Seismic Behaviour of Lightweight Reinforced Concrete Shear Walls

Von der Fakultät für Bauingenieurwesen und Geodäsie
der Gottfried Wilhelm Leibniz Universität Hannover
zur Erlangung des Grades eines

DOKTORS DER INGENIEURWISSENSCHAFTEN

Dr.-Ing.

genehmigte Dissertation
von

M.Eng. Werasak Raongjant
geboren am 19.10.1974 in Samutsakorn, Thailand

2007

1. Referent: Prof. Dr.-Ing. Nabil   A. Fouad
2. Referent: Prof. Dr.-Ing. Jürgen Grünberg
Vorsitz: Prof. Dr.-Ing. Martin Achmus

Tag der Promotion: 17.07.2007

Abstract

The lighter weight of lightweight concrete permits a saving in dead load as well as a reduction in the costs of both superstructures and foundations. In addition, the better thermal insulation, the higher fire resistance and the substantially equivalent sound-proofing properties benefit for its familiar use in recent years. Structural lightweight reinforced concrete shear walls seems to be a very convenient alternative to conventional reinforced concrete shear walls for structures in seismic zones. However, there are still few attention which focus on the seismic behaviour of lightweight reinforced concrete shear walls. So that it is important to study the hysteresis behaviour of this system and find an optimized reinforcement placement to increase its ductility and shear resistance.

This work studied the shear resistance, the crack development, the lateral deformation, the hysteretic behaviour, the failure mode and shear transfer mechanism, etc. of lightweight reinforced concrete shear walls with different web reinforcement ratios and orientations on the base of experimental and theoretical results of four shale ceramsite concrete shear wall specimens.

The experimental study indicated that, walls with lightweight aggregate concrete exhibited high shear capacity, large ductility and a satisfactory energy dissipation mechanism. It appears that lightweight reinforced concrete shear walls can be used as structural walls in seismic zones. Diagonal web reinforcement provided a more effective mechanism for transferring lateral forces into the foundation, resulted in lower shear strains near the base of the wall, and improved the energy dissipation characteristics. Due to the economic reason and the difficulties associated with placement of diagonal bars during construction, the placement

of fewer inclined bars together with conventional reinforcements provided an attractive alternative for the web reinforcement in walls.

An appropriate finite element analysis program was developed by ANSYS software for modeling the nonlinear behaviour of lightweight reinforced concrete shear walls. The analysis results showed good agreement with the experimental results. It clearly supported the validity of the finite element models developed in this study for predicting the nonlinear response of lightweight reinforced concrete shear walls. Some numerical studies which focus on the influence factors of shear resistance of lightweight reinforced concrete shear walls were processed in this way.

Keywords: lightweight concrete, reinforced concrete shear walls, seismic behaviour, cyclic load, diagonal web reinforcement, finite element analysis, hysteresis behaviour

Kurzfassung

Die geringe Dichte des Leichtbetons ermöglicht eine Reduktion des Eigengewichts und somit einer Verringerung der Kosten des Tragwerkes und der Gründung. Zusätzlich liefern sie bessere thermische Dämmwerte, grössere Feuerwiderstandsfähigkeit und im wesentlichen gleichwertige Schallschutz Eigenschaften für deren vertrauten Gebrauch in den letzten Jahren. Wandscheiben aus Stahlleichtbeton sind eine bewehrte Alternative zu den herkömmlichen Wandscheiben für Bauwerke in den seismischen Zonen. Bisher gibt es nur wenige Untersuchungen über das Tragverhalten von Stahlleichtbeton Wandscheiben unter Erdbebenbeanspruchung. Daher ist es wichtig, das hysteresis Verhalten derartige System zu untersuchen und die Bewehrungsanordnung zu optimieren, um die Duktilität und den Schubwiderstand zu erhöhen.

In dieser Arbeit werden die Schubwiderstandsfähigkeit, die Rissentwicklung, die seitlichen Verformungen, das hysteretic Verhalten, der Versagensmechanismus und Scherübergangseinheit, der Stahlleichtbeton Wandscheiben mit unterschiedlichen Bewehrungsverhältnissen und unterschiedliche Anordnungen der Bewehrung auf der Grundlage von experimentellen und nummerische Untersuchungenan vier Schieferbeton-wandscheibenproben untersucht.

Die experimentelle Studie zeigte, dass Wände aus Beton mit Leichtzuschlagstoffen eine hohe Schubkapazität, grosse Duktilität und eine zufriedenstellende Energieableitung aufweisen können. Es scheint, dass Stahlleichtbeton Wandscheiben als lastabtragende Wände in den seismischen Zonen eingesetzt werden können. Eine diagonale Bewehrungsanordnung stellte eine wirkungsvollere variante dar für das Einleiten der seitlichen Kräfte in die Fundamente. Es ergeben sich niedrigere Scherbelastungen nahe der Unterseite der Wand und eine verbesserte Energiedissipation. Aus wirtschaftlichen Gründen und auf Gründ von Konstrucktiven Schwierigkeiten, die sich durch die Anordnung der diagonalen Stäbe während des Aufbaus ergeben, ist die Plazierung weniger geneigter Stäbe zusammen mit

herkömmlichen Bewehrung eine attraktive Alternative für die Bewehrungsanordnung in den Wänden.

Ein passendes Finite Elementanalyse Programm wurde durch ANSYS Software für das Modellieren des nichtlinearen Verhaltens der Stahlleichtbeton Wandscheiben entwickelt. Die Berechungsergebnisse zeigen eine gute Ubereinstimmung mit den experimentellen Resultaten. Sie stützte offenbar die Gültigkeit der Finiten Elementmodelle, die in dieser Studie für das Voraussagen der nichtlinearen Antwort der Stahlleichtbeton Wandscheiben entwickelt wurde. In einer Parameterstudie werden die zahlreichen Einflussfaktoren für die Schubtragfähigkeit der Stahlleichtbeton Wandscheiben ausgewertet.

Schlagwörter: Leichtbeton, Stahlleichtbeton Wandscheiben, seismisches Verhalten, zyklische Last, diagonale Netzverstärkung, begrenzte Elementanalyse, hysteresis Verhalten

Acknowledgments

First of all, I would like to thank my advisor, Prof. Dr.-Ing. Nabil A. Fouad, for giving me the opportunity to contribute to this project, moreover, giving advices, insights, and guidance along the way. I am honoured to work with him, for his mastery of seismic theory of concrete structure making me put things in the right perspective.

I am grateful to the members of my promotion committee: Prof. Dr.-Ing. Jürgen Grünberg, Institute of Concrete Construction (IFMA) and Prof. Dr.-Ing. Martin Achmus, Institute of Soil mechanics, Foundation engineering and Waterpower engineering (IGBE). And especially. I'd like also to thank all my colleagues in the Institute of Concrete Construction (IFMA) and Institute of Building Techonolgy and Timber Construction (IBH), Leibniz Universität Hannover, who have provided me with their valuable suggestions, many contributions and true friendship.

I thank Rajamangala University of Technology Thunyaburi in Thailand for financial support throughout my study. I also thank Hebei University of Technology, Prof. Lai Wang and Prof. Xian Rong for their help during the whole experiment course.

I greatly thank my beloved family and all my friends in Thailand for always being there when I needed them. I also thank all Thai people in Hannover whose name I don't mention explicitly.

Finally, a special word of thanks goes to my wife, Meng Jing, for all her love, moral support and help.

Hannover, in July 2007   **Werasak Raongjant**

Table of Contents

List of Figures

List of Tables

To my Father, Sun Raongjant

To my Mother, Wannee Raongjant

To my Aunty, Varin Suphang

To my Wife, Jing Meng

Chapter 1

Introduction

1.1 Overview

During the past fifty years, reinforced concrete shear walls have been widely used as the primary lateral-load resisting systems for both wind and earthquake loading in multi-story building around the world. Observations from previous earthquakes have indicated that well-designed structural walls can be used effectively as the primary lateral-load resisting system for both wind and earthquakes loading in multistory building [Ebe95] [Fin74]. Because it is not economical to design slender structural walls to remain elastic during strong earthquakes [Oes84], the inelastic response of structures should be considered during the design process [Der79][Oes76]. To survive in case of strong ground motions from severe earthquakes, structural walls must be able to dissipate energy after yielding and should not be susceptible to sudden failures due to shear or local instabilities [Pau77].

At the time, structural lightweight aggregate concrete (LWAC) is being used in many civil engineering applications as a very convenient alternative to conventional concrete. LWAC is manufactured by using different kinds of lightweight aggregates, available in nature or artificially produced. The properties of LWAC depend on the properties of the particular lightweight aggregate being used. Two major categories, natural and processed, are utilized to classify lightweight aggregate. Natural lightweight aggregates include pumice and scoria (volcanic cinder). They have been used as an aggregate in the production of lightweight concrete in many countries of the world. In particular, it can be found in the Mediterranean area (Italy, Turkey, Greece, and Spain) [Cav03]. In the USA it is mined mainly in the South-Central States. Processed or manufactured lightweight aggregates include perlite, vermiculite, expanded clay, shale, slate, blast furnace slag and coal cinders. Thereinto, shale ceramsite is a type of manmade lightweight aggregate, which was made from natural shale by crushing, burning and expanding. It has the features of lightness, high strength, heat preservation, heat insulation, sound insulation, fire resistance and corrosion resistance. It can be also added to

materials which are heat resistant, acid resistant, sound-proof, filtering, and to materials for gardening and organism raising [Min04].

As a matter of fact lighter weight of LWAC permits a saving in dead load with a reduction in the costs of both superstructures and foundations. In addition, the better thermal insulation, the greater fire resistance and the substantially equivalent sound-proofing properties benefit for its familiar use. In the last five decades the use of LWAC has been extended to structural elements, thanks to the improvement in performances obtainable (in terms of stiffness, strength and ductility) by means of appropriate ingredient mix proportions [Arn86] and appropriate design of the reinforcement. Naturally, the use of lightweight concrete has been confined to large structures (where the beneficial influences of the reduced weight are greater), and more in particular, to structures where a high dead load to live load ratio occurs. Further, the reduced weight may make LWAC preferable for structures in seismic zones because of the reduced dynamic actions, and for precast structures, because it makes it easier to move the elements to be connected. More recently, lightweight concrete was also applied in marine structures (offshore structures and ships), and later for long span bridges, buildings and grandstands [Bar93]. Referring to buildings, LWAC can be used in structural frames, but it proves to be more suitable for wall system structures, where the local ductility demand (in seismic zones) and the required strength of the materials are reduced and the dead load to live load ratio is very high.

Results from previous investigations [Oes76][Oes79][Oes84][Oes86] have demonstrated that structural walls that deform primarily in shear and experience large shear distortions have lower energy dissipation than structural walls that deform primarily in flexure. In addition, it was found that walls that experience large shear distortions were more likely to fail by web crushing, which is caused by deterioration of the compressive strength of the concrete struts in the web [Oes84]. Experimental results [Oes76][Oes79] have indicated that increasing the amount of conventional vertical and/or horizontal web reinforcement in walls that were susceptible to shear failure did not significantly reduce the inelastic shear distortion nor appreciably improve the energy dissipation capacity. Web crushing failures were still observed in walls designed with a nominal shear strength that exceeded the nominal flexural strength [Woo91]. Subsequent analytical studies [Sitp93][Sit95] have indicated that the hysteretic response of walls susceptible to shear failures could be improved if diagonal reinforcement was used in the web. Diagonal web reinforcement provided a more effective mechanism for transferring lateral forces into the foundation, resulted in lower shear strains near the base of the wall, and improved the energy dissipation characteristics.

On the other hand, the major problems of the nonlinear finite element analysis of reinforced concrete structures are the large amount of CPU time required for the analysis due to the complicated material models and the difficulties encountered in the stability and accuracy of the solutions. Some material models for concrete include excessively refined analyses, such as fracture mechanics and detailed crack localizations, which cause unneeded expenses. Most previous models for the cyclic behavior of reinforced concrete were tested and verified successfully at the element level (the finite element model consists of one and few elements), but when these material models were used in the structural level problems (the finite element model consists of a large number of elements, such as the modeling of actual reinforced concrete structures), numerical problems associated with the complex stress-strain relationships prevented the completion of most analyses [Ste87]. Therefore, the need exists to develop new material models for concrete and reinforcing steel that can avoid these problems.

The research work in this paper is actually part of an ongoing investigation of the cyclic behavior of reinforced concrete shear walls because that lightweight reinforced concrete (shale ceramsite concrete) was used. In this study lightweight reinforced concrete shear walls with different reinforcement ratios and orientations were tested and some of the important behavior aspects were reported. At the same time, the appropriate analytical models were developed by ANSYS software for modeling the inelastic behavior of lightweight reinforced concrete shear walls. The finite element method was chosen as the numerical technique in this investigation because this method, when combined with the proper constitutive models for concrete and reinforcing steel, offers a very powerful tool to investigate the response of shear walls with different configurations subjected to generalized loadings. Furthermore, finite element analysis also yields important detailed information on the behavior of shear walls, including the stress-strain relationships in concrete and reinforcing steel, deflected shapes, and crack patterns, which cannot be obtained from other analytical methods such as truss models [Oes86] and shear hysteresis models [Ozc89].

The analytical models for lightweight concrete and reinforcing steel, developed and verified using experimental results, will play an important role in the ongoing research. With these analytical models, the finite element method can be used to explore in detail the behavior of lightweight reinforced concrete shear walls that have different configurations and reinforcement details tested in the laboratory.

1.2 Research significance

Experience during the 1989 Loma Prieta and 1994 Northridge earthquakes has shown that economic losses can be significant in buildings that satisfied the life-safety design criteria in current building codes. As a result, procedures to consider the post–earthquake condition of a building when establishing design limit states are currently being developed. For lightweight reinforced concrete shear wall, shear failure is more serious and brittle than normal reinforced concrete shear wall. So that it is important to find an optimized reinforcement placement to increase its ductility and shear capacity. Diagonal web reinforcement in structural walls appears to be one way to control structural damage using conventional methods of construction.

1.3 Objective

The main objective of this research program is aimed at evaluating experimentally the cyclic force behavior of lightweight reinforced concrete shear walls with different web reinforcement under cyclic displacement controlled load reversals and to predict analytically the nonlinear static response of this system under earthquake loading.

The detailed objectives of this research are:

(1) Four lightweight reinforced shear wall specimens with conventional and diagonal web reinforcement will be designed according to the requirements of Eurocode 8 (EC 8) and ACI 318-05[ACI05] codes.

(2) An experimental program will be undertaken to obtain information on the seismic behavior of lightweight reinforced concrete shear walls with conventional web reinforcement, with diagonal web reinforcement, with more diagonal web reinforcement

and with combined conventional web reinforcement and diagonal web reinforcement. Some of the important behavior aspects will be reported, such as the overall hysteresis response, the energy dissipation capacity, shear walls with openings response, the contribution of flanges to shear walls response, deflected shapes, crack patterns, and observed failure modes.

(3) Considering various solutions, an idealized numerical model of the composite system, capable of predicting the response of the lightweight reinforced concrete shear walls with different arrangement of web reinforcement, will be developed and its accuracy will be assessed in comparison with the experimental data. Nonlinear material models for both reinforcing steel and concrete that are capable of reproducing the nonlinear response of the lightweight concrete shear wall are presented. The material models used must be simple, stable, and reliable in order to make the analyses feasible and economical with respect to CPU time and the convergence of nonlinear solutions.

(4) By the experimental and theoretical analysis, the shear transfer mechanism for lightweight reinforced shear wall with different web reinforcement will be studied in detail and the influence of diagonal web reinforcement on the seismic behavior of shear walls will be evaluated.

1.4 Scope

This thesis is divided into eight chapters. The opening chapter addressed the usefulness of structural lightweight reinforced concrete shear walls as lateral load resisting element for buildings in seismic zones and gives a brief description of the proposed lightweight wall system.

The second chapter describes microstructure and mechanical properties of shale ceramsite concrete. General information of shale, occurrence of shale, deposits of shale and pyroprocessed aggregates are presented.

In the third chapter, both the principle aspects of lightweight reinforced concrete shear wall design, as given in two codes, namely, the European Seismic Code 8 (EC 8) and the American Concrete Institute Building Code (ACI 318-05), and the design considerations of lightweight structural walls are discussed. The seismic design of four lightweight reinforced concrete shear wall specimens using simplified equivalent static lateral-load analysis procedures as defined in the EC 8 and ACI 318-05 code are presented in detail.

The experimental programs of four lightweight reinforced concrete shear walls are described in chapter 4. Material properties, specimen details, test procedures and the instrumentation layout are given.

The experimental results are presented in chapter 5. Several aspects of the test results, including the load vs. top deflection curves, the load vs. shear distortion curves, the energy dissipation capacity, the deflected shapes, crack patterns and observed failure modes, are given and discussed in detail.

A nonlinear FEA (Finite Element Analysis) computer program is developed in chapter 6 to evaluate the overall cyclic response of the lightweight reinforced concrete shear walls with

different arrangement of web reinforcement. Element type, material properties, geometrical modeling and finite meshing are being studied in detail.

In chapter 7, the accuracy of the mathematical model to predict the cyclic nonlinear behavior of lightweight reinforced concrete shear walls with different arrangement of web reinforcement is assessed by comparing the analytical results with the experimental results of the four tested specimens. Shear transfer mechanisms for lightweight reinforced concrete shear walls with conventional and diagonal reinforcements are discussed by theoretical results and a further study on the shear resistance of lightweight aggregate shear wall is processed.

Finally, chapter 8 coveres the summary, conclusions and recommendations for the research and design improvement.

Chapter 2

Microstructure and Mechanical Properties of Shale Ceramsite Concrete

Since the 1990s, the research on lightweight aggregate has been carried out in many fields. Lightweight aggregate can be classified into sintered lightweight aggregate and lightweight aggregate exempted from sintering according to its production technology. When it comes to raw materials, light aggregate includes shale ceramsite, fly ash ceramsite, pumice ceramsite, glass ceramsite, diatomite ceramsite, etc.

This chapter introduces shale ceramsite as an aggregate for structural lightweight concrete which used in the experimental study of this paper. This aggregate has low apparent density, high strength and high durability. The microstructure and mechanical properties of shale ceramsite concrete are discussed in detail here.

2.1 Shale ceramsite as an aggregate for lightweight concrete

2.1.1 General information

Shale is a sedimentary rock composed predominantly of clay-sized particles, as shown in Fig.2-1. It is formed by the lithification of clay or mud, commonly with admixed silt. Shales is easily to be split into thin flat plates or sheets parallel to bedding (fissile). When freshly exposed, its colour is commonly very dark gray or nearly black. Less commonly, shale may be light gray, greenish, or reddish in color. Black and gray shales owe their color to finely divided carbonaceous matter or pyrite. Greenish shale owes its color to the presence of ferrous iron and/or chlorite, and reddish shale to the presence of iron oxide. But weathering shades it to very light gray or buff [Nue81]. The chemical composition of Ithaca shale is provided in Table 2-1.

Fig.2-1 Shale

Throughout most of the interior highlands, shale is the dominant sedimentary rock. Most shale occurs in very thick units. Units consisting almost entirely of shale may be more than 300 feet thick. Shale is more easily eroded than most other sedimentary rocks. Consequently, it underlies valley floors and the lower flanks of mountains where it is less likely to be exposed in outcrop than the more resistant sedimentary rocks occupying higher elevations. It is often exposed in creek beds, along the banks of the major rivers, and in road cuts. Shale, containing the mineral talc, developed from the alteration of shale adjacent to soapstone deposits in Saline County. Ground talcose shale has potential value as filler in pottery clay and additives to paints and plastics. Baking of shale that occurred in the zone of contact metamorphism at the Magnet Cove intrusion in Hot Spring County, created hornets, a rock that is usable as a crushed stone product. Shale resources are considered inexhaustible. However, there have shortages of particular types or colors. Markets for shale products are limited by competition from substitute materials and the relatively few industries utilizing slate granules and flour (fines) [Sto84].

Table 2-1 Chemical composition of Ithaca shale [Roy60]

Component	% Mass
SiO_2	62.00
Al_2O_3	18.50
Fe_2O_3	7.70
MgO	2.00
CaO	0.34
TiO_2	0.12
K_2O	4.70
Na_2O	1.20
Ig Loss	4.40
Carbon	0.22
SO_3	0.24

2.1.2 Pyroprocessed aggregates

The process, by expansion and vesiculation under scientific control of raw shale, slates or clays having suitable characteristics in a rotary kiln at kiln temperatures of from 1800 to 2100ºF(1,000 degrees C), is called "pre-processing". This process was first perfected at Kansas City in 1917 by Stephen J. Hayed, a chemist, who found that by heating certain shales, clays and slates to incipient fusion he was able to develop a lightweight aggregate of high structural strength. Gases formed within the shale thus expand, forming myriads of tiny air cells within the mass, which are retained upon cooling and solidification. The resultant product is therefore made up of a cellular aggregate of great structural strength, each cell being surrounded by a hard vitreous membrane.

Clay is a very fine-grained, moisture-retentive, naturally occurring material composed principally of silicates of alumina, derived from the decay of igneous micas and feldspars, such as those found in granite. Sedimentary rock made from clay is called shale, and if it is metamorphosed, it becomes slate. The pyroprocessing of all three materials results in essentially the same product: a lightweight aggregate that is ceramic in nature [Tom05]. Expanded shale ceramsite, as a high grade building material, has been recognized by the building industry for more than a third of a century.

2.2 Microstructure and strength of shale ceramsite concrete

The structure of lightweight aggregate concrete is piled with lightweight aggregate particle bonded by cement paste. The difference between lightweight aggregate (LWA) and normal weight aggregate (NWA) is that LWA has porous interior and a micropore-micropipe system. This kind of system has a hydrophilic effect in lightweight aggregate concrete (LWAC). When the relative humidity in the hardened paste drops, a moisture flow starts from the lightweight aggregate particles to the drying paste, providing for the continuous hydration action of unhydrated cement particles. The micro-pumping effect of water absorption and release results in a low local water/cement ratio on the surface of aggregate. In other words, the compactness of mortar near the aggregate will be increased. The pockets of water below coarse aggregate caused by inner lamination phenomenon can be reduced or avoided. The interface bond strength between coarse aggregate and paste can be increased. The effective area between LWA and cement paste is larger than that of NWA due to roughened surface and porous character of LWA. Besides these features, chemical reaction between with calcium hydroxide in the cement paste can take place. So the interface bonding power between LWA and cement paste is much stronger than NWA. The interface structure of LWAC is different with that of normal weight concrete[Zha90][Zha02].

The interface structure between LWA and cement paste influences considerably the physical and mechanical properties of LWAC. So the study of its interface structure has a significant meaning for the high strength lightweight aggregate concrete. It has something to do with the type, surface structure, water absorbability of aggregate, mortar composition and consistence. The effect of absorption and release water of shale ceramsite has a significant influence to microstructure of interfacial zone [Min04].

The microstructure of the ceramsite sealing course has been testified by SEM (Scanning electron microscope) testing. The hydration phases are illustrated in Fig.2-2, have a needle

-like crystal and a compact structure, which has a high strength [Min04]. A compact layer shale ceramsite body can be seen from Fig.2-3.
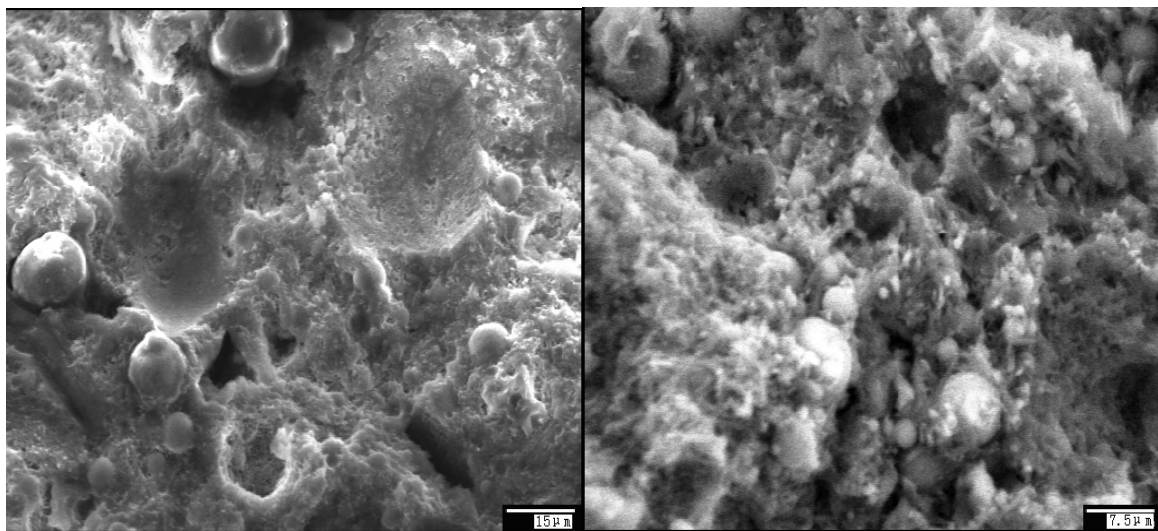
(a) 1000 times　　　　　　　　　　　　　　(b) 2000 times
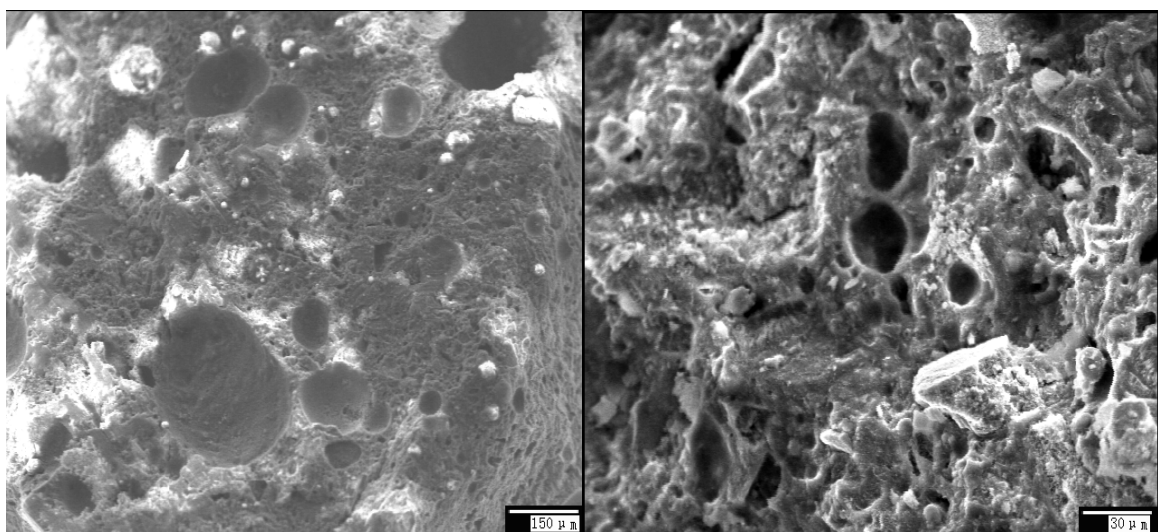
(c) 100 times　　　　　　　　　　　　　　(d) 500 times

Fig.2-2 Microstructure in SEM of the shale ceramsite [Min04]
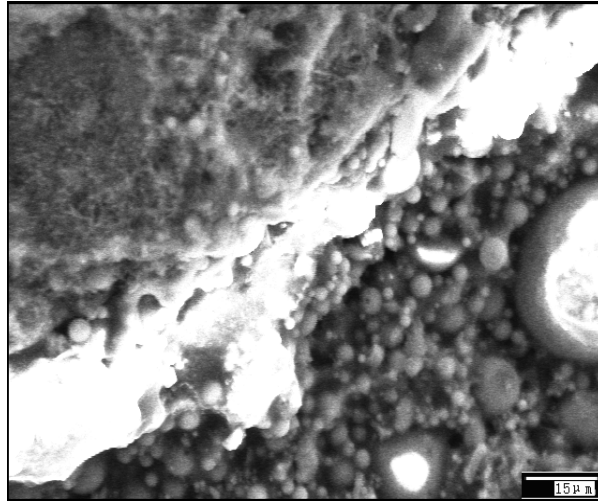
Fig.2-3 Sealing layer structure of the shale cereamsite [Min04]

2.2.1 Early strength and microstructure of shale ceramsite concrete

The influence of pre-wetting time on strength of shale ceramsite concrete was studied by former researchers. The aggregate was pre-wetted for 0, 5 min, 60 min and boiled for 120 min, respectively. The concrete specimens made by them were marked with A_0, A_5, A_{60}, A_b correspondingly [Jia03] [Zhe06]. It showed that the early compressive strength decreased gradually with the pre-wetted degree increasing. The compressive strength at 7 days can reach 93.3% of that at 28 days. However, the compressive strength of normal concrete at 7 days was about 70% to 80% of that at 28 days. With the pre-wetted degree increasing, the strength growth rate at 7 days decreased, but the early strength was still fairly high. This is because that water absorbing force of coarse aggregate decreased with the pre-wetted degree increasing. The descent scope of localized water/binder ratio of concrete in the interfacial zone between ceramsite and cement paste turned smaller and smaller, and the bond strength between ceramsite and cement paste decreased. So the early strength of concrete decreased gradually.

The microstructures of the interfacial zone of shale ceramsite concrete at 7 days are shown in Fig.2-4. There were almost no cracks on the interfacial zone between aggregate and cement paste. The rough surface made mortar permeate into aggregate available, so the mechanical occlusion between aggregate and cement paste was well, and there was no distinct weak transition zone in the concrete composite, so the LWAC has higher early strength than normal concrete.

Fig.2-5 exhibits the microstructures of cement paste at the distance of 1 micron to aggregate surface at 7 days. It was seen that the microstructure of the interfacial zone at the vicinity of aggregate turned looser and looser, but the microstructures of the bulk cement paste had no distinct difference and had nothing to do with the pre-wetted degree. On the contrary, when the design strength of concrete was rather high and water/binder ratio was very low, the pre-wetted aggregate would release the water to cement paste. So the water/binder ratio of interfacial zone was nearly the same, even higher than that of cement matrix. With the pre-

wetted degree increasing, water absorbing force from mortar to ceramsite decreased, and the descent scope of water/binder ratio on the interface between ceramsite and mortar decreased. The bond strength of the interfacial zone is lower than that of the bulk cement paste. The compressive strength of concrete depends on the strength of the interfacial zone. So the compressive strength of concrete at 7 days decreased gradually with the pre-wetted degree increasing.

| a) Concrete A_0 | b) Concrete A_{60} | c) Concrete A_b |
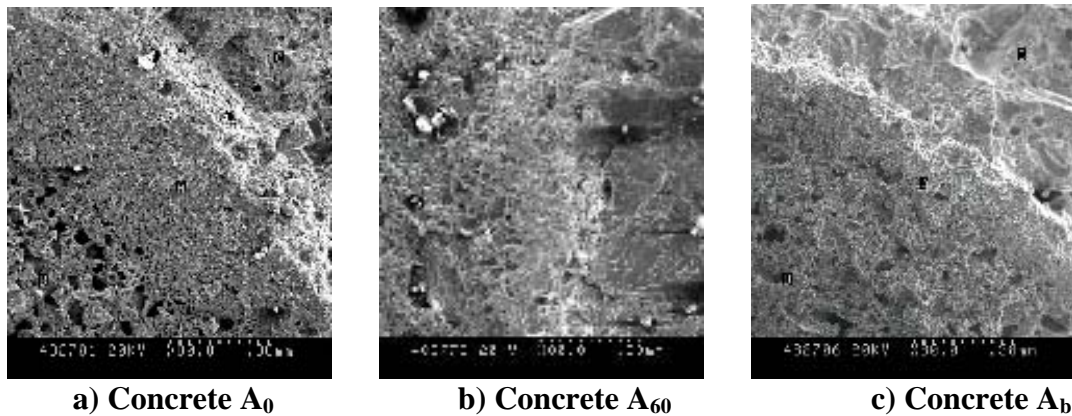
Fig.2-4 Microstructure of the interfacial zone between aggregate and cement paste at 7 days (×80) [Min04]

| a) Concrete A_0 | b) Concrete A_{60} | c) Concrete A_b |
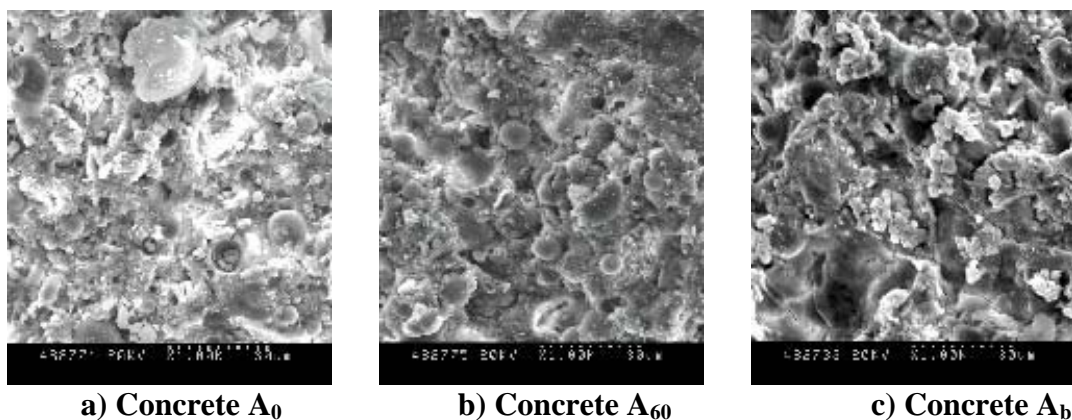
Fig.2-5 Microstructure of cement paste at the vicinity of aggregate at 7 days (×1K) [Min04]

2.2.2 Later strength and microstructure of shale ceramsite concrete

The test results showed that the later cube compressive strengths of all concretes with different pre-wetting degree of shale ceramsite were almost the same after 28 days [Qin99].

The main reason was that with the prolongation of curing age, relative moisture in the cement paste decreased gradually due to the consumption of water when cement hydrated. The relative humidity of cement paste changed fast in early stage and changed slowly in later stage. When relative humidity of cement paste was lower than that of aggregate, water in aggregate would be released and played a self-curing action inside the concrete, and

accelerated cement hydration and made cement in the interfacial zone hydrated sufficiently. And water supply capacity increased with the increasing of pre-wetting degree of shale ceramsite. That is, the increase of pre-wetting degree of shale ceramsite increased the self-curing ability of LWAC. The self-curing action improved the bond strength between aggregate and cement paste. It appeared that in case of self-curing there were more advantages than external curing. When the bond strength of interfacial zone or cement matrix reached an upper level for the aggregates, and the strength did not benefit very much from a further improvement in the matrix strength, the strength of concrete had no obvious increase with further prolongation of curing age. The long-term strength of LWAC was mainly decided by the self-strength of LWA.

The 140-day microstructures of concrete were presented in Fig.2-6. There was almost no crack on the interfacial zone between aggregate and mortar, the microstructure of interfacial zone between aggregate and cement paste was hardly homogeneous. The hydrate structure was very dense and had no obvious difference from all concretes. This demonstrates that water return of ceramsite play a very important role in the self-curing enhancement effect of concrete. On the other hand, LWA is a type of fired clay material and has some certain activity on the surface after high-temperature calcinations. Then chemical reaction with calcium hydroxide in the cement paste can occur. As a result of both physical and mechanical occlusion effect and chemical effect, the structure of cement paste became denser, and the boundary between aggregate and cement paste could not be observed obviously.

a) Concrete A_0 b) Concrete A_{60} c) Concrete A_b
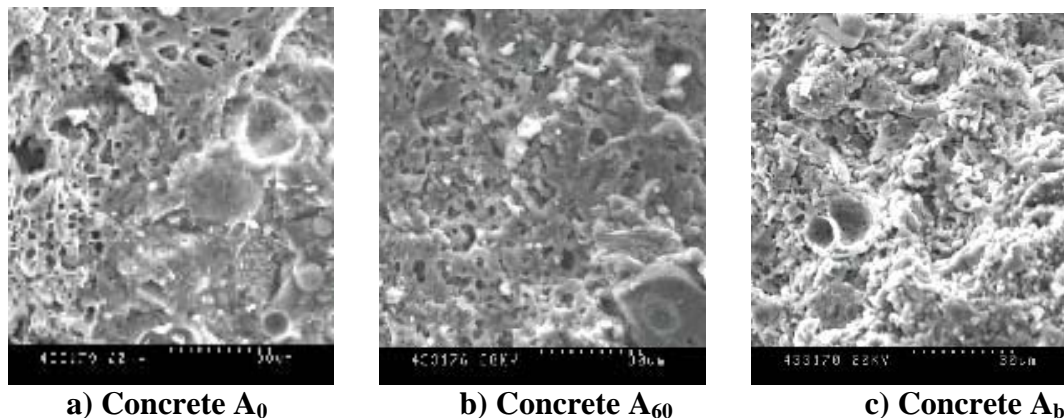
Fig.2-6 Microstructure of cement paste at the vicinity of aggregate at 140 days [Min04]

2.3 Mechanical properties of shale ceramsite concrete

The ultimate difference between lightweight aggregate concrete and normal concrete is the coarse aggregate, which induces the differences of concrete mechanical properties. In normal concrete, the strength of coarse aggregate is much higher than the strength of cement paste. Because of that, the crack, firstly appearing inside of the cement paste and in the interface between aggregate and cement paste, will go round the aggregate and continue to develop in the cement paste. The coarse aggregate has the effect to prevent the crack's development. Finally, the crack and failure of concrete occur only in the cement paste. However, the coarse aggregate has no damages.

It is different for lightweight aggregate concrete. Because lightweight aggregate has normally porous interior and brittle property, its compressive strength, tensile strength and modulus of deformation are very low, even lower than the corresponding values of cement paste around them. So that, when lightweight aggregate concrete subject to load, the stress distribution in coarse aggregate and cement paste is different to that of normal concrete. Due to the relatively lower strength of coarse aggregate, cement paste will bear more stresses. So that lightweight aggregate concrete works almost like a mechanical model, in which aggregate works as filling and cement paste works as frame. Furthermore, the rough surface of lightweight aggregate makes mortar permeate into aggregate available, so the mechanical adhesive between aggregate and cement paste is well, and there were no distinct weak transition zone in the concrete composite.

So the interface cracks appear later and develop slower in lightweight aggregate concrete than in normal concrete. Due to the larger deformation of coarse aggregate, the deformation of lightweight aggregate concrete is increased, also the peak strain of it. After cracks appeared in the cement paste, coarse aggregate can not hold back the development of cracks and then cracks go through the coarse aggregate easily. It results in the abrupt descend curve of its stress-strain curve with quickly decreased strength and relatively fewer crack quantity. It can be seen distinctly that coarse aggregate is split at the failure zone of specimens. The strength and deformation capacity of lightweight aggregate concrete depend some degree on the mechanical properties of its coarse aggregate.

Chapter 3

Seismic Design of Lightweight Reinforced Concrete Shear Walls

3.1 Introduction

Structural codes are legal documents which provide guidelines for the design, detailing and construction of structures. Experimental and analytical research and field observations are the main source in the development of seismic code requirements. Code provisions can be seen as a minimum demand for structures with a more or less conventional and regular configuration. Most seismic building codes permit the determination of the design lateral forces using either a static lateral force procedure or a dynamic force analysis method. Worldwide, the simple equivalent lateral force method combined with the capacity design concept is the most commonly used method to evaluate the earthquake design forces.

For the preliminary seismic design of shear walls used in this study, the simple static lateral force procedures defined in the European and ACI codes (respectively the Eurocode 2, Eurocode 8 and ACI 318-05), have been used. The use of these codes is justified as the prototype structure is regular in layout as defined in the both codes. These two seismic design codes are used here in order to show the current design methods practiced in Europe and the USA.

Basically, the two codes reflect a design philosophy by which the structures should be able to resist minor earthquakes without damage, moderate earthquakes without structural damage but possibly with some nonstructural damage, and major earthquakes without collapse but with both structural and nonstructural damage. The basic reason to permit substantial building damage under major earthquake exposure lies in the high construction cost of a structure designed to resist seismic forces without damage.

As current codes have not yet codified design procedures for the proposed lightweight wall system, procedures specified for reinforced concrete (RC) shear walls were used. So that, in this study the lightweight reinforced concrete shear wall is designed as a RC panel. In order to

achieve a cyclic behavior of the lightweight walls, different arrangement of web reinforcement designs have been developed and tested as part of this study.

In the following section, a brief description of the principal requirements of each code, Eurocode 8 (EC 8) [Eur00] and ACI 318-05 [ACI05], with respect to the seismic design of lightweight reinforced concrete shear walls are summarized. The design procedures of four lightweight reinforced shear wall specimens are presented, which were mainly according to ACI 318-05 code.

3.2 Design procedure according to Eurocode 8

Eurocode 8 is a European seismic code issued by the Commission of the European Communities for the design and construction of buildings in seismic regions. The general purpose of the code is to protect human lives and limit structural damages under earthquakes. The capacity design criteria based on the ultimate limit state of structural systems and the serviceability limit state of such systems are considered in this code. EC 8 classifies two distinct types of failure for RC walls, namely flexural and shear failure. The behavior factor to be used in the analysis procedure reflects the expected ductility of the system as reflected by the anticipated type of failure. Based on these failure modes, design expressions are given. A brief description of the design procedures for shear wall is listed in the following sections.

3.2.1 Design requirements of lightweight reinforced concrete shear walls

The design of earthquake resistant lightweight shear walls is aimed at providing a structural system with adequate energy dissipation and a sustained capacity to resist both horizontal and vertical loads. In general, the designer needs to know the maximum possible shear and moment values which can be expected considering the pattern of seismic forces. The designer should be able to determine the shear and flexural capacities in the critical wall regions in order to predict, given the different load combinations, if either flexural or shear failure can be expected. In order to develop a ductile system, it is desired to provide structural walls with a shear capacity greater than the maximum shear associated with the available moment capacity. Hence, the wall design may call for a shear load capacity twice as large as the shear force related directly with the flexural capacity of the walls.

The different design provisions in EC 8 for RC slender and squat walls consider the different modes of failures as reflected in the different "ductility classes" used in earthquake resistant concrete design. Slender walls are defined as walls with a height to length ratio greater than 2 and squat walls as walls with a corresponding ratio less than or equal to 2. The basic two types of the failure, namely flexural failure and shear failure, are shown in Fig.3-1.

		Failure mode
		Flexural, ductile
		Flexural, brittle
		Shear, web diagonal failure in compression
		Shear, web diagonal failure in tension
		Shear, horizontal sliding
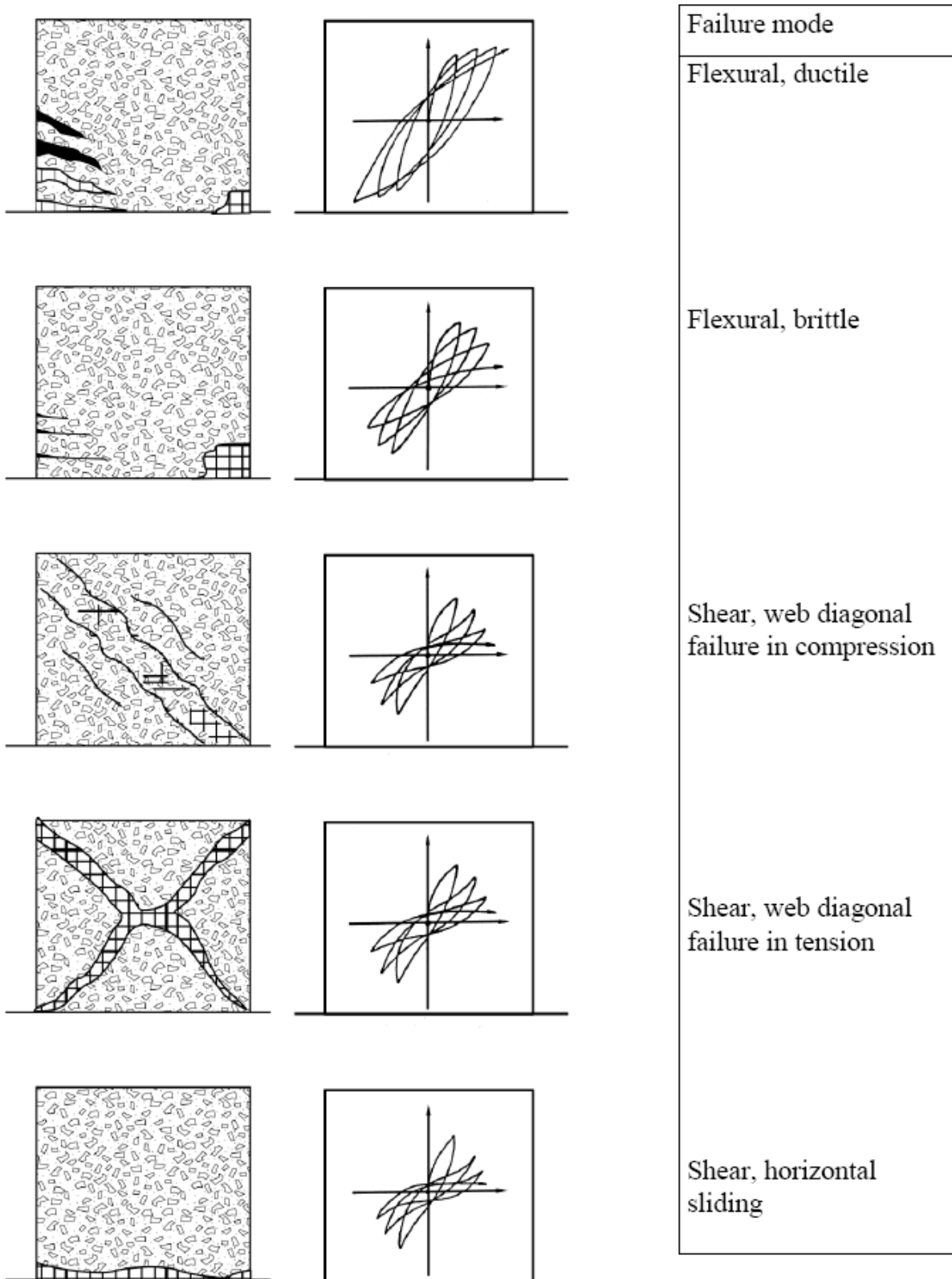
Fig.3-1 Failure modes of the RC wall with expected response

3.2.2 Standard method of shear design

In general, the distinction between the two types of failure may be made on the basis of the ratio:

$$\upsilon = \frac{V_{Rd}}{\gamma_{Rd} \cdot V_{(M_{Rd})}}$$

(3-1)

Where V_{Rd} — The minimum value of the design strength at shear failure mode (diagonal compression, diagonal tension or shear sliding);

$V_{(M_{Rd})}$ — The shear force corresponding at the state of the design flexural failure of the critical wall region;

γ_{Rd} — A global factor, intended to counterbalance the chosen partial safety factor of steel and to cover partial hardening effects as well as uncertainties of the models involved; it may taken equal to 1.25 in case of a high ductility class design and 1.15 for the medium ductility class design.

In the preliminary design of the wall reinforcement it is necessary to assume a realistic υ-value to assure the intended mode of failure. For slender walls (height-to-length ratio larger than 2.0) designed for high ductility class (DC H) or medium ductility class (DC M) and intended to experience a flexural mode of failure, a υ-value of more than 1.0 should be assumed. In case of squat walls (height-to-length ratio less than 0.75) designed for one of the above ductility classes, a υ-value of less than 0.50 should be assumed if the wall is to experience shear failure. For the walls with height-to-length ratio between 0.75 and 2.0, a υ-value between 0.5 and 1 are assumed with a mixed type of wall failure (flexural and shear failure).

In assessing the potential development of a flexural or shear mode of failure, the reinforcing layout in the "critical" region of the wall should be considered. This region extends over part of the lower portion of the shear wall with a height of about equal to the length of the wall or 1/6 of the height of the building.

In evaluating the shear capacity of the wall, the shear resistance of both the concrete and reinforcing steel has to be considered for several different modes of failure. For the concrete, both the diagonal compression and tension failure, the following inequality should be satisfied, namely:

(1) For diagonal compression failure of the web,

$$V_{Sd} \le V_{Rd2}$$

(3-2)

Where V_{Rd2} may be calculated:
For the critical region as:

$$V_{Rd2} = 0.4 \cdot (0.7 - f_{ck}/200) \cdot f_{cd} \cdot b_{wo} \cdot z$$

(3-3)

And for the zone outside of the critical region as:

$$V_{Rd2} = 0.5 \cdot (0.7 - f_{ck}/200) \cdot f_{cd} \cdot b_{w0} \cdot z \qquad (3\text{-}4)$$

Where z — The internal lever arm, which may be taken equal to $0.8l_w$;

    b_{w0} — The web thickness of the wall;

    f_{ck} — The characteristic strength for concrete in MPa, which is limited to 40 MPa.

(2) For diagonal tension failure of the web,

$$V_{Sd} \le V_{Rd3} \qquad (3\text{-}5)$$

In which the shear resistance V_{Rd3} is defined as:

$$V_{Rd3} = V_{cd} + V_{wd} \qquad (3\text{-}6)$$

Where V_{cd} — The contribution of the concrete, with a distinction made for the critical region with normal tensile or compressive forces;

    V_{wd} — The contribution of the reinforcement.

As the diagonal tension failure is affected by both the horizontal and vertical reinforcement, acting in a simplified truss model in equilibrium with the concrete providing the diagonal compressive strut elements, the web reinforcing bars together with the concrete should satisfy the following conditions that differentiate on the basis of the shear span ratio of the wall, α_s.

$$\alpha_s = M_{sd} \Big/ V_{sd} l_w \qquad (3\text{-}7)$$

Where M_{Sd} — The design bending moment at the base of the wall;

    V_{sd} — The design shear force;

    l_w — The length of the wall.

(1) For $\alpha_s \ge 2.0$, the wall can be designed as a column.

(2) For $2.0 > \alpha_s > 1.3$, horizontal web reinforcing bars (fully anchored to the wall boundary elements) should satisfy the following conditions:

$$V_{sd} \le \rho_h \cdot f_{yd,h} \cdot b_{wo} \cdot z + V_{cd} \qquad (3\text{-}8)$$

Where ρ_h — The reinforcement ratio of the horizontal web bars ($\rho_h = \dfrac{A_h}{b_{wo} \cdot s_h}$);

A_h — Cross section area of horizontal web reinforcement in a wall;

s_h — Spacing of horizontal web reinforcement;

$f_{yd,h}$ — The design yield strength of the horizontal web reinforcement;

V_{cd} — The shear resistance due to mechanisms others than axial resistance of the reinforcement and concrete-to-concrete friction.

Vertical web reinforcement (properly anchored and spliced along the height of the wall) should satisfy the following conditions:

$$V_{sd} \le \rho_V \cdot f_{yd,V} \cdot b_{wo} \cdot z + V_{cd} + \min N_{Sd} \tag{3-9}$$

Where ρ_V — The reinforcement ratio of the vertical web bars ($\rho_V = \dfrac{A_V}{b_{w0} \cdot s_V}$);

A_V — Cross section area of vertical web reinforcement in a wall;

s_V — Spacing of vertical web reinforcement;

$f_{yd,V}$ — The design value of the yield strength of the vertical web reinforcement;

N_{Sd} — The compressive force, taken positive.

(3) For $\alpha_s \le 1.3$, the following expression should be satisfied:

$$V_{sd} \le \left[\rho_h(\alpha_s - 0.3) f_{yd,h} + \rho_V(1.3 - \alpha_s) f_{yd,V} \right] b_{wo} z + V_{cd} \tag{3-10}$$

Where $\rho_V f_{yd,V} / \rho_h f_{yd,h} \le 1.0$;

For $\alpha_s < 0.3$, α_s is normally taken as 0.3.

For all the above expressions, the term V_{cd} can be calculated as follows:
In case of axial tension in the critical region V_{cd} is equal to zero; And in the zone outside of the critical region,

$$V_{cd} = \left[C_{Rd,c} k (100 \rho_1 f_{ck})^{1/3} + k_1 \sigma_{cp} \right] b_w d \tag{3-11}$$

In case of axial compression in the critical region:

$$V_{cd} = \tau_{Rd} \cdot (1.2 + 40\rho) \cdot b_{wo} \cdot z \tag{3-12}$$

Where τ_{Rd} — The basic design shear strength as given in Table 3-1;

$$\tau_{Rd} = 0.035 f_{ck}^{2/3} \tag{3-13}$$

f_{ck} — Concrete grades;

ρ — The reinforcement ratio in the tension zone ($\rho = \dfrac{A_s}{b_{wo} \cdot z}$).

And in the zone outside of the critical region, V_{cd} can be calculated according to Eq.(3-11).

Table 3-1 Values of τ_{Rd} (N/mm^2) for different concrete grades

f_{ck}	12	16	20	25	30	35	40	45	50
τ_{Rd}	0.18	0.22	0.26	0.30	0.34	0.37	0.41	0.44	0.48

As a minimal measure against lateral instability, the thickness b_{wo} of the web should not be less than stipulated in the following:

$$b_{wo} = \min\{150mm; q \cdot l_w/60; h_s/20\} \qquad (3\text{-}14)$$

The web reinforcement should form two identical orthogonal grids of bars with the same bond characteristics. The minimum amount of reinforcement in both directions, to prevent premature web shear cracking of the walls, should not be less than $\rho_{h,\min} = \rho_{V,\min} = 0.002$.

3.2.3 Design of specimens according to EC 8

The lightweight reinforced concrete shear wall specimen LW-1, LW-2, LW-3 and LW-4 have been designed based on the procedures described hereinbefore. For the preliminary design, a 100 mm thick wall panel with a 250 mm square edge element has been selected. The following material properties have been used for the calculation:

For LW-1, the design shear force V_{sd} for the wall is V_{Sd} = 440 kN. Characteristics strength of lightweight concrete is f_c' = 30 MPa. Yield strength of reinforcement is f_y = 400 N/mm^2.

Checking the diagonal compression failure of the web, the shear resistance is calculated from Eq.(3-3) and Eq.(3-4) for both inside and outside of the critical region as 448.8 kN (inside) and 561 kN (outside), respectively. Both values satisfy the inequality in Eq.(3-2).

For checking the diagonal tension failure of the web, considering the design shear force of 440 kN and the material and dimensional parameters $f_{yd,h} = f_{yd,V}$ = 400 N/mm^2, b_{wo} = 0.1 m, $z = 0.8 l_w = 0.8 \times 1.5 = 1.2$ m, α_s =1.43, $\rho_v f_{yd,v}/\rho_h f_{yd,h} = 0.75$ and τ_{Rd} = 0.34 N/mm^2, the reinforcement ratios were found to be ρ_h = 0.78 % and ρ_V = 0.58 % respectively.

For LW-2, the design shear force V_{sd} for the wall is $V_{Sd} = 433.2$ kN. Characteristics strength of lightweight concrete is $f'_c = 30$ MPa. Yield strength of reinforcement is $f_y = 400$ N/mm^2.

Checking the diagonal compression failure of the web, the shear resistance is calculated for both inside and outside of the critical region as 833.04 kN (inside) and 945.24 kN (outside), respectively. Both values satisfy the inequality in Eq.(3-2).

For checking the diagonal tension failure of the web, considering the design shear force of 433.2 kN and the material and dimensional parameters $f_{yd} = 400$ N/mm^2, $b_{wo} = 0.1$ m, $z = 0.8l_w = 0.8 \times 1.5 = 1.2$ m, $\alpha_s = 1.43$ and $\tau_{Rd} = 0.34$ N/mm^2, the diagonal reinforcement ratios in each 45° direction was found to be $\rho = 0.57$ %.

For LW-3, the design shear force V_{sd} for the wall is $V_{Sd} = 558.8$ kN. Characteristics strength of lightweight concrete is $f'_c = 30$ MPa. Yield strength of reinforcement is $f_y = 400$ N/mm^2.

Checking the diagonal compression failure of the web, the shear resistance is calculated for both inside and outside of the critical region as 957.8 kN (inside) and 1070 kN (outside), respectively. Both values satisfy the inequality in Eq.(3-2).

For checking the diagonal tension failure of the web, considering the design shear force of 558.8 kN and the material and dimensional parameters $f_{yd} = 400$ N/mm^2, $b_{wo} = 0.1$ m, $z = 0.8l_w = 0.8 \times 1.5 = 1.2$ m, $\alpha_s = 1.43$ and $\tau_{Rd} = 0.34$ N/mm^2, the diagonal reinforcement ratios in each 45° direction was found to be $\rho = 0.75$ %.

For LW-4, the design shear force V_{sd} for the wall is $V_{Sd} = 530$ kN. Characteristics strength of lightweight concrete is $f'_c = 30$ MPa. Yield strength of reinforcement is $f_y = 400$ N/mm^2.

Checking the diagonal compression failure of the web, the shear resistance is calculated for both inside and outside of the critical region as 910 kN (inside) and 1023 kN (outside), respectively. Both values satisfy the inequality in Eq.(3-2).

For checking the diagonal tension failure of the web, considering the design shear force of 440 kN and the material and dimensional parameters $f_{yd,h} = f_{yd,V} = 400$ N/mm^2, $b_{wo} = 0.1$ m, $z = 0.8l_w = 0.8 \times 1.5 = 1.2$ m, $\alpha_s = 1.43$, $\rho_v f_{yd,v} / \rho_h f_{yd,h} = 0.75$ and $\tau_{Rd} = 0.34$ N/mm^2, the conventional reinforcement ratios were found to be $\rho_h = 0.87$ % and $\rho_V = 0.65$ % respectively.

3.3 Design procedure according to ACI 318-05

The building code requirements for reinforced concrete, ACI 318-05, is the common building code in the US and covers the design requirements to the structural safety of buildings. The earthquake resistant design requirements of this code are aimed primarily to safeguard against major structural failures and loss of life. The minimum seismic design forces stipulated by this code are determined in accordance with a seismic-equivalent static lateral force procedure. A short summary of the design analysis is given in the following section.

3.3.1 Determination of nominal shear strength for structural concrete wall

The nominal shear strength (v_n) for structural walls shall not exceed:

$$v_n = 2.1 \sqrt{f_c'} \tag{3-15}$$

Where f_c' — The specified compressive strength of concrete, ksc.

Shear strength of concrete (V_c) shall be computed by Eq.(3-16) and Eq.(3-17), where V_c shall be the lesser of Eq.(3-16) and Eq.(3-17).

$$V_c = 0.875\sqrt{f_c'}hd + \frac{N_u d}{4l_w} \tag{3-16}$$

or

$$V_c = \left[0.159\sqrt{f_c'} + \frac{l_w\left(0.331\sqrt{f_c'} + 0.2\dfrac{N_u}{l_w h}\right)}{\dfrac{M_u}{V_u} - \dfrac{l_w}{2}} \right] \tag{3-17}$$

Where $\dfrac{M_u}{V_u} - \dfrac{l_w}{2} \geq 0$;

V_u — Factored shear force at section, kg;

M_u — Factored moment at section, cm·kg;

N_u — Factored axial load normal to cross section occurring simultaneously with V_u; taken as positive for compression, negative for tension, and include effects of tension due to creep and shrinkage, kg;

h — The thickness of lightweight concrete wall specimen, cm;

d — The distance from extreme compression to centroid of longitudinal tension reinforcement, but shall be not less than $0.8l_w$, cm;

l_w — The width of lightweight concrete wall specimen, cm.

Shear strength (V_s) of steel shall be computed by Eq.(3-18).

$$V_s = \frac{A_v f_y d}{s} \qquad (3\text{-}18)$$

Where A_v — Area of shear reinforcement within a distance s , or area of shear reinforcement perpendicular to flexural tension reinforcement within a distance s for deep flexural members, cm^2;

f_y — Specified yield strength of reinforcement, ksc;

s — Spacing of transverse reinforcement measured along the longitudinal axis of the structural member, cm.

The shear strength (V_n) for walls can be calculated as

$$V_n = V_c + V_s \qquad (3\text{-}19)$$

Where V_c — Shear strength provided by concrete, kg;

V_s — Shear strength provided by steel, kg.

3.3.2 Determination of shear reinforcement ratio

Ratio of horizontal shear reinforcement area to gross concrete area of vertical section shall not be less than 0.0025.

The minimum vertical reinforcement ratio ρ_n is a function of h_w / l_w and of the horizontal reinforcement as shown below:

$$\rho_n = 0.0025 + 0.5 \left[2.5 - \frac{h_w}{l_w} \right] \left[\rho_h - 0.0025 \right] \geq 0.0025 \qquad (3\text{-}20)$$

Where ρ_h — Ratio of area of distributed reinforcement parallel to the plane of A_{cv} to gross concrete area perpendicular to that reinforcement;

A_{cv} — Gross area of concrete section bounded by web thickness and length of section in the direction of shear force considered, cm^2;

h_w — The distance between the base of the lightweight concrete wall and the lateral load, cm;

l_w — The width of lightweight concrete wall specimen, cm.

Also, the vertical shear reinforcement ratio need not exceed the required horizontal shear reinforcement ratio.

3.3.3 Amount of longitudinal reinforcement for flexural moment in boundary element

The wall suffered not only the shear strength but also the flexural strength. Therefore, the design has been done to assure that its flexural strength is equal to its shear strength. So the flexural moment is defined as following expressions:

$$
\begin{aligned}
M_u &= V_u h_w \\
&= \phi_{shear} V_n h_w \\
&= \phi_{shear} \left(2.1\sqrt{f_c'} hd \right) h_w
\end{aligned}
\tag{3-21}
$$

Where V_u — Factored shear force at section, kg;

ϕ_{shear} — Strength reduction factor for shear.

3.3.4 Amount of shear reinforcement in diagonal direction

The calculation method used here is the same as calculating inclined stirrups in reinforced concrete beams. Therefore amount of shear reinforcement can be calculated as following:

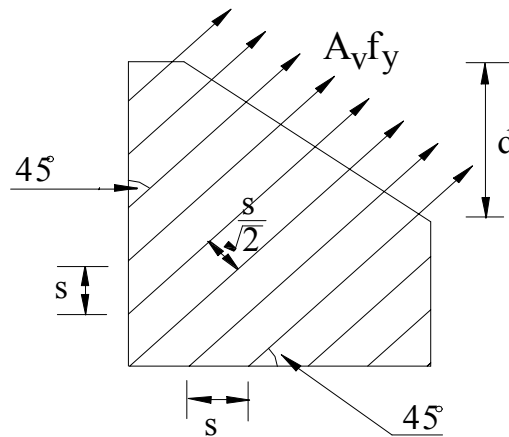

Fig.3-2 Reinforcement in diagonal direction

From Fig.3-2, V_s (shear strength provided by diagonal shear reinforcement) was got by

$$
V_s = A_v f_y (\sin 45 + \cos 45)\frac{d}{s}
\tag{3-22}
$$

Since in Eq.(3-19),

$$
V_n = V_c + V_s
$$

then

$$V_n - V_c = V_s = A_v f_y (\sin 45 + \cos 45) \frac{d}{s} \tag{3-23}$$

3.3.5 Design of four lightweight reinforced concrete shear wall specimens

Let $f_c' = 300$ ksc, (specified compressive strength of lightweight concrete);

$f_y = 4000$ ksc, (specified yield strength of reinforcement);

$\phi_{flex} = 1.0$, (strength reduction factor for flexure);

$\phi_{shear} = 1.0$, (strength reduction factor for shear);

$d = 0.8\,l_w$, (distance from extreme compression to centroid of longitudinal tension reinforcement, but shall be not less than 0.8 l_w)

$l_w = 150$ cm, (the width of lightweight concrete wall specimen);

$h_w = 210$ cm, (the distance between the base of the lightweight concrete wall and the lateral load);

$h = 10$ cm, (the thickness of lightweight concrete wall specimen).

The reinforcement in specimen LW-1 was selected that the nominal shear and flexural strength of the wall were nearly equal, and was designed according to the American Concrete Institute Building Code (ACI 318-05). The design nominal shear strength in seismic zone (v_n) at any horizontal section shall be not greater than $2.1\sqrt{f_c'}$.

Specimen LW-1 (Fig. 4-2(a))

1. Shear strength provided by concrete, V_c

Critical section for shear strength calculation shall locate a lesser distance of $l_w/2$ or $h_w/2$ above the base, so that $l_w/2$ (75 cm) was used here.

$$\begin{aligned}
V_{c1} &= 0.875\sqrt{f_c'}\,hd + \frac{N_u d}{4l_w} \\
&= 0.875\sqrt{300} \times 10 \times 120 + 0 \\
&= 18.20 \text{ tons}
\end{aligned}$$

and

$$V_{c2} = \left[0.159\sqrt{f_c'} + \frac{l_w\left(0.331\sqrt{f_c'} + 0.2\dfrac{N_u}{l_w h}\right)}{\dfrac{M_u}{V_u} - \dfrac{l_w}{2}} \right] hd$$

$$= \left[0.159\sqrt{300} + \frac{150(0.331\sqrt{300}+0)}{(210-75)\dfrac{V_u}{V_u}-75} \right] \times 10 \times 120$$

$$= 20.50 \text{ tons}$$

Therefore, $V_c = 18.20$ tons

and $v_c = \dfrac{18.20 \times 1000}{10 \times 120}$

$$= 15.16 \text{ ksc} \cong 0.875\sqrt{f_c'}$$

2. Shear strength provided by reinforcement, V_s

Since $V_n = V_c + V_s$

then $V_s = V_n - V_c = (2.1 - 0.875)\sqrt{f_c'}hd = 1.225\sqrt{f_c'}hd$

3. Area of horizontal shear reinforcement, A_{vh}

$$\frac{A_{vh}}{s} = \frac{V_s}{f_y d}$$

$$= \frac{1.225\sqrt{300} \times 10 \times 120}{4000 \times 120}$$

$$= 0.053 \text{ cm}^2/\text{cm} = 5.30 \text{ cm}^2/\text{m}$$

Therefore, HRB335Φ10@0.15 was used to have the rate of horizontal shear reinforcement $\rho_h = 0.523$ %.

4. Area of vertical shear reinforcement, A_{vv}

Since $\rho_n = 0.0025 + 0.5\left[2.5 - \dfrac{h_w}{l_w}\right]\left[\rho_h - 0.0025\right]$

$$= 0.0025 + 0.5\left[2.5 - \frac{210}{150}\right]\left[0.00523 - 0.0025\right]$$

$$= 0.0040$$

then $\dfrac{A_{vv}}{s} = \rho_n h$

$$= 0.0040 \times 10$$

$$= 0.04 \text{ cm}^2/\text{cm} = 4 \text{ cm}^2/\text{m}$$

Therefore, HRB335Φ10@0.20 was used to have the rate of vertical shear reinforcement $\rho_n = 0.393$ %.

5. Amount of longitudinal reinforcement for flexural moment in boundary element
The wall suffered not only the shear forces but also the flexural moment, so the flexural moment is

$$M_u = V_u h_w$$
$$= \phi_{shear} V_n h_w$$
$$= \phi_{shear} \left(2.1\sqrt{f_c'}hd\right)h_w$$
$$= 1.0 \times 2.1\sqrt{300} \times 10 \times 120 \times 210 / 100$$
$$= 91660 \text{ kg·m}$$

$$M_n = \frac{M_u}{\phi_{flex.}}$$
$$= \frac{91660}{1.0} = 91660 \text{ kg·m}$$

6HRB335Φ16 + 2HRB335Φ12 were used as longitudinal reinforcement in the boundary element. Strain compatibility method was used to find the flexural moment in specimen LW-1, as shown in Fig.3-3.
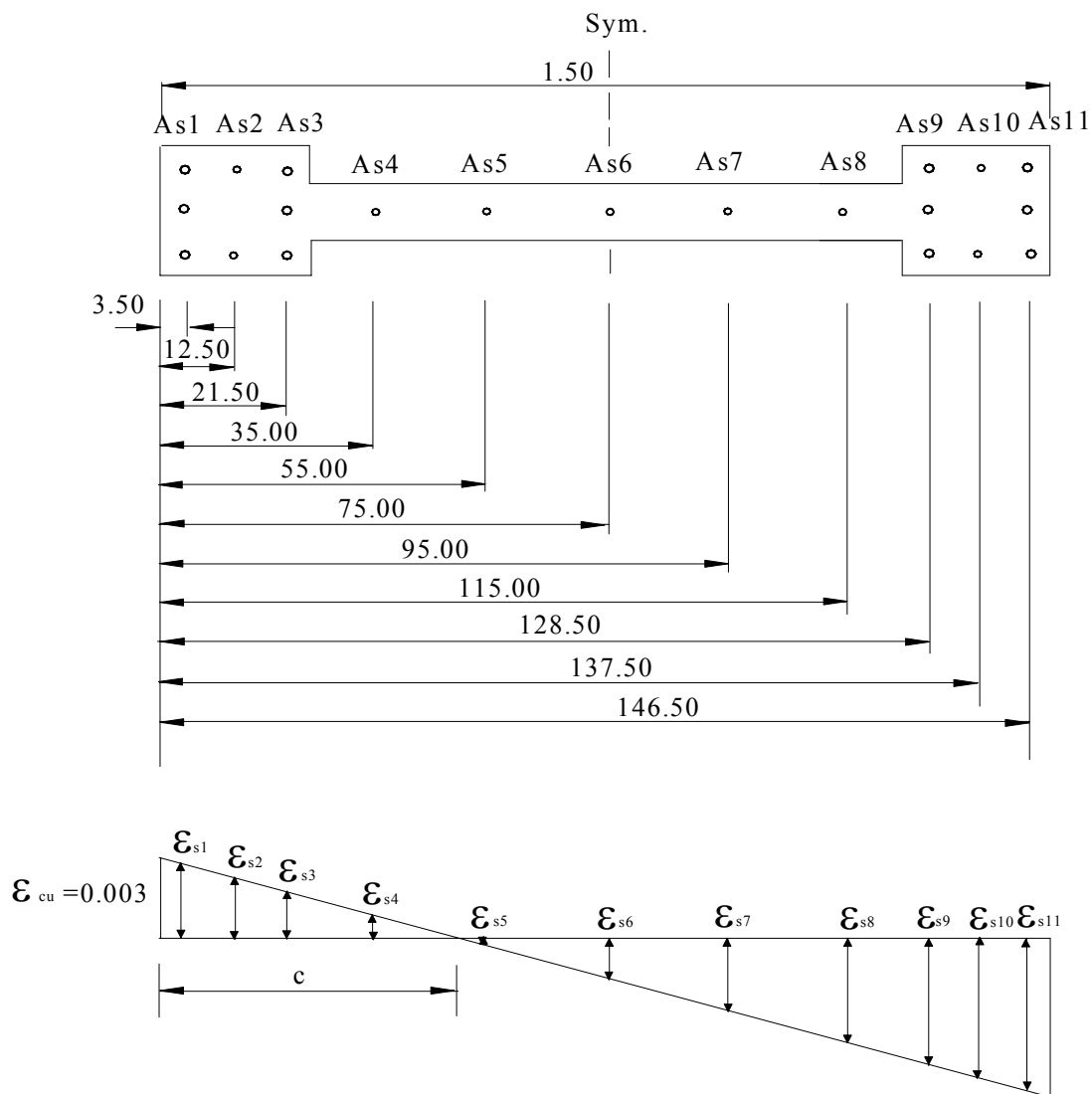
Note: ε_{cu} = Compressive strain at crushing of concrete.

Fig.3-3 Strain distribution of cross section area in specimen LW-1

β_1 is the ratio of the average compressive stress to the maximum stress of concrete. For concrete with strengths f_c' up to and including 280 ksc, $\beta_1 = 0.85$; for concrete with f_c' between 280 and 560 ksc, $\beta_1 = 1.05 - 0.05 \cdot \dfrac{f_c'}{1000}$; for concrete with f_c' greater than 560 ksc, $\beta_1 = 0.65$. So that, for specimen LW-1, $f_c' = 300$ ksc, $\beta_1 = 0.836$.

Therefore, $a = \beta_1 c = 0.836c$, where c is the distance from the extreme compression edge to neutral axis of cross section area, cm.

1st Trial: Let the c=13.45 cm, then obtain a=11.24 cm.

Layer	y(cm)	ε_s	f_s (ksc)	A_s(cm^2)	F_s(kg)	C_c(kg)
Comp. Zone	-	-	-	-	-	71655.00
A_{s1}	3.5	0.00196	3745.0	6.03	22582.35	-
A_{s2}	12.5	0.00021	428.4	2.26	968.18	-
A_{s3}	21.5	-0.00180	-3672.0	6.03	-22142.16	-
A_{s4}	35.0	-0.00196	-4000.0	0.785	-3140.00	-
A_{s5}	55.0	-0.00196	-4000.0	0.785	-3140.00	-
A_{s6}	75.0	-0.00196	-4000.0	0.785	-3140.00	-
A_{s7}	95.0	-0.00196	-4000.0	0.785	-3140.00	-
A_{s8}	115.0	-0.00196	-4000.0	0.785	-3140.00	-
A_{s9}	128.0	-0.00196	-4000.0	6.03	-24120.00	-
A_{s10}	137.5	-0.00196	-4000.0	2.26	-9040.00	-
A_{s11}	146.5	-0.00196	-4000.0	6.03	-24120.00	-
	Σ				-71571.63	71655.00

Note: 1) ε_s, f_s and F_s are positive in compression.

2) $-\varepsilon_y \le \varepsilon_{si} \le \varepsilon_y$ with yielding strength of $\varepsilon_y = \dfrac{4000}{2.04 \times 10^6} = 0.00196$. For a bar located at distance y below the extreme compressive edge, the strain is $\varepsilon_s = 0.003 - 0.003\dfrac{y}{c}$.

3) If $y < a$, this layer of steel is assumed to be stressed in compression. Then f_s =4000-0.85 f_c'

Where F_s — Calculated force in reinforcement, $F_s = f_s \cdot A_s$, kg;

f_s — Calculated stress in reinforcement, ksc;

A_s — Area of longitudinal tension reinforcement in wall segment, cm^2;

C_c — The compressive force resisted by concrete, $C_c = 0.85 \cdot f_c' \cdot \beta_1 \cdot c \cdot b$, kg;

c — Distance form the extreme compression specimen (load to perform) to neutral axis of cross section area, cm;

b — Width of compression face of member, effective compressive flange width, cm;

Therefore, $\sum F_s + \sum C_c = 83.37$ kg. <u>O.K.</u>

So that $P = \sum F_s + \sum C_c$. For a wall without vertical load, P is equal to zero. If the calculated value of P is not equal to zero, the strain distribution will be adjusted and first step will be repeated until P is as close to zero as desired. The imbalance should not exceed 0.1% to 0.5% of C_c [Jam92].

Flexural strength of specimen was calculated by

M_n = 71655(75-11.24/2)+22582.35(75-3.5)+968.18(75-12.5)-22142.16(75-21.5)-3140(75-35)-3140(75-55)-3140(75-75)+3140(95-75)+3140(115-75)+24120(128.5-75)+9040(137.5-75)+24120(146.5-75)

= 9041967.62 kg-cm.

M_n = 90.42 t-m. approach to 91.66 t-m. <u>O.K.</u>

Then,

V_n = 91.66/2.10

$\cong$ 44 tons

Hence, flexural strength and shear strength of specimen 1 were 44 tons ($\cong$ 440 kN).

Specimen LW-2 (Fig. 4-2(b))

1. Amount of shear reinforcement in diagonal direction

From Fig.3-2, V_s (shear strength provided by diagonal shear reinforcement) was got by

$$V_s = A_v f_y (\sin 45 + \cos 45) \frac{d}{s}$$

Since

$$V_n = V_c + V_s$$

then

$$V_n - V_c = V_s = A_v f_y (\sin 45 + \cos 45) \frac{d}{s}$$

where $V_n = 44$ tons and $V_c = 18.20$ tons obtained by specimen LW-1.

Therefore, $(44-18.20) \times 1000 = 0.785 \times 4000 \times \sqrt{2} \times \dfrac{120}{s}$

s = 20.65 cm.

The spacing of reinforcement in diagonal direction is $\dfrac{s}{\sqrt{2}} = \dfrac{20.65}{\sqrt{2}} = 14.60$ cm. HRB335Φ10@0.15 was used for reinforcement in diagonal direction.

2. Shear strength of specimen
Shear strength provided by reinforcement

$$V_s = A_v f_y (\sin 45 + \cos 45) \frac{d}{s}$$

$$= 0.785 \times 4000 \times \sqrt{2} \times \frac{120}{15\sqrt{2}}$$

$$= 25.12 \text{ tons}$$

Then

$$V_n = V_c + V_s$$
$$= 18.20 + 25.12$$
$$= 43.32 \text{ tons}$$

Shear strength of specimen LW-2 was 43.32 tons ($\cong$ 433.2 kN).

3. Flexural strength of specimen
Due to this specimen having only the web reinforcement in diagonal direction, the longitudinal reinforcement in boundary element sustains the flexural moment. Strain compatibility method was used to find the flexural moment in specimen LW-2, as shown in Fig.3-4.

1st Trial: Let c=11.30 cm, then a= 9.45 cm.

Layer	y(cm)	ε_s	f_s (ksc)	A_s(cm²)	F_s(kg)	C_c(kg)
Comp. Zone	-	-	-	-	-	60243.75
A_{s1}	3.5	0.00196	3745.0	6.03	22582.35	-
A_{s2}	12.5	0.00032	-652.8	2.26	-1475.33	-
A_{s3}	21.5	-0.00196	-4000.0	6.03	-24120.00	-
A_{s4}	128.5	-0.00196	-4000.0	6.03	-24120.00	-
A_{s5}	137.5	-0.00196	-4000.0	2.26	-9040.00	-
A_{s6}	146.5	-0.00196	-4000.0	6.03	-24120.00	-
Σ					-60292.98	60243.75

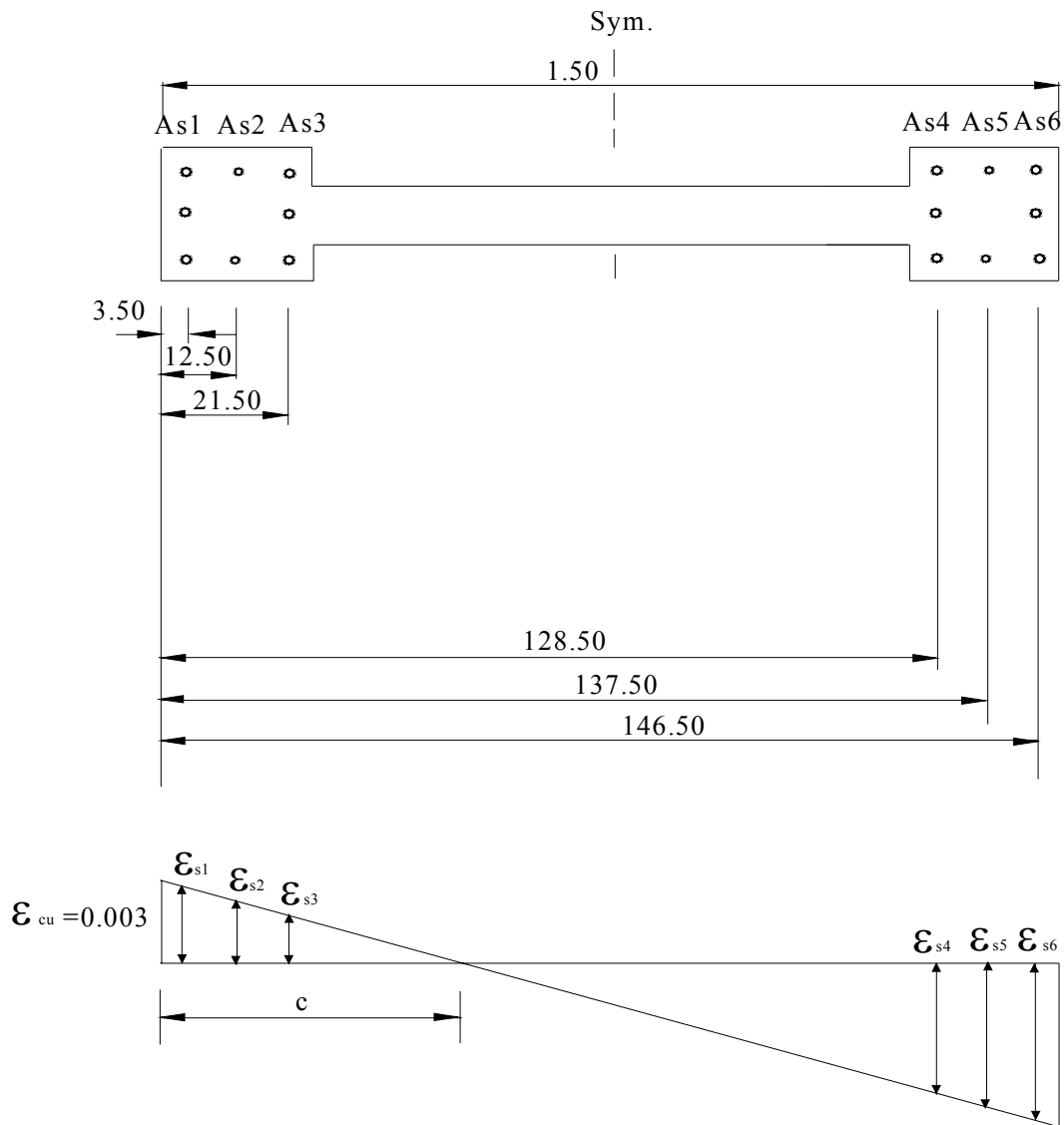Therefore, $\Sigma F_s + \Sigma C_c$ = -49.23 kg.   O.K.

Flexural strength of specimen was calculated by

$$M_n = 60243.75(75-9.45/2)+22582.35(75-3.5)-1475.33(75-12.5)-24120(75-$$
$$21.5) +24120(128.5-75)+9040(137.5-75)+24120(146.5-75)$$
$$= 8045639.43 \text{ kg-cm.}$$
$$M_n = 80.46 \text{ t-m.}$$

Then,

$$V_n = 80.46/2.10$$
$$\cong 38 \text{ tons}$$

Hence, flexural strength of specimen LW-2 was 38 tons.

Note: ε_{cu} = Compressive strain at crushing of concrete.

Fig.3-4 The strain distribution of cross section area in specimen LW-2

Specimen LW-3 (Fig. 4-2(c))

This specimen was designed similar to specimen LW-2 while its shear reinforcement ratio was more than that of specimen LW-2. HRB335Φ10@0.10 was used for web reinforcement in diagonal direction in specimen LW-3.

1. Shear strength provided by web reinforcement, V_s

$$V_s = 0.785 \times 4000 \times \sqrt{2} \times \frac{120}{10\sqrt{2}}$$
$$= 37.68 \text{ tons}$$

2. Shear strength (V_n) of specimen

$$V_n = V_c + V_s$$
$$= 18.20 + 37.68$$
$$= 55.88 \text{ tons}$$

So that, shear strength of specimen LW-3 was 55.88 tons ($\cong$ 558.8 kN).

3. Flexural strength of specimen

Due to this specimen having only the web reinforcement in diagonal direction, the longitudinal reinforcement in boundary element sustains the flexural moment. So that, flexural strength of specimen LW-3 was 38 tons, the same as that of specimen LW-2.

Specimen LW-4 (Fig. 4-2(d))

In the web of specimen LW-4, there are not only the conventional reinforcements, which are the same as those in specimen LW-1, but also additional inclined steels, which intersect each other at the midpoint of the base of the wall. The conventional reinforcements (HRB335Φ10@0.15 in horizontal direction and HRB335Φ10@0.20 in vertical direction) provide the same resistance to shear force and flexural moment as in specimen LW-1. The additional bidiagonal steels form a truss to resist shear force, as shown in Fig.3-5.
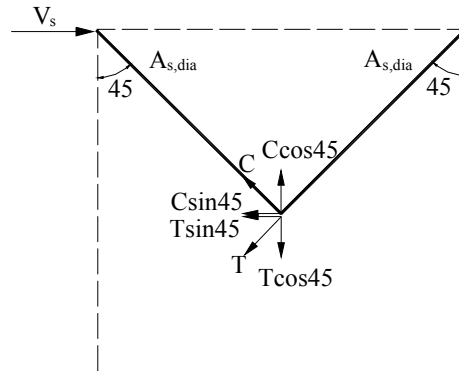

Fig.3-5 Truss model of diagonal steels

1. Amount of diagonal steels

From Fig.3-5, it can be gained that

$$\sum F_y = 0: \ T = C = A_s f_y$$
$$\sum F_x = 0: \ V_{s,dia} = 2T \sin 45° = 2A_s f_y \sin 45°$$

Since $V_n = V_c + V_s = V_c + V_{s,dia} + V_{s,nor}$

Where $V_{s,nor}$ — Shear strength provided by conventional web reinforcement;

$V_{s,dia}$ — Shear strength provided by diagonal web reinforcement.

For specimen LW-3, $V_n = 55.88 \text{ tons}$

For specimen LW-1, $V_c + V_{s,nor} = 44 \text{ tons}$

Then, in order to get the same shear strength as specimen LW-3, the nominal shear strength provided by diagonal steel in specimen LW-4 should be calculated that

$$V_{s,dia} = V_n - V_c - V_{s,nor} = 55.88 - 44 = 11.88 \text{ tons}$$

So that,
$$11.88 = 2A_s f_y \sin 45° / 1000$$
$$A_s = 2.1 \text{ cm}^2$$

2HRB335Φ10 ($A_s = 1.58 \text{ cm}^2$) was used in 45 degree direction.

2. Shear strength (V_n) of specimen

$$V_{s,dia} = 2 \times 1.58 \times 4000 \times \sin 45° / 1000 = 9 \text{ tons}$$
$$V_n = V_c + V_{s,nor} + V_{s,dia} = 44 + 9 = 53 \text{ tons} \cong 530 \text{ kN}$$

3. Flexural strength of specimen
Because the bidiagonal steels don't sustain the flexural moment, only the conventional reinforcement and the longitudinal reinforcement in boundary element sustain the flexural moment in specimen LW-4. Hence, flexural strength of specimen LW-4 was 44 tons, the same as that of specimen LW-1.

3.4 Comparison of EC 8 and ACI 318-05

For shear design of reinforced concrete shear walls, ACI 318-05 and EC 8 present some notable differences. The ACI Code recognizes the increased shear strength of walls with low shear aspect ratio by specifying a concrete contribution of $0.25\sqrt{f_c'}$ MPa for $h_w/l_w \leq 1.5$ (h_w is the height of the wall and l_w is the width of the wall), reducing to $0.17\sqrt{f_c'}$ MPa for $h_w/l_w \geq 2.0$. In contrast to this, the EC 8 does not provide for increased concrete contribution in low slenderness walls. However, it differentiates the design equation for shear carried by web reinforcement on the basis of the shear span ratio α_s, as Eq.(3-1) through (3-14). Eq.(3-10) implies that for α_s=1.3, only horizontal reinforcement is contributing to shear strength, whereas for $\alpha_s \leq 0.3$, only the vertical reinforcement is resisting shear; both type of web reinforcement are considered effective for $0.3 < \alpha_s < 1.3$. The ACI Code simply requires that for aspect ratio $h_w/l_w < 2.0$, the vertical reinforcement ratio need not be greater than the horizontal ones. Another important difference between the ACI Code and EC8 concerns the possibility of sliding shear failure of squat walls, which is explicitly recognized in the EC 8, but is not explicitly accounted for in the ACI Code, which controls it directly by specifying an upper bound of $0.65\sqrt{f_c'}$ MPa at the nominal shear stress.

In design the wall reinforcement in accordance to both codes, the design according to EC 8 leads to a less economic design than in case of a design according to ACI 318-05. The EC 8 design is conservative, as compared to the ACI 318-05 design.

Chapter 4

Experimental Program

4.1 Introduction

In recent years, many attentions have been focus on the seismic behavior of lightweight concrete (LWC) shear walls. Y.H. Chai and John D. Anderson [Y.H.05] tested two full-scale precast lightweight concrete prototype panels for construction of low-rise modular school buildings. The test results, in particular with respect to the lateral strength, deformation capacity and hysteretic loops of the panels, were presented in the paper. Y. Z. Zhuang [Zhu00] discussed the mechanical properties of self-combusted gangue reinforced concrete shear walls based on the test results of six cantilever shear wall. The results showed that mechanical properties and failure modes of the walls were almost the same as of the normal concrete shear walls. But the former was greater than the later in the capability of energy dissipation. H. J. Tao et al. [Tao94] gave the discriminating formulas for balanced shear span ratio and the condition of dividing strength control zone. Based on the experiments of seven ash ceramsite concrete shear walls and one normal concrete shear wall, the calculation method for shear capacity of LWC shear wall was derived. L. Cavaleri et al. [Cav03] compared the cyclic behavior of three different kinds of reinforced wall panels which were made using lightweight pumice stone concrete, lightweight expanded clay concrete and normal concrete. The comparison showed the effectiveness of pumice as an aggregate in manufacturing concrete.

However, there are few studies on the seismic behavior of lightweight shale ceramsite concrete shear wall. Especially information on the influence of diagonal reinforcement on cyclic behavior of LWC shear walls is limited. A similar conclusion was drawn in recent research work on normal concrete shear walls, which demonstrated that, walls with diagonal web reinforcement displayed the ability to dissipate more energy at a given level of lateral deformation than walls with conventional web reinforcement [Cha01]. Diagonal web reinforcement is one approach to control structural damage reliably during earthquake. In view of the preceding, developing optimum reinforcement mode to effectively improve seismic properties of LWC shear walls are the current research points. So the measured cyclic

---

responses of reinforced ceramsite concrete structural walls with different web reinforcements are discussed in this thesis.
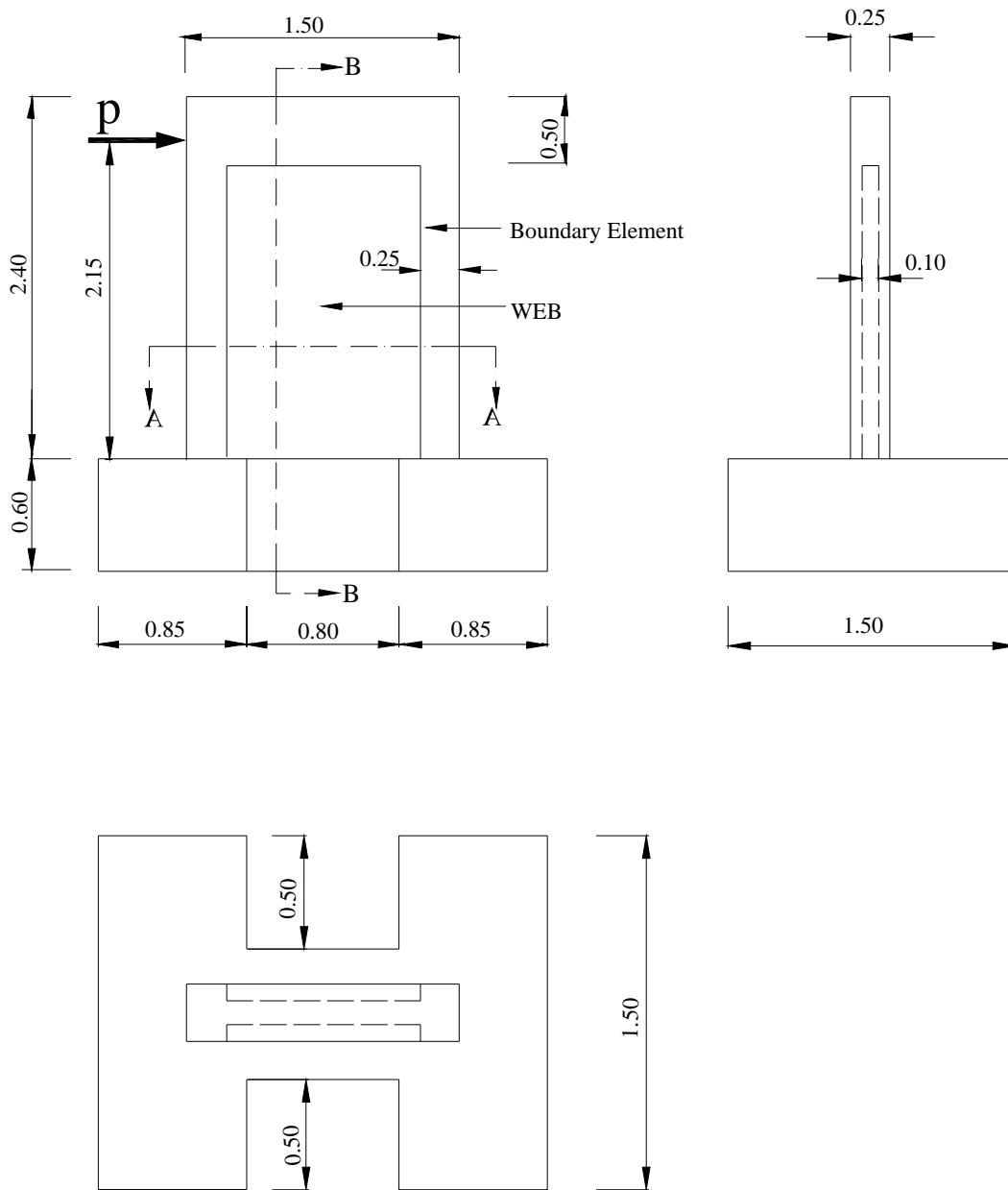
4.2 Test specimens

Four lightweight reinforced concrete shear wall specimens were constructed and tested to investigate the influence of diagonal web reinforcement on the hysteretic response of structural LWAC walls. One wall contained conventional horizontal and vertical web reinforcement, one wall contained not only conventional web reinforcement but also additional diagonal web reinforcement, and two walls contained inclined wed reinforcement.

The dimensions of the specimens are shown in Fig.4-1. All walls had a barbell-shaped cross section with a web thickness of 100 mm and 250x250 mm boundary elements. The overall length of the cross section was 1500 mm. Vertical and diagonal reinforcement was anchored in a 600 mm thick base girder that was bolted to the laboratory floor. A 250 mm wide by 500 mm deep beam was cast on top of the wall panel, and a hydraulic actuator was attached to the specimen at mid depth of the top beam. Lateral loads were applied 2150 mm above the base of the wall.

The specimens tested here address the behavior of reinforced lightweight concrete walls with low slenderness under reversed cyclic loading. Shear walls with low slenderness are common in low-rise construction, characterized by normalized moment M to shear V ratios $a_s=M/(Vl_w)<=1.5$, where l_w is the wall length, as is commonly referred to as shear-span ratio or shear ratio. Whereas the behaviors of properly designed walls with $a_s>=2$ is dominated by flexure and that of walls with $a_s<1$ is dominated by shear, shear span ratio around 1.5 typically results in the least predictable behavior, as either flexure or shear, or in fact, a mixed mode of failure may result under seismic loading [Pen97]. The shear-span ratio of four specimens is 1.43.

The primary experimental parameters were the amount and orientation of the web reinforcements. The longitudinal and transverse reinforcement in the boundary elements and the top beams were the same in all four specimens (shown in Fig.4-l (b.c)). A single layer of web reinforcement was used in all walls. Such a reinforcement arrangement, which is not usual in real walls where a double plane is generally adopted, is not effective for the concrete confinement. Nevertheless, it allows one to observe the mechanical behavior of the shear wall with different kinds of reinforcement. The study of the reinforcement confinement effect was ignored in presented test. The transverse reinforcements in the boundary elements were not intended to provide confinement of the concrete core. Only the web reinforcements of four specimens are shown in Fig.4-2. The reinforcement ratios of four specimens are shown in Table 4-1.
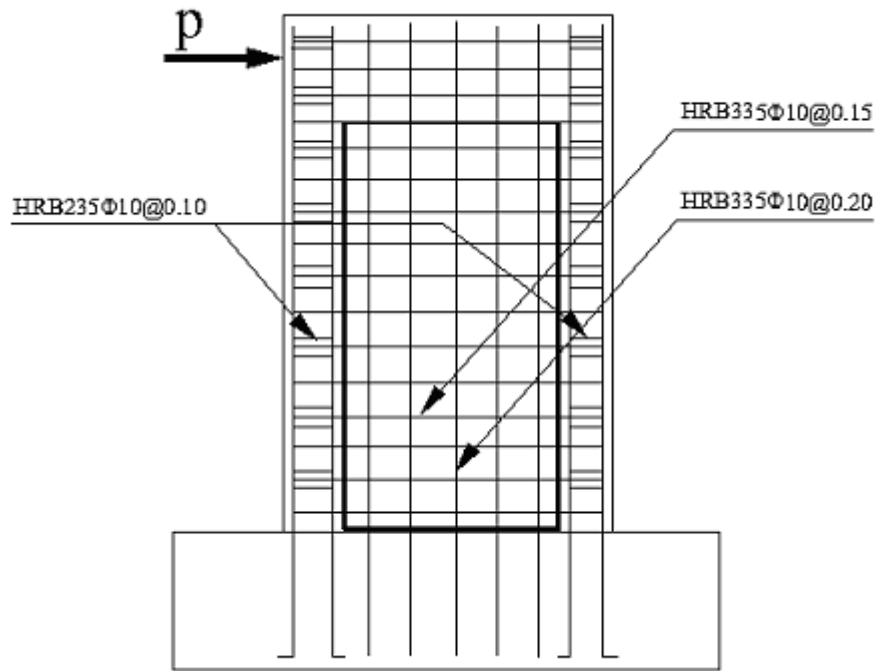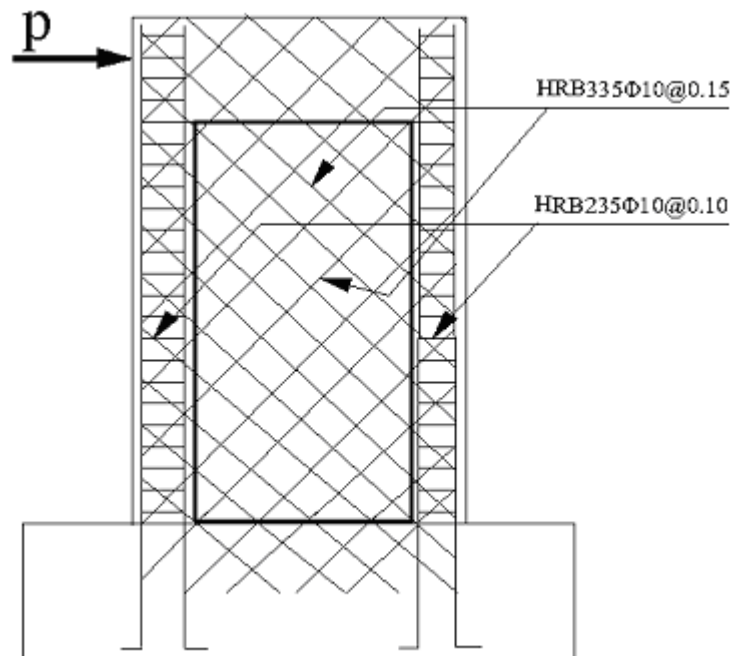
(a) Overview of test specimens
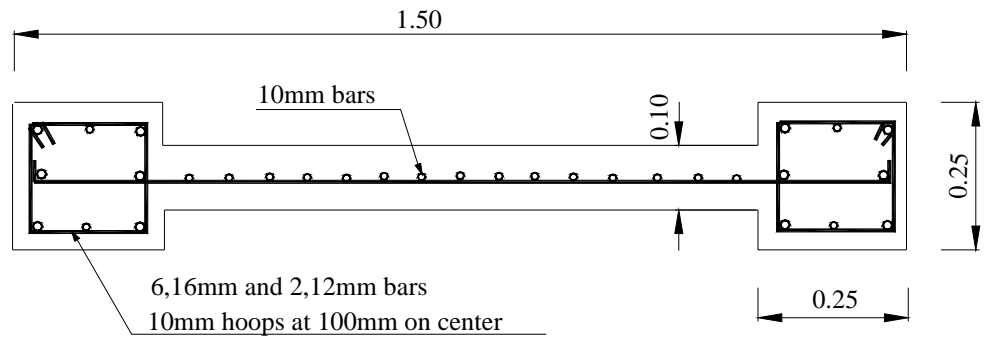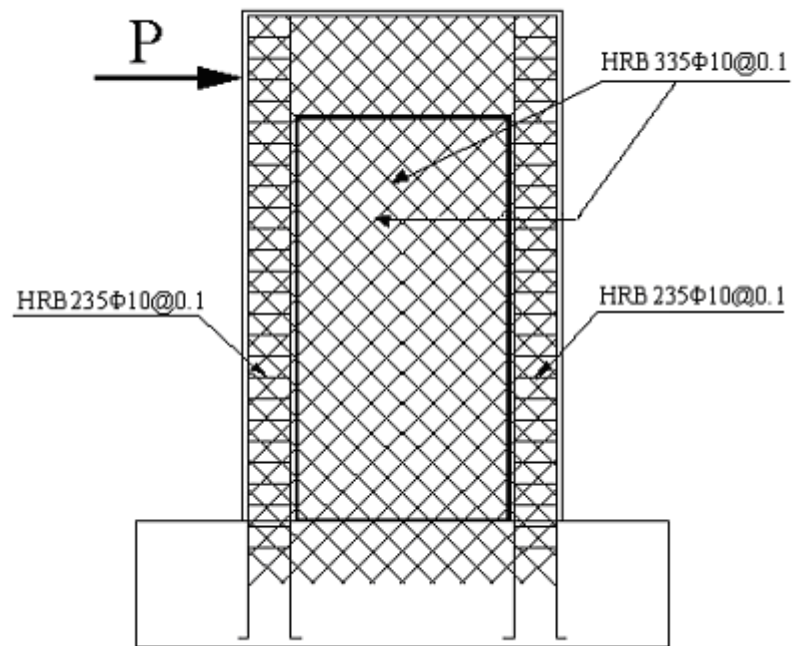
(b) Cross section A-A
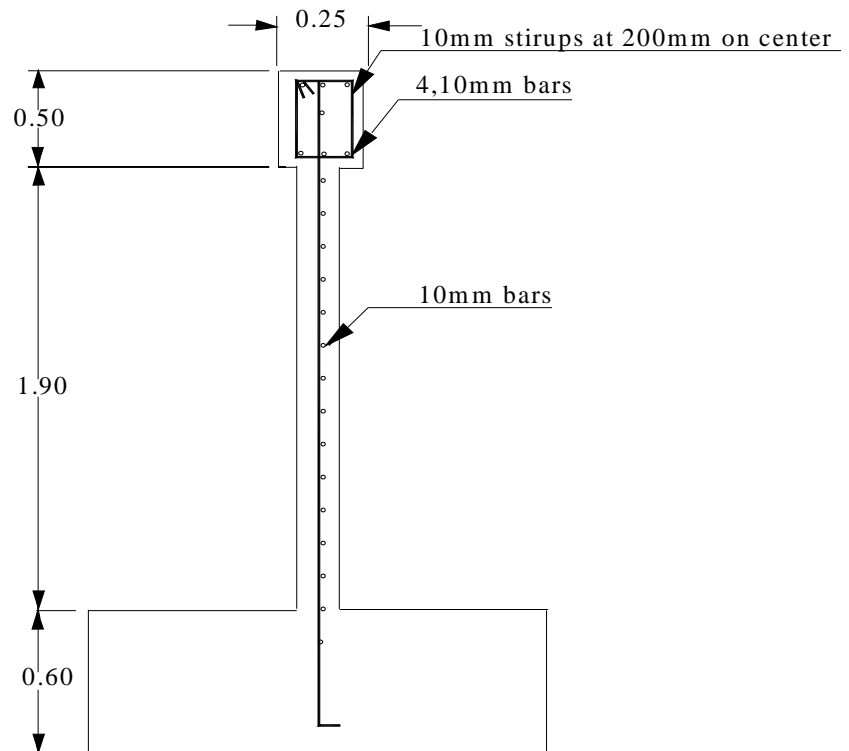
(c) Cross section B-B

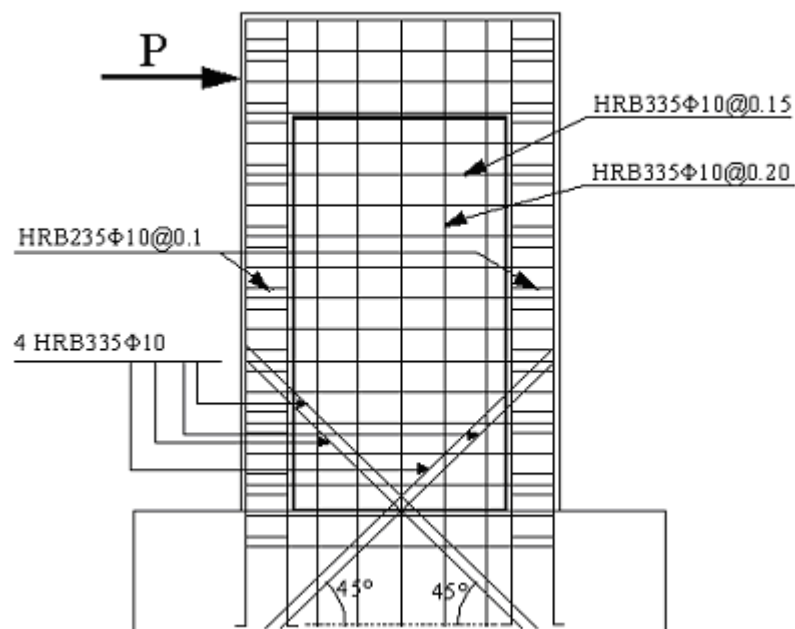**Fig.4-1 Dimensions of test specimens**

(a) Specimen LW-1

(b) Specimen LW-2

(c) Specimen LW-3

(d) Specimen LW-4

Fig.4-2 Arrangement of web reinforcements in four test specimens

Table 4-1 Reinforcement ratios of four specimens

		LW-1	LW-2	LW-3	LW-4
Horizontal web reinforcement	Spacing, mm	150	----	----	150
	Reinforcement ratio, %	0.52	----	----	0.52
Vertical web reinforcement	Spacing, mm	200	----	----	200
	Reinforcement ratio, %	0.39	----	----	0.39
Diagonal web reinforcement	Spacing, mm	----	150	100	50
	Reinforcement ratio, %	----	0.52	0.79	0.31
Longitudinal reinforcement in boundary elements	Area, mm^2	1430	1430	1430	1430
	Reinforcement ratio, %	2.29	2.29	2.29	2.29
Transverse reinforcement in boundary elements	Spacing, mm	100	100	100	100

The reinforcement in specimen LW-1 was selected such that the nominal shear and flexural strengths of the wall were nearly equal, based on the assumed material properties. Horizontal web reinforcement was spaced at 150 mm on center, and vertical web reinforcement was spaced at 200 mm on center.

The spacing of the web reinforcement in specimen LW-2 was the same as the spacing of the horizontal web reinforcement in specimen LW-1 (Table 4-1). The web reinforcement in specimens LW-2 was rotated 45 degrees with respect to the longitudinal axis of the wall. The nominal strengths of specimens LW-1 and LW-2 were essentially the same.

Spacing of 45 degree diagonal bar was decreased to 100 mm in specimen LW-3. This change in spacing had a negligible influence on the calculated flexural capacity but increased the nominal shear strength by 25%, relative to specimen LW-2.

Specimen LW-4 were similar to specimen LW-1 in every aspect, expect that a total of two 10-mm bars inclined by 45 degrees were added in each direction, as shown in Fig.4-2(d). The selection of the bidiagonal reinforcement was made in such a way as to achieve an effective reinforcement ratio for bars crossing the potential (horizontal) sliding plane almost identical to that of vertical web reinforcement in specimen LW-3. This selection was expected to yield a meaningful comparison of the relative effectiveness of the two types of shear reinforcement. The intersection of the 45 degrees inclined bars is at the base of the wall; hence no increase in flexural capacity is expected in the critical region.

Table 4-2 shows the finial mixture proportions of the shale ceramsite concrete used in all the specimens. The design procedures in the American Concrete Institute Building Code (ACI 318-05) [ACI99] for regions of low and moderate seismic risk were used to proportion the walls. During design, the concrete compressive strength was assumed to be 30 MPa, and the yield stress of the reinforcement was assumed to be 400 MPa. The measured strengths of the materials used to construct the walls exceeded these values and are summarized in Table 4-3.

Table 4-2 Mix proportions of lightweight shale ceramsite concrete

Ingredients of lightweight concrete	Quantities (kg/m^3)
Portland cement (P.O 42.5)	442
Sand	676
Expanded shale	568
Mix water	170
Admixture	9.0
Water / Cement Ratio	0.39

**Table 4-3 Material properties of lightweight concrete and reinforced bars**

	Specimen	Fresh density (kg/m^3)	Over-dry density (kg/m^3)	Compressive strength (MPa)	Tensile strength (MPa)	Elastic modulus (MPa)
Concrete	LW-1 LW-2	1900	1865	35.7	2.96	21899
	LW-3 LW-4	1905	1850	32.8	2.81	21632
	Type	Yielding strength (MPa)		Ultimate strength (MPa)		Elastic modulus (MPa)
Reinforced bars	HRB335 10mm bar	450		590		225000
	HRB335 12mm bar	455		645		227500
	HRB400 16mm bar	460		625		230000
	HRB235 10mm bar	405		480		202500

4.3 Test setup and instrumentation

Each specimen was loaded laterally as a vertical cantilever with forces applied by one double-effect horizontal jack through the top beam. Since a collapse lateral load of ca 600 kN was predicted, horizontal jack having 1000 kN was used. No axial load is applied to any of the specimens. The experimental setup is shown in Fig.4-3.

The horizontal loading was applied at the top beam of the specimens where two metal plates were attached. The use of a stiff beam at the top of wall specimens has been questioned by some researchers who pointed out that it tends to overestimate the shear capacity of the walls.

It is a fact, however, that in most practical situations, beams are framing into the walls at the level of floor slabs, although these beams are usually less stiff than those used in the test specimens.

1 Concrete reaction wall
2 Screw jack
3 Wall panel
4 Bolts
5 Strong floor
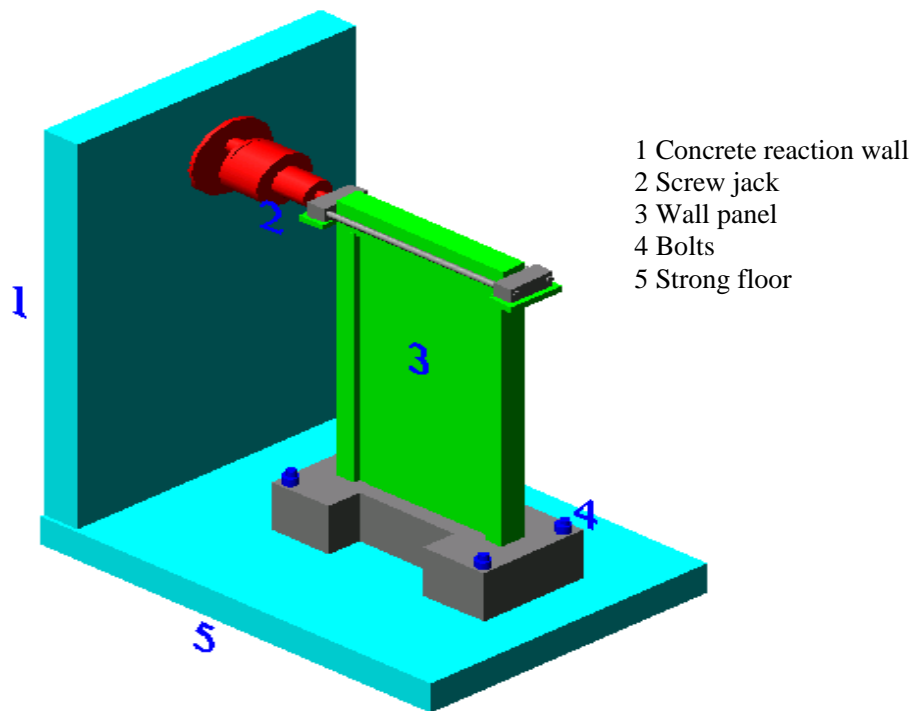
(a) AutoCAD picture of experimental setup

(b) Photograph of experimental setup

Fig.4-3 Experimental setup
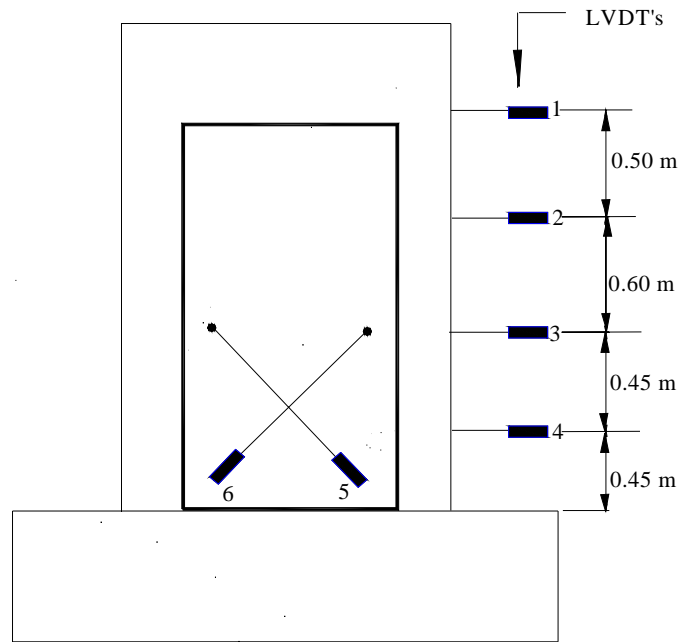
Fig.4-4 Positions of LVDT on side surfaces of four specimens
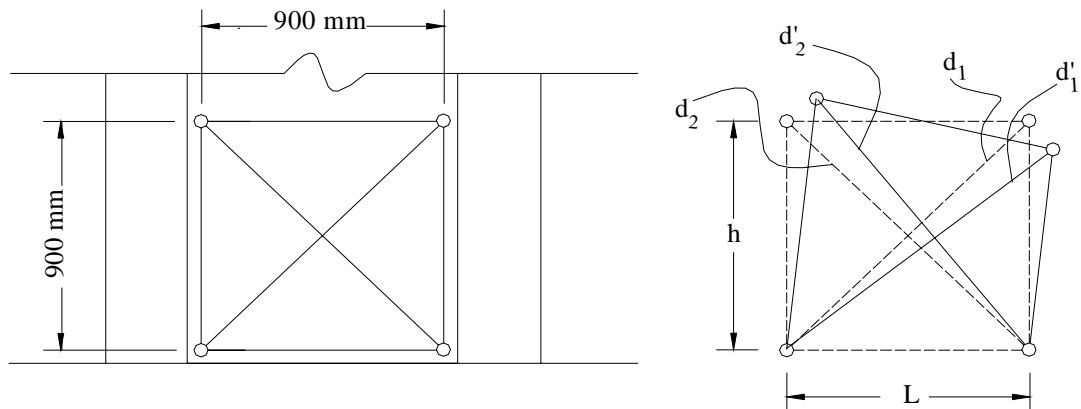
Note: Average shear distortion $\gamma_{avg} = \dfrac{(d_1' - d_1)d_1 - (d_2' - d_2)d_2}{2hL}$

where, $d_i = $ Original length of diagonal

$d_i' = $ Deformed length of diagonal

Fig.4-5 Estimation of average shear distortion from measured data

Instrumentation was selected to monitor applied loads, deformations and strains in the concrete and reinforcing bars. Lateral deflections were measured at four levels above the base (0.45 m, 0.90 m, 1.50 m and 2.00 m) by the linear variable displacement transducers (LVDT), as shown in Fig.4-4. Average shear distortions in the hinging region were calculated from deformations measured along diagonals of a square located in the lower 900mm of the web. Two LVDT inclined at 45 degree were installed in the lower region of the wall to measure

shear deformation. The procedure used to calculate the average shear distortion from the measured data is shown in Fig.4-5.

Possible horizontal displacement of the foundation was measured in order to verify that the foundation was fixed to the laboratory strong floor. Meanwhile, vertical displacements were measured on the surface of the base girder. All the displacement transducers used to measure them were shown in Fig.4-6.
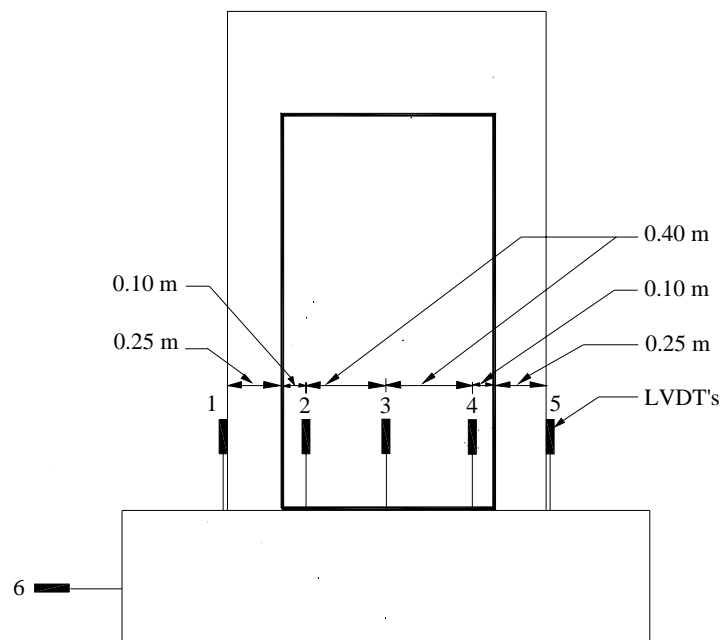

Fig.4-6 Positions of LVDT on bottom surfaces of four specimens

For specimen LW-1, six strain gauges (S7-S12) were pasted on the longitudinal steels in the two boundary columns to determine the initial yield displacement, as shown in Fig.4-7 (a). Four strain gauges (S1-S4) were pasted on the horizontal web reinforcements and two strain gauges (S5, S6) were pasted on the vertical web reinforcements to measure the strains in steel bars, as shown in Fig.4-8(a).

For specimen LW-2, six strain gauges (S7-S12) were pasted on the longitudinal steels in the two boundary columns (Fig.4-7(a)). Six strain gauges (S1-S6) were pasted on the diagonal reinforcements to measure the strains in steel bars, as shown in Fig.4-8(b).

For specimen LW-3, six strain gauges (S21-S23, S26-28) were pasted on the longitudinal steels and four strain gauges (S24, S25, S29, S30) were pasted on the stirrups in the two boundary column, as shown in Fig.4-7(b). Eight strain gauges (S1-S8) were pasted on the diagonal web reinforcements, as shown in Fig.4-8(c).

For specimen LW-4, there are in all 26 strain gages pasted on the reinforcements before concrete casting. Six strain gauges (S21-S23, S26-28) were pasted on the longitudinal steels and four strain gauges (S24, S25, S29, S30) were pasted on the stirrups in the two boundary columns, as shown in Fig.4-7(b). Four strain gauges (S1-S4) were pasted on the horizontal web reinforcements and four strain gauges (S5-S8) were pasted on the vertical web

reinforcements to measure the strains in steel bars. Other eight strain gages were pasted on the four additional diagonal web steels, as shown in Fig.4-8(d).
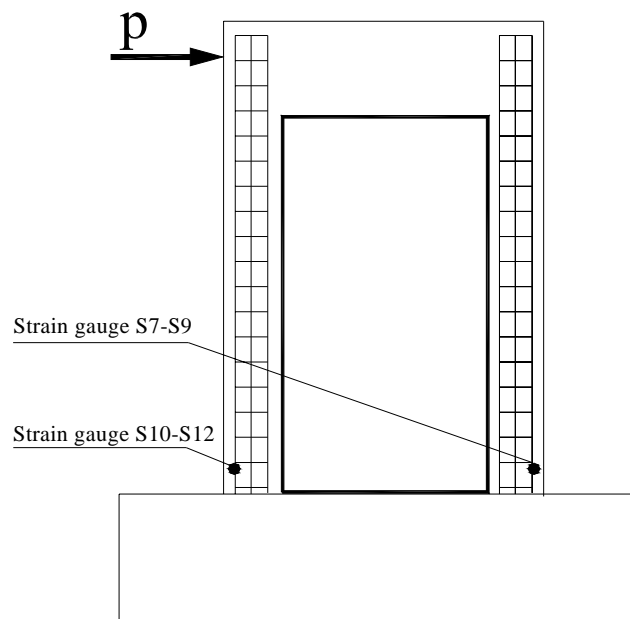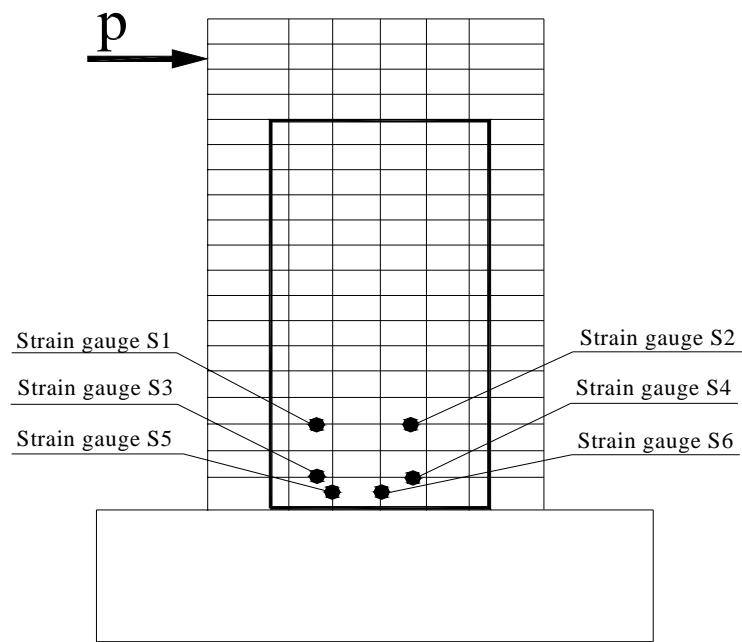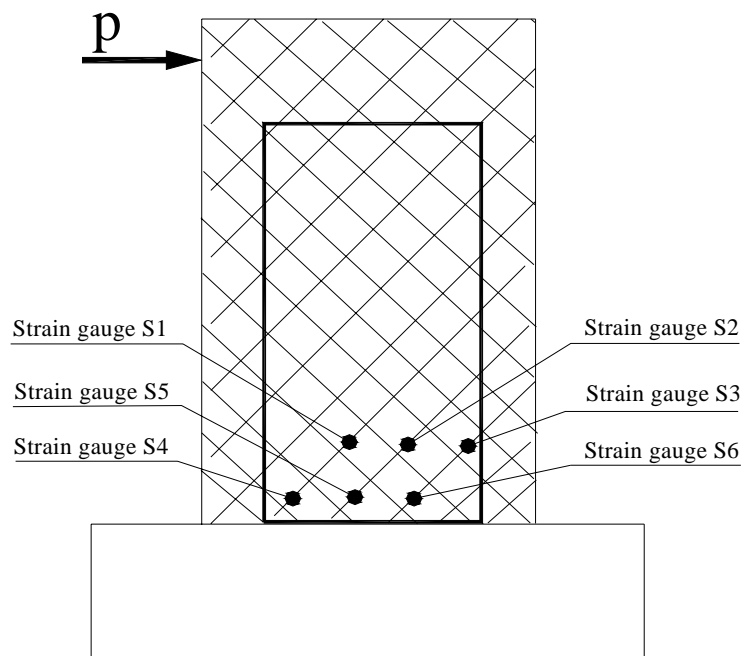

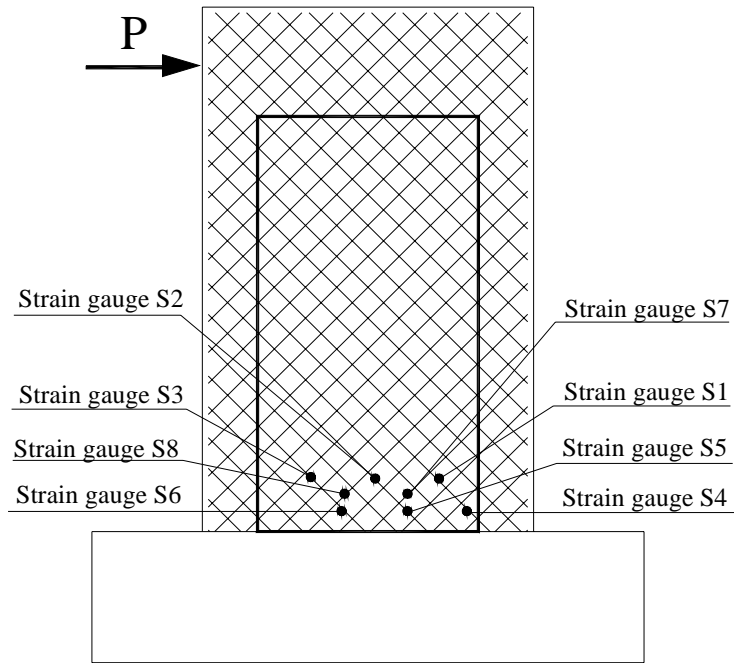(a) Specimen LW-1, LW-2
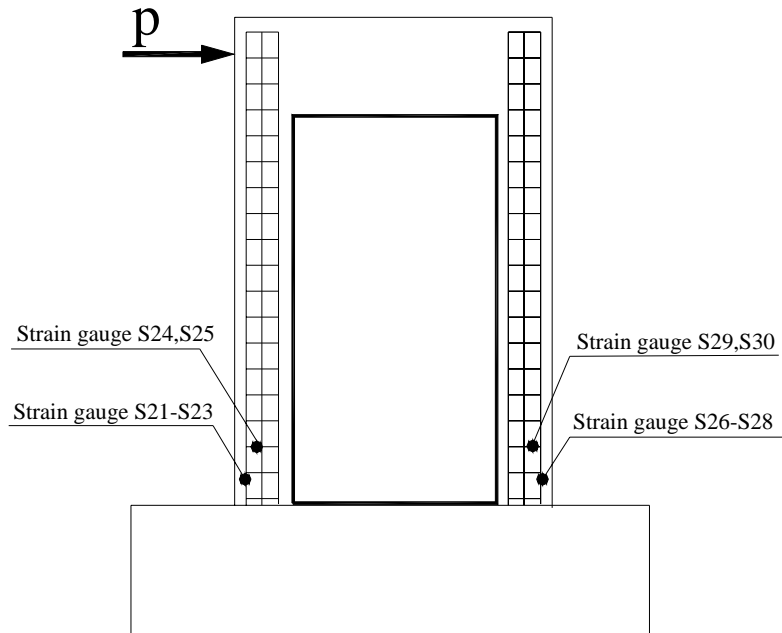
(b) Specimen LW-3, LW-4

Fig.4-7 Positions of strain gauges in the boundary elements

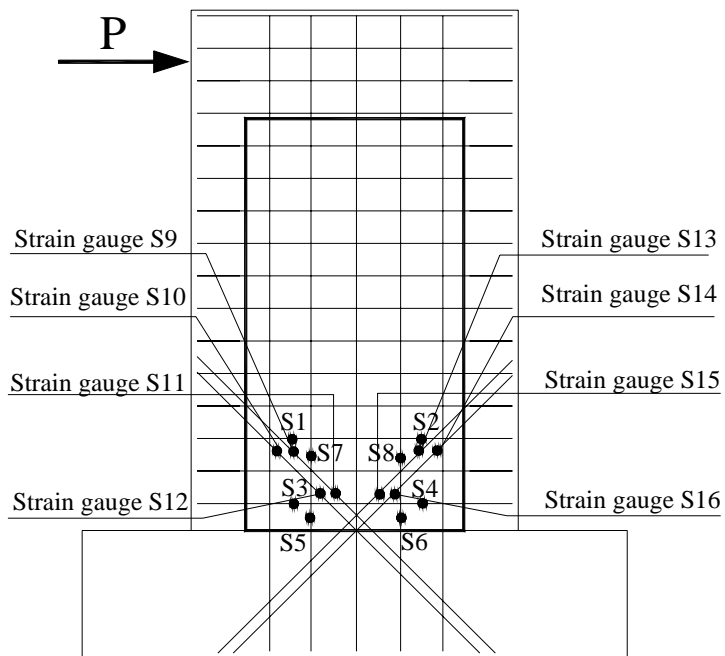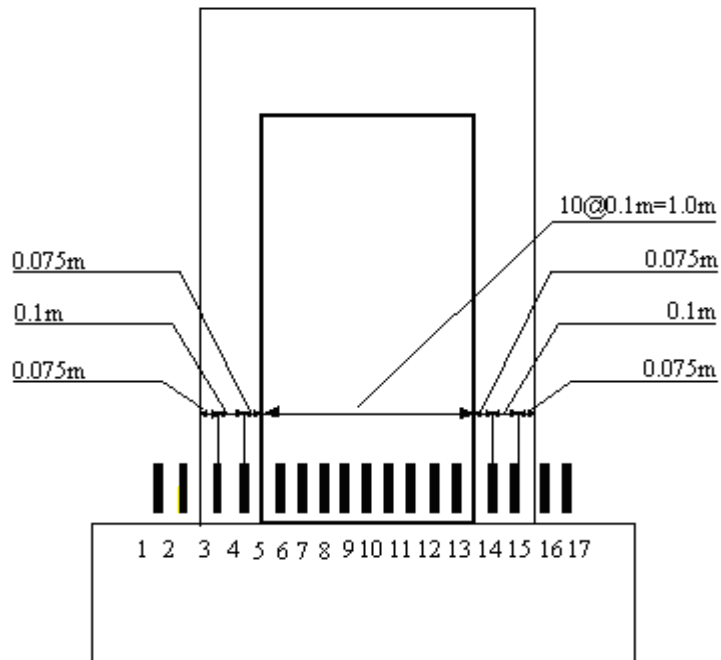(a) Specimen LW-1

(b) Specimen LW-2
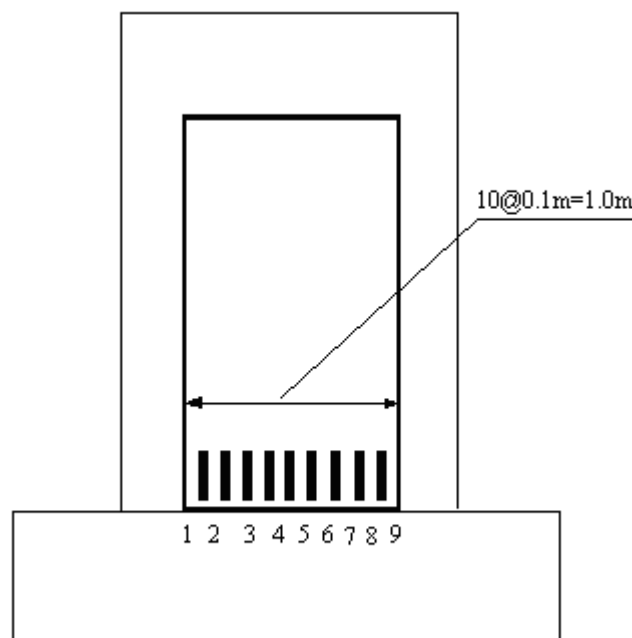
(c) Specimen LW-3

(d) Specimen LW-4

Fig.4-8 Positions of strain gauges in web reinforcements of four specimens

The locations of strain gauges used to measure the strains on concrete surface are shown in Fig.4-9. For specimen LW-1 and LW-2, there are 17 strain gauges pasted on the base of the web and columns of each wall respectively. For specimen LW-3 and LW-4, there are 9 strain gauges pasted only on the web of each wall respectively.

(a) Specimen LW-1, LW-2

(b) Specimen LW-3, LW-4

Fig.4-9 Positions of strain gauges on concrete surface of four specimens

4.4 Loading history and testing procedures

The same loading history was used to test all four specimens described in this research.

Before formal loading of the test, pre-loading should be processed so that the setup and the specimen can be in proper contact at normal working condition, the reliability of the loading system can be verified and all instrumentation can be adjusted. For this test, a 50 kN pre-load was applied on the specimen, which was less than 70% of the predicted cracking load.

Each complete load cycle consisted of one half cycles in the positive direction and one half cycles in the negative direction. The loading history was divided into two parts. Load control was used during the first several cycles to push the specimens to the yielding load in both directions; and displacement control was used in subsequent cycles to push the specimens such that the top deflection reached integer multiples of the yield displacement in both directions. The specimen was pushed to the same displacement level for three complete cycles before the displacement level was increased. At each increment the load was maintained constant for at least two minutes to measure the load and deformation response of the walls, mark the cracks and take photographs on the wall crack pattern. Pressure transducers in the hydraulic supply line of the rams provided accurate measurement of the applied load. Each test continued until the specimen experienced a significant loss of capacity. Fig.4-10 shows the loading history of the test program.
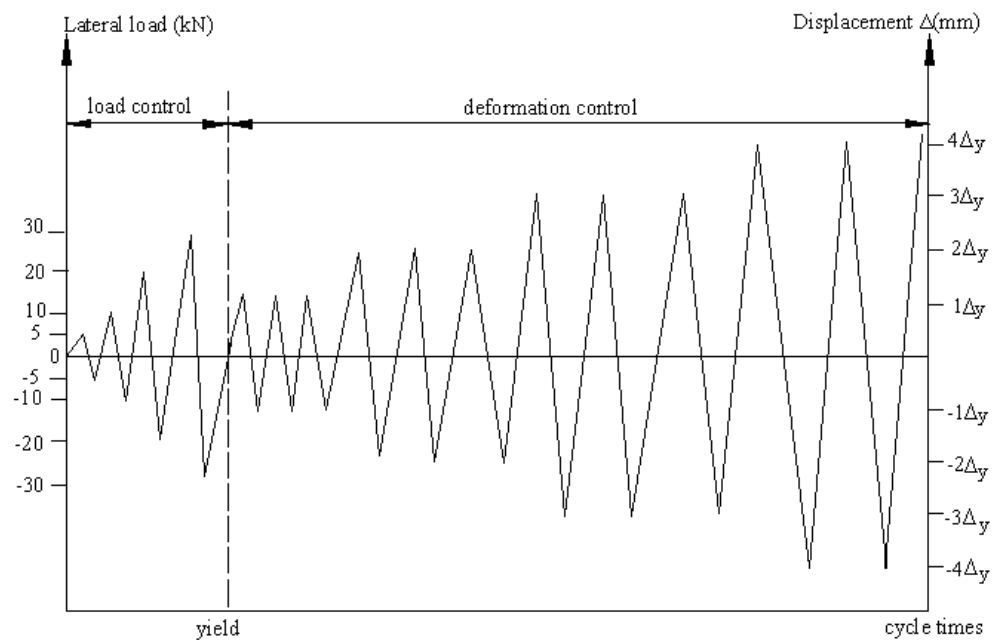

Fig.4-10 Loading history of four specimens

Chapter 5

Test Results and Discussions

The main results of the tests, together with information necessary for their interpretation, are given in Table 5-1, Table 5-2 and Fig.5-1 through 5-17. Table 5-1 summarized code predictions for wall strength and compares them with the experimental results. Table 5-2 provides information related to the experimental data and the principal results of the specimens tested in the program. Fig.5-1 through Fig.5-3 are the crack patterns of four specimens. Fig.5-4 through 5-7 provides the horizontal load versus top displacement curves established from the tests for all the specimens. Fig.5-8 shows the shear distortion of walls. Fig.5-9 is the relationship between shear distortion and accumulated ductility ratios for all the specimens at half cycle increments. Fig.5-10 through 5-13 illustrates variations of steel strains with increasing horizontal load for a typical specimen of the series, while Fig.5-14 shows the concrete strain at the base of every wall. The deflection shape, stiffness destination and energy dissipation of four specimens are compared respectively in Fig.5-15 through 5-17.

The experimental results indicate that diagonal web reinforcement can significantly improve the energy dissipation characteristics of the walls and prevent web crushing. The amount of diagonal web reinforcement also has an influence on the magnitude of shear distortion observed in the specimens.

5.1 Cracking processes and failure mode

There are extinct differences in cracking processes of four specimens. So everyone was described in detail as follows.

Specimen LW-1

Before the horizontal load increased to 100 kN, no cracks appeared on the surface of specimen. The whole wall behaved as an elastic body. All the deformation could be reverted after unloading. At the load level of 130 kN, some horizontal cracks emerged on the boundary

column subjected to tensile stress, which were 300 mm, 750 mm, 950 mm and 1150 mm apart from the wall base. The maximum width of these cracks was 0.05 mm. At this load level, the tensile stress in the longitudinal steel of column was 54.28 N. Correspondingly, the tensile stress in vertical reinforcement was 33.25 N while in horizontal reinforcement only 2.63 N. Until the load of –150 kN, one crack appeared on the surface of another column, 700 mm apart from the base.

As the horizontal load approached to 200 kN, significant inclined cracks initiated at the web near the tension column of the wall, 1700 mm, 1450 mm, 1250 mm, 1050 mm, 600 mm and 400 mm apart from the base, and penetrated deeply into the web near the compressive zone. The slope of all cracks was circa 45 degree to the horizontal axis. They could be closed when unloading. The tensile stress in the longitudinal steel of column was 164.45 N. Correspondingly, the tensile stress in vertical reinforcement was 117.675 N while in horizontal reinforcement only 72.675 N. All the reinforcements were still not yield at this moment. All diagonal cracks could not be observed when horizontal load was applied in negative direction. Some new inclined cracks initiated at the web near the tension column at the load of –200 kN, 1600 mm, 1450 mm, 1250 mm, 1000 mm, and 400 mm apart from the base, and penetrated deeply into the web near the compressive zone. These cracks formed an orthogonally crisscrossing crack pattern, which had a higher intensity for specimen subjected to cycles of loading to higher ductility levels, as Fig.5-1(a) demonstrates.

With the increase of load cycle, diagonal cracks appeared more in the web and the original cracks were extended, widen or connected through out. All the inclined cracks were approximately parallel and distributed uniformly. At the same time, horizontal cracks due to tensile stress on the columns were increased also. However, no diagonal cracks appeared on the column.

As the horizontal load approached to 330 kN, the longitudinal reinforcements in the boundary columns were yield with the top horizontal displacement of 7.84 mm. The maximum width of diagonal cracks in the web was 0.54 mm. However, steel bars in the web were still not yield at this moment.

After specimen yielding, it could continue to subject increasing load. But the positive cracks could not be closed when negative load was applied. The parallel diagonal cracks divided the web concrete up to some inclined compressive struts, which resisted the most of the shear forces in the web of the wall. Conventional horizontal web reinforcements acted as ties that cross diagonal concrete struts to distribute the shear force to them. In fact, due to the crisscrossing diagonal cracks under cyclic load, the concrete compressive struts were formed with several concrete blocks and the vertical reinforcements acted as ties that cross these blocks. So that, all lateral force in walls was transferred through concrete by compressive struts and aggregate interlock and by dowel action in the reinforcement at the base of the wall. When the specimen was near to collapse, splitting of the concrete in compressive zone was observed.

At the peak load of 454 kN, with the top horizontal displacement being treble of the yield displacement, most reinforcements in the web yielded. The maximum crack width was reach to 1.21 mm and the concrete cover at the lower compressive zone of the wall crushed. Then the shear capacity of specimen was decreased quickly to about 85% of the ultimate load. Specimen failure was determined as this point.

Specimen LW-2

Before the horizontal load increased to 70 kN, no cracks appeared on the surface of specimen. The whole wall behaved as an elastic body. All the deformation could be reverted after unloading. At the load level of –70 kN, some horizontal cracks emerged on the boundary column subjected to tensile stress, which were 600 mm, 750 mm, 950 mm 1020 mm, 1150 mm and 1270 mm apart from the base. Until the load of 100 kN, horizontal cracks appeared on the surface of another column, 675 mm, 820 mm, 900 mm and 1050 mm apart from the base. The maximum width of these cracks was 0.06 mm. At this load level, the tensile stress in the longitudinal steel of column was 31.28 N. Correspondingly, the tensile stress in the web diagonal reinforcement was 13.65 N.

As the horizontal load approached to 200 kN, significant inclined cracks initiated at the web near the tension column of the wall, 1900 mm, 1000 mm and 500 mm apart from the base, and penetrated deeply into the web near the compressive zone. They could be closed when unloading. When negative load of –200 kN was applied on the specimen, all diagonal cracks of positive load could not be observed while some new inclined cracks initiated at the web near another column, 1900 mm, 900 mm and 470 mm apart from the base. All the cracks have the angle of about 45 degree to the horizontal axis and formed an orthogonally crisscrossing crack pattern, as Fig.5-1(b) demonstrates. The tensile stress in the longitudinal steel of column was 173.5 N. Correspondingly, the tensile stress in diagonal web reinforcement was 142.05 N. All the reinforcements were still not yield at this moment.

With the increase of load cycle, diagonal cracks appeared more in the web and the original cracks were extended, widen or connected through out. All the inclined cracks were approximately parallel distributed uniformly. At the same time, horizontal cracks due to tensile stress on the columns were increased also. However, no diagonal cracks appeared on the column. Compared with specimen LW-1, the diagonal cracks in the web of LW-2 was sparser while the width of crack was bigger.

As the horizontal load approached to 300 kN, the longitudinal reinforcements in the boundary columns were yield with the top horizontal displacement of 7.13 mm. The maximum width of diagonal cracks in the web was 0.61 mm. Some steel bars in the web were yield at this moment also.

After specimen yielding, it could continue to subject increasing load. But the positive cracks could not be closed when negative load was applied and few new inclined cracks formed. The parallel diagonal cracks divided the web concrete up to some inclined compressive struts. Diagonal web reinforcement not only acted as tie that cross concrete struts but also helped transfer part of shear force directly to the foundation by tension in the web reinforcement. So the tensile strain in diagonal reinforcement of LW-2 was much higher than that of LW-1. As a result, the shear forces carried by the compressive struts were reduced.

At the load of 430 kN, with the top horizontal displacement being double of the yield displacement, all reinforcements in the web were yield. The maximum crack width was reach to 1.29 mm. However, the concrete cover at the lower compressive zone of the wall didn't spalled off. As the horizontal load reached to the ultimate level of 490 kN, with the top horizontal displacement of 29 mm, the maximum crack width was reach to 2.9 mm.

Specimen LW-2 failed when the concrete in the boundary elements crushed. Then the shear capacity of specimen was decreased quickly to about 85% of the ultimate load. Specimen failure was determined as this point. Although specimen LW-2 was subjected to a maximum shear force greater than that resisted by specimen LW-1 with conventional reinforcement, the concrete in the web of LW-2 was still in good condition after failure.

Specimen LW-3

Before the horizontal load increased to 100 kN, no cracks appeared on the surface of specimen. The whole wall behaved as an elastic body. All the deformation could be reverted after unloading. At the load level of −100 kN, some horizontal cracks emerged on the boundary column subjected to tensile stress, which were 600 mm, 750 mm and 900 mm apart from the wall base. The maximum width of these cracks was 0.02 mm. At this load level, the tensile stress in the longitudinal steel of column was 48.4 N. Correspondingly, the tensile stress in web diagonal reinforcement was 15.75 N. Until the load of 129 kN, two cracks appeared on the surface of another column, 50 mm and 750 mm apart from the base respectively.

As the horizontal load approached to −200 kN, significant inclined cracks initiated at the web near the tension column of the wall, 1800 mm, 850 mm, 600 mm and 400 mm apart from the base, and penetrated deeply into the web near the compressive zone. They could be closed when unloading. When positive load of 250 kN was applied on the specimen, some new inclined cracks initiated at the web near another column, 1900 mm, 1650 mm, 1500 mm, 950 mm and 350 mm apart from the base. All the cracks have the angle of about 30~45 degree to the horizontal axis and formed an orthogonally crisscrossing crack pattern, as Fig.5-1(c) demonstrates. The tensile stress in the longitudinal steel of column was 399 N while the tensile stress in web diagonal reinforcement was 137.9 N.

As the horizontal load approached to 302 kN, the longitudinal reinforcements in the boundary columns were yield with the top horizontal displacement of 5.87 mm. The maximum width of diagonal cracks in the web was 0.42 mm. Some steel bars in the web were yield at this moment also.

At the load of 432 kN, with the top horizontal displacement being double of the yield displacement, all reinforcements in the web were yield. Compared with specimen LW-1 and LW-2, the amount of diagonal cracks in the web was obviously sparser and narrower. Until failure the concrete cover at the lower compressive zone of the wall didn't peel.

Specimen LW-3 failed when the concrete in the boundary elements crushed at the load of 497 kN.

Specimen LW-4

Before the horizontal load increased to 100 kN, no cracks appeared on the surface of specimen. The whole wall behaved as an elastic body. All the deformation could be reverted after unloading. At the load level of 100 kN, some horizontal cracks emerged on the boundary column subjected to tensile stress, which were 500 mm, 600 mm, 850 mm and 1550 mm apart from the wall base. The maximum width of these cracks was 0.03 mm. At this load level, the tensile stress in the longitudinal steel of column was 32.2 N. Correspondingly, the tensile stress in vertical reinforcement was 6.1 N and in bidiagonal bar was 5 N while in horizontal

reinforcement was only 0.7 N. At the load level of –100 kN, cracks appeared on the surface of another column, 700 mm, 900 mm and 1450 mm apart from the base.

As the horizontal load approached to 150 kN, significant inclined cracks initiated at the web near the tension column of the wall, 1750 mm, 1400 mm, 1250 mm, 900 mm and 600 mm apart from the base, and penetrated deeply into the web near the compressive zone. They could be closed when unloading. When negative load of –150 kN was applied on the specimen, some new inclined cracks initiated at the web near another column, 1800 mm, 1450 mm, 1000 mm, 750 mm, 600 mm, 450 mm and 350 mm apart from the base. All the cracks have the angle of about 30~45 degree to the horizontal axis and formed an orthogonally crisscrossing crack pattern, as Fig.5-1(d) demonstrates. The maximum width of these cracks was 0.16 mm.

As the horizontal load approached to 300 kN, the longitudinal reinforcements in the boundary columns were yield with the top horizontal displacement of 5.86 mm. The maximum width of diagonal cracks in the web was 0.52 mm. Steel bars in the web were not yield at this moment.

At the load of 410 kN, with the top horizontal displacement being double of the yield displacement, all the reinforcements in the web expect the horizontal steels were yield. The horizontal web steels yield at load level of 564 kN. Until failure the concrete cover at the lower compressive zone of the wall didn't peel. Specimen LW-4 failed when the concrete in the boundary elements crushed at the load of 474 kN.

For specimen LW-1, a major horizontal crack running through the entire base of the wall formed. However, in the case of the specimen with bidiagonal reinforcement intersection in the middle of the base section (LW-4), the width of the horizontal crack was smaller. These bars have also contributed to better control of the inclined shear cracks in the web of specimens.

Fig.5-2 shows crack patterns at failure load level for each of the specimen and Fig.5-3 shows the details of failure place. Two modes of failure were observed in the specimens. Walls LW-1 failed abruptly due to web crushing and extensive damage to the concrete in the web can be observed in Fig.5-3. Walls LW-2, LW-3 and LW-4 failed when the concrete in the boundary elements crushed. Although each wall was subjected to a maximum shear force greater than that resisted by its companion wall LW-1, the concrete in the web of walls LW-2, LW-3 and LW-4 were still in good condition after failure.
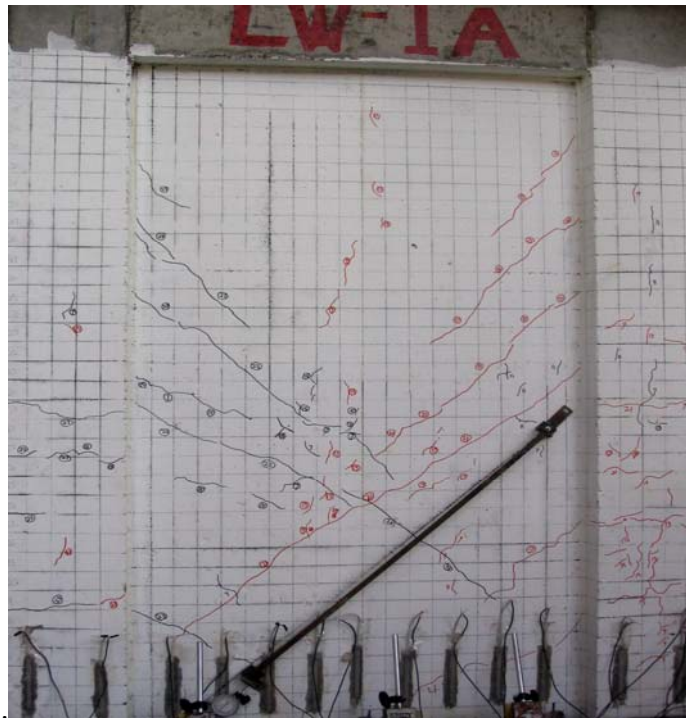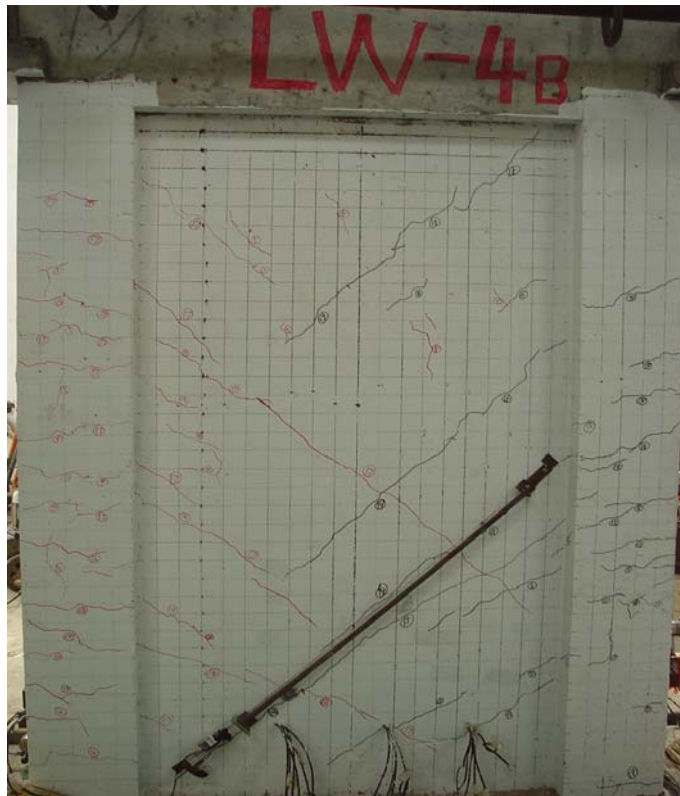
(a) LW-1 (load=200 kN)
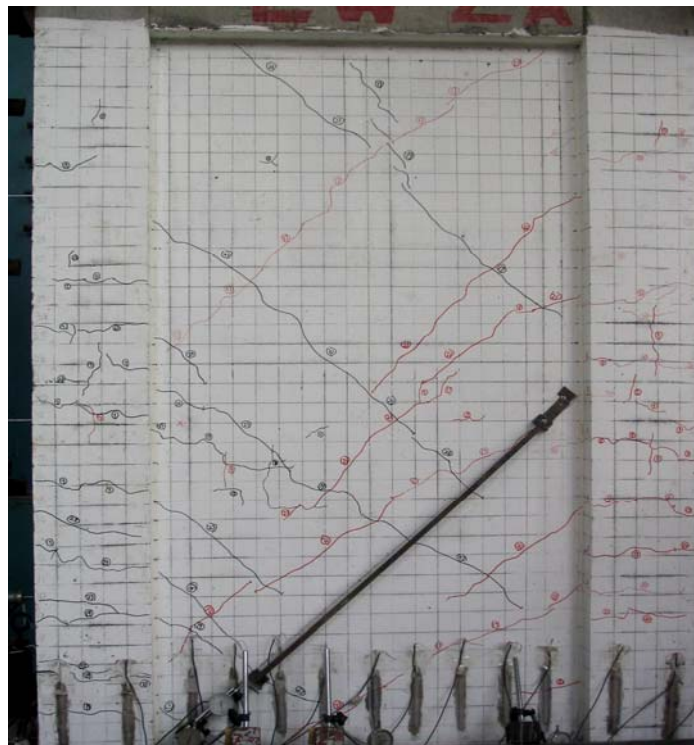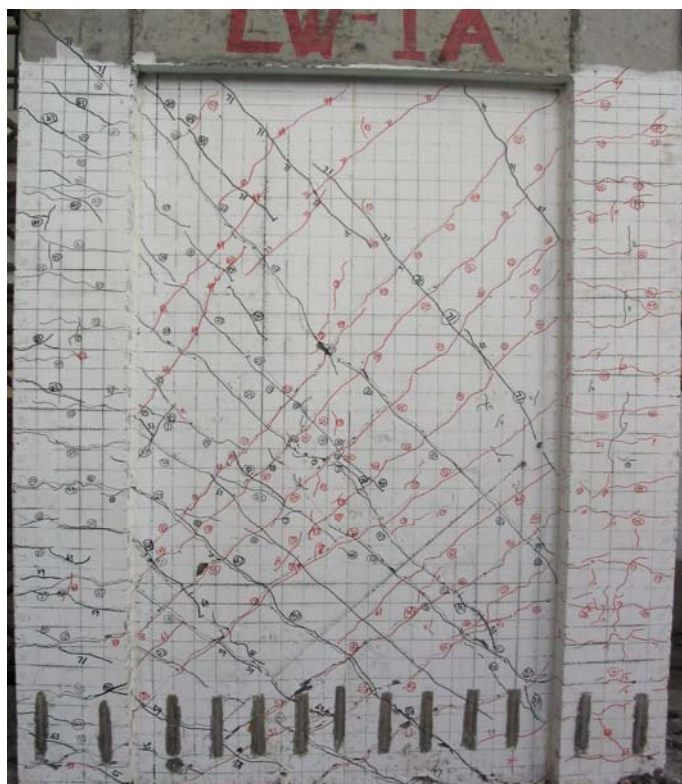

(b) LW-2 (load=200 kN)
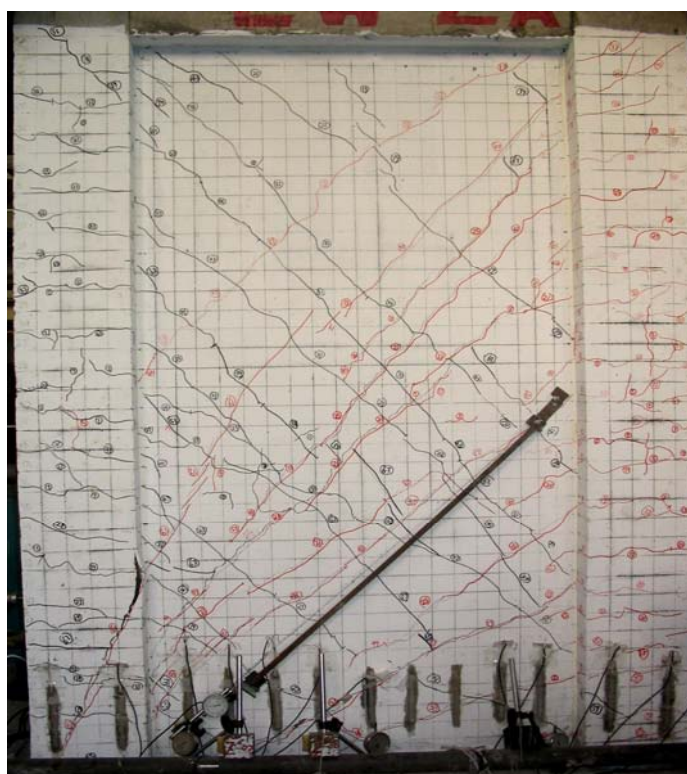
(c) LW-3 (load=200 kN)
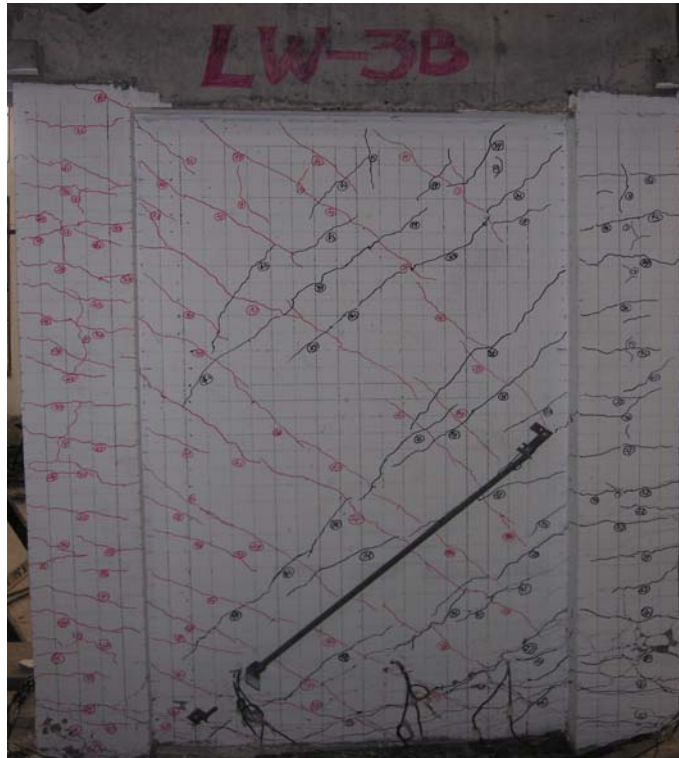

(d) LW-4 (load=200 kN)
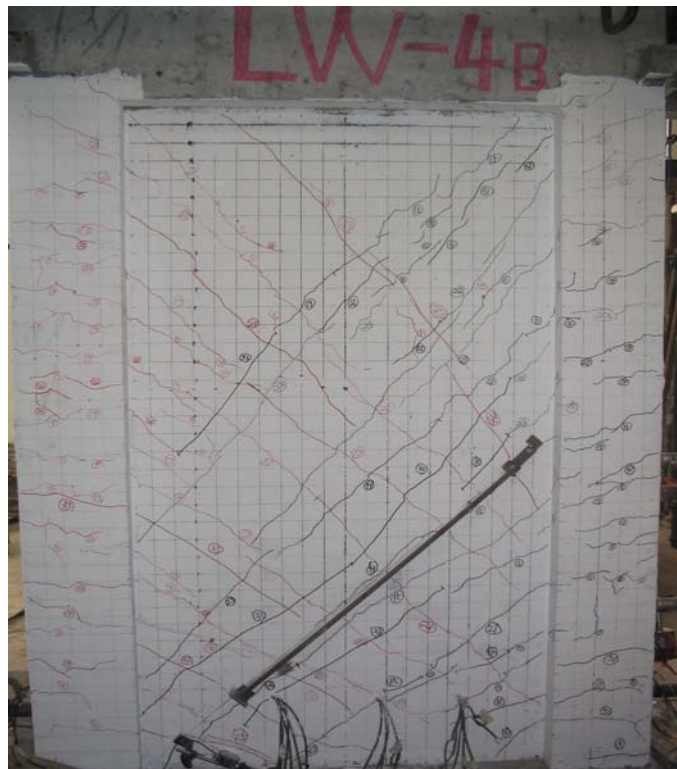**Fig.5-1 Significant stages of cracking process by four specimens**

(a) LW-1

(b) LW-2

(c) LW-3

(d) LW-4

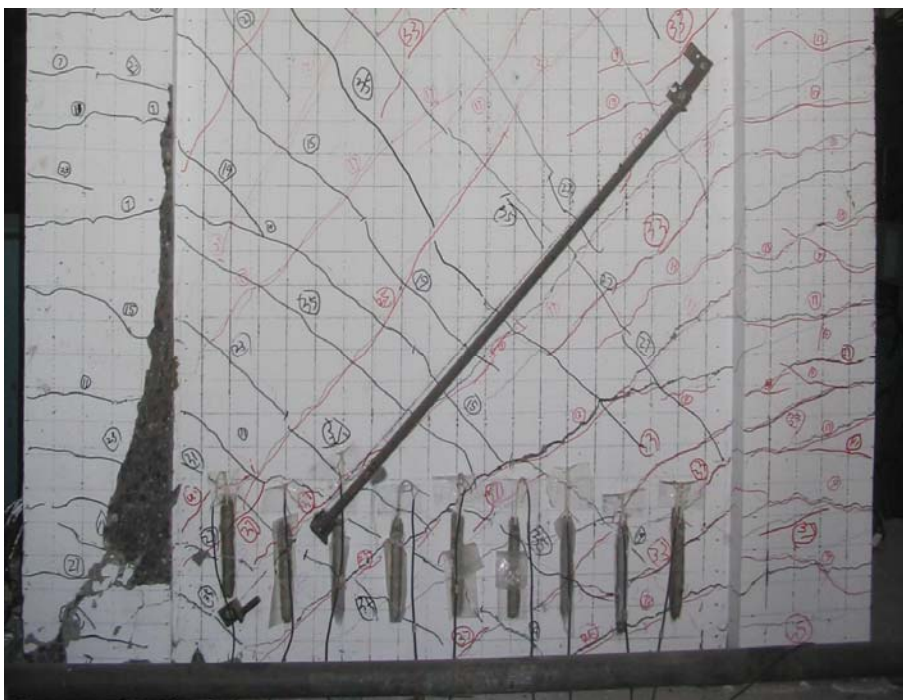**Fig.5-2 The crack patterns of four specimens at failure point**

(a) LW-1

(b) LW-2

(c) LW-3

(d) LW-4

Fig.5-3 Failure details of four specimens

5.2 Capacity, deformation and ductility characteristics

Table 5-1 summarizes calculated nominal capacities, maximum loads and observed failure modes of four specimens. All four specimens sustained maximum loads that exceeded the calculated nominal capacities. Comparing the result of LW-1 with those of LW-2 and LW-3, it can be seen that, the walls with diagonal web reinforcement resisted higher loads than the companion walls with conventional reinforcement and the increase in strength was significant for the walls with higher web reinforcement ratios. Comparison of the results among LW-1, LW-3 and LW-4 showed that, additional 45 degree diagonal steels helped the conventional reinforcement to sustain the load so that the specimen LW-4 had the increased strength like specimen LW-3 with higher diagonal web reinforcement ratio.

Specimen LW-1 failed abruptly due to web crushing. Extensive damage to the concrete in the web may be observed in Fig.5-3. Specimen LW-2, LW-3 and LW-4 failed when the concrete in the boundary elements crushed. This observation indicates that different shear transfer mechanisms controlled the behavior of the walls reinforced with conventional web reinforcement and walls reinforced with diagonal web reinforcement.

Table 5-1 Calculated and measured capacity of specimens

Specimen	Calculated per ACI 318-05		Observed response		
	Flexural capacity (kN)	Shear capacity (kN)	Maximum load (kN)	Load at web crushing (kN)	Mode of failure
LW-1	440	440	460	387	Web crushing
LW-2	380	433.2	490	---	Crushing of boundary element
LW-3	380	558.8	572	---	
LW-4	440	530	562	---	

The crack horizontal load, crack top deflection, yield horizontal load, yield top deflection, ultimate load, ultimate deflection, failure load, failure deflection, shear distortion at every load level and ductility factor for all the tested walls are listed in Table 5-2.

Different reinforcement placing has few effects on the crack load, crack deflection, yield load and yield deflection. However, diagonal web reinforcement is more effective in improving the shear capacity and shear stiffness of specimen LW-2. Although the yield top displacement of specimen LW-1 and LW-2 are almost the same, diagonal web reinforcement in specimen LW-2 resulted in decrease of 4.6% in top horizontal displacement and 20.19% in shear distortion corresponding to the relatively high ultimate load. Higher diagonal web reinforcement ratio (specimen LW-3) improved the shear capacity by up to 18% (mean value in positive and negative direction), comparing with specimen LW-2. However, the top horizontal displacement and shear distortion decreased distinctly. Due to the additional diagonal crossing steels, the shear capacity of specimen LW-4 was improved by up to 20.41% with smaller ultimate shear distortion, comparing with specimen LW-1.

Table 5-2 Test results of load, deflection and ductility

Specimen		LW-1		LW-2		LW-3		LW-4	
Load direction		positive	negative	positive	negative	positive	negative	positive	negative
Crack stage	Crack load (kN)	134	-137	103	-102	129	-100	99.4	-100
	Crack top displace--ment (mm)	1.3772	-1.1976	0.929	-0.853	1.54	-1.28	1.68	-2.01
	Crack shear distortion (rad)	0.00048	-0.00029	0.000124	-0.00039	0.00013	-0.00011	0.00012	-0.00015
Yield stage	Yielding load (kN)	340	-338	297	-305	302	-298	303	-292
	Yielding top displace--ment (mm)	7.844	-7.844	7.13	-7.245	5.87	-5.95	5.86	-6.28
	Yield distortion (rad)	0.00159	-0.0024	0.0008	-0.0009	0.00197	-0.00195	0.00113	-0.00106
Peak stage	Peak load (kN)	460	-453	475	-490	572	-566	562	-541
	Peak top displace--ment (mm)	25.089	-24.731	28.9	-29.4	23.46	-23.46	23.95	-23.95
	Peak distortion (rad)	0.00397	-0.00428	0.00376	-0.00382	0.00312	-0.00306	0.00353	-0.00341
Ultimate stage	Ultimate load (kN)	387	-386	405	-415	497	---	473	-508
	Ultimate top displace--ment (mm)	39.7	-39.6	38.1	-37.65	27.88	---	32	-29.2
	Ultimate distortion (rad)	0.00557	-0.00592	0.00442	-0.00475	0.00392	---	0.00425	-0.00389
Ductility factor		5.061	5.01	5.34	5.20	4.75	---	5.46	4.65

Note: Ductility factor is defined as the ratio of ultimate top displacement to yield top displacement of one specimen.

It can also be noticed that ductility factor of specimen LW-2 is superior to that of specimen LW-1 and ductility ratio of specimen LW-4 are close to that of LW-2. It means that diagonal web reinforcement is a good way to increase the seismic behaviors of shear wall.

5.3 Overall hysteretic response

Continuous plots of applied horizontal load versus top horizontal displacement (P- Δ hysteretic response) for specimens LW-1 to LW-4 are shown in Fig.5-4 through 5-7. The well-known characteristics of RC members subjected to cyclic loading, such as unloading and reloading stiffness reduction as cyclic displacement amplitude increases, and pinching of hysteresis loops, can be clearly seen in the figure. The degree of pinching, which is a manifestation of crack closing and consequent loss of stiffness during reloading in the opposite direction, varies significantly. Fig.5-4 through 5-7 clearly indicate the difference between four specimens.

Four specimens exhibited the same non-linear deformation response under horizontal load. Before concrete cracking, wall exhibited elastic properties with high shear rigidity. With the increase of loading, hysteresis loop formed. After concrete cracking, especially after wall yielding, shear rigidity reduced quickly and horizontal displacement increased obviously. The area in one hysteresis loop was increased obviously. At this moment, specimen dissipates energy mainly through boundary column and the opening and closing of diagonal cracks in the web. The slope of curve in positive loading period was relatively small at first and then had a little improvement. This is because that during the unloading and reverse loading periods the opened cracks were closed partly which make it possible that concrete between cracks can touch with each other and transfer more shear forces. At the same deformation stage, the corresponding horizontal loads in the second and third cycles were less than the load in the first cycle, which is named strength deterioration. This is due to the accumulated damage at the hinging region of the wall. For the shear walls presented here, the accumulated damage are mainly caused by diagonal cracks development, concrete protective coating spalling in cracks and cohesion failure.
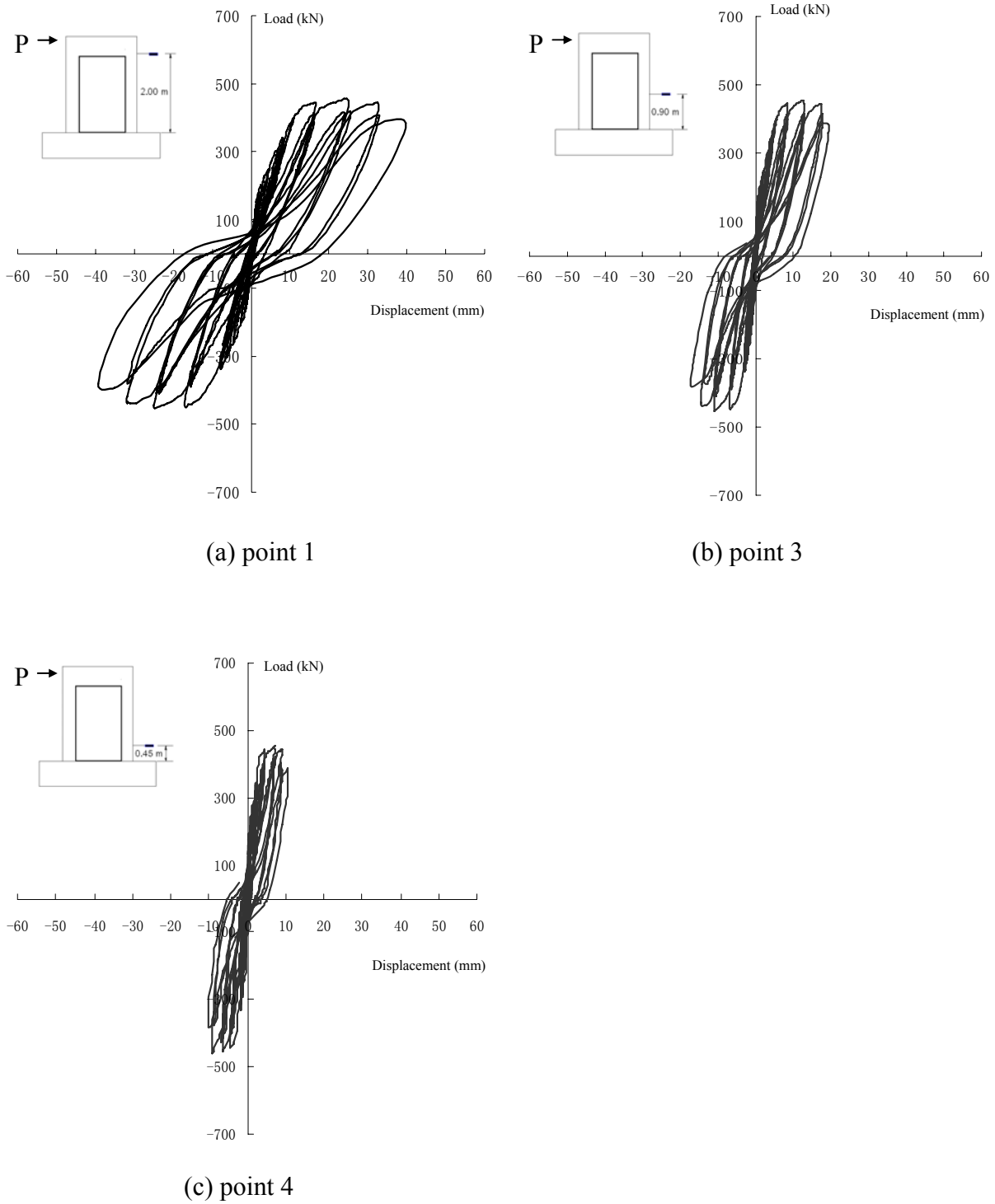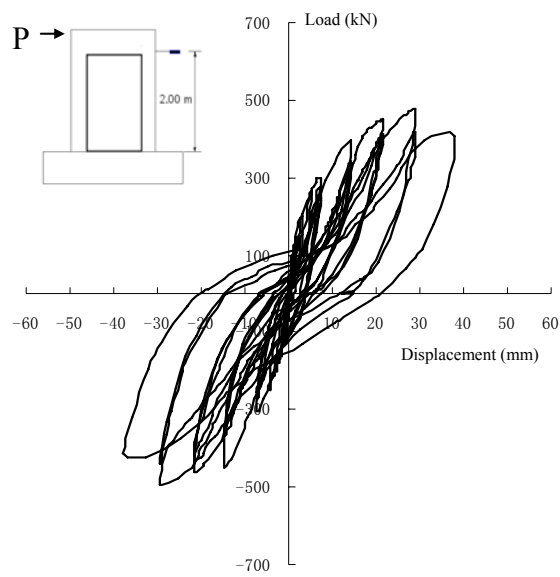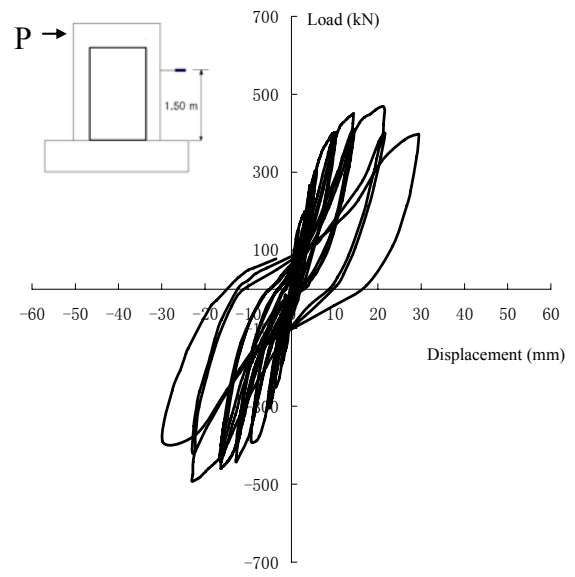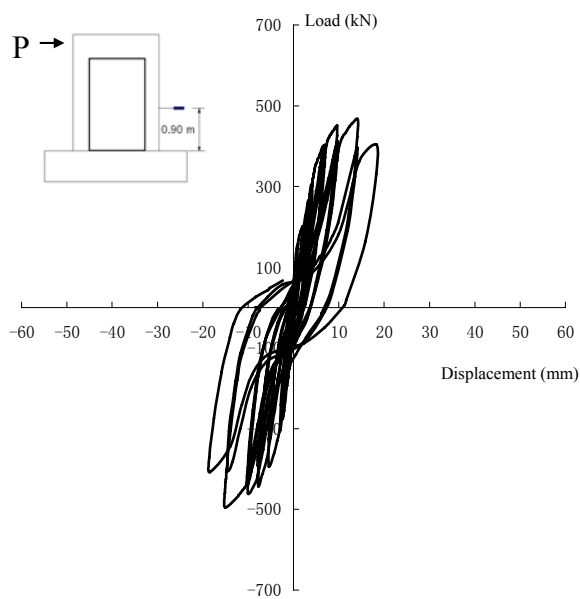
(a) point 1

(b) point 3

(c) point 4

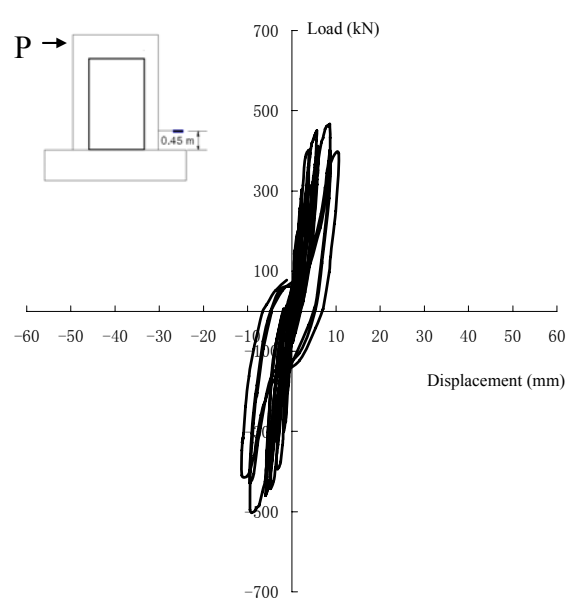**Fig.5-4 Horizontal load versus horizontal displacement curve of specimen LW-1**
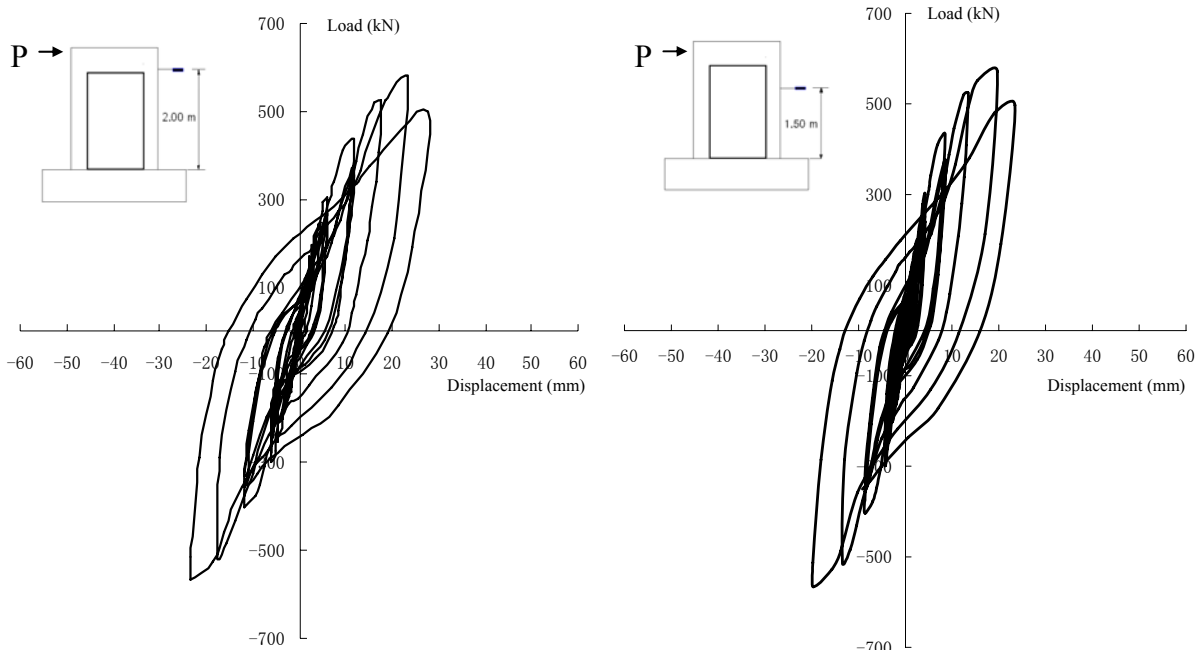
(a) point 1

(b) point 2
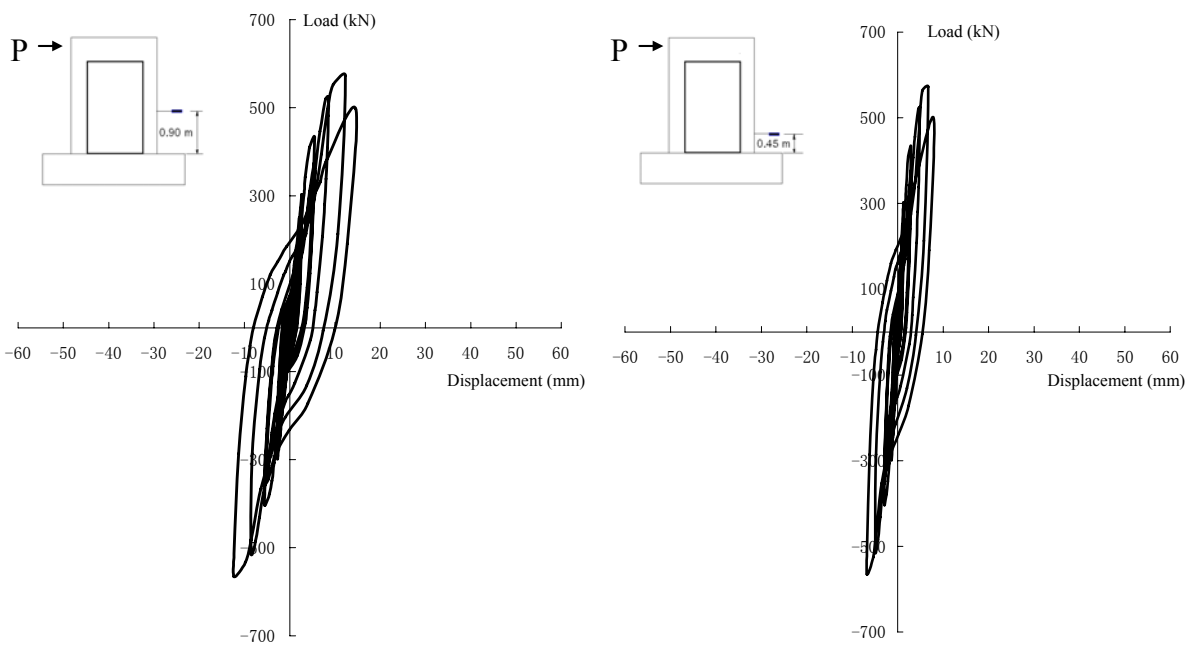

(c) point 3

(d) point 4

Fig.5-5 Horizontal load versus horizontal displacement curve of specimen LW-2

(a) point 1

(b) point 2

(c) point 3

(d) point 4

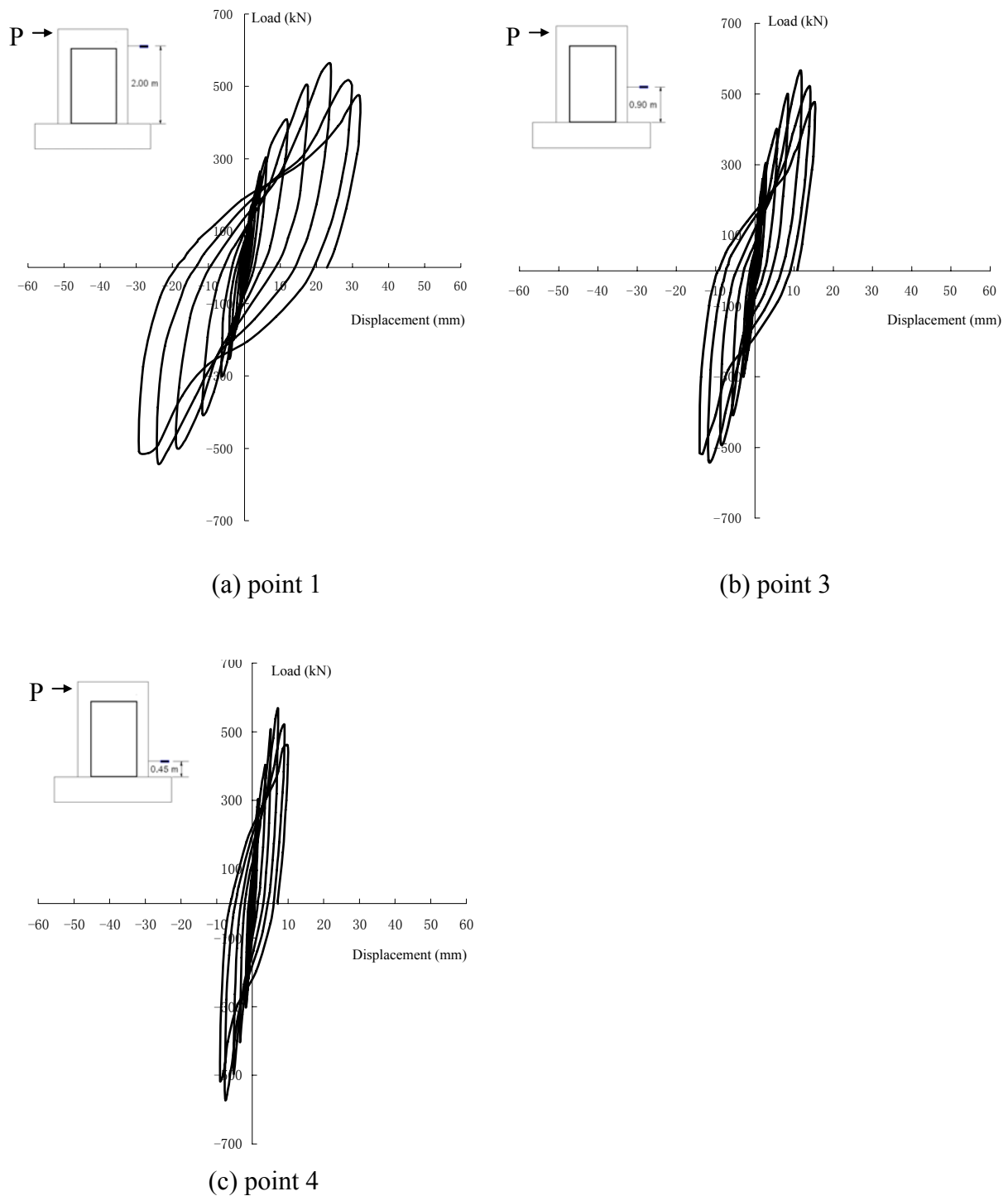**Fig.5-6 Horizontal load versus horizontal displacement curve of specimen LW-3**

(a) point 1

(b) point 3

(c) point 4

Fig.5-7 Horizontal load versus horizontal displacement curve of specimen LW-4

The P-Δ relationship of wall LW-1 experienced significant pinching caused by the low shear rigidity of the wall in hinging region. In the conventionally reinforced wall, applied shear force is transferred to foundation by compressive struts in the concrete. When the applied load was close to zero, most cracks in the lower portion of the wall remained open and the compressive struts could not transfer compressive force effectively. This significantly reduced

the shear rigidity in the hinging region of the wall and caused large shear distortions at low levels of applied load.

The degree of pinching is visibly lower in specimen LW-2 and LW-3. The P-Δ relationships of them exhibited a more rounded shape and did not experience significant pinching. This is due to the fact that part of shear force was transferred to the foundation directly by diagonal reinforcing steel in walls with diagonal web reinforcement. As a result, the shear rigidity in the hinging region was also controlled by the reinforcing steel and did not deteriorate as inelastic shear deformation increased.

A lower degree of pinching is also observed in the loops of the specimens LW-4, apparently due to the effect of inclined reinforcements, which affect the bond-slip mechanisms. These bidiagonal bars contribute to better control of the inclined shear cracks in the web of specimen LW-4. The main reason for this better control is that bidiagonal bars intersect the inclined shear cracks almost at right angle (refer to the cracking pattern in Fig.5-2). Hence, they work essentially in direct tension, whereas the bars in the orthogonal grid intersect the shear cracks at 35 to 45 degree and tend to work primarily as dowels.

5.4 Shear distortion at base of walls

Continuous plots of applied horizontal load versus shear distortion (P-γ) in the lower 900 mm of the specimens for wall LW-1 to LW-4 are shown in Fig.5-8. The P-γ relationship of wall LW-1 experienced significant pinching. Wall LW-1 experienced larger shear distortions than wall LW-2, especially in the later loading cycles. The P-γ relationships of walls LW-2, LW-3 and LW-4 did not display an obvious pinched shape.

(a) Specimen LW-1   (b) Specimen LW-2
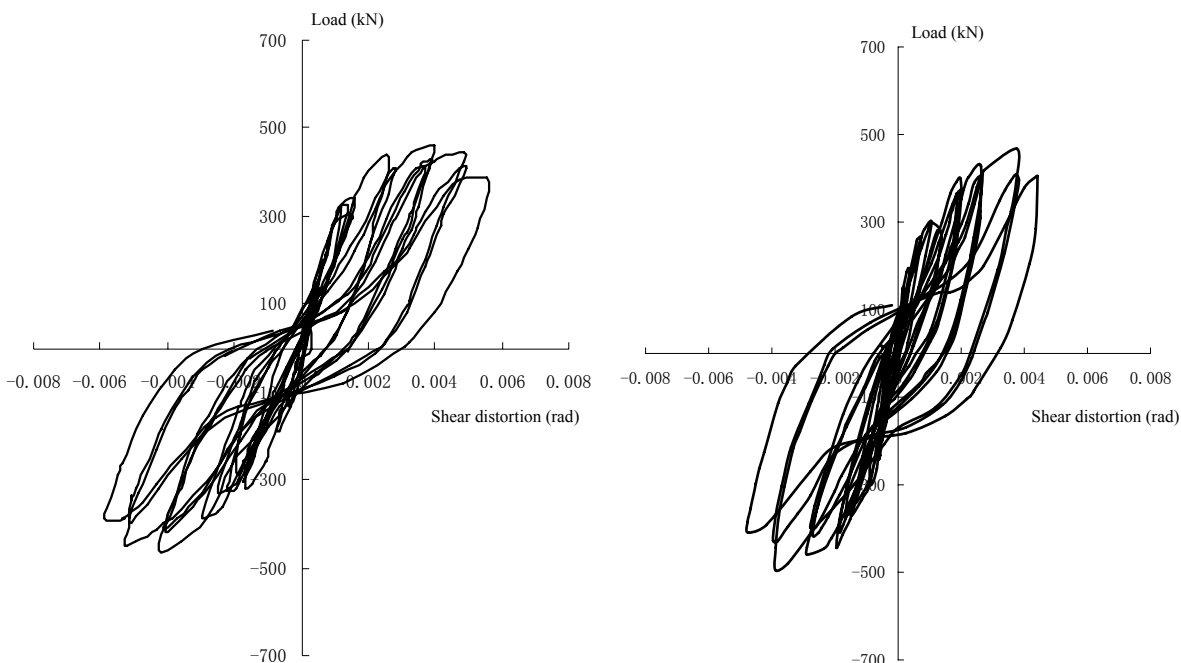
(c) Specimen LW-3   (d) Specimen LW-4
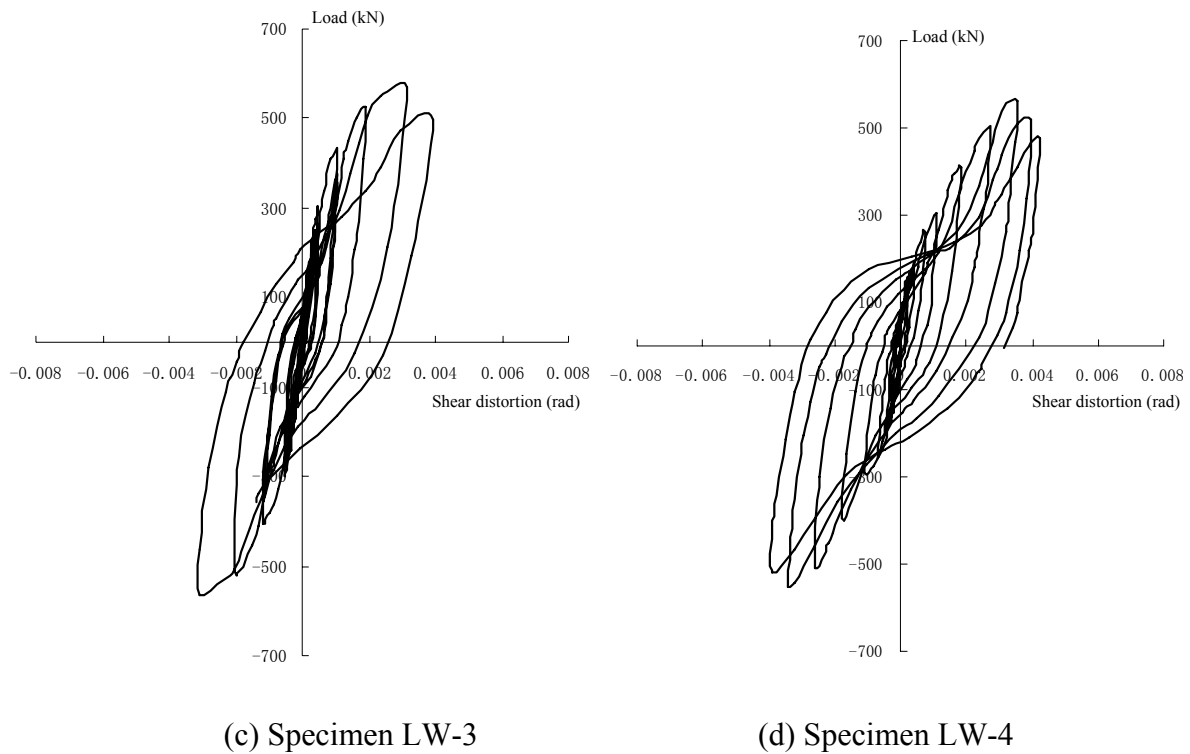
Fig.5-8 Shear distortion at base of four specimens

Because the amplitudes of the imposed displacements were not the same for corresponding loading cycles for the four walls, normalized parameters were used to compare the hysteric characteristics of the walls. For each loading cycle, the maximum ductility ratio, defined as the ratio of the maximum displacement during that cycle to the yield displacement, was calculated. The accumulated ductility ratio was then defined as the maximum ductility ratio for a given cycle plus the sum of the maximum ductility ratios in all previous cycles.

Fig.5-9 shows the relationship between shear distortions and accumulated ductility ratios for all the specimens at half cycle increments. At a given level of accumulated ductility, the shear distortion experienced by wall LW-1 is larger than that of wall LW-2. Moreover, wall LW-2 experiences nearly 1.5 times as much shear distortion as wall LW-3. This observation shows that diagonal web reinforcement contributes obviously to controlling the shear stiffness and increasing the amount of diagonal web reinforcement significantly decreased the shear distortion in the hinging region.

Specimen LW-4 experiences the shear distortion closing to wall LW-2 and wall LW-3, but less than that of wall LW-1. It means that the additional bidiagonal bars have the effect on the decrease of shear distortion also.
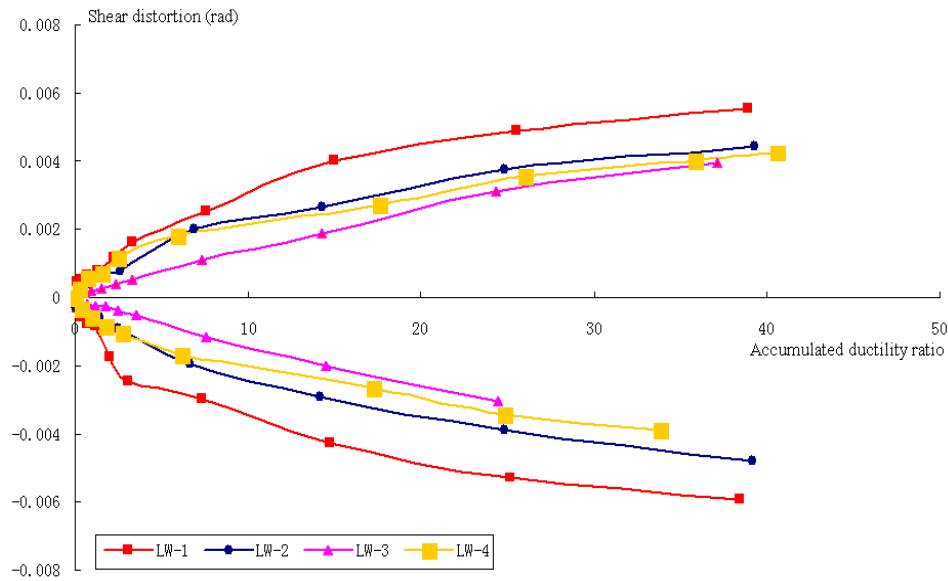
Fig.5-9 Variation of shear distortions at the base of walls with accumulated ductility ratios of four specimens

5.5 The relationships between applied load and the strains in reinforcing steels

Differences in the response of the test specimens may also be observed by considering the measured strains in the boundary elements and the web reinforcements. The locations of the representative strain gauges discussed in this section are shown in Fig.4-7 and Fig.4-8 respectively.

Because the test specimens suffered cyclic load, which decreased the bond force between lightweight concrete and reinforcing steel and induced slip between surfaces of their material, some strain gages pasted on reinforcements were failure by getting loose from reinforcing steels before failure of tested specimen. However, the load versus steel strain curves presented here (Fig.5-10 to Fig.5-13) were sufficient to explain the mechanical behavior of each tested specimen.

5.5.1 Strains in boundary element

Observations from curves in Fig.5-10(c), Fig.5-11(b), Fig.5-12(b) and Fig.5-13(d) have indicated that, reinforcing steels in boundary elements yielded at first and their strains continued to increase until the specimen's failure. It means that, cracks in the boundary elements were not closed completely in unloading stage and the boundary columns helped support shear force until wall's failure.

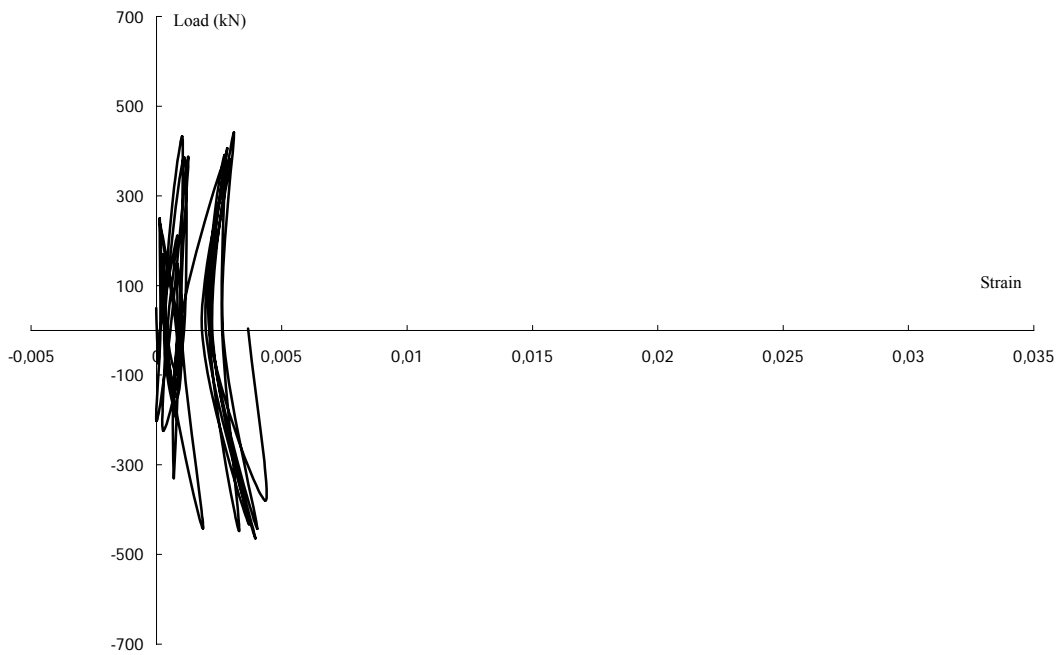## 5.5.2 Strains in web reinforcement

Measured strains in the vertical and horizontal web reinforcement in wall LW-1 are shown in Fig.5-10(a) and (b). Permanent tensile strains were observed in both the vertical and horizontal bars, but the maximum strains in vertical reinforcement were nearly an order of magnitude larger than in the horizontal bars. Yielding was observed at load of 350 kN for the vertical reinforcement and 447 kN for the horizontal bars. The same phenomenon was also observed in the vertical and horizontal bars of specimen LW-4, which indicated that, although there were additional bidiagonal steels, the conventional bars acted the same mechanism when subjected to horizontal shear load.

Measured strains in the diagonal reinforcement in wall LW-2 are shown in Fig.5-11(a). The diagonal web reinforcement yielded in tension at load level of 400 kN and remained in tension throughout the remainder of the loading history. Fig.5-12(a) shows the strain development in the diagonal reinforcement of specimen LW-3. It exhibited the same development rule as wall LW-2. The diagonal bar yielded at load level of 400 kN and then its strain increased quickly until ultimate strain of 0.026.

Fig.5-13(a, b and c) shows the strain developments in the reinforcements of specimen LW-4. The additional bidiagonal steel yielded after the yielding of longitudinal reinforcement in boundary element (in Fig.5-13(c)). In the positive and negative load level, it acted as tensile bar and compressive bar alternately.

Results from LW-2, LW-3 and LW-4 have indicated that reinforcing steels in diagonal direction have not only tensile strains. The compressive strains were also observed in reinforcing steels in diagonal direction, which demonstrated that reinforcing steels in diagonal direction can be used helpfully for compressive struts to transferring shear force into foundation of walls.
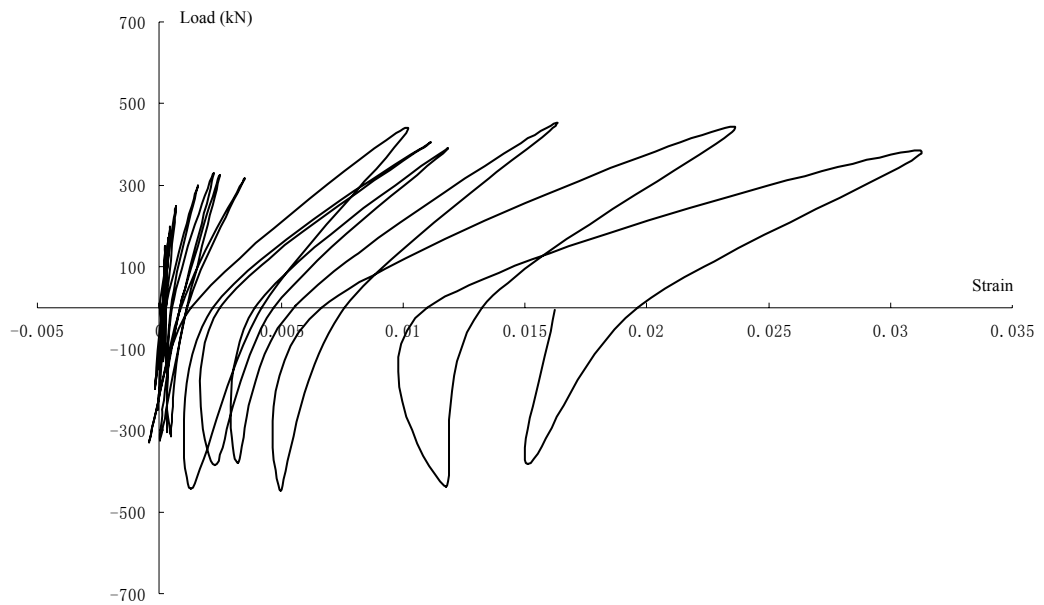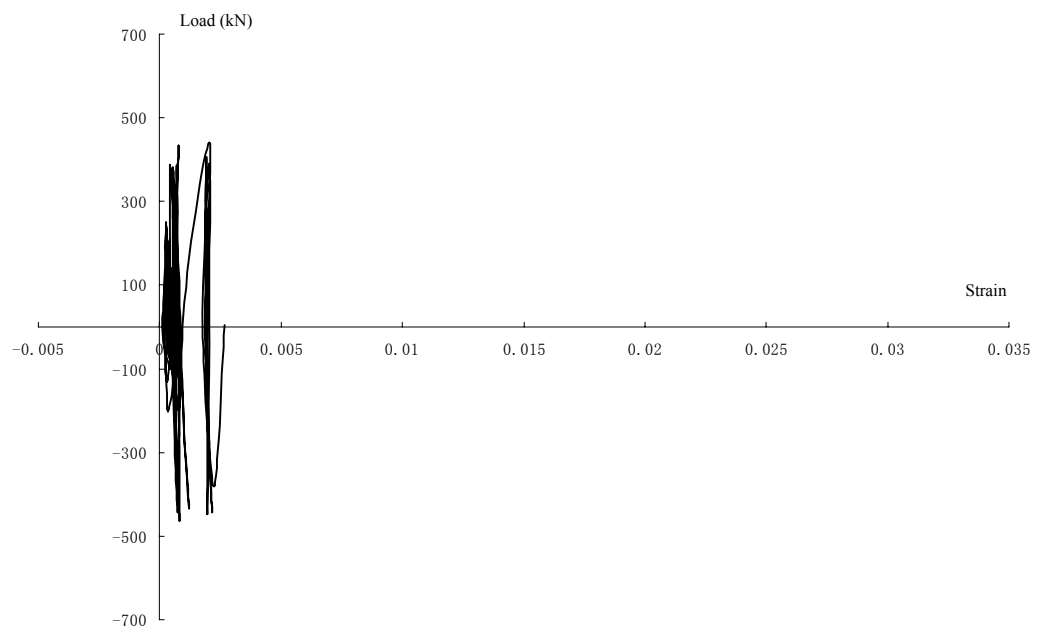
Load vs. Strain of Reinforcing Bar in Web (S1)
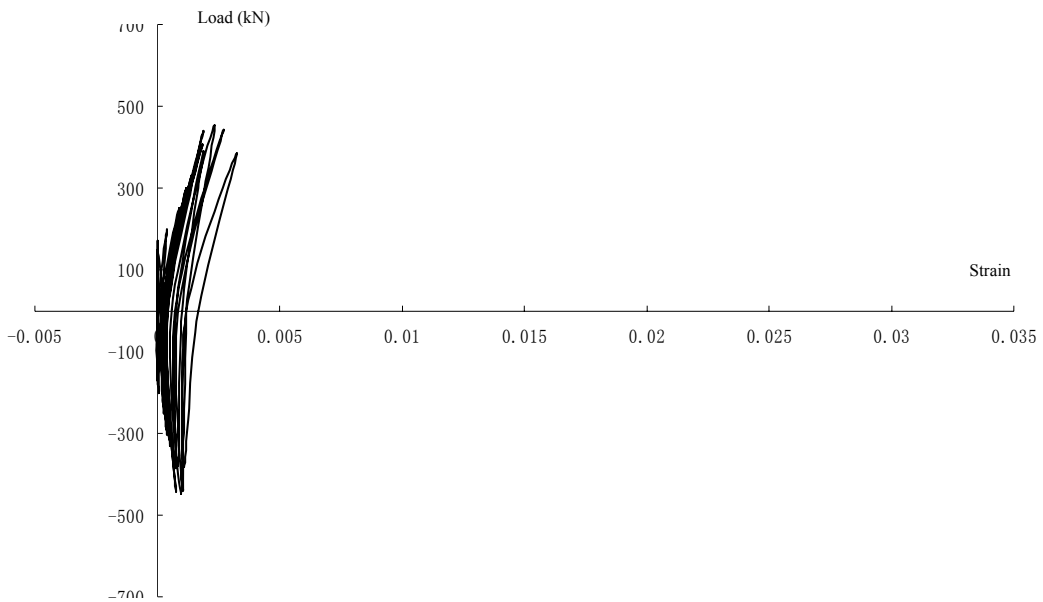
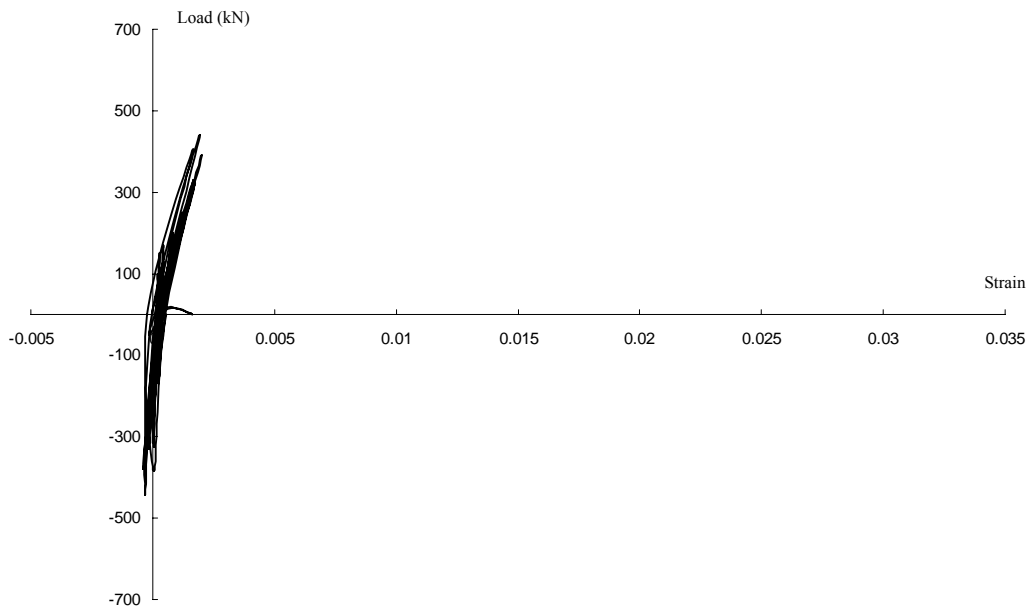*Load vs. Strain of Reinforcing Bar in Web (S2)*

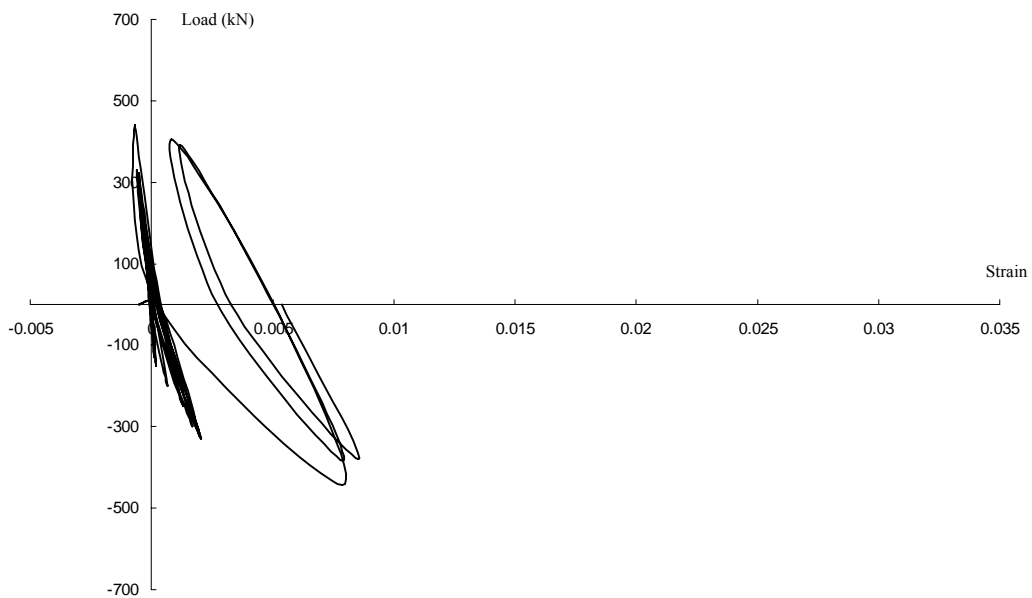(a)   in horizontal web reinforcement

Load vs. Strain of Reinforcing Bar in Web (S5)

Load vs. Strain of Reinforcing Bar in Web (S6)

(b)   in vertical web reinforcement

Load vs. Strain of Reinforcing Bar in BE. (S8)

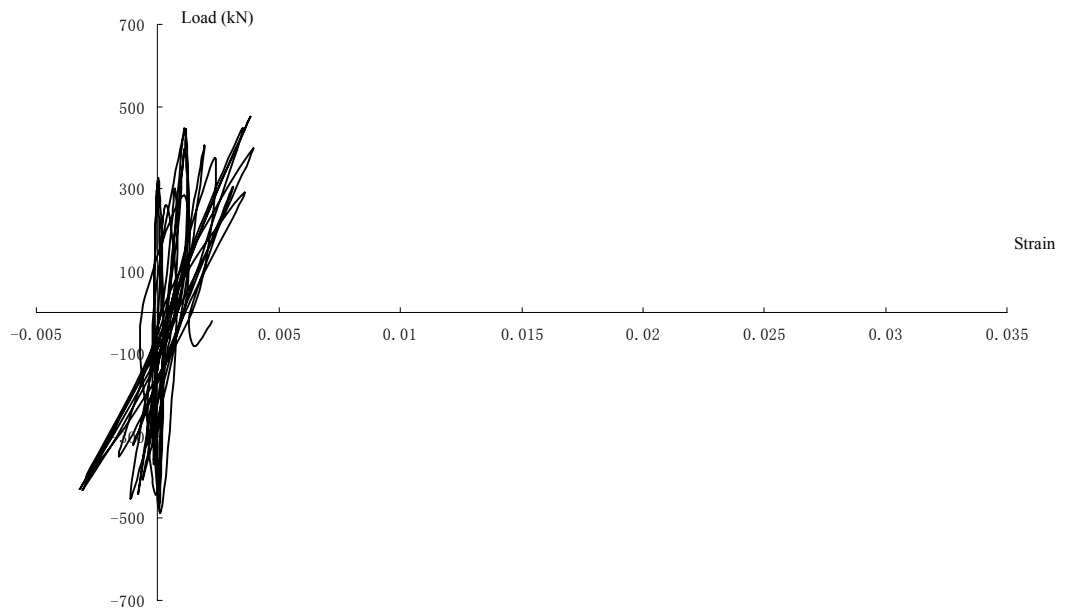*Load vs. Strain of Reinforcing Bar in BE. (S11)*

(c) in boundary element

Fig.5-10 Measured strains of specimen LW-1

Load vs. Strain of Reinforcing Bar in Web (S2)

Load vs. Strain of Reinforcing Bar in Web (S3)

Load vs. Strain of Reinforcing Bar in Web (S5)

Load vs. Strain of Reinforcing Bar in Web (S6)

(a) in diagonal web reinforcement
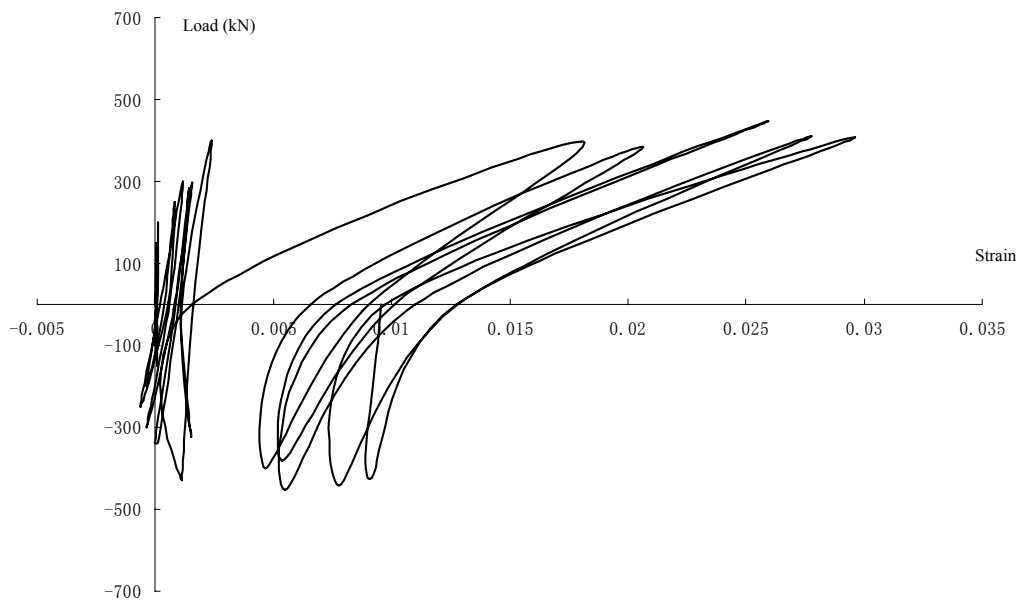
Load vs. Strain of Reinforcing Bar in BE (S7)

Load vs. Strain of Reinforcing Bar in BE (S12)
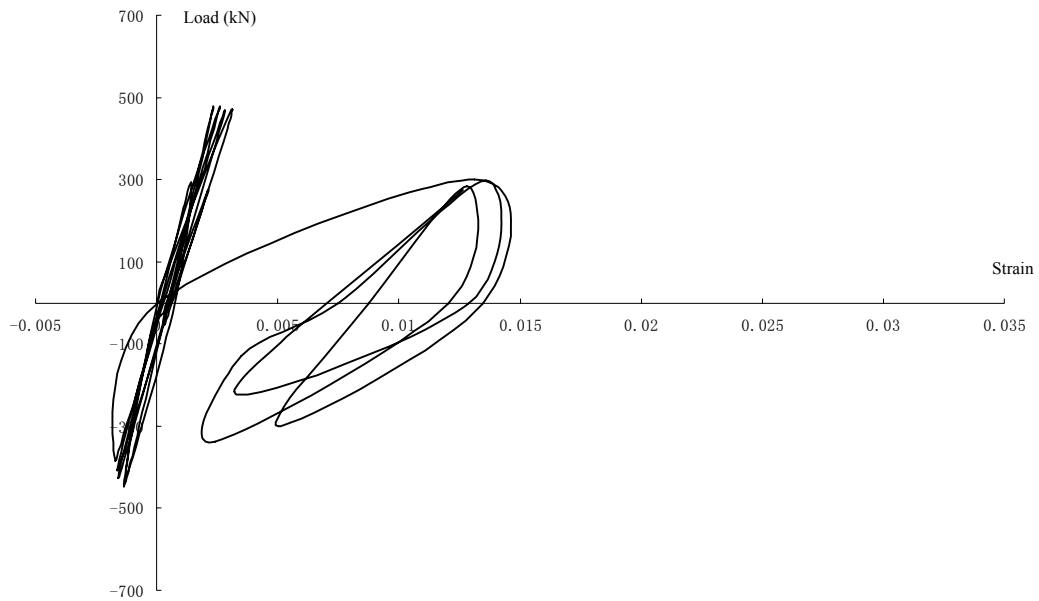

(b) in boundary element

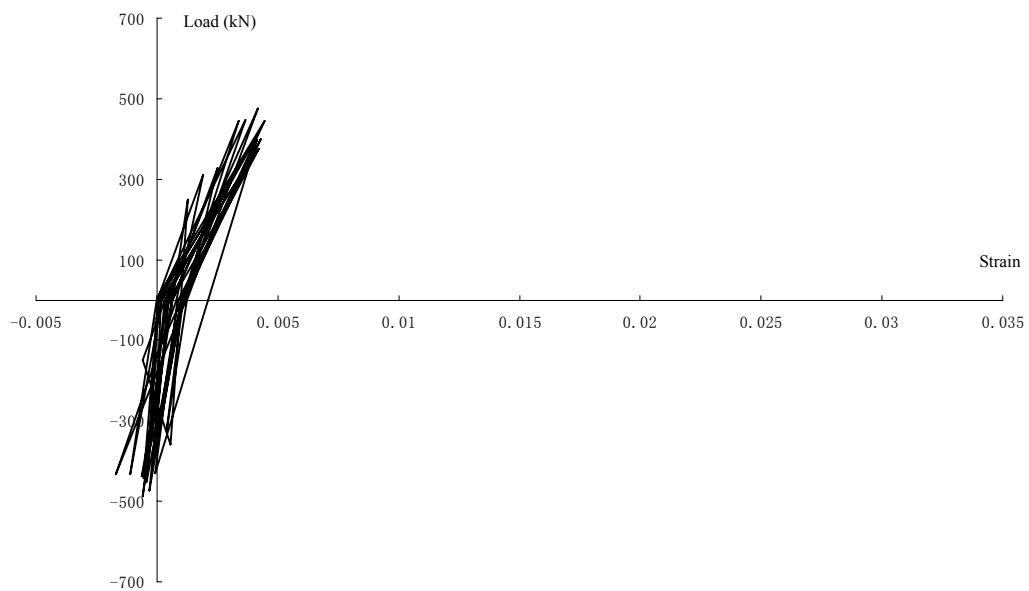**Fig.5-11 Measured strains of specimen LW-2**

Load vs. Strain of Reinforcing Bar in Web (S1)

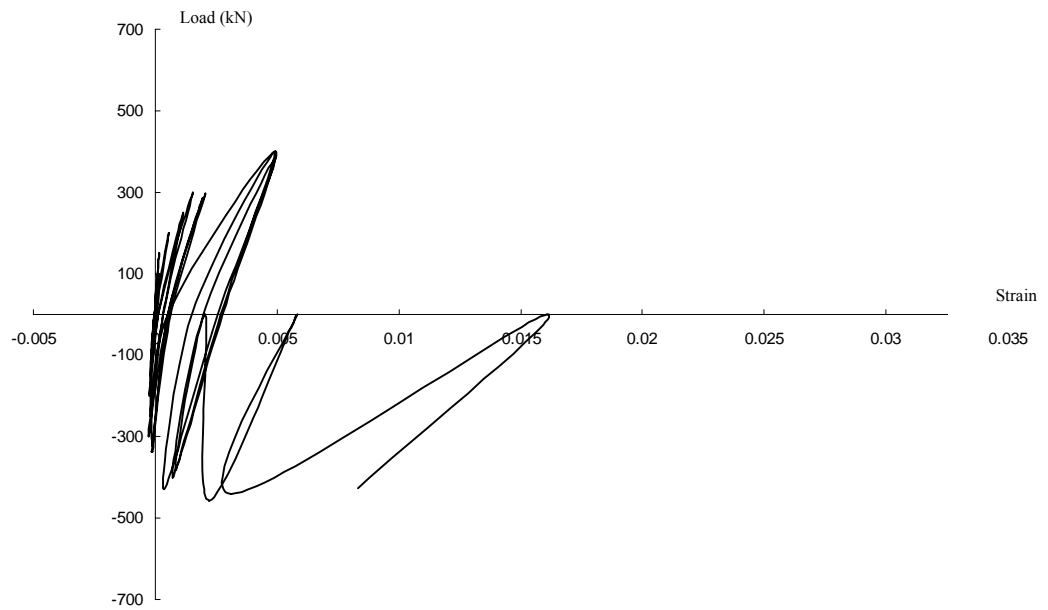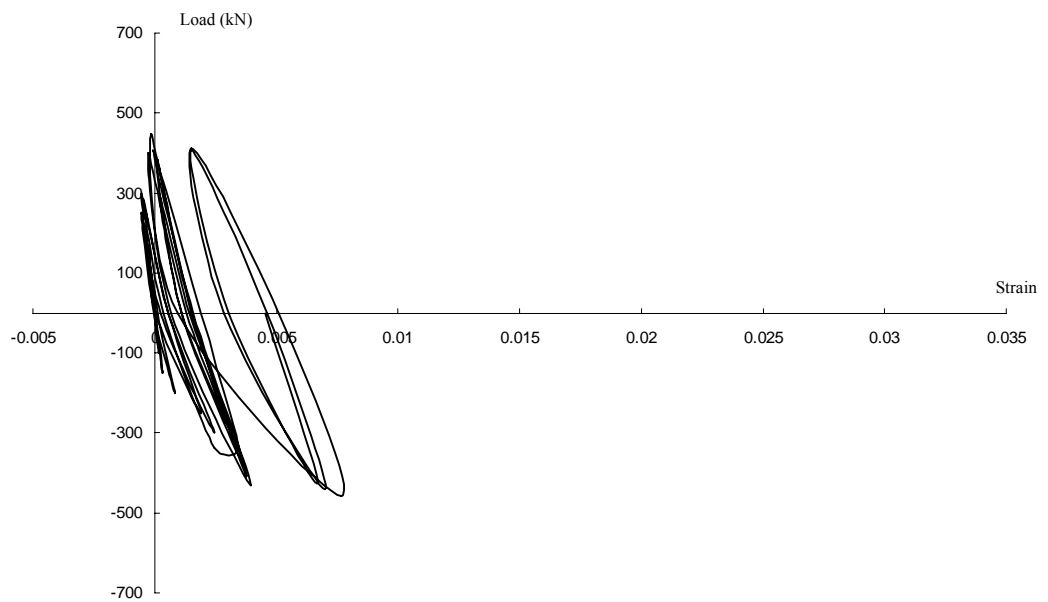*Load vs. Strain of Reinforcing Bar in Web (S4)*

Load vs. Strain of Reinforcing Bar in Web (S5)

Load vs. Strain of Reinforcing Bar in Web (S8)

(a) in diagonal web reinforcement

Load vs. Strain of Reinforcing Bar in BE (S23)
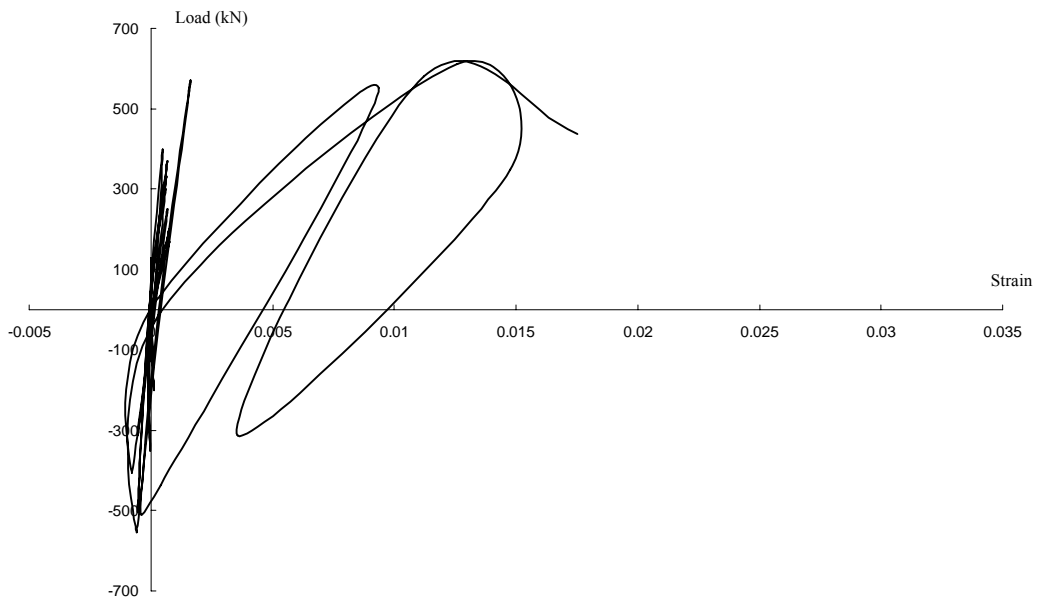
Load vs. Strain of Reinforcing Bar in BE (S26)
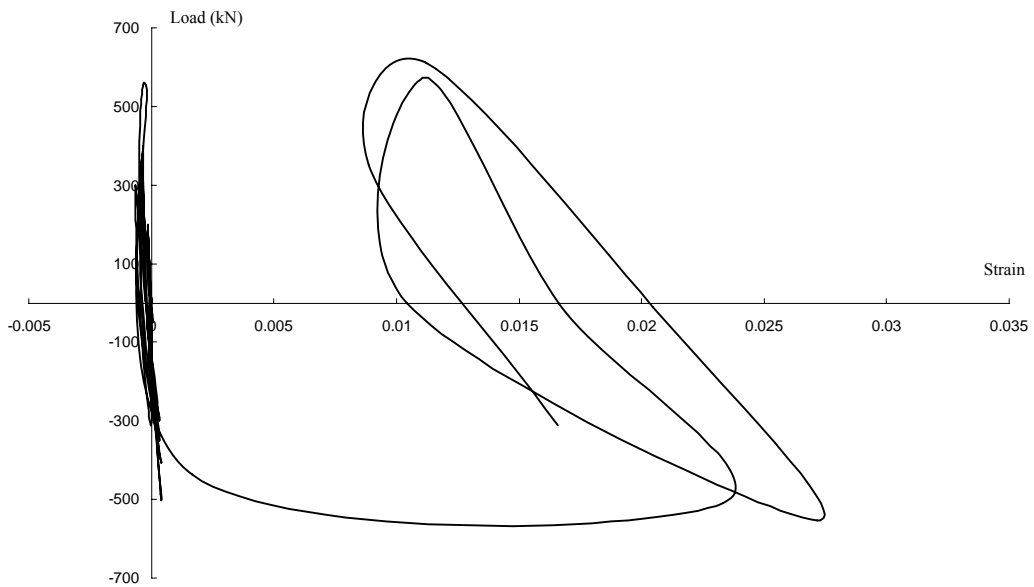
(b) in boundary element

Fig.5-12 Measured strains of specimen LW-3

Load vs. Strain of Reinforcing Bar in Web (S1)
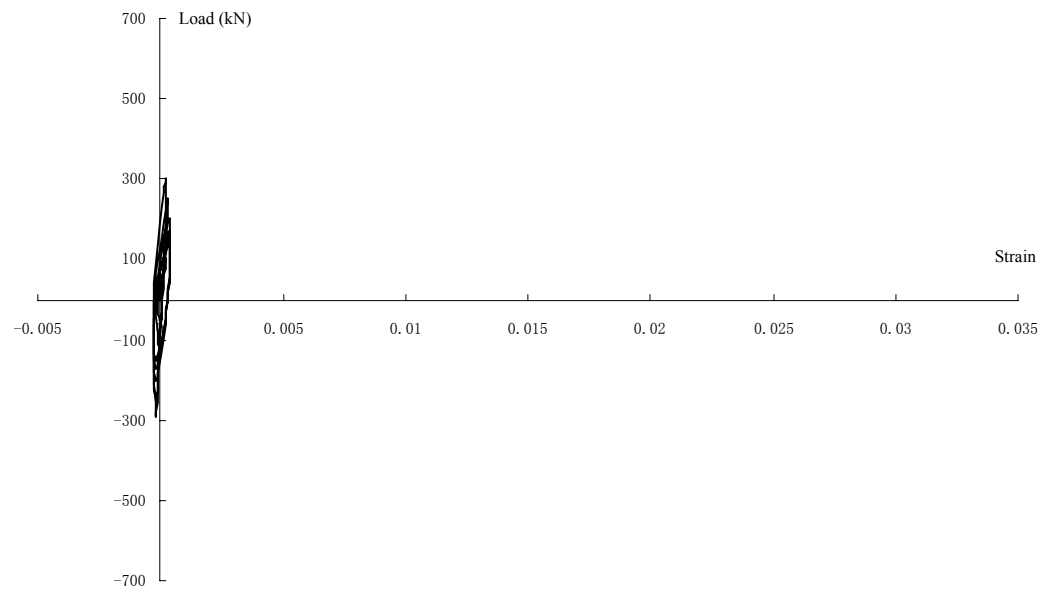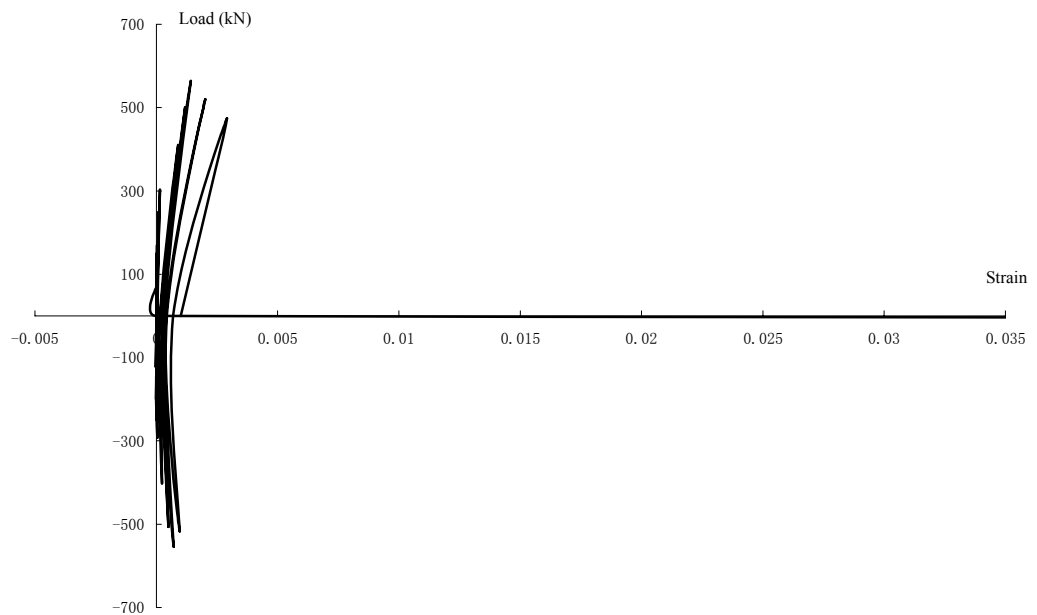
Load vs. Strain of Reinforcing Bar in Web (S2)

(a) in horizontal web reinforcement

Load vs. Strain of Reinforcing Bar in Web (S5)
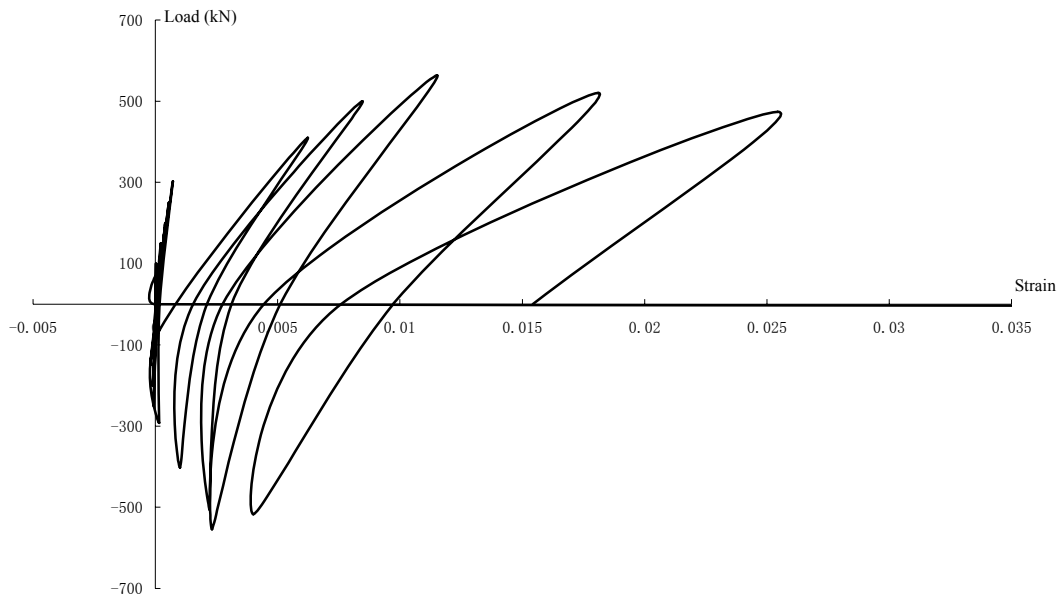
Load vs. Strain of Reinforcing Bar in Web (S8)
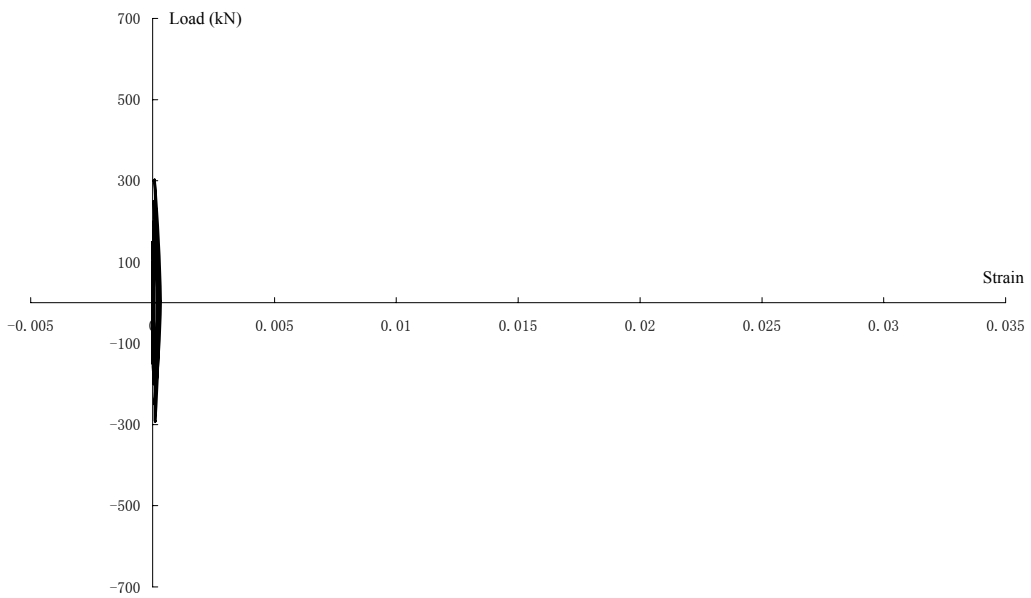
(b) in vertical web reinforcement

Load vs. Strain of Reinforcing Bar in Web (S13)
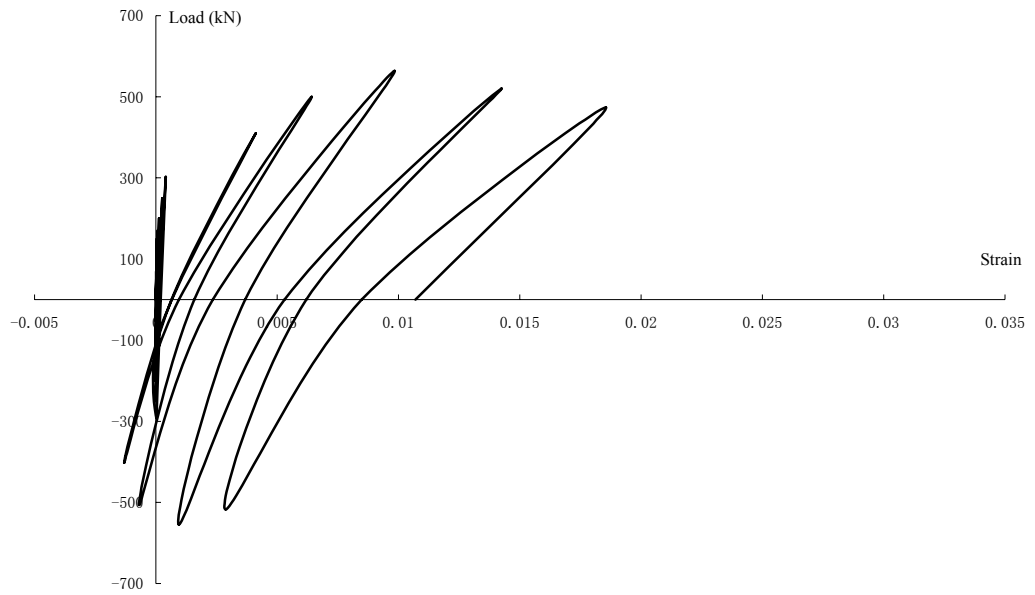
Load vs. Strain of Reinforcing Bar in Web (S14)
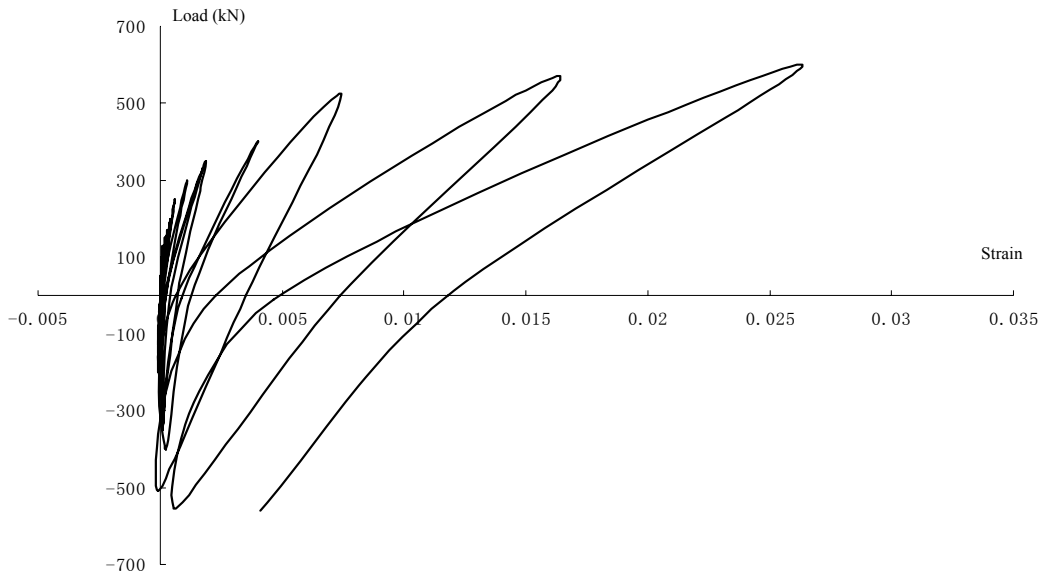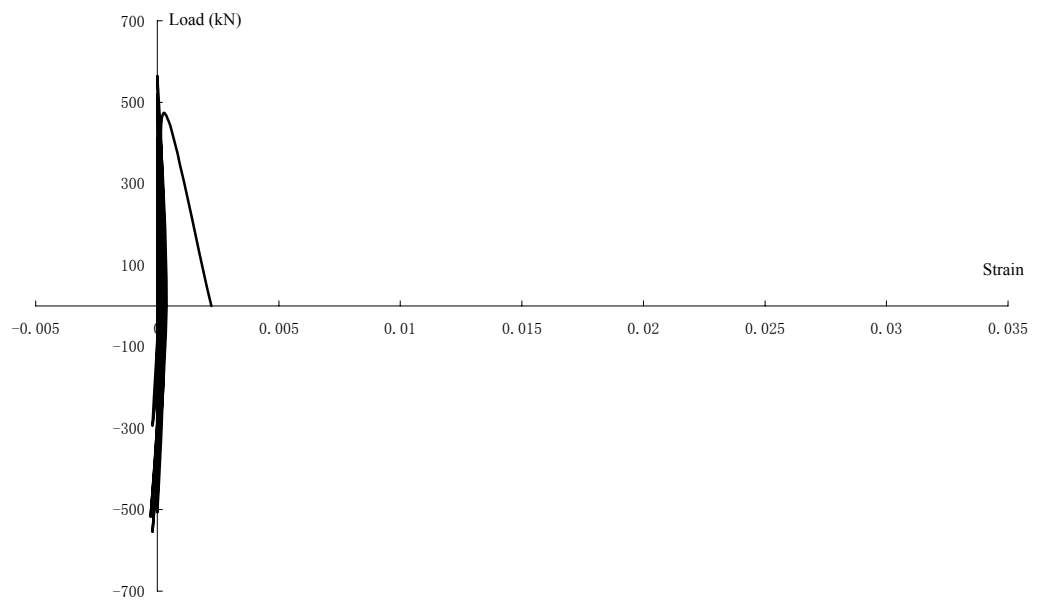

(c) in bidiagonal web reinforcement

Load vs. Strain of Reinforcing Bar in BE. (S21)
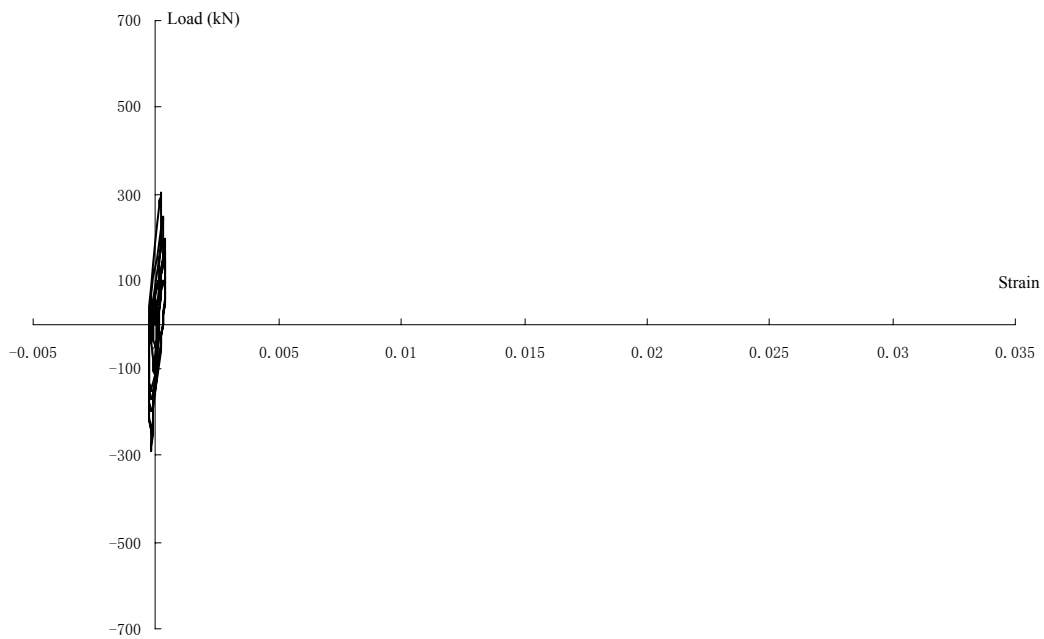
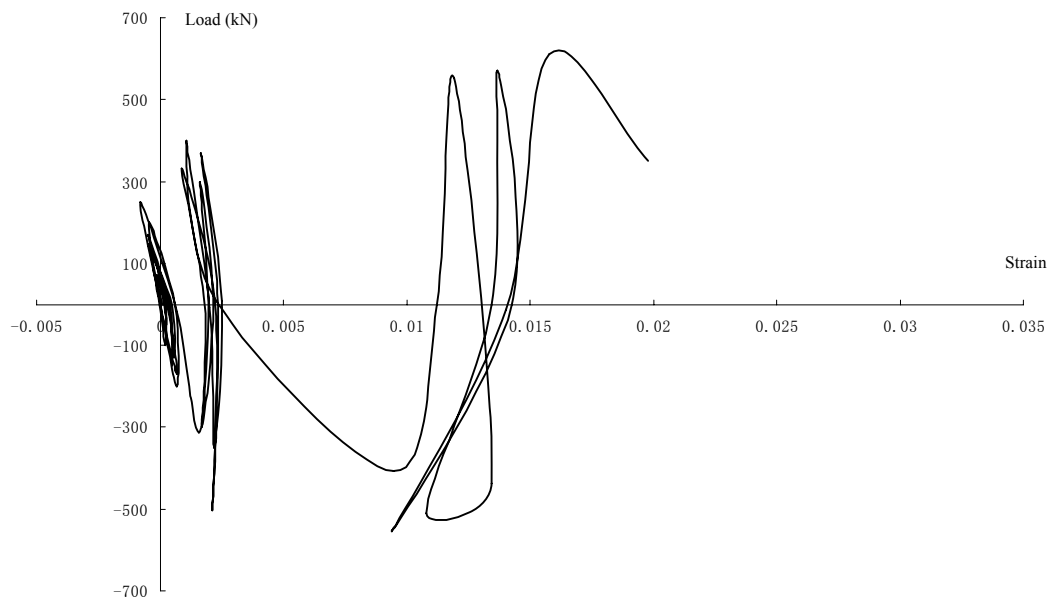

Load vs. Strain of Reinforcing Bar in BE. (S26)
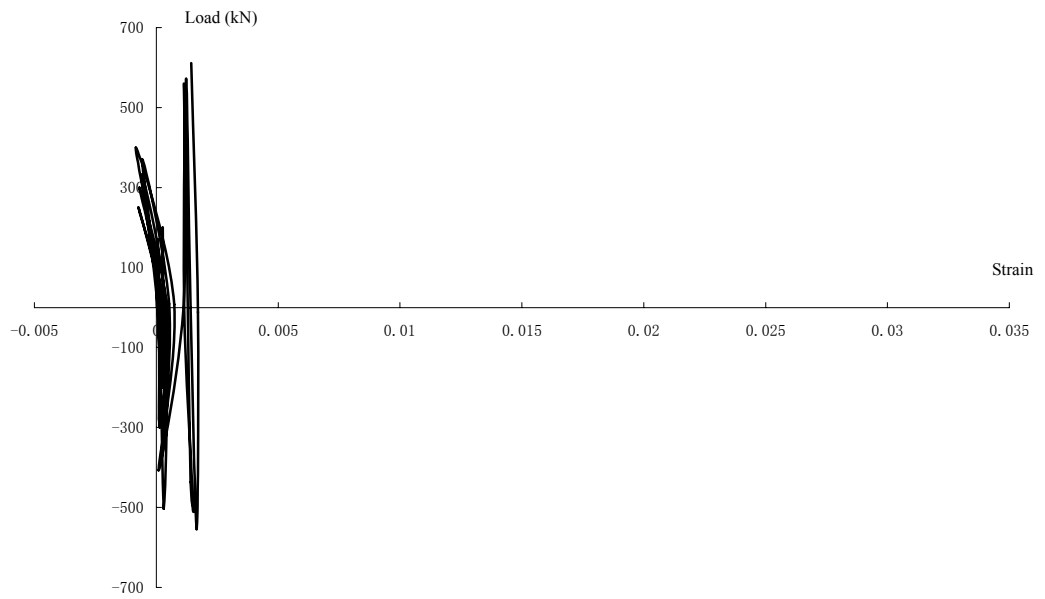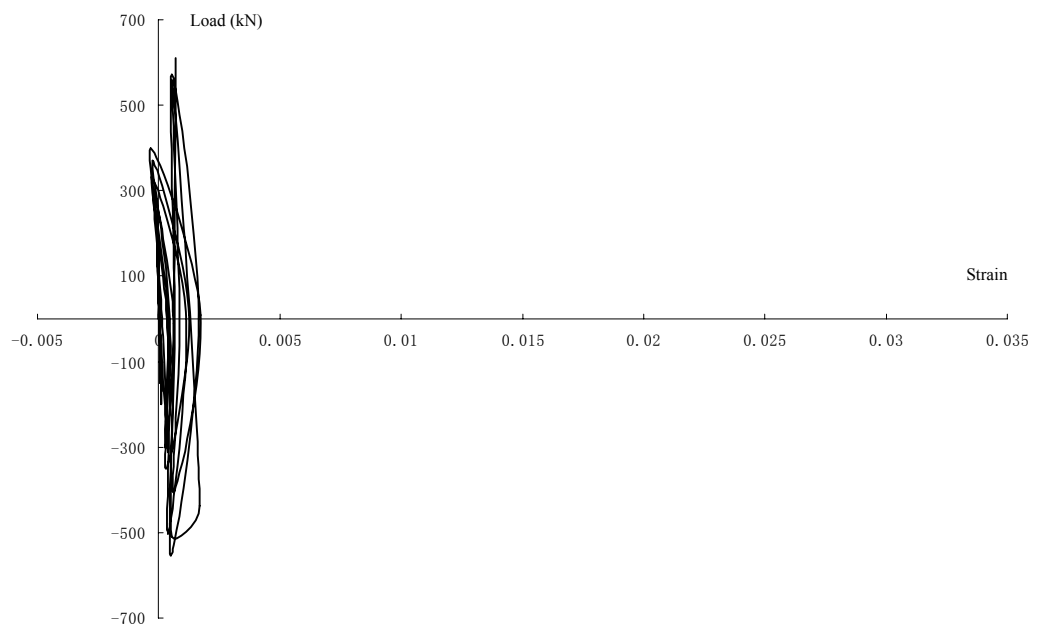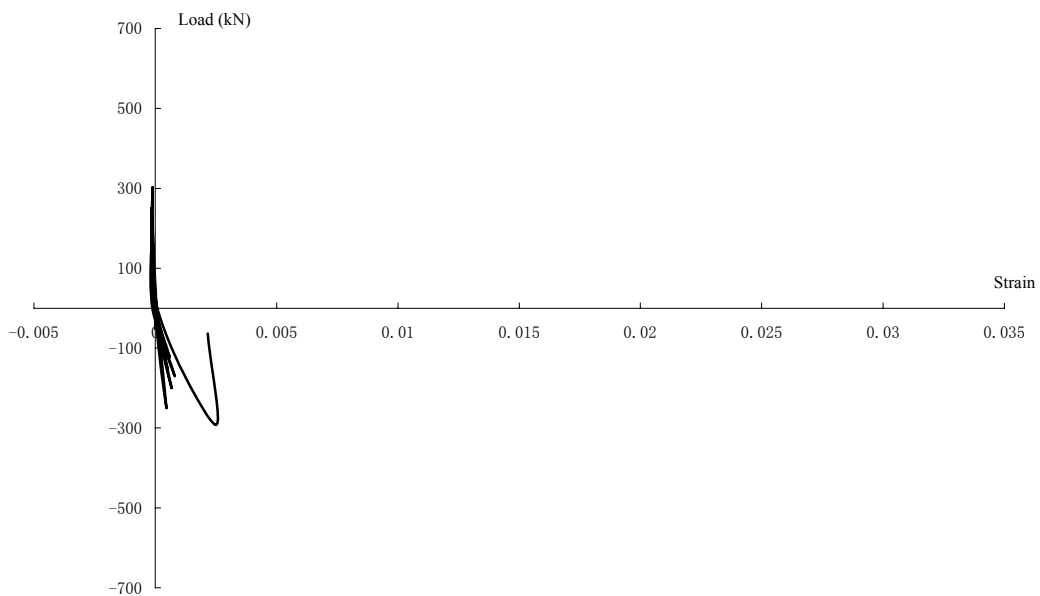

(d) in boundary element

Fig.5-13 Measured strains of specimen LW-4

5.6 Strains in concrete at base of walls

Taking the distance from every concrete strain gauge to the midline of the web wall as X axis and the strains of concrete measured by every strain gauge at each load level as Y axis, Fig.5-14 provides the distribution of concrete strains at the base of four specimens before concrete cracking. The locations of the representative strain gauges discussed in this section are shown in Fig.4-9.
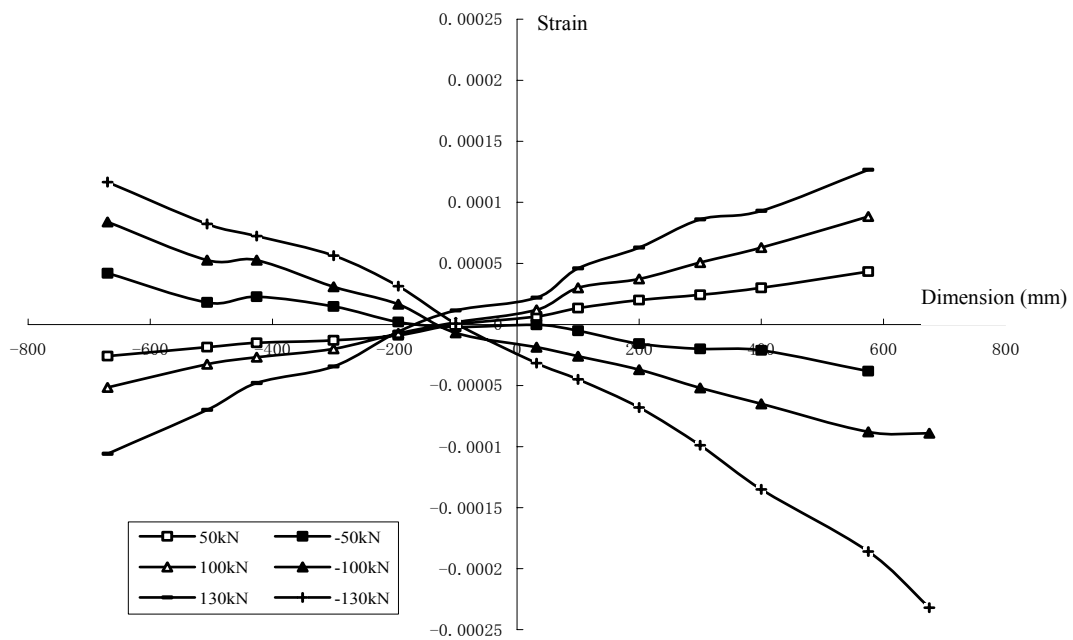
(a) Specimen LW-1
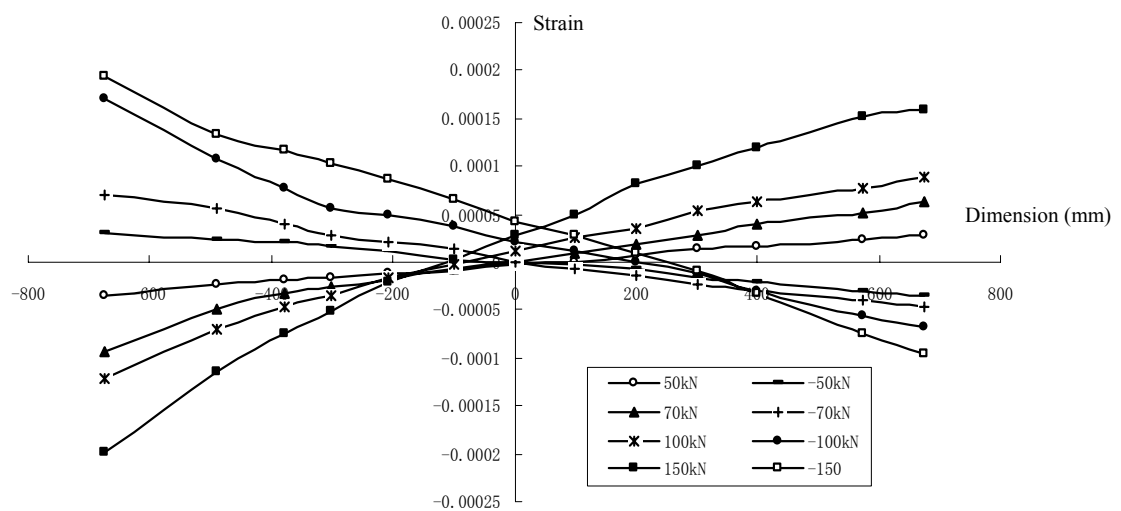
(b) Specimen LW-2
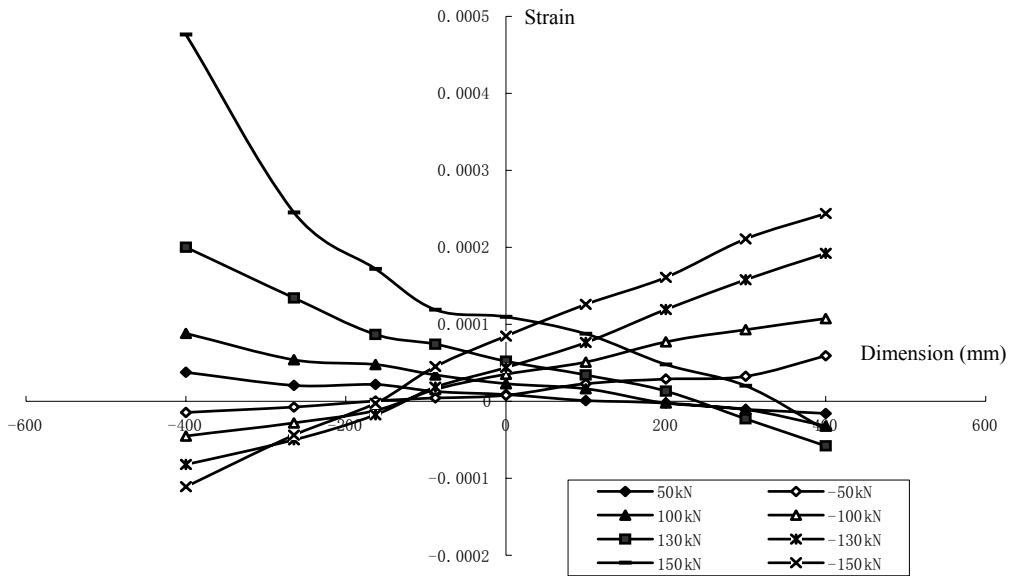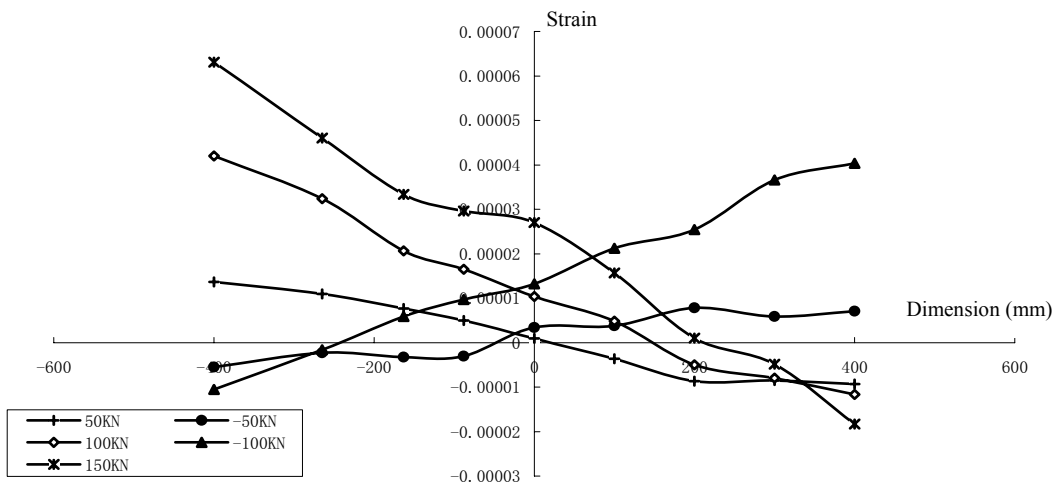
(c) Specimen LW-3

(d) Specimen LW-4

Fig.5-14 Concrete strains at the base of four specimens

It can be noticed that, at every load level before concrete cracking, the concrete strain distribution of every cross section accorded with plane cross section assumption. With the increase of the horizontal load, the neutral axis of the wall moved from the middle of the web to compressive zone. So that four specimens can be calculated as elastic bodies before concrete cracking. However, after concrete cracking, there were extinct changes in concrete strains of every cross section and never behaved as plane cross section assumption, which means that internal strain redistribution occurred in the specimens due to the rigidity variation in column and web panel after cracking.

5.7 Deflection shape

Taking the lateral deflection measured by every LVDT at each load level as X axis and the height of LVDT for measuring lateral deflection as Y axis, Fig.5-15 provides the deflection shapes of four specimens.

(a) Specimen LW-1

(b) Specimen LW-2

(c) Specimen LW-3

(d) Specimen LW-4
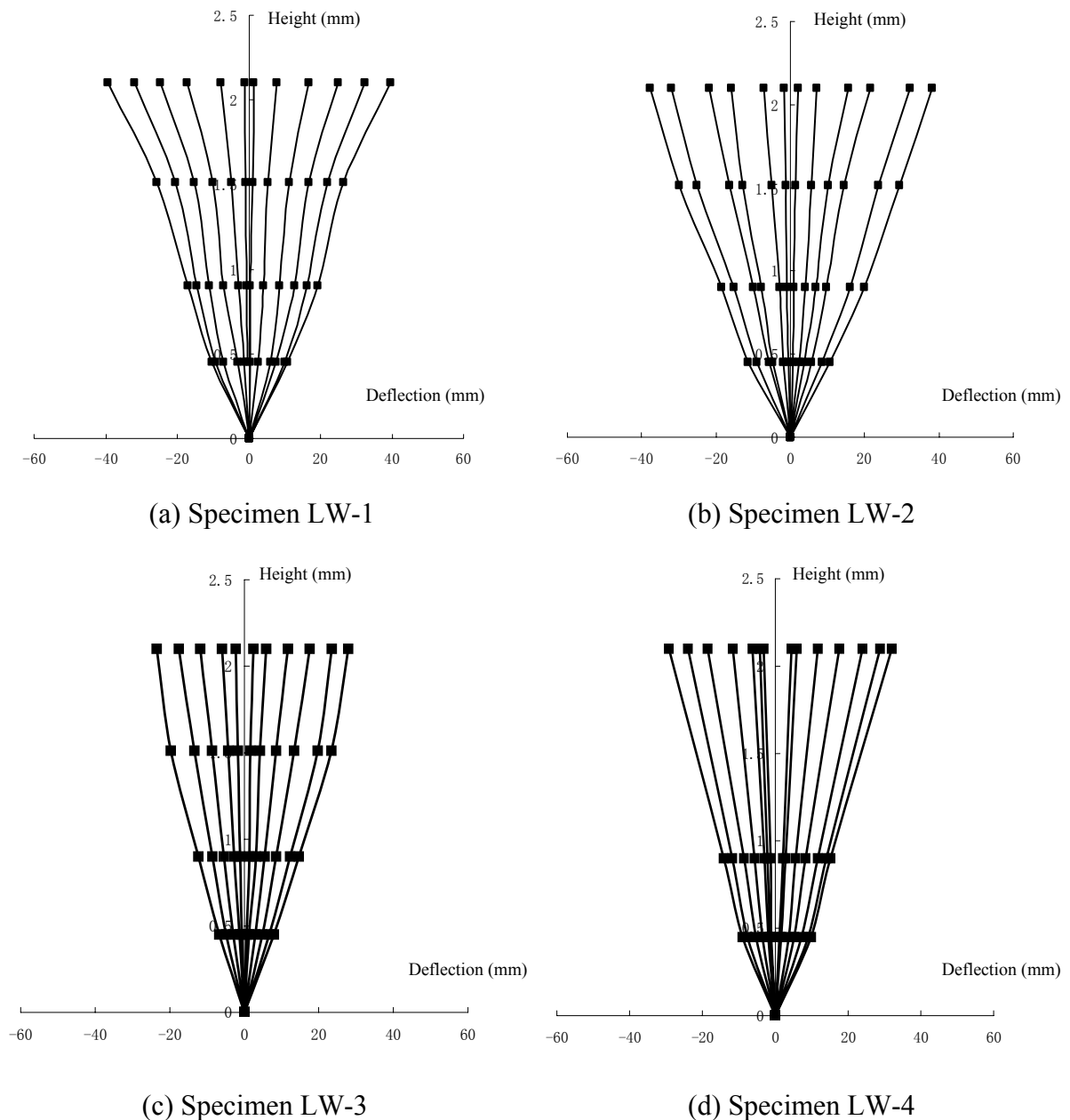
Fig.5-15 Deflection shapes of four specimens

5.8 Rigidity attenuation

Dividing the summation of absolute values of positive and negative peak horizontal load in each cycle by the summation of corresponding absolute values of positive and negative horizontal top displacement, the result can be defined as the shear rigidity in each cycle (K_i, i means the loading cycle number). K_0 denote the initial shear rigidity of specimen. The K_i/K_0

versus horizontal top displacement curves of four specimens in this test are shown in Fig.5-16.

It can be seen that the rigidity attenuation of each shear wall reduced with the increase of top displacement. The shear rigidity reduced rapidly along with the concrete cracking and specimen yielding and slowly prior to complete failure. The rigidity attenuation was mainly induced by the plastic property of the shear wall after its yielding and accumulated damage, which includes cracks occurring and development, yielding and plastic behaviour of reinforcement and the slide between concrete and reinforcements. Comparison of the curve of specimen LW-1 with that of LW-2 shows that, diagonal web reinforcement resulted in relatively slow rigidity attenuation. Increasing the amount of diagonal web reinforcement, just like in specimen LW-3, can significantly increase the shear rigidity attenuation. Specimen LW-4 behaved similar to specimen LW-3 in lightening the shear rigidity attenuation. This can also be proved in the crack pattern of specimen LW-3 and LW-4, which have fewer and narrower cracks in the web of the wall to keep a better state to sustain shear force.
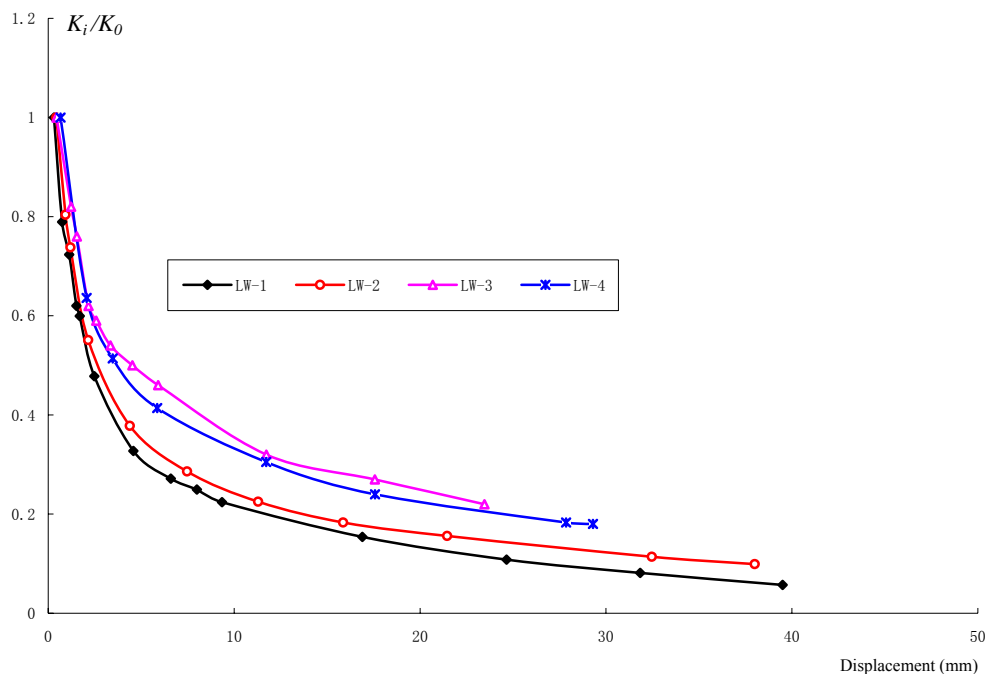
Fig.5-16 The rigidity attenuation of four specimens

5.9 Energy dissipation capacity

To survive a severe earthquake, structural walls must be able to dissipate energy. The energy dissipation mechanisms in a given wall depend on the inelastic behavior of the materials and the orientation of the reinforcement. Walls with conventional web reinforcement transfer shear through compressive struts and aggregate interlock within the concrete and dowel action of the web reinforcement. These mechanisms degrade when subjected to cyclic deformations. In contrast walls with diagonal web reinforcement transfer shear through tensile forces in the web reinforcement. This energy dissipation mechanism was stable and did not degrade with cycling during the tests. Therefore, walls with diagonal web reinforcement exhibit better energy dissipation characteristics than walls with conventional reinforcement.

The accumulated energy dissipation was used in this investigation to compare quantitatively the behavior of the walls. The energy dissipated by wall in one load cycle was defined as the area enclosed by the overall hyeteresis curve of each cycle. So that the accumulated energy dissipation was calculated as the sum of the area enclosed by all previous hysteresis loops. The relationship between the accumulated energy dissipation and the accumulated ductility ratio for four specimens is plotted in Fig.5-17.

The rate of increase was considerably higher for the walls with diagonal web reinforcement, which indicated their ability to dissipate more energy at a given level of distortion. This confirms the qualitative observations based on the shape of the hysteresis curves.
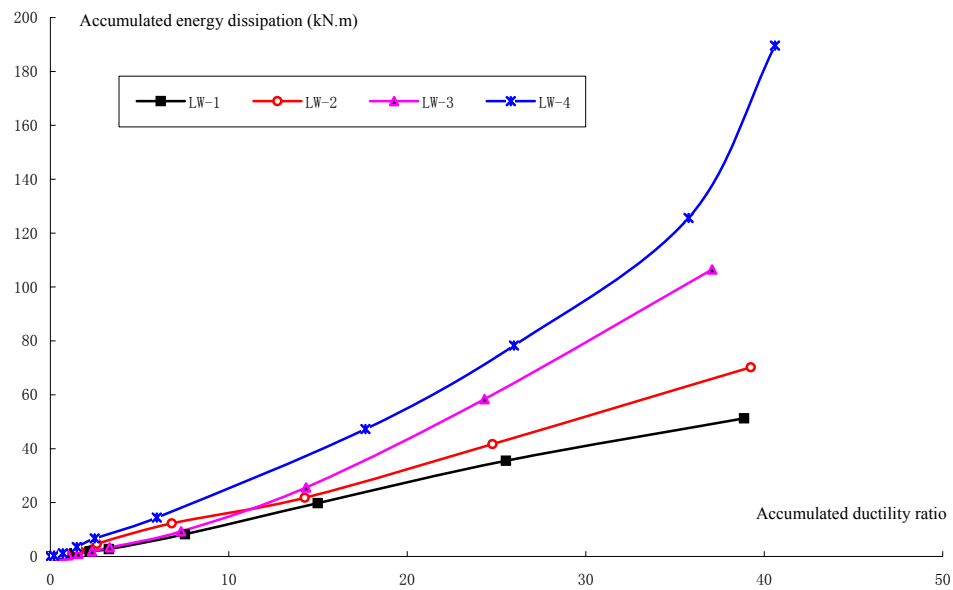
Fig.5-17 Variation of accumulated energy dissipation with accumulated ductility ratio of four specimens

Chapter 6

Analytical Model
of Test Specimens

6.1 Introduction

In the last decades, lightweight reinforced concrete shear walls have been used for reducible dead load of reinforced concrete structural members. However, further research work is needed to explore the seismic behavior and the compute theory of this system. Due to the financial and the time reason, it is not enough that only getting the results from experiments. Finite element method supplied a new way to study the strengthened members by computer, which can help the researcher to analyze and complete the experimental results and have a better understanding of it.

The finite element method is a powerful structural analysis tool that has been widely used in many different types of problems. The strength of the finite element method is based primarily on its fundamental concept of discretization, which models a structure as an assemblage of several finite elements. This concept simplifies the modeling of complex structure and allows the formulation of the problem to be written in a matrix form, which is appropriate to be incorporated into computer programs. The concept of descretization is also useful for the study of problems with material and geometric nonlinearities, because it allows a variety of material and element models to be installed at the element level. Finite element users can select or develop the material and the element models that have the proper kinematics and constitutive relationships for the problems under study. As a result, with the proper material and element models for concrete and reinforcing steel, the finite element method can be a very powerful analytical tool for studying the behavior of reinforced concrete structures.

The accurate prediction of the behavior of the structure during earthquake excitation depends on the development of reliable analytical models of the critical regions. Analytical models for RC structures have generally been based on replacing the reinforced concrete composite continuum by an assembly of finite elements representing the concrete and the steel

reinforcement. These models should be able to reflect the behavior of concrete in tension and compression, the response of the reinforcing bars and their interaction with the concrete Hence, a realistic stress-strain relationship for both concrete and steel bars and a failure theory are required to obtain basic information through an analytical model of the structure.

Several approaches for defining the stress-strain behavior of the concrete under various stress states are available, namely, nonlinear elasticity, plasticity based model, plastic fracturing theory and end chronic theory of plasticity. However, by using the finite element method and performing a nonlinear analysis with appropriate constitutive relations, deformational and failure characteristics of reinforced concrete structures can be accurately predicted.

Basically, the nonlinear response is caused by two major material effects, cracking of the concrete and plasticity of the reinforcement and of the compression concrete. Other time–independent effects arise from the nonlinear action of the individual constituents of reinforced concrete, such as bond slip between steel and concrete, aggregate interlock of a cracked concrete and dowel action of reinforcing steel. The time dependent effects such as creep, shrinkage, and temperature change also contribute to the nonlinear response. In this study, only the time-independent material nonlinearities (cracking and plasticity) will be considered in the nonlinear analysis of the specimens.

The implementation of nonlinear constitutive relations in finite element analysis codes is generally undertaken in one of two ways. In the first case the material behavior is programmed independently of the elements. Using this approach the choice of elements for a particular structural system is not limited and best practice modeling techniques can be used in identifying an appropriate element type to which any of the nonlinear material properties are assigned. This is the most adaptable approach and does not limit the analyst to specific element types in configuring the problem of interest. In spite of this, however, following the second approach, certain software developers provide specific nonlinear material capabilities only for dedicated element types. ANSYS provides a dedicated three-dimensional eight node solid isoparametric element, SOLID 65, to model the nonlinear response of brittle materials based on a constitutive model for the triaxial behaviour of concrete after Williams and Warnke [Will75].

In this chapter, a brief review of the previous work in the finite element analysis of reinforced concrete is presented. This review emphasizes three areas related to the major objectives of this investigation: the finite element analysis of shear wall, the cyclic response of reinforced concrete members and the applications of the finite element method. A non-linear finite element analysis on seismic behavior of lightweight reinforced concrete shear wall by ANSYS 8.0 is presented.

6.2 Literature review

6.2.1 Overview

The earliest publication of the finite element analysis of reinforced concrete was written by Ngo and Scordelis [Baz79] in 1967. In this paper, simply supported reinforced concrete beams with predefined cracks were analyzed using the finite element method. Since then, a large number of works on the finite element analysis of reinforced concrete have been published. Due to the computational effort required in the analysis and the lack of knowledge

concerning the behavior of concrete in a three-dimensional state of stress [Tas82], most of the early investigators limited their work to two-dimensional plane stress problems and used the finite element method to investigate the behavior of reinforced concrete beams tested in laboratories [Sit93]. Jofriet and McNiece [Jof71] used the finite element method to study behavior of reinforced concrete slabs by using plate bending element and a modified stiffness approach. Subsequently, several other research successfully used plate and shell elements to investigate the behavior of slabs and reinforced concrete shell structures.

Suidan and Schnobrich [Sui73] used three-dimensional isoperimetric elements to model reinforced concrete beams. Meyer and Bathe [Mey82] used three-dimensional elements and shell elements to model reinforced concrete nuclear reactor that were subjected to internal pressure and temperature loadings. Bathe and Ramaswamy [Bat79] used the three-dimensional finite element to analyze prestressed concrete reactor vessels. Richard, Cheng-Tzu and Ali [Ric04] used three-dimensional to analyze concrete columns for biaxial bending. Susanto, Yu and Chee-Kiong [Che05] also used three-dimensional continuum model to analyze concrete slabs using shell element with assumed strain. The extensive summary of the previous work in the finite element analysis of reinforced concrete can be found in the State-of-the-Art report published by the American Society of Civil Engineers [Tas82].

6.2.2 Previous work on reinforced concrete shear wall

During the past twenty years, some researchers used the finite element method to study the effects of different design parameters on the response of reinforced concrete members. In 1972, Yuzugullu [Yuz72] used the finite element method to study the monotonic behavior of a shear wall-frame system which was tested at the University of Tokyo. This research is one of the earliest attempts to model reinforced concrete shear walls by the finite element model. Aktan and Hanson [Akt80] analyzed the monotonic and cyclic responses of slender reinforced concrete shear walls by using a finite element model that separated the walls into sub regions. In each of the sub regions, the linear behavior was represented by elastic plane stress element, and the nonlinear behavior was represented by joint elements connected to the boundary of the sub region. Bolander and Wight [Bol89] [Bol91] developed the finite element program SNAC primarily for use as a tool to investigate the inelastic response of shear wall dominant buildings subjected to quasi-static loadings. Daniel and Frank [Dan04] also used provisional constitutive models, which are provided to show that the procedures employed are stable, compliant, and provide reasonably accurate simulations of behavior in reinforced concrete.

Ueda and Kawai [Ued85] conducted finite element analyses of reinforced concrete shear walls with different amounts of reinforcement and axial load. Mikame et al. [Mik89] used the finite element method to conduct an extensive parametric study of reinforced concrete shear walls. The parameters studied included reinforcement ration, axial stress, compressive strength of concrete, cross section of columns, and presence of openings. Massicotte et al. [Mas90] used the finite element method to analyze five reinforced concrete panels which were tested under axial and lateral loadings at the University of Alberta. The finite element analyses were then extended to investigate the behavior of twenty six reinforced concrete panels with different aspect ratios, thickness, amount of reinforcement, magnitudes of in-plane load, in-plane and rotational edge restraints, and the loading sequence. The analysis of last researchers, Daniel and Frank [Dan04], also indicated that two-dimensional analyses capture main features of behavior, but three-dimensional analyses are required to capture some important second-order mechanisms.

Research in the finite element analysis of reinforced concrete shear walls in Japan is much more active than in the U.S. Most of the shear wall research in Japan deals with the behavior of low-rise shear walls (height/length is less than 1.0), which represent the reinforced concrete walls used in the nuclear power plants. Yamaguchi and Nomura [Yam89] used the finite element method based on the plastic-fracture theory proposed by Bazant and Kim [Baz79] to analyze four reinforced concrete shear walls subjected to monotonic and cyclic loadings. Sotomura and Marazumi [Sot85] analyzed a series of reinforced concrete shear walls with openings by using a simple smeared crack model for concrete, and an elastic-plastic model for reinforcing steel. Inoue et al [Ino85] developed the reinforced concrete material model based on the results from Vecchio and Collins'panel test [Vec82], where thirty reinforced concrete panels subjected to different uniform stress conditions were tested, and used the model in the analysis of several shear walls that had different reinforcement ratios and different shear span ratios. In all these previous analyses of reinforced concrete walls, most of the reinforced concrete models were simple, and, regardless of the differences in the material and element models, most of the analytical results agreed with the experimental result.

6.2.3 Previous work on cyclic response of reinforced concrete

Although there was a large amount of research in the past three decades on the finite element analysis of reinforced concrete members, there were few studies on the behavior of reinforced concrete members subjected to cyclic loading. Some of the pioneer researchers who used finite element analysis to model the cyclic response of reinforced concrete members include Cervenka [Cer80], Cervenka and Gerstle [Cer71], Darwin and Pecknold [Dar76], Bergan and Holand [Ber79], Aktan and Hanson [Akt80], and Agrawal et al [Agr76]. Despite the promising results from some of these studies, none of these studies is truly successful in modeling the cyclic response of reinforced concrete members. This is due to the fact that the reinforced concrete members studied in all these analyses were subjected to only a few cycles of load reversals. As a result, the cyclic response of these reinforced concrete members did not demonstrate important hysteresis characteristics, such as the hinging effects in load vs. deflection curves, the effects of cyclic shear deformation, and the deterioration of concrete because of cyclic compressive loadings.

Two major obstacles that most researchers experienced in the development of cyclic models for reinforced concrete are the lack of understanding in the cyclic response of reinforced concrete and the numerical problems associated with complex rules for load reversals and stress-strain relationships in material models. In order to obtain a detailed understanding of the cyclic behavior of reinforced concrete element and to gather essential experimental data needed for the formulation of such behavior, Stevens et al [Ste87] conducted cyclic tests on three reinforced concrete panels. In these tests, two panels with different amounts of reinforcement were subjected to load reversals in pure shear, while one other panel was subjected to reversed cyclic shear combined with biaxial compression. The average stress-strain relationship for these panels was then used as a basis for the development of a material model for concrete. Two other researchers also used the results from these panel tests to verify their concrete models. Stevens et al. also proposed a concrete model based on the modified compression field theory. Xu [Xu91] proposed the model using a smeared non-orthogonal cracking approach, and Izumo et al [Izu89] developed the hysteresis constitutive law for reinforced concrete by combining several existing constitutive laws developed in Japan. The analytical results at the element level (a finite element model consist of one element) of these three models agreed well with the results of the panel tests.

However, because of the complexities of these models, numerical problems usually occurred in the analysis of problems at the structural level (a finite element model consist of several element) and, hence, prevented the completion of most analyses. Such problems greatly reduced the usefulness of these models. In the numerical model for simulating the nonlinear response of reinforced concrete shear walls subject to cyclic loadings by Kwak and Kim [Kwa04], the material behavior of cracked concrete is described by an orthotropic constitutive relation with tension-stiffening and compression softening effects defining equivalent uniaxial stress-strain relation in the axes of orthotropy. Especially in making analytical predictions for inelastic behavior of reinforced concrete walls under reversed cyclic loading, some influencing factors inducing the material nonlinearities have been considered.

6.2.4 Applications of ANSYS software

Many researchers have used the finite element method in two ways. Some researchers developed the special element to simulate the behavior of structural member in their own projects and compiled the compute program. But the precision of the calculated results and the applicability of the program are still in doubt. Some researchers used the large universal software, such as MARC, ANSYS and ABAQUS, to do the study work. These softwares have plentiful element types and offer some default parameters, which make it easy to develop the model to simulate the cooperation work of concrete and other materials.

In recent years, using ANSYS finite element software, many research works have been done successfully to simulate the seismic behavior of reinforced concrete shear wall. Monique C. Hite and Harry W. Shenton [Mon02] presented modeling the nonlinear behavior of wood frame shear walls. A study has been undertaken to investigate the effect of vertical load on the static and cyclic lateral load response of wood frame shear walls. And then Johnn P. Judd and Fernando S. Fonseca [Joh02] presented nonlinear analysis of wood diaphragms and shear walls using commercial finite-element software (ANSYS and ABAQUS). In this method sheathing-to-framing connections were represented using a pair of uncoupled orthogonal nonlinear spring elements. N. Mohammad [Moh02] studied afterwards a numerical study on a hybrid shear wall system under cyclic load by ANSYS 5.7. However, the only work that has been done recently was the research of Lu Xinzheng and Jiang Jianjing [Lux03], which presented analysis for concrete structure under complex stress condition with element SOLID 65 of ANSYS. This study show that ANSYS can simulate concrete precisely.

6.3 Finite element analysis on lightweight reinforced concrete shear walls

Former studies proved that software ANSYS was capable of handling dedicated numerical models for the non-linear response of concrete under static and dynamic loading. So that, in this study, ANSYS 8.0 was used to do the numerical study on the mechanical behavior of lightweight reinforced concrete shear wall.

6.3.1 Element types

6.3.1.1 Reinforce concrete

Concrete is a quasi-brittle material and has different behavior in compression and tension. Development of a model for the behavior of concrete is a challenging task. An eight-node solid element, SOLID 65, was used in this analysis to model the concrete. This solid element has eight nodes with three degrees of freedom at each node-translation in the nodal x, y, and z directions. The geometry and node locations for this element type are show in Fig.6-1. This element includes a smeared crack analogy for cracking in tension zones and a plasticity algorithm to account for the possibility of concrete crushing in compression regions.

Cracking or crushing of an element is initiated once one of the element principal stresses, at an element integration point, exceeds the tensile or compressive strength of the concrete. Cracked or crushed regions are then formed perpendicular to the relevant principal stresses being redistributed locally. The element is thus nonlinear and requires an iterative solver. The crushing algorithm follows a plasticity law in which, once the ultimate strength has been reached, any further application of load in that direction develops increasing strains at constant stress. After reaching the ultimate strain (ε_u) the concrete is assumed to loose its resistance completely. In case of cracking, following the formation of initial cracks, stresses tangential to the crack face may cause a second or third crack at the integration point.
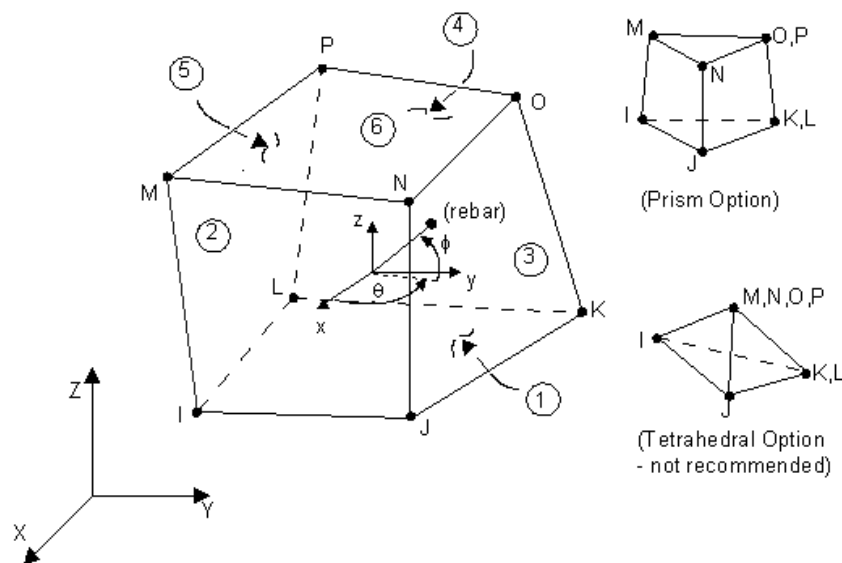
Fig.6-1 SOLID 65 geometry

The reinforcement bars may be incorporated in the finite element model according to either a discrete model (individual bars), or through a smeared model. In the discrete model, one dimensional elements carrying axial force are used. For the smeared model, the steel is assumed to be distributed over the concrete element with a particular orientation angle. In that case, a perfect bond between the concrete and reinforcing steel is assumed. In this study, the smeared model was used to simulate reinforcements in specimen LW-2 and LW-3 for its convenience reason, since only reinforcement ratio and steel properties of each direction need to be introduced. For specimen LW-1 and LW-4, reinforcements were modeled by using separate element called LINK 8, a 3-D spar element. The element is uniaxial tension-

compression and also capable of plastic and large deformation. The bond between concrete and reinforcements is assumed to be perfect and modeling of bond itself is not undertaken in this study.

The geometry and node locations for LINK 8 are show in Fig.6-2. Two nodes are required for this element. Each node has three degrees of freedom, translations in the nodal x, y and z directions.
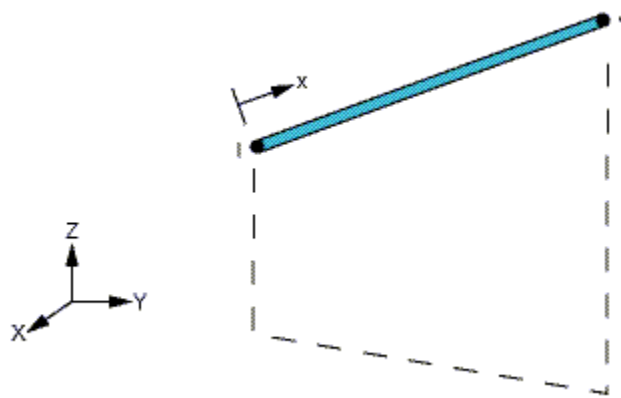
Fig.6-2 LINK 8 geometry

6.3.1.2 Steel plates
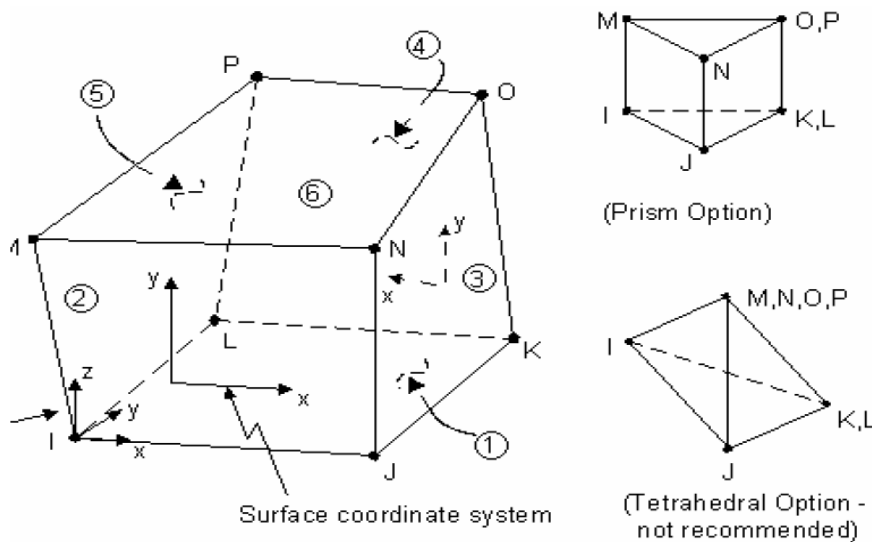
Fig.6-3 SOLID 45 geometry

A 25 mm thick steel plate, modeled by using element SOLID 45, was added at the load application location in order to avoid stress concentration problems and to prevent localized crushing of concrete elements near the load application locations. Element SOLID 45 is defined with eight nodes having three degrees of freedom at each node and translations in the nodal x, y and z directions. The stiffness of it is assumed about ten times of that of steel bars. The geometry and node locations for this element type are shown in Fig.6-3.

6.3.2 Failure criteria of concrete

Concrete is a nonlinear, inelastic and nonhomogeneous material with a very complex physical behavior, having a high compressive strength and low tensile strength. The load carrying capacity of concrete under multiaxial stress conditions is a function of the state of stress, and can be properly predicted by using appropriate failure criteria. Most failure criteria are given as a hypothesis whose application to different materials should be evaluated from tests.

The constitutive model applied to concrete modeling available in the commercial finite element code ANSYS 8.0 characterizes the concrete failure in four distinct domains. This model is represented through a failure surface described in terms of the invariants of the stress tension and compression, the main characteristics presented in pressure dependent materials (quasi brittle materials). The failure surfaces are dependent of the hydrostatic component of the stress, are curved, smooth and convex having well defined compression and tension meridians. The cracking and crushing behavior are both considered in this model

Two dimensional failure curves for concrete is shown in Fig.6-4. The most significant nonzero principal stresses are in the x and y directions, represented by σ_{xp} and σ_{yp}, respectively. Three failure curves are shown as projections of the three dimensional failure surface on the σ_{xp}-σ_{yp} plane. The mode of failure is a function of the sign of σ_{zp} (principal stress in the z direction). For example, if σ_{xp} and σ_{yp} are both negative (compressive) and σ_{zp} is slightly positive (tensile), cracking would be predicted in a direction perpendicular to σ_{zp}. However, if σ_{zp} is zero or slightly negative, the material is assumed to crush [ANS05].
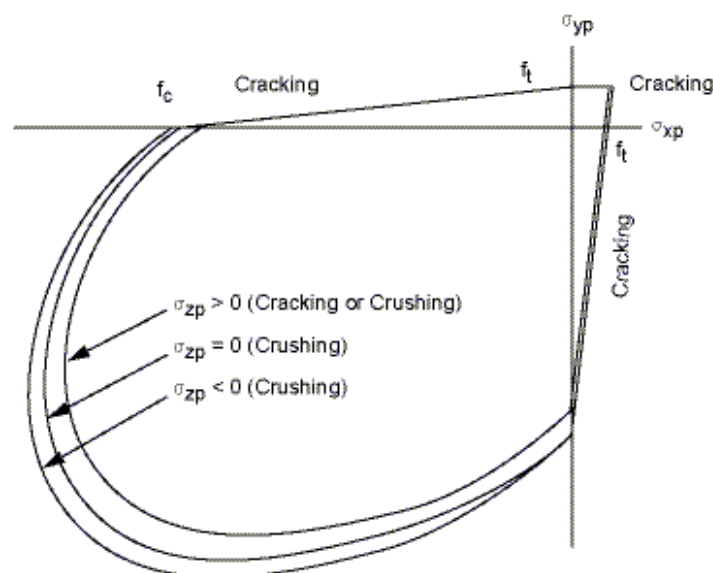

Fig.6-4 Failure surface in principal stress space with nearly biaxial stress

6.3.3 Material properties

6.3.3.1 Concrete

The two input strength parameters, ultimate uniaxial tensile and compressive strength, are needed to define a failure surface for the concrete. The crushing capability of the SOLID 65 element was turned off in this study in order to avoid a "rapid collapse" in the finite element simulation. Since cracked concrete cannot transfer tensile stresses, the tensile strength drops suddenly after cracking. The tensile strength was assumed to be $0.273 f_c^{'2/3}$ MPa, with $f_c^{'}$ being the compressive strength of 30 MPa. The poisson's ratio for the concrete was assumed to be 0.2. The amount of shear transfer across a crack can be varied between full shear transfer and no shear transfer at a cracked section. Then the shear transfer coefficient of open crack $\beta_t = 0.5$ and the shear transfer coefficient of closed crack $\beta_c = 0.8$. For the compressive uniaxial stress-strain relationship of concrete, the multilinear isotropic hardening model (Concrete + Miso) was used.

In this study, the lightweight concrete stress-strain curve has been assumed by the mathematical equation. One of the most important parameters affecting the ascending and descending portion of the concrete stress – strain curve is concrete strain at peak stress. In the case of LWC, the equation proposed by Almusallam and Alsayed [Alm95] was that

$$\begin{aligned}
\varepsilon_o &= \left(65.57 f_c^{'0.44} - 6.748\right) \times 10^{-5} \\
&= \left[\left(65.57 \times 30^{0.44}\right) - 6.748\right] \times 10^{-5} \\
&= 0.00286
\end{aligned} \tag{6-1}$$

Where ε_0 — Concrete strain at peak stress;

$\qquad f_c^{'}$ — Concrete compressive strength.

The modulus of elasticity of concrete has an important effect also on the behavior of reinforced concrete members, and directly affects the stiffness and deformation of the RC structural components. It should be noted that the design of RC members is dominantly based on flexural behavior and should not be used for less ductile failure modes, particularly for structures in earthquake prone areas. Therefore, the force deformation ratio of RC members changes the stiffness during the application of load. Furthermore, the actual value of the elastic modulus in a structure, as built, is not known at the stage of analysis and design. In the case of lightweight concrete, the equation to calculate elastic modulus, E_{itm}, proposed by Wang et al.[Wan78] was

$$\begin{aligned}
E_{itm} &= 2.1684 f_c^{'0.535} \\
&= 2.1684(30^{0.535}) \\
&= 1.33783e10 \text{ Pa.}
\end{aligned} \tag{6-2}$$

Once the value of $f_c^{'}$ is known, ε_o and E_{itm} can easily be determined. Numerical expression, Eq.(6-3), was used to construct the uniaxial compressive stress-strain curve for lightweight concrete in this study.

$$f_c = (2\beta - 3)\left\{\frac{\varepsilon_c}{\varepsilon_o}\right\}^4 + (4 - 3\beta)\left\{\frac{\varepsilon_c}{\varepsilon_o}\right\}^3 + \beta\left\{\frac{\varepsilon_c}{\varepsilon_o}\right\} \qquad (6\text{-}3)$$

Where f_c — Concrete stress;

ε_c — Concrete strain;

$\beta = E_{itm}\dfrac{\varepsilon_o}{f_c'}$.

Then this stress-strain curve for lightweight concrete was adopted to suitable simulation in ANSYS program, as shown in Fig.6-5.
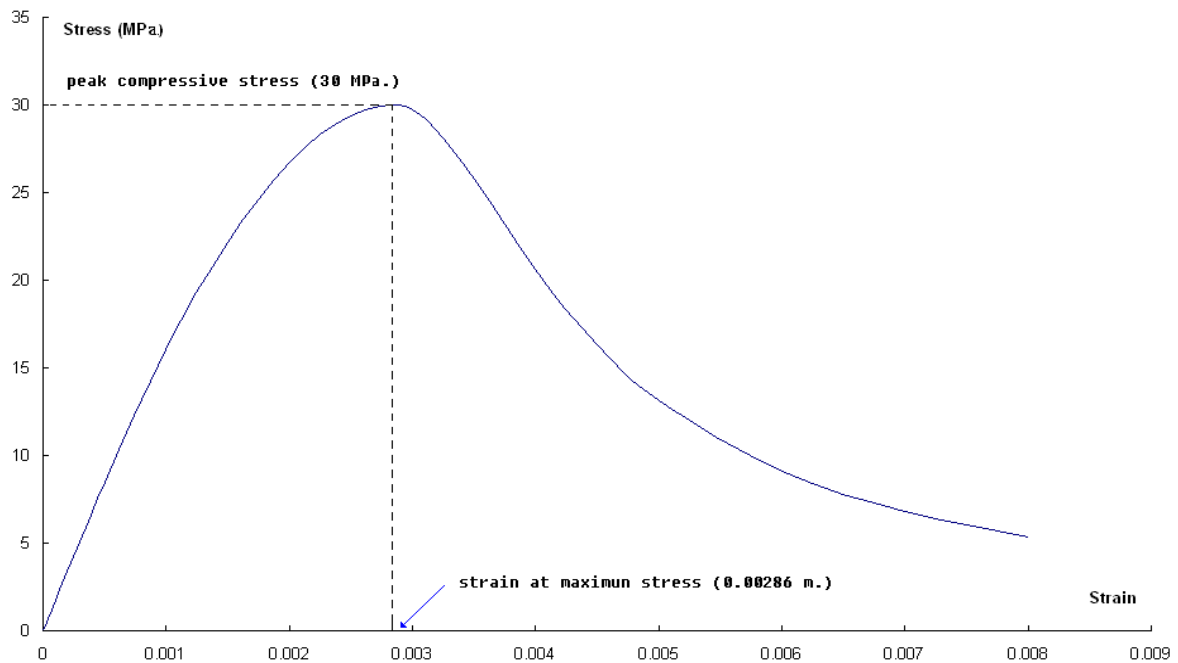

Fig.6-5 Simplified compressive stress-strain curve for LWC used in FE model

6.3.3.2 Reinforcement

As the reinforcing bars are long and relatively slender, they are generally assumed capable of transmitting axial forces only. Hence, a uniaxial stress-strain relationship has been adopted. Steel reinforcement stress-strain curve for the finite element model was based on the actual stress-strain curve obtained from tensile tests. For example case, The bar HRB335 10 mm. is chose for this study. The actual stress-strain curve is shown in Fig.6-6. However, this stress-strain curve was modified to improve the convergence of finite element model by removing the negative slope portion of the curve. Also the zero slop portions after yielding was slightly modified to a mild positive slope. Fig.6-7 shows the stress-strain relationship used in this study. The bilinear kinematic hardening model (BKIN) was used.

Material properties for steel reinforcement model are as follows:
Elastic modulus (E_s) = 225,000 MPa, Yield stress (f_y) = 450 MPa, Poisson's ratio (ν) =0.3.

Constitutive law for steel $\left\{\begin{array}{lll} \sigma_s = E_s \varepsilon_s & , & \varepsilon_s \leq \varepsilon_y \\ \sigma_s = f_y + E_s' \varepsilon_s & , & \varepsilon_s > \varepsilon_y \end{array}\right.$ (6-4)

Where σ_s — Steel stress;

ε_s — Steel strain;

ε_y — Yielding strain;

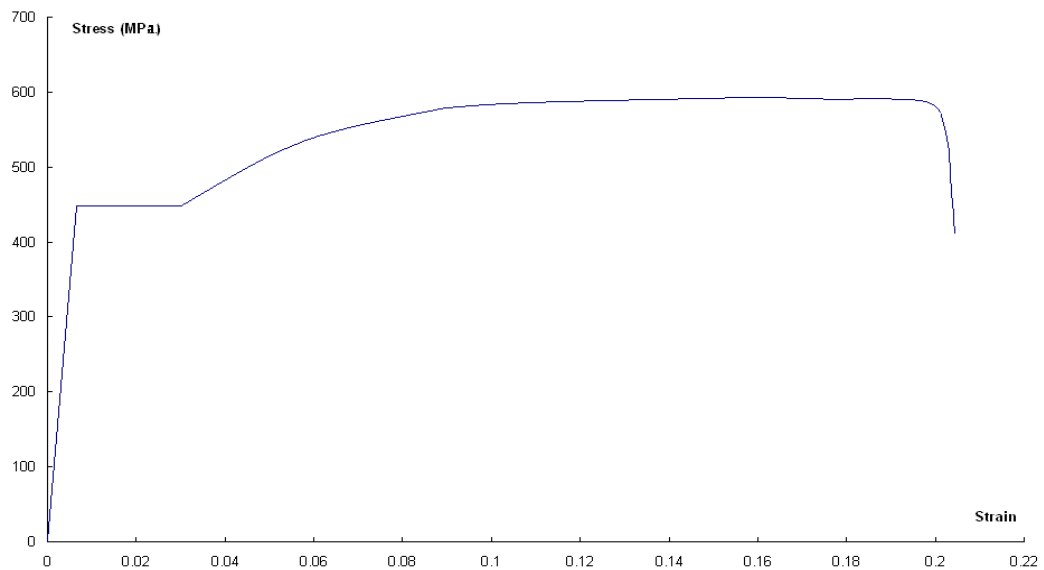E_s' — Tangent modulus of steel after yielding, $E_s' = 0.01\,E_s$;

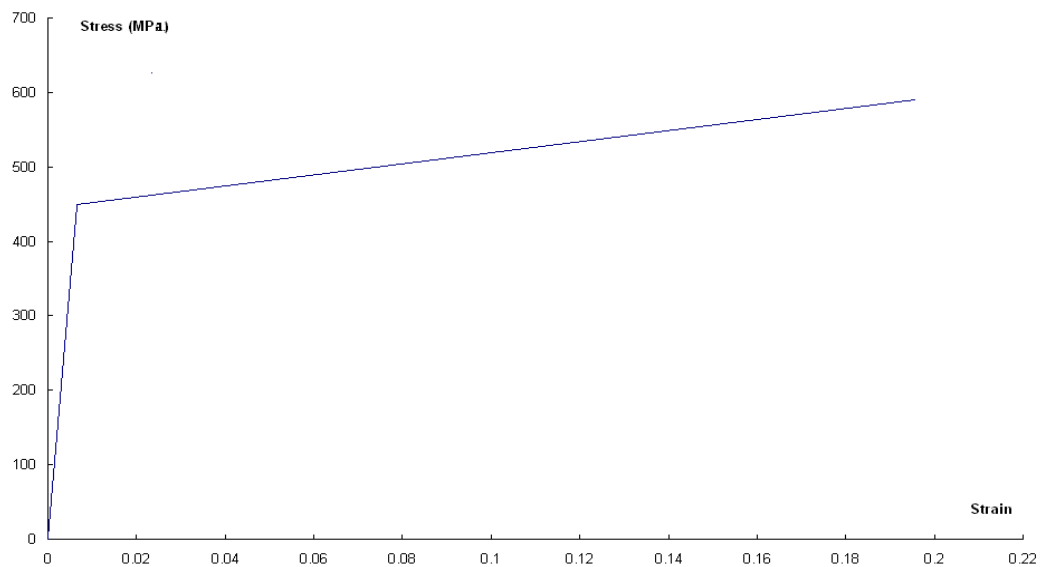**Fig.6-6 Stress-strain curve for steel (obtained from tested results of HRB335 10 mm bar)**

Fig.6-7 Modified stress-strain curve for steel (adopted in ANSYS model)

6.3.4 Geometrical modeling and finite mesh

Under loading, micro and macro cracks occur in the concrete. The stress-strain behavior of concrete is affected by the development of these cracks. There are two main approaches for modeling the cracking of the concrete, namely, the discrete and smeared crack approach. The former one treats cracking by adapting the geometry of the structure and keeping the interior of the body linear elastic, whereas the second approach keeps the geometry fixed, and models the cracking process entirely via a constitutive law. In early studies the tension cut-off was used, assuming that after exceeding the tensile strength a complete loss of coherence occurred in the direction of the major principle stress. The performance of the smeared fixed-crack model has been improved with the introduction of tension stiffening, tension softening and degradation of shear capacity due to cracking. The fixed-crack model has been further developed to fixed multi crack and rotating crack models in order to account for the formation of cracks in other directions. In this study, smeared crack model was used.

In the finite element model, nodes of solid elements (SOLID 45) were connected to those of adjacent concrete solid elements (SOLID 65) in order to satisfy the perfect bond assumption. Because a perfect bond between concrete and steel rebar was assumed due to the limitations in ANSYS, the elements LINK 8 for the reinforcing steel were connected with nodes of each adjacent concrete solid element. Fig.6-8 illustrates the element connectivity.
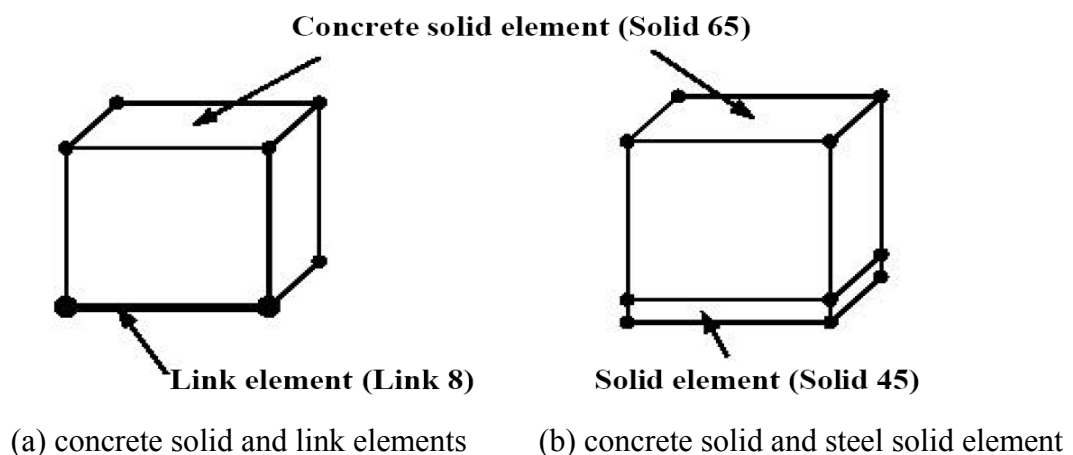

(a) concrete solid and link elements   (b) concrete solid and steel solid element

Fig.6-8 Element connectivity

In this study, four different three dimensional finite element models (FEM) representing the four specimens with different reinforcement were generated to analytically predict the response of them under the pertinent load condition.

The appropriate element layout and size (meshing) is an important aspect in finite element modeling to capture the behavior of interest. It takes experience to find the "best" mesh. If the mesh is too fine, one might get singularities in the solution, stress concentrations where they should not appear, or the solver will take an extraordinarily long time to run. But if the mesh is too coarse, then the solution will not be accurate enough. For four models in this study, concrete of the shear wall specimen was meshed with cubes element of dimension 25 mm or 50 mm and all the reinforcements were meshed with 50 mm or 100mm long link element.

A typical finite element mesh layout of specimens is shown in Fig.6-9. For specimen LW-1, the finite element model included about 9680 SOLID 65 elements, 2027 LINK 8 elements and 400 SOLID 45 elements. Fig.6-10 provides the concrete and reinforcement element layout of specimen LW-1. For specimen LW-4, the finite element model included 9680 SOLID 65 elements, which was the same as that in LW-1, 2265 LINK 8 elements and 400 SOLID 45 elements. Fig.6-11 displays the reinforcement model of specimen LW-4.

For specimen LW-2 and LW-3, due to the computer limit, element SOLID 65 with smeared rebar were used. The internal reinforcement may be modelled as an additional smeared stiffness distributed through SOLID 65 element in a specified orientatation. Each finite element model included about 9680 SOLID 65 elements, 312 LINK 8 elements and 200 SOLID 45 elements. Fig.6-12 displays the SOLID 65 element with internal lines that present rebar sizes and orientations for specimen LW-2 and LW-3. The rebar with the largest volume ratio in each element plots as a red line, the next largest as green, and the smallest as blue. The difference of reinforcement in LW-2 and LW-3 is only the volume ratio of every steel bars.
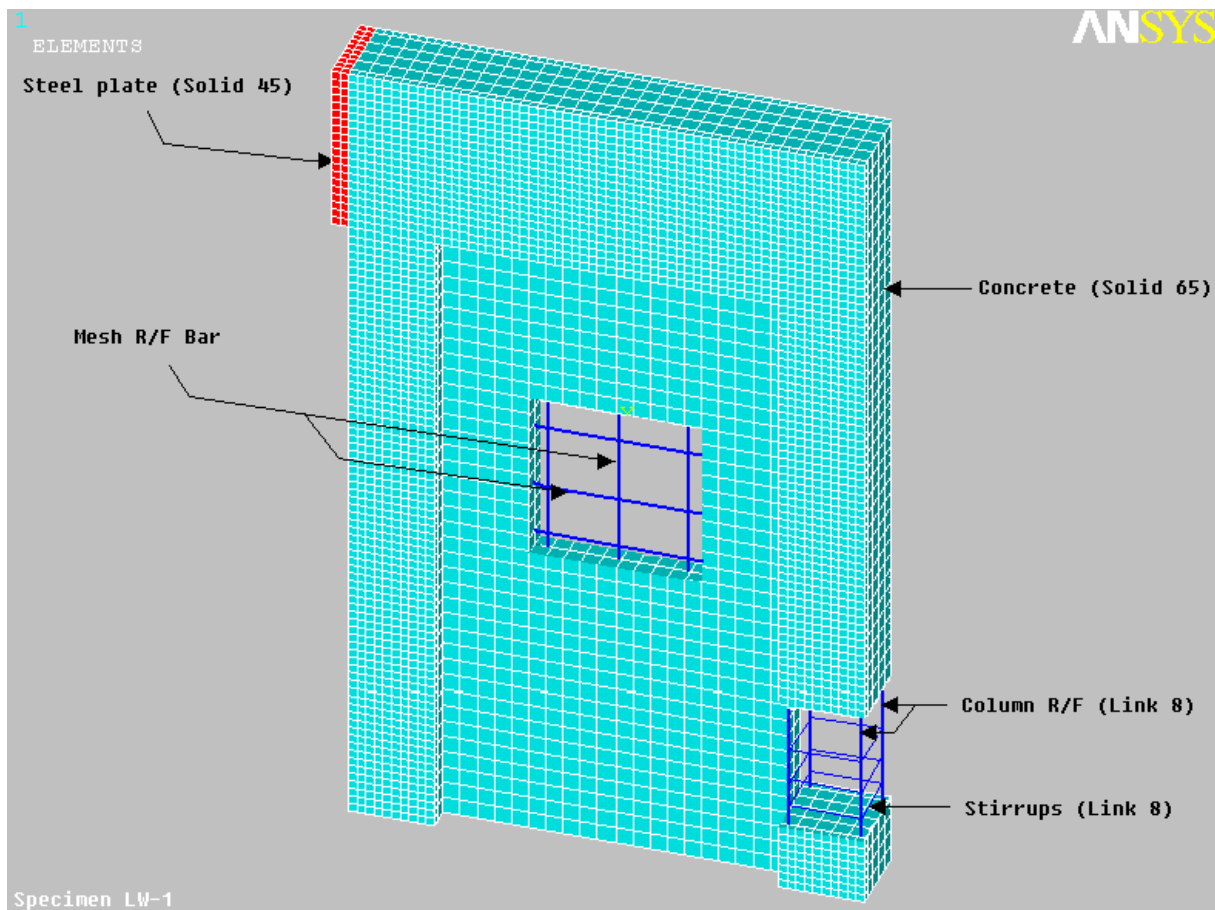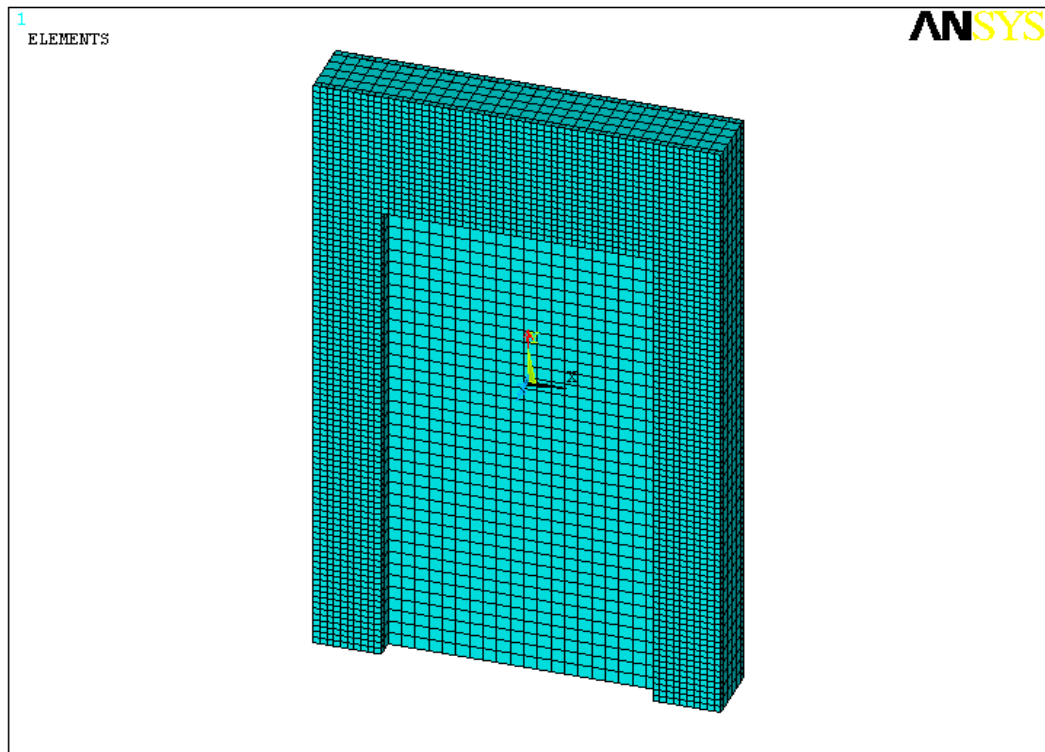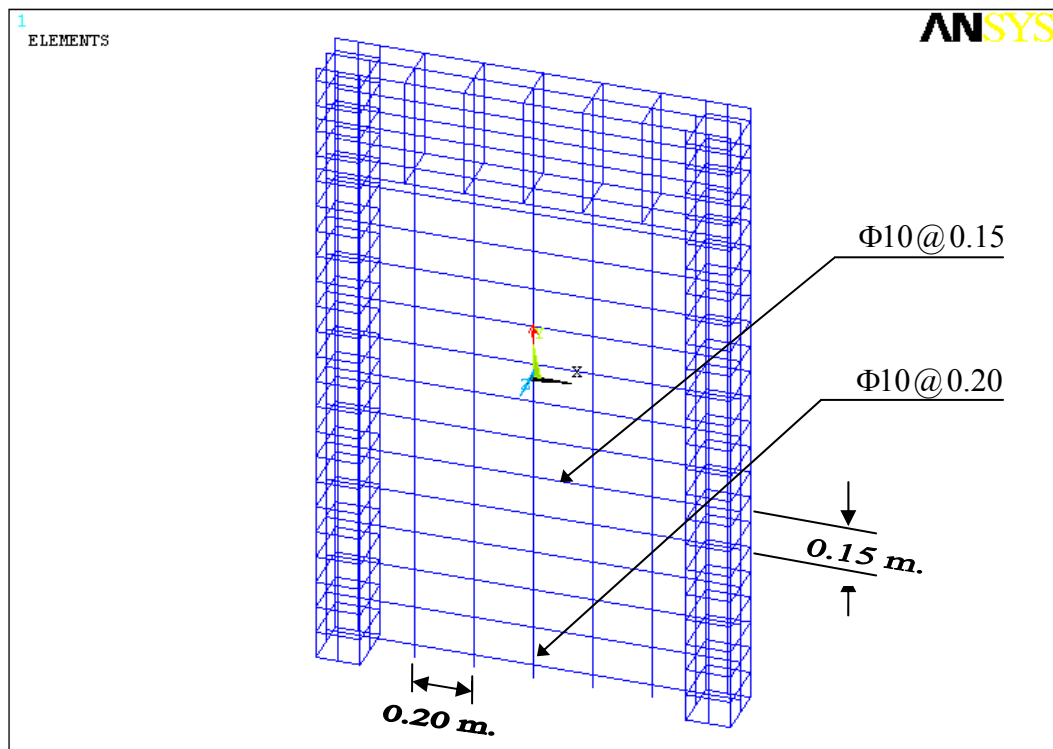

Fig.6-9 Finite element mesh layout (selected concrete elements were removed to illustrate internal reinforcement)

(a) concrete model

(b) reinforcement model

Fig.6-10 Finite element model for specimen LW-1
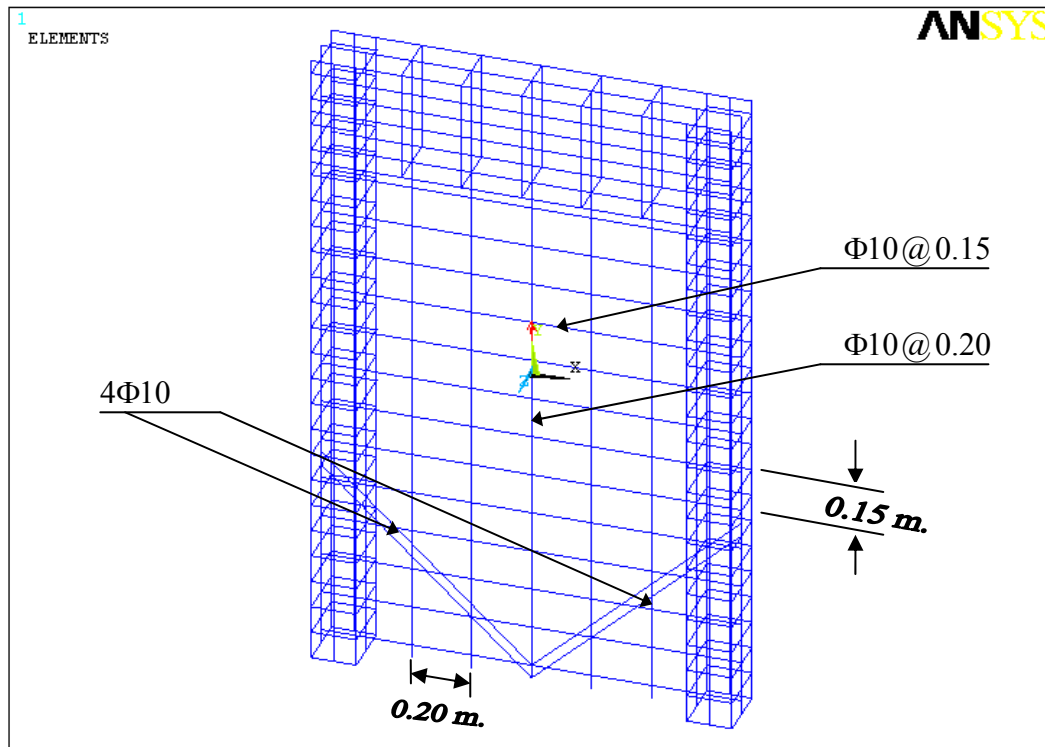
Fig.6-11 Finite element model of reinforcement for specimen LW-4
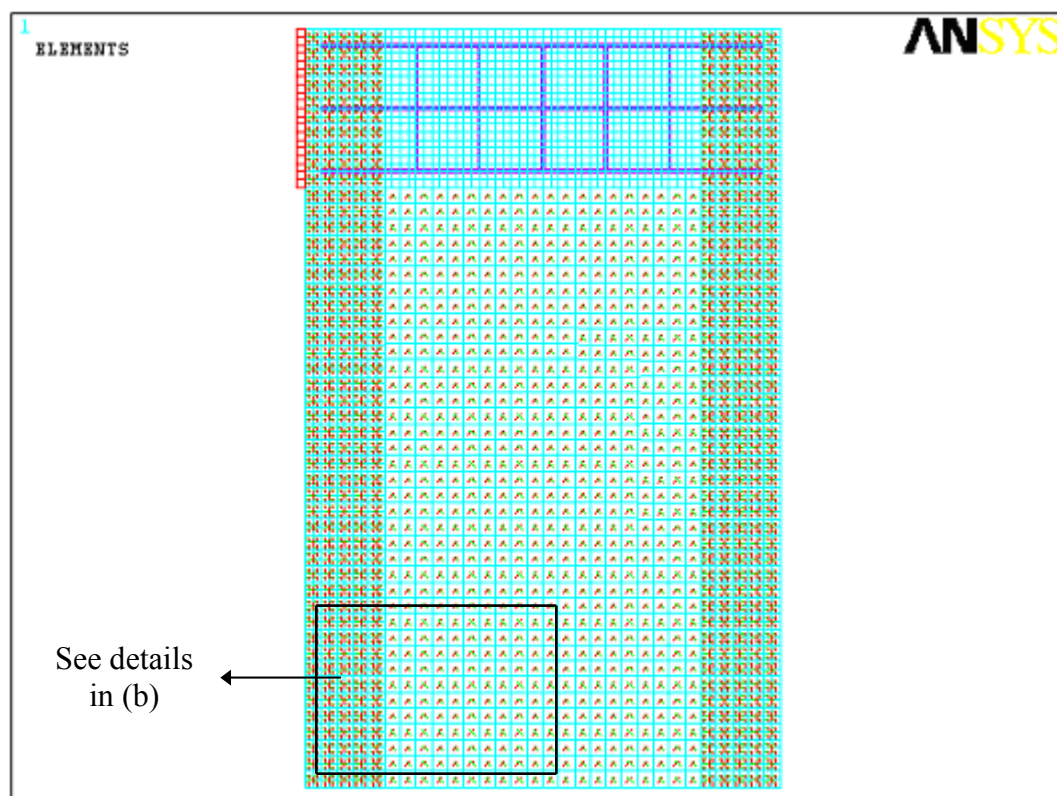
(a) concrete element with smeared rebar
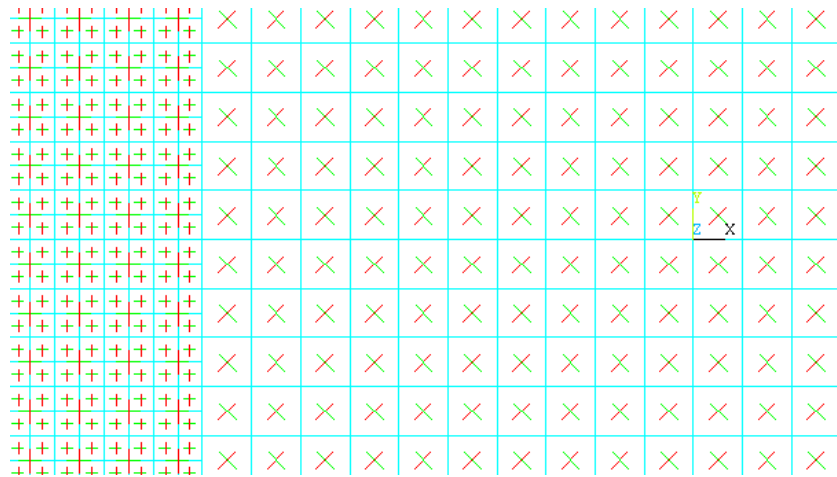
(b) details of smeared rebar

Fig.6-12 Finite element model for specimen LW-2 and LW-3

6.3.5 Boundary conditions

The boundary conditions were exactly simulated as in the test setup shown in Fig.4-3. Restraints for three coordinate axes represent a fix connection applied at the base of the shear wall. Fig.6-13 shows the restraints used in the finite element model at column end and web end.
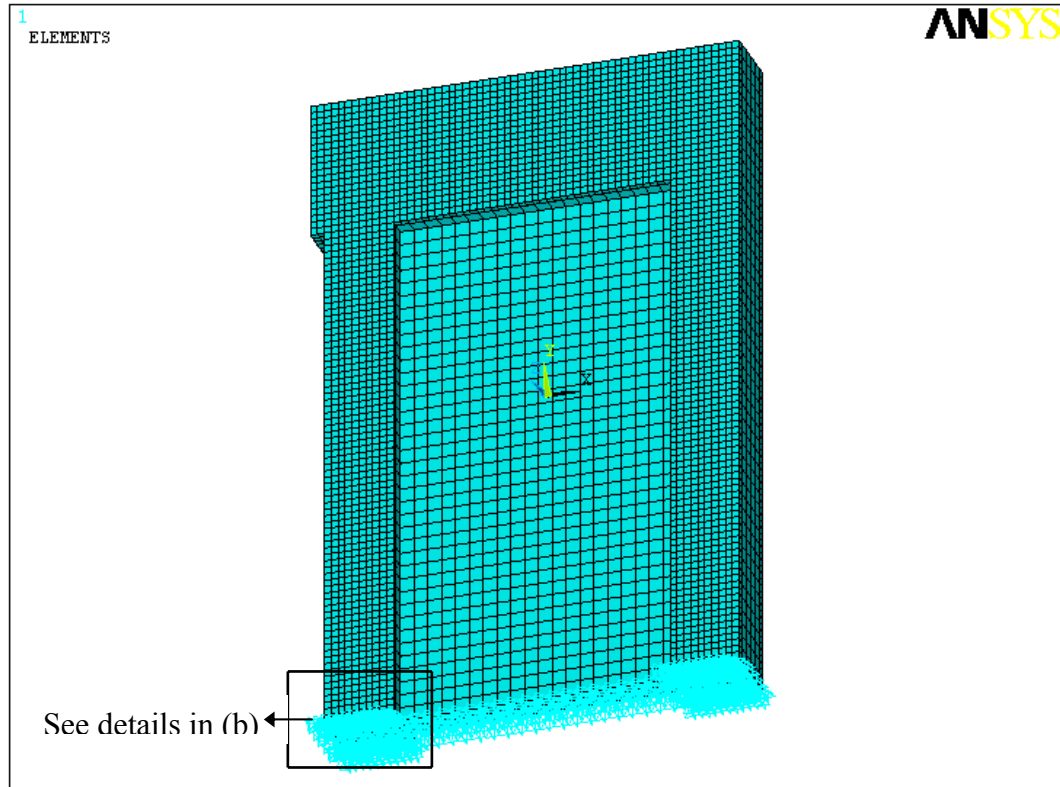
(a) boundary conditions for lightweight reinforced concrete shear wall
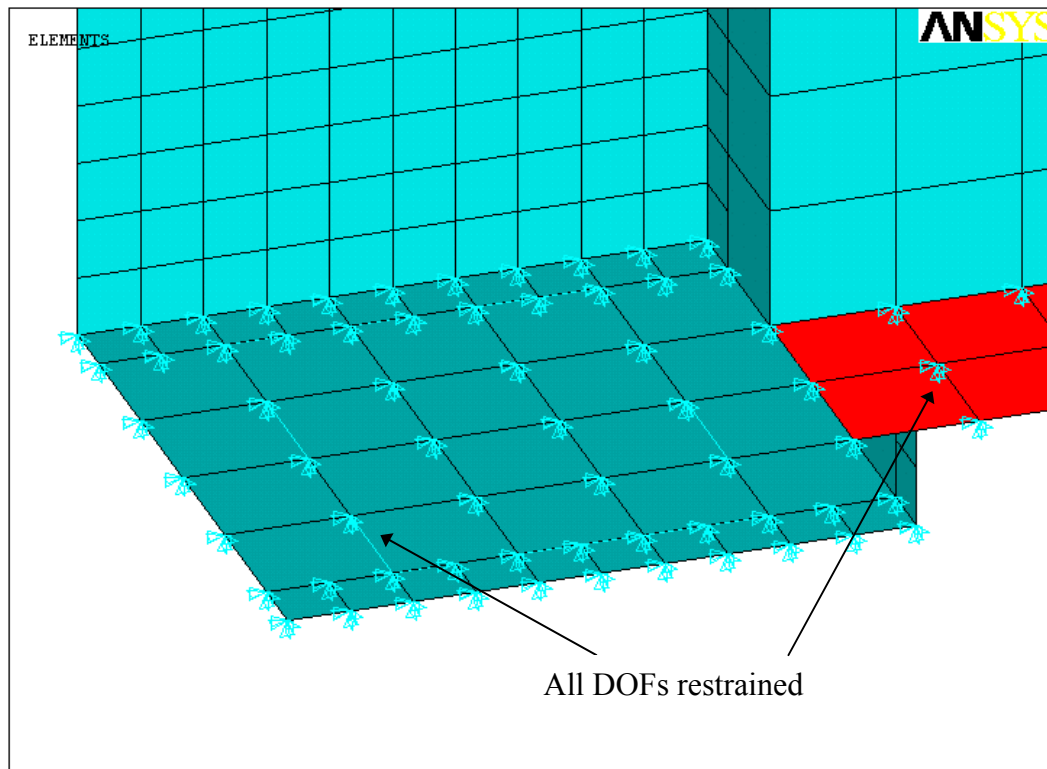
(b) details for column end and web end restraints

Fig.6-13 Column end and web end restraints in FE model

6.3.6 Nonlinear solution

In nonlinear analysis, the total load applied to a finite element model is divided into a series of load increments called load steps. At the completion of each incremental solution, the stiffness matrix of the model is adjusted to reflect nonlinear changes in structural stiffness before proceeding to the next load increment. The ANSYS program [ANS05] use Newton-Raphson equilibrium iterations for updating the model stiffness.

Newton-Raphson equilibrium iterations provide convergence at the end of each load increment within tolerance limits. Fig 6-14 shows the use of the Newton-Raphson approach in a single degree of freedom non-linear analysis.

Prior to each solution, the Newton-Raphson approach assesses the out-of-balance load vector, which is the difference between the forces (the loads corresponding to the element stresses) and the applied loads. Subsequently, the program carries out a linear solution, using the out-of-balance loads, and checks for convergence. If convergence criteria are not satisfied, the out-of-balance load vector is re-evaluated, the stiffness matrix is updated, and a new solution is attained. This iterative procedure continues until the problem converges [ANS05].

For the non-linear analysis, automatic time stepping in the ANSYS program predicts and controls load step sizes. Based on the previous solution history and the physics of the models, if the convergence behaviour is smooth, automatic time stepping will increase the load increment up to a selected maximum load step size. If the convergence behaviour is abrupt,

automatic time stepping will bisect the load increment until it is equal to a selected minimum load step size. The maximum and minimum load step sizes are required for the automatic time stepping.
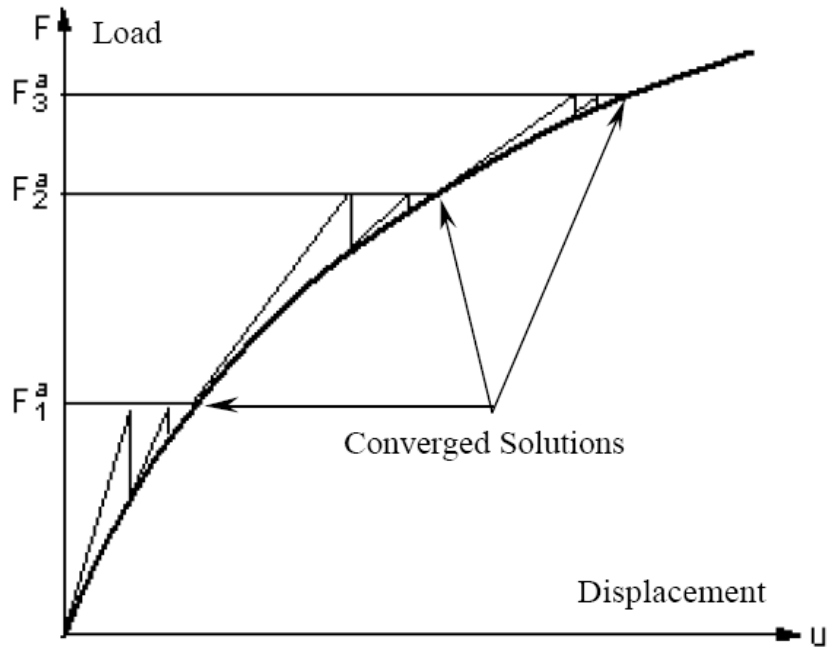

Fig. 6-14 Newton-Raphson iterative solutions (2 load increments)

Chapter 7

# Comparison of Analytical and Experimental Results

7.1 General

In this chapter, the analytically predicted response of the lightweight aggregate concrete shear wall specimens are compared with the experimental test results. Specifically, the analytical derived force-displacement behavior under monotonic loading is compared with the experimentally determined cyclic peak load values for successively increased displacement levels. Also the development of strain and stress in reinforcements and concrete are analyzed based on the finite element analysis results and tested results. A further study on the shear resistance of lightweight aggregate shear wall is considered in this chapter.

7.2 Comparison of analytical and experimental results

7.2.1 Force-displacement behaviors of four specimens

The deformation shapes of four specimens calculated by ANSYS are provided in Fig.7-1. The test and ANSYS results of top horizontal force versus top horizontal displacement curves of four specimens are shown in Fig.7-2. The test results in Fig.7-2 present in fact the positive loading branch of the envelope of the cyclic alternating hysteretic load-displacement curves of four specimens, which cover only the first peak load values at the predetermined displacement levels. Comparing the numerical results with the experimental data, ANSYS results show similar trends to the test results and capture well the non-linear load-displacement response of the specimens up to peak load. It is clear from the numerical model that the response of the model is linear until the first diagonal crack in the web of the walls has formed. It indicates that the finite element analyses are capable of predicting the experimental behavior of the specimens when these are subjected to a monotonic horizontal load.
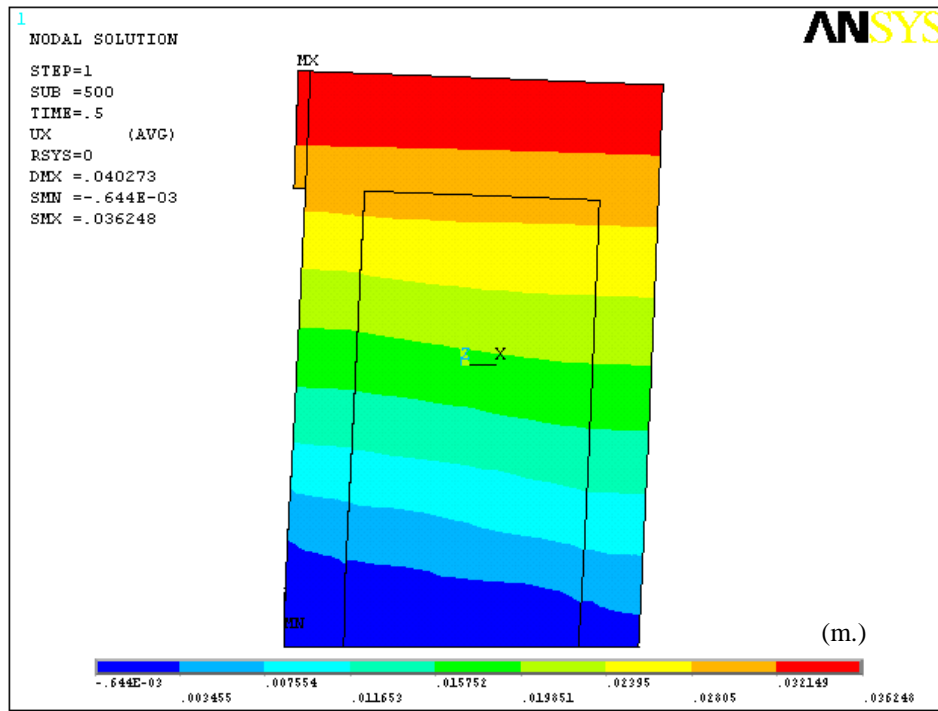
(a) LW-1
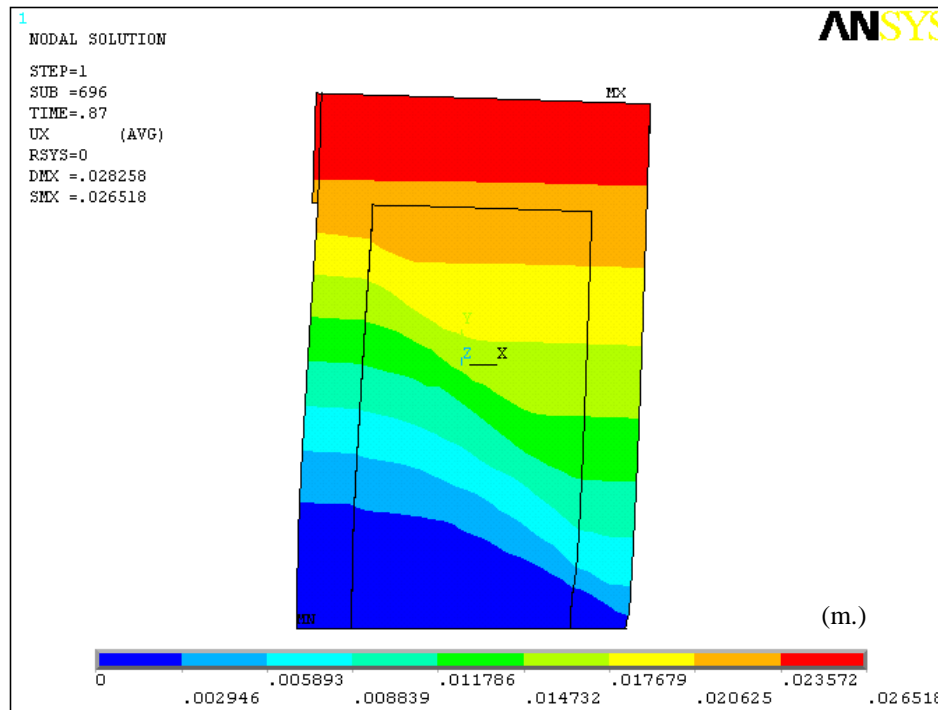
(b) LW-2

Fig.7-1 a: Deformation shapes of four specimens in ANSYS

(c) LW-3

(d) LW-4

Fig.7-1 b: Deformation shapes of four specimens in ANSYS

(1) LW-1

(2) LW-2

Fig.7-2 a: Force-displacement comparison for four specimens

(3) LW-3

(4) LW-4

Fig.7-2 b: Force-displacement comparison for four specimens

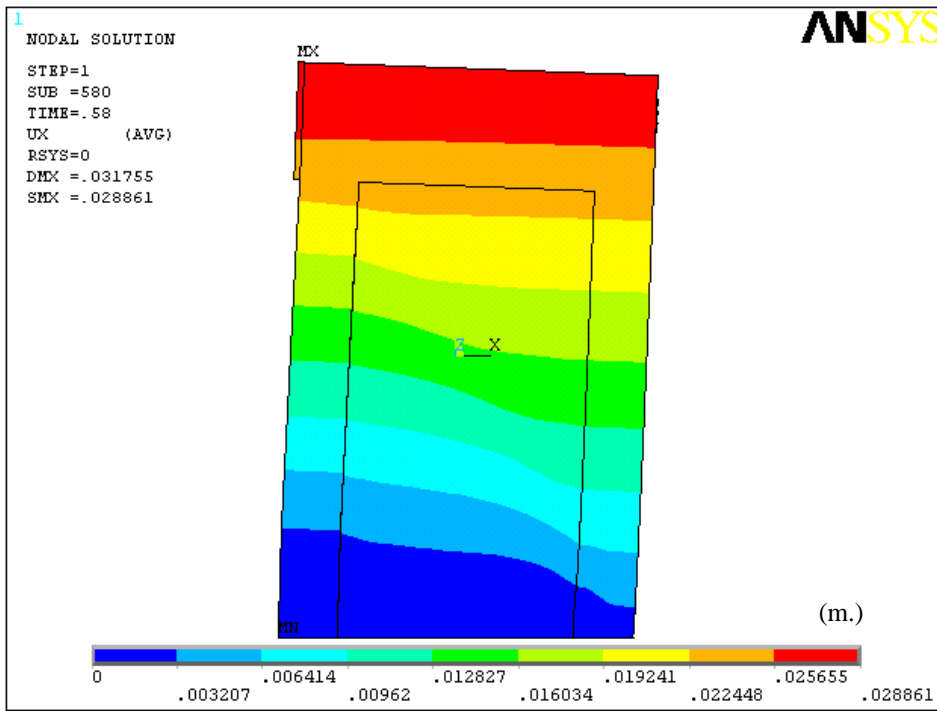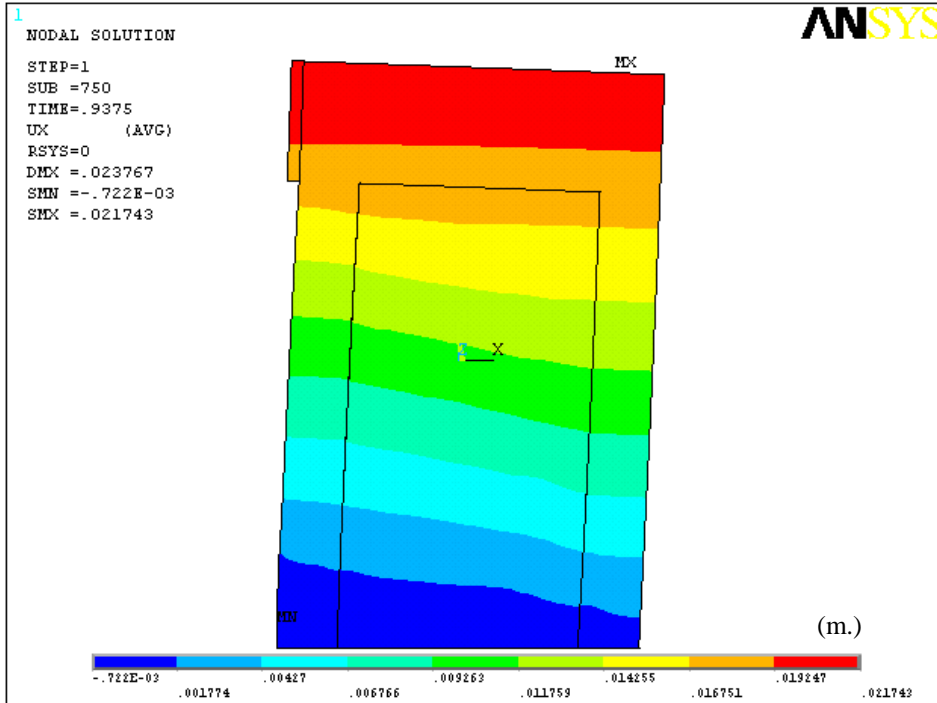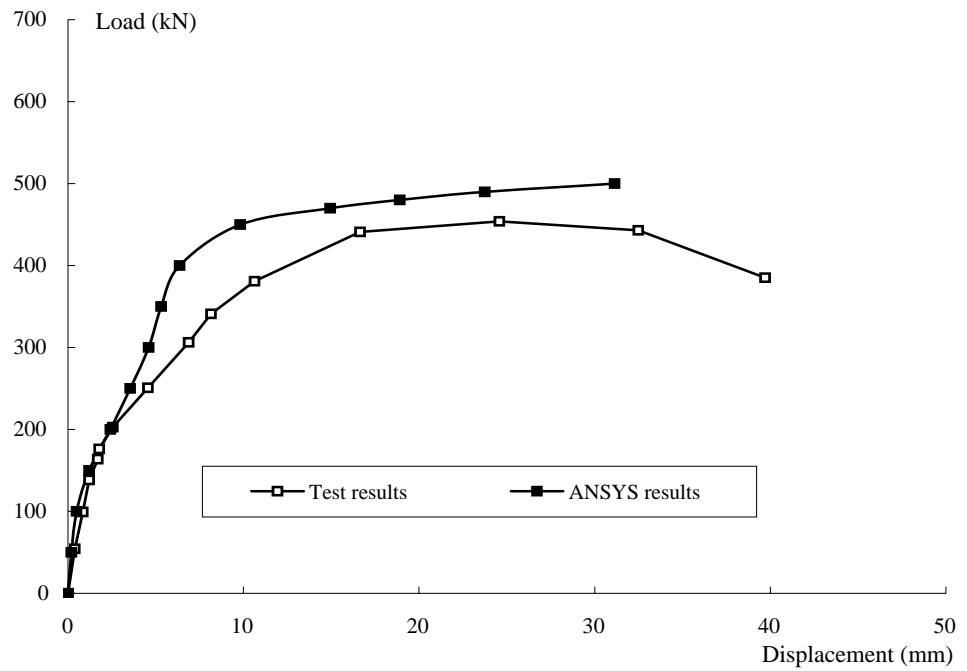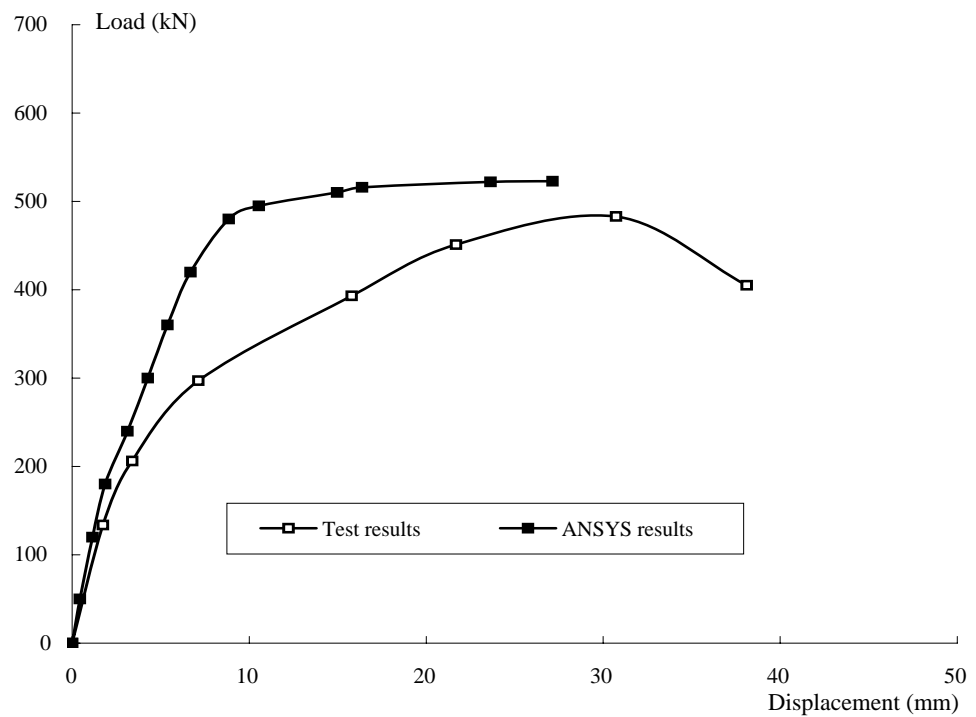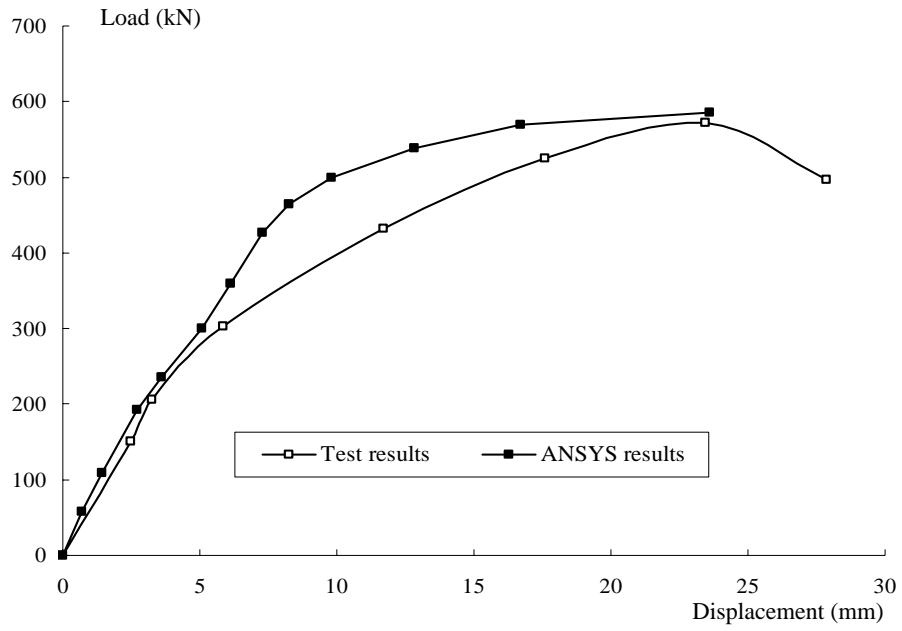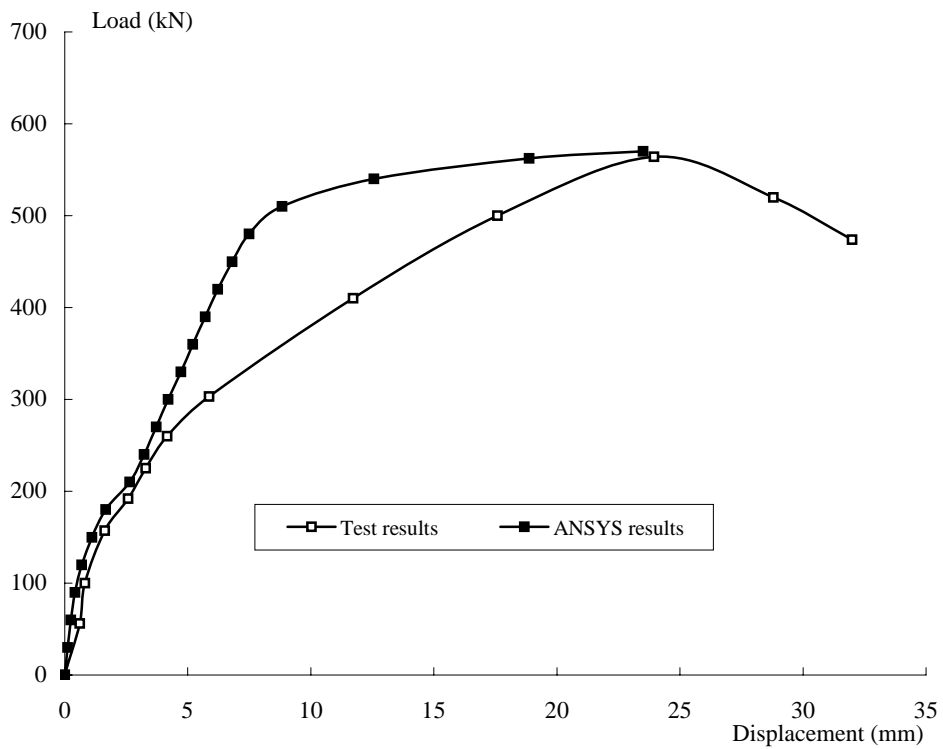In additional, the ANSYS shear walls are stiffer than the tested ones. One reason for this is because materials used to model the finite element model are perfectly homogenous, unlike those in the actual structure. Moreover, the boundary conditions are strictly defined in the finite element (FE) model and the discretization itself impose additional constrains on the displacements. These also trend to make the FE model stiffer. Additionally, in the actual reinforced lightweight aggregate concrete shear walls micro-cracks in the concrete and bond slip between the stiffness of the concrete and reinforcing steel bars, as well as other imperfections in construction, may lessen the stiffness of the actual structure.

Table 7-1 shows the comparison between the ANSYS calculated results and the test results of four specimens LW-1, LW-2, LW-3 and LW-4. It is also substantiated by the good coincidence of the peak loads that, the analytical model is indeed capable to successfully predict the shear resistance of lightweight aggregate concrete shear walls. The analytical peak load values for the four specimens are within 10% bigger than their peak tested load values.

Table 7-1 Comparison of shear resistance of four specimens

	LW-1	LW-2	LW-3	LW-4
Test results, V^{exp} (kN)	460	475	572	562
ANSYS results, V^{ansys} (kN)	500	510	585	570
V^{ansys} / V^{exp}	1.087	1.074	1.023	1.014
Average value	1.0495			

7.2.2 Shear transfer mechanisms for walls with conventional and diagonal web reinforcements

Finite element analyses were used to investigate shear transfer mechanisms for specimen LW-1, LW-2 and LW-3. Fig.7-3, Fig.7-4 and Fig.7-5 provide respectively the stress distribution in reinforcements and concrete of specimen LW-1, LW-2 and LW-3 at its failure point. Because element SOLID 65 with internal rebar was used in ANSYS analysis for specimen LW-2 and LW-3, Fig.7-4 and Fig.7-5 shows the stress in rebar of every concrete element.

It can be seen from Fig.7-3(a), Fig.7-4(a) and Fig.7-5(a) that, stresses in most web reinforcements of the walls reached to or even exceeded yield strength when wall failed. Fig.7-3(b), Fig.7-4(b) and Fig.7-5(b) shows that, concrete stress reached to its compressive strength also when wall failed. Furthermore, for specimen LW-2 and LW-3, in which diagonal web reinforcement was used, stress in concrete distribution are more even. The more diagonal reinforcement it has, the more obvious this phenomenon is. It proves that web diagonal reinforcement can effectively improve the mechanism of web concrete for shear wall. This is also evident in the test walls.
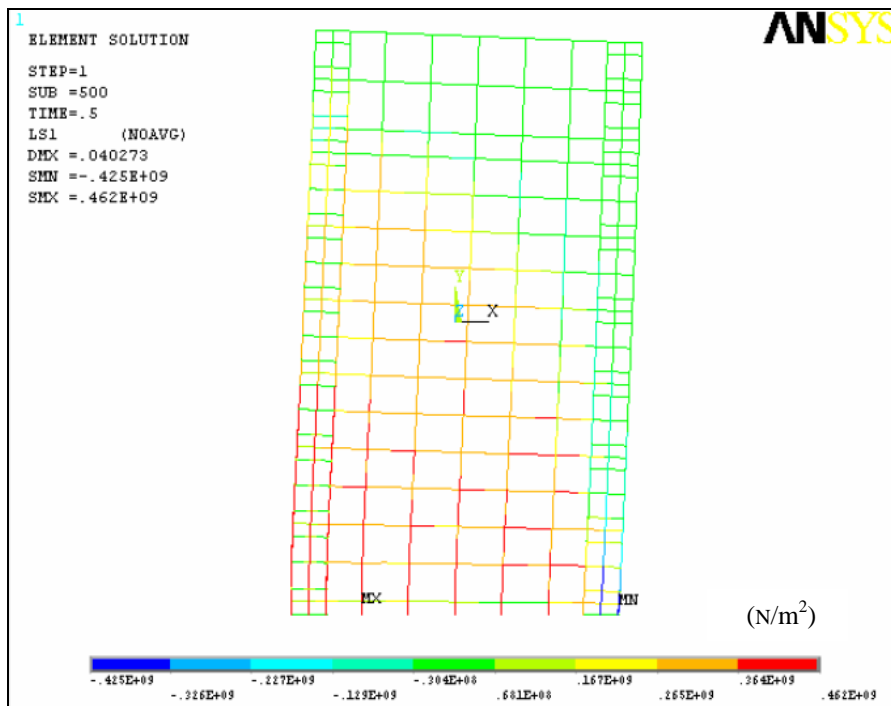
(a) Stress in steel bars
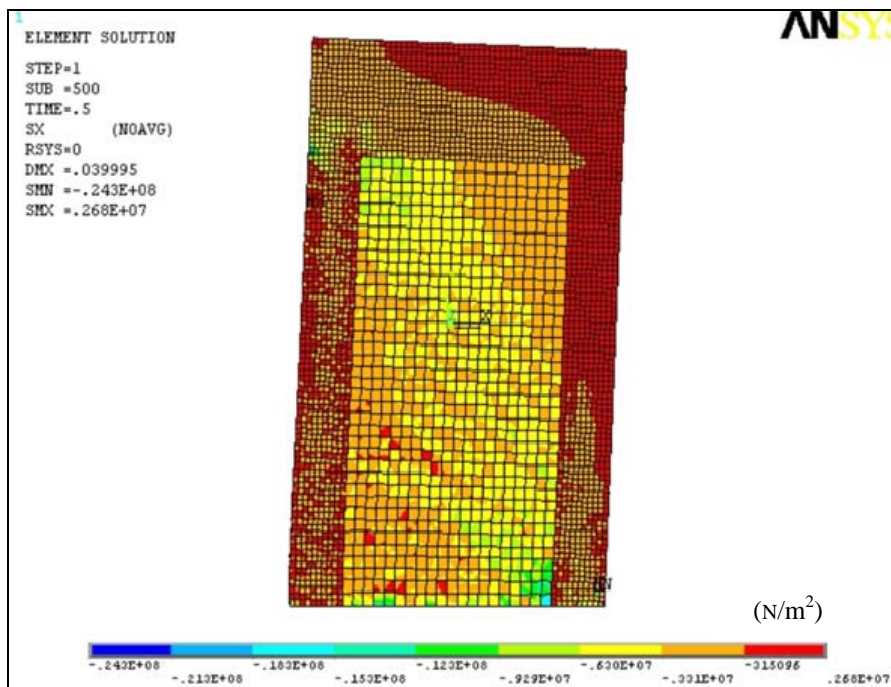
(b) Stress in concrete

Fig.7-3 Stress distribution of specimen LW-1 in ANSYS
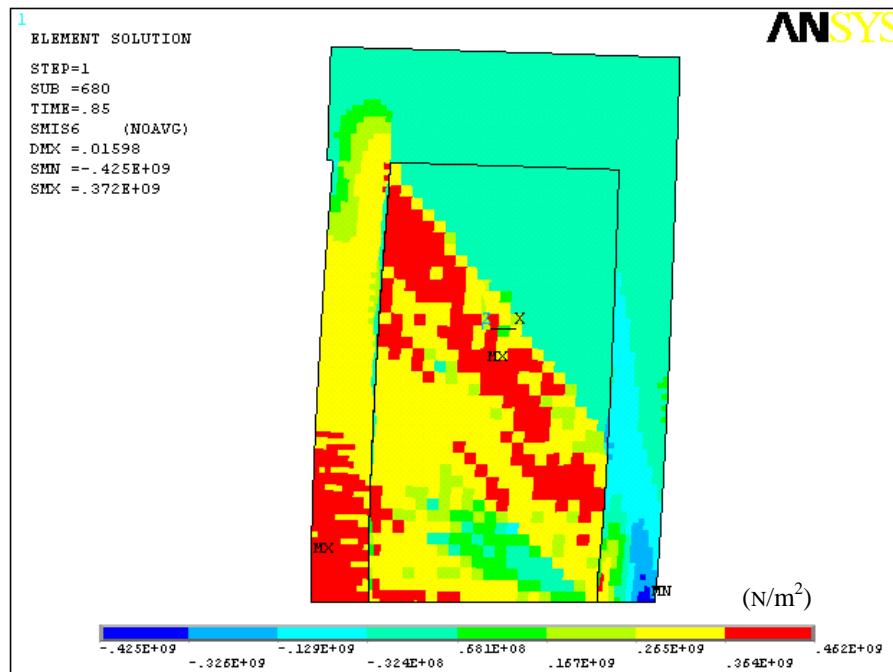
(a) Stress in steel bars
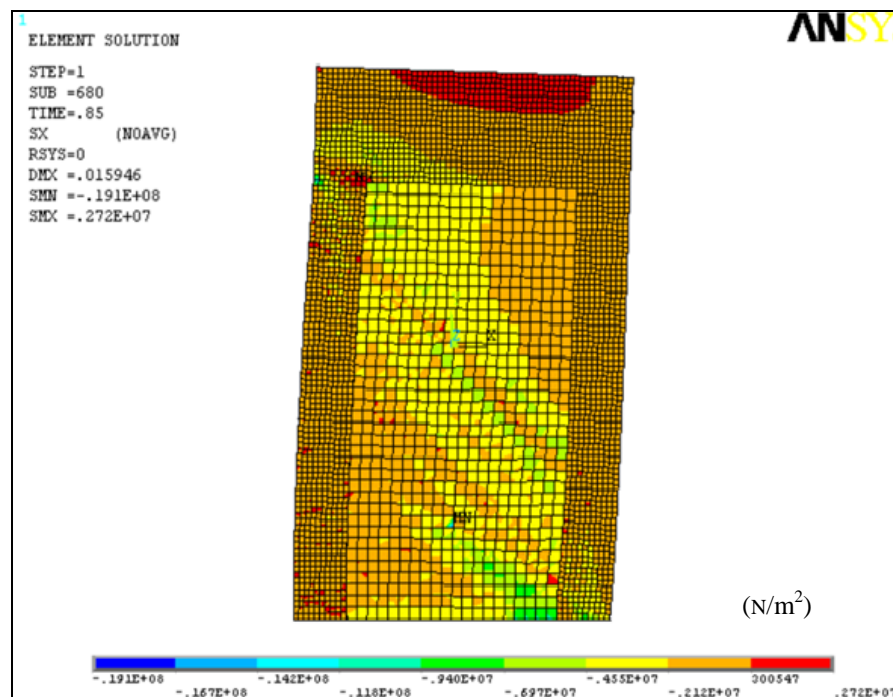
(b) Stress in concrete

Fig.7-4 Stress distribution of specimen LW-2 in ANSYS
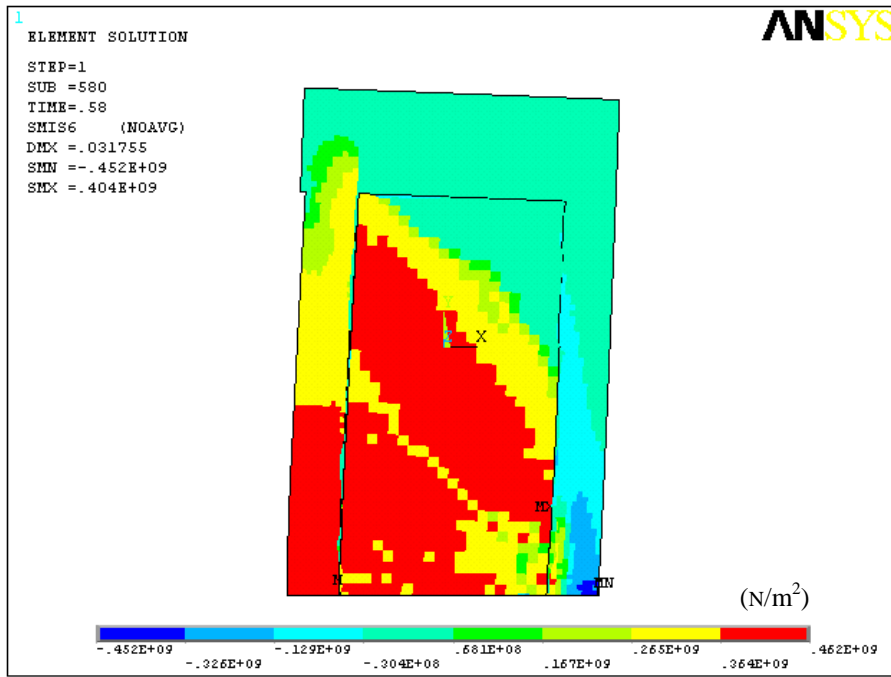
(a) Stress in steel bars
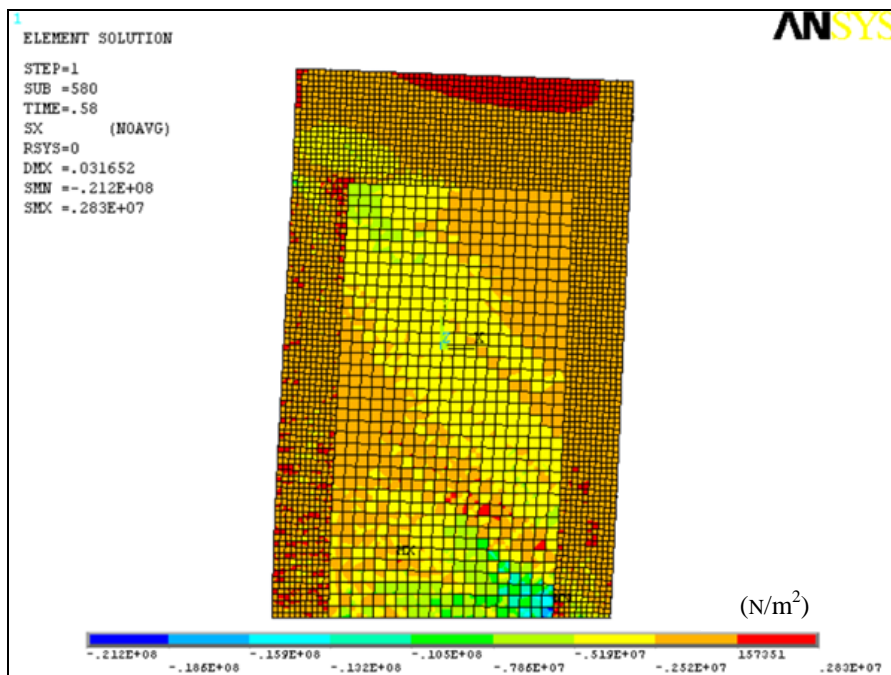
(b) Stress in concrete

Fig.7-5 Stress distribution of specimen LW-3 in ANSYS

The numerical and experimental results of the strain development with increase of load in web reinforcement for specimen LW-1 are compared in Fig.7-6. The element chose to observe its strain lies at the same position as strain gauge S5 (vertical web steel) and S2 (horizontal web steel) of specimen LW-1 in the test. The test results in Fig.7-6 present in fact the positive branch of the envelope of the cyclic alternating load–strain curves of strain gauge S2 and S5, which cover only the peak load values at the predetermined displacement levels.
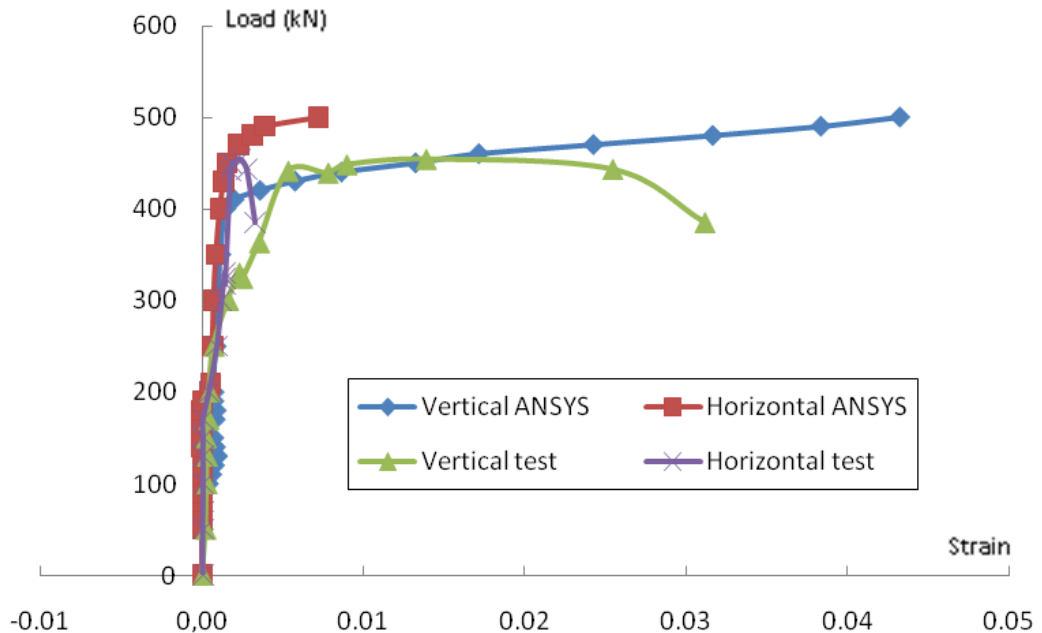
Fig.7-6 Strain in steel of LW-1
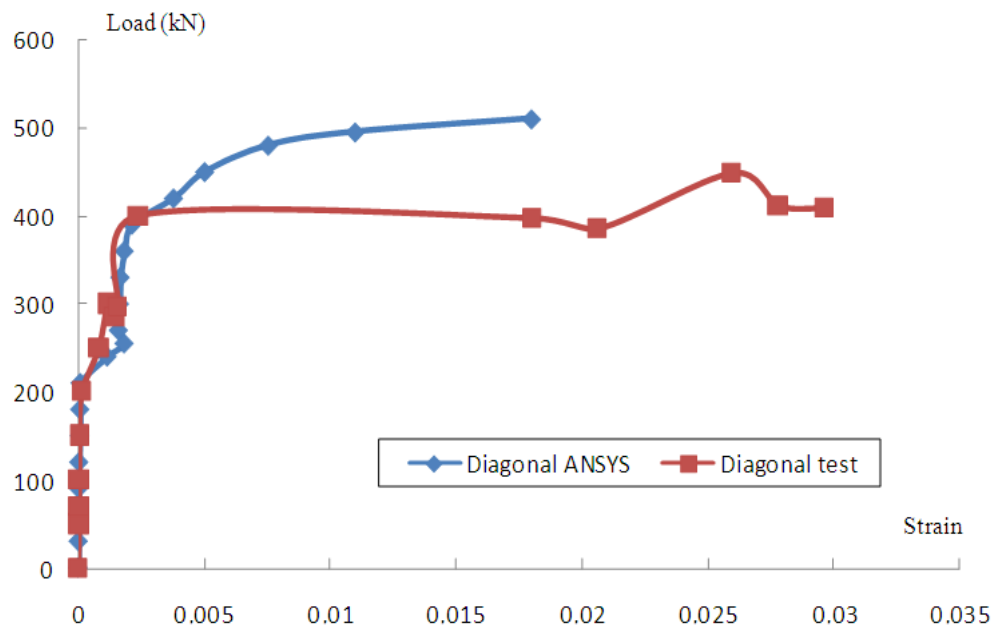
Fig.7-7 Strain in steel of LW-2
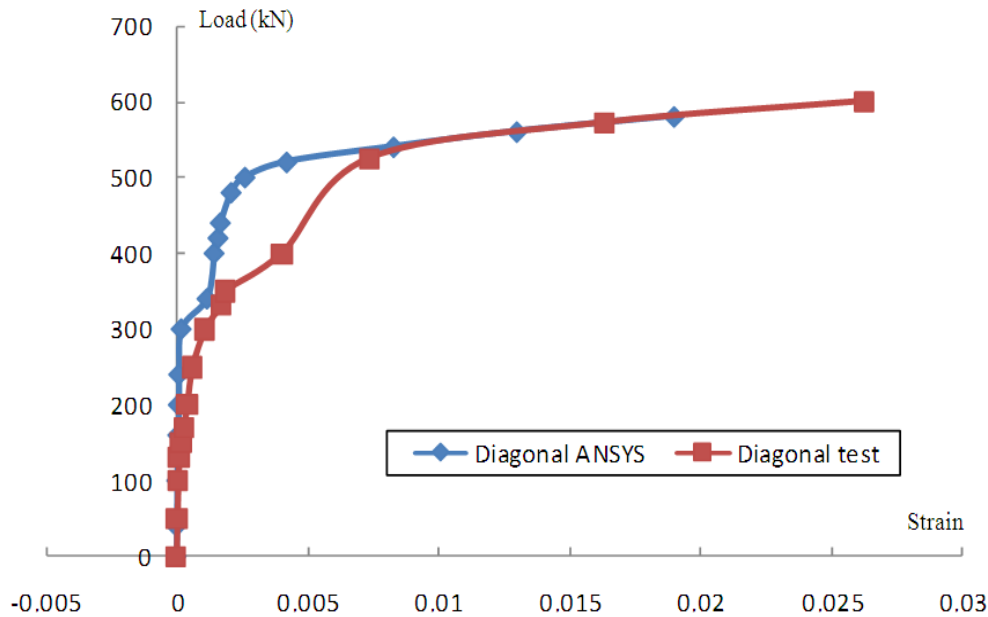
Fig.7-8 Strain in steel of LW-3

Similarly, the load–strain responses in web diagonal steel for specimen LW-2 from the test program are plotted with the finite element results in Fig.7-7. The element chose to observe its steel strain lies at the same position as strain gauge S3 of specimen LW-2 in the test. Fig.7-8 shows the strain development curves in web diagonal steel for specimen LW-3 from numerical and test programs. The element chose to observe its steel strain lies at the same position as strain gauge S1 of specimen LW-3 in the test.

The load–strain responses for three walls are captured well by the numerical simulation. The difference between the experiment and FE results is mainly because that, the position of strain gauge in the test is not absolutely consistent with the calculated point in FE model. The difference of smear crack and cracks in actual shear wall, the measure error of the strain gauge may also results in the differences.

Fig.7-9 shows idealized shear transfer mechanisms for walls with different web reinforcement. Conventional web reinforcement acts as ties that cross diagonal cracks and contribute to the shear resistance. All lateral force in walls with conventional web reinforcement must be transferred through concrete by compressive struts and aggregate interlock and by dowel action in the reinforcement at the base of the walls (Fig.7-9(a)). Web crushing failures occur when the compressive stress exceeds the average compressive strength of the concrete in the strut $kf_c^{'}$, where k is a factor that represents the decrease in strut compressive strength due to large inelastic shear distortion [Oes84]. On the other hand, diagonal web reinforcement helps transfer part of shear force directly to the foundation by tension in the web reinforcement (Fig.7-9(b)). As a result, the shear force carried by the compressive struts is reduced.
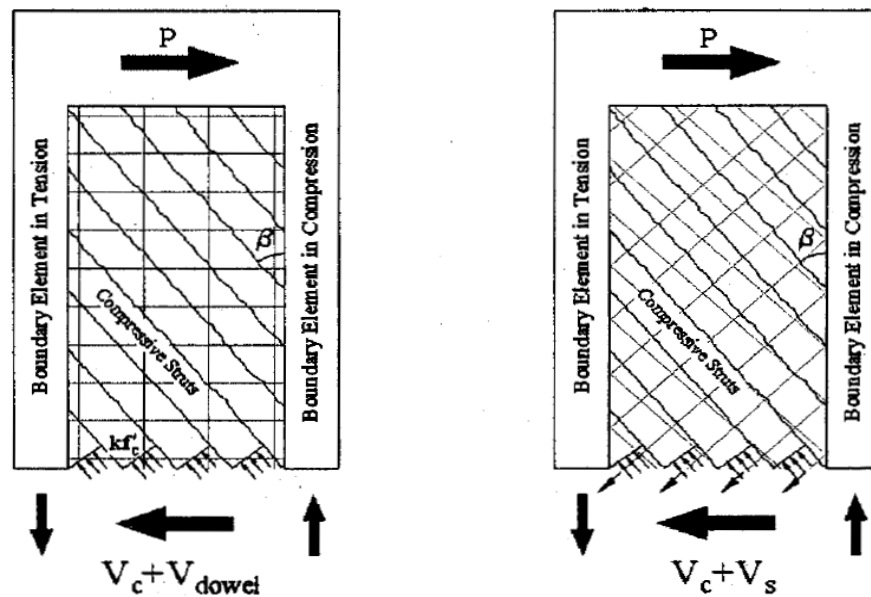
(a) Wall with conventional reinforcement   (b) Wall with diagonal reinforcement

Fig.7-9 Mechanisms for transferring shear into foundation

Finite element analysis was used to study this mechanism in detail. The load–stress development curves for concrete element of specimen LW-1, LW-2 and LW-3 based on the finite element model results are compared in Fig.7-10. The element discussed here lie at the same position as strain gauge S5 in wall LW-1 in the test. It can be seen that, increase speeds of concrete stress for wall LW-2 and LW-3 are distinctly slower than that for wall LW-1. The more web diagonal reinforcements it has, the more obvious this phenomenon is. It indicates that the shear force carried by the compressive struts is evidently reduced due to the existing of diagonal web reinforcement.

The load–stress development curves for reinforcement element of specimen LW-1, LW-2 and LW-3 based on the finite element model results are compared in Fig.7-11. The steel rebar element discussed here lie at the same position as the concrete element discussed in Fig.7-10. It can be seen that, stresses in steel rebar were small when walls began to suffer top horizontal load. At that moment there was no diagonal crack in web concrete and most of the loads were supported by concrete. At the load level of about 200 kN, diagonal cracks appeared in the web concrete and stress redistribution took place between the concrete and reinforcements, which was represented as the abrupt increase of stress in steel. This has been observed in experiment also. From Fig.7-11 it can be also seen that, increase speeds of steel stress in specimen LW-2 and LW-3 are evidently slower than that of specimen LW-1. The more diagonal reinforcement the wall has, the more evident this rule is. It proves that, diagonal web reinforcement has better mechanisms for transferring shear force so that stress can develop more evenly in the web steel bars. As a result more web reinforcements reached to or exceed its yielding strength. This conclusion is consistent with the conclusions got from Fig.7-3 (a), Fig.7-4 (a) and Fig.7-5 (a).

Fig.7-10 Comparison of concrete stress development in LW-1, LW-2 and LW-3
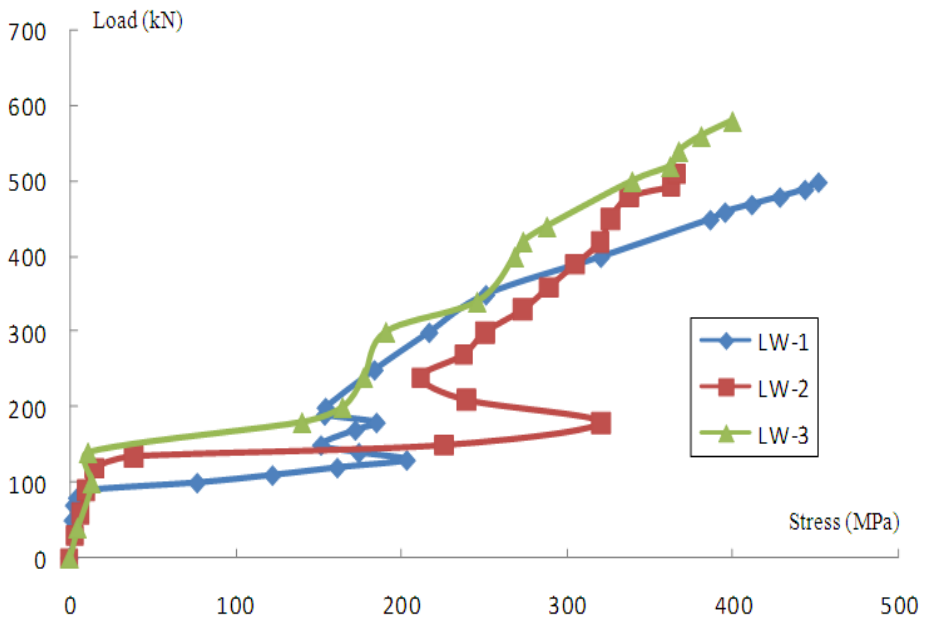
Fig.7-11 Comparison of steel stress development in LW-1, LW-2 and LW-3

7.2.3 Function of web bidiagonal steel bars in specimen LW-4

Fig.7-12 provides the stress distribution in reinforcements and concrete of specimen LW-4 at its failure point. Two diagonal web rebar in one direction reached to its tensile yielding strength and another two diagonal web rebar in another direction were compressed to its yielding strength. It proves that the mechanism used in chapter 3 for specimen LW-4 design is reasonable.
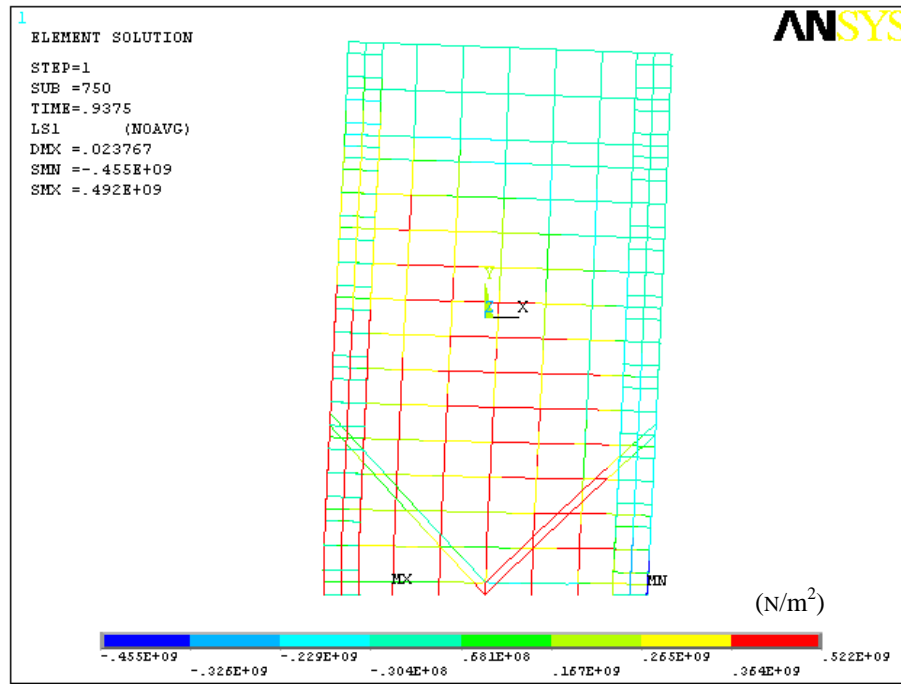
(a) Stress in steel bars
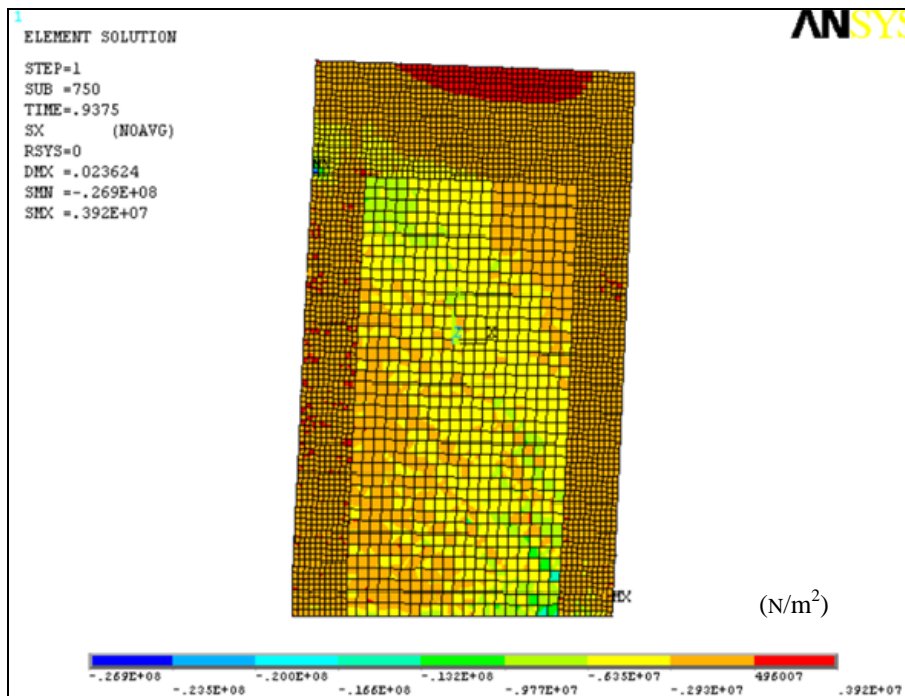
(b) Stress in concrete

Fig.7-12 Stress distribution of specimen LW-4 in ANSYS

Compare Fig.7-12(a) and Fig.7-3(a), it can be seen that, due to existence of additional web diagonal rebar, more web conventional (horizontal and vertical) reinforcements yielded when wall failed. Comparison of Fig.7-12(b) with Fig.7-3(b) also shows that, stress distribution in web concrete of wall LW-4 is more even than that in wall LW-1.

The numerical and experimental results of the strain development with increase of load in web reinforcement for specimen LW-4 are compared in Fig.7-13. The element chose to observe its strain lies at the same position as strain gauge S5 (vertical web steel), S2 (horizontal web steel) and S13 (tension diagonal web steel) of specimen LW-4 in the test. The test results in Fig.7-13 present in fact the positive branch of the envelope of the cyclic alternating load–strain curves of strain gauge S2, S5 and S13, which cover only the peak load values at the predetermined displacement levels. The finite element analysis results have good coincidence with the tested results.
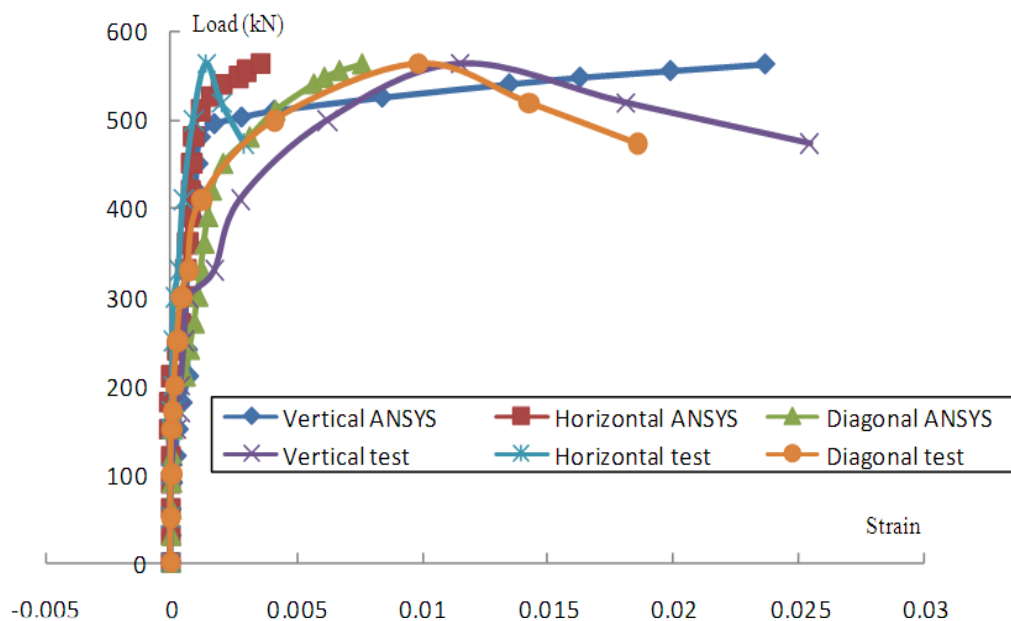
Fig.7-13 Strain in steel of LW-4

The load–stress development curves for concrete element of specimen LW-1 and LW-4 based on the finite element model results are compared in Fig.7-14. The element discussed here lie at the same position as strain gauge S5 in wall LW-1 in the test. The increase speeds of concrete stress with increase of load for wall LW-4 is distinctly slower than that for wall LW-1. It indicates that web diagonal steels can transfer shear force directly to the wall foundation so that the compressive stress in diagonal concrete strut was reduced.

The load–stress development curves for vertical and horizontal web reinforcement of specimen LW-1 and LW-4 based on the finite element model results are compared in Fig.7-15. The steel rebar element discussed here lie at the same position as the concrete element discussed in Fig.7-14.

After diagonal cracks appeared in web concrete, stress redistribution between concrete and reinforcements took place, which is behaved as sudden increase of steel stress in Fig.7-15 at about horizontal load level of 150 kN. Stress in horizontal and vertical reinforcements of wall LW-4 increase slower with the increase of load than those of wall LW-1.
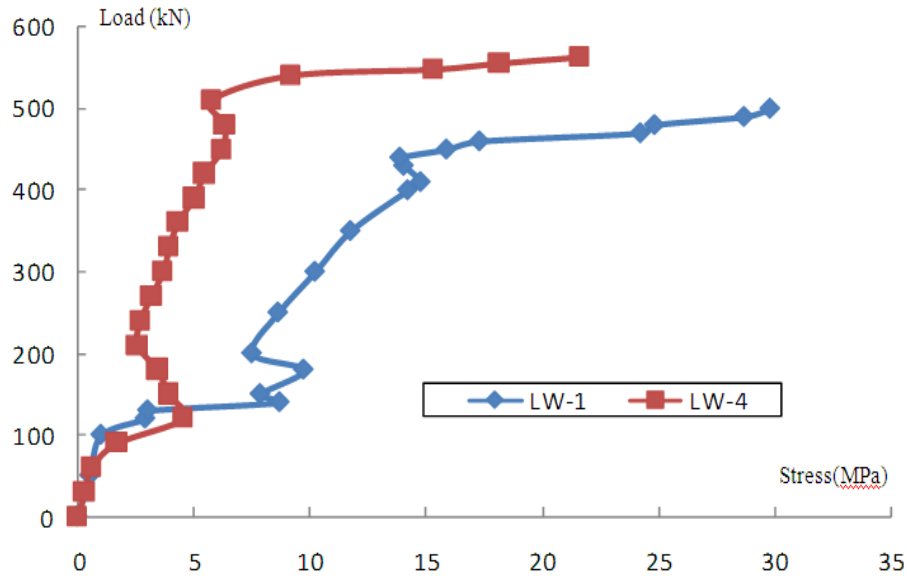
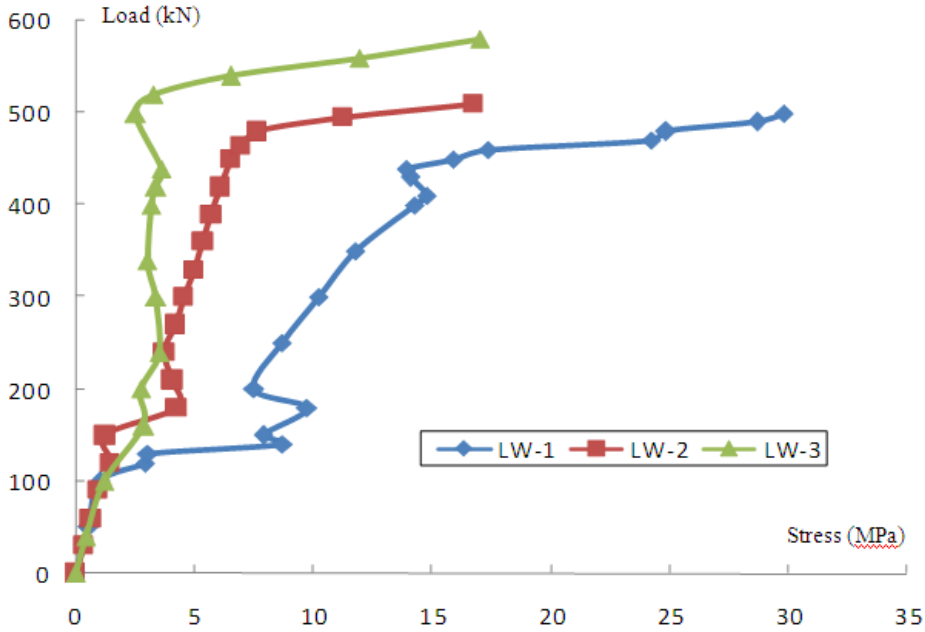**Fig.7-14 Comparison of concrete stress development in LW-1 and LW-4**
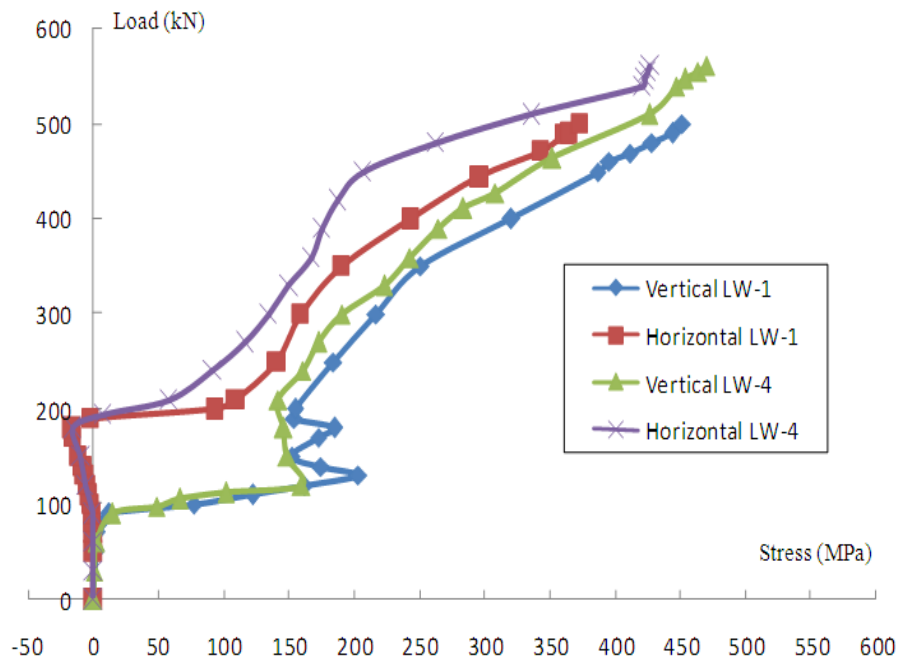
Fig.7-15 Comparison of steel stress development in LW-1 and LW-4

7.3 Influence factors on shear resistance of lightweight reinforced concrete shear wall

For the shear resistance of lightweight aggregate concrete shear walls, it can be calculated as normal concrete shear walls which were put forward in former chapter 3. It can be seen that, there are so many factors which influence the shear resistance of shear walls, such as strength of concrete, shear span ratio, web reinforcement, column dimension and column reinforcement, etc. Due to the different microstructure and mechanical properties of shale ceramsite concrete and normal concrete, it is necessary to consider the influence of these

factors on shear resistance of shale ceramsite concrete in order to provide more accurate coefficients to the calculated expressions of shear resistance which especially established for lightweight reinforced concrete shear walls.

From the upwards analysis it can be concluded that the finite element analysis method developed in this study can well simulate the shear resistance of shale cerasmite concrete shear wall. So it is possible to continue to do some numerical experiments by this way. The main influence factors for shear resistance of lightweight aggregate concrete shear wall are studied as following.

7.3.1 Shear span ratio

Six shear walls with different shear span ratios of 0.76, 1.43, 1.96, 2.5, 2.9 and 3.17 respectively are calculated by ANSYS 8.0. All the six shear walls have the same reinforcements, the same column cross section, the same web thickness and the same concrete strength as those parameters in specimen LW-1. So that it can be studied clearly the effect of the only variable, shear span ratio, on shear resistance of lightweight aggregate concrete shear walls. Taking shear span ratio as X-axis and horizontal force as Y-axis, Fig.7-16 shows the results of numerical walls. It can be concluded that, with the increase of shear span ratio, shear resistance of lightweight aggregate shear wall reduced. The relationship between shear span ratio and shear resistance behaves approximately an inclined line.
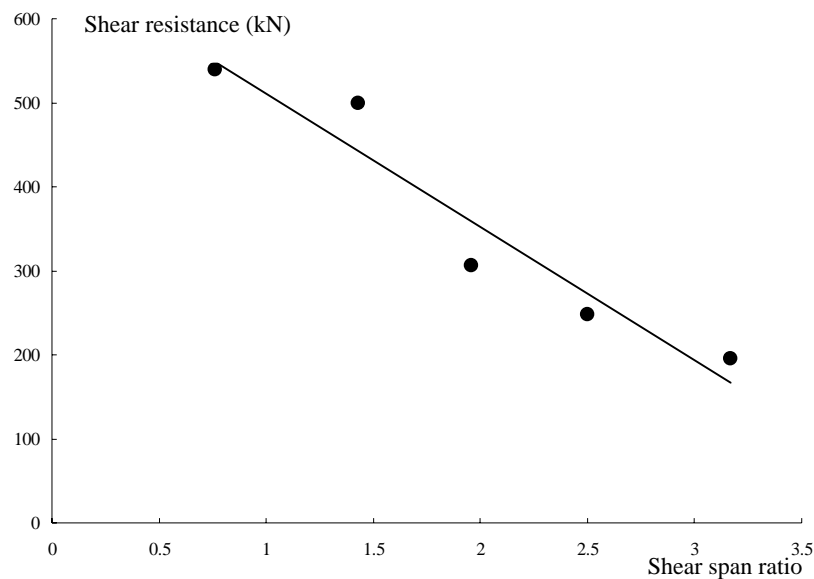
Fig.7-16 Influence curve of shear span ratio on shear resistance

7.3.2 Web horizontal reinforcement ratio

Seven shear walls, similar with specimen LW-1 except the web horizontal reinforcement ratio, are analyzed by the ANSYS 8.0. The web horizontal reinforcement ratios of the seven walls change from 0.1% to 4%. The calculated results, as shown in Fig.7-17, indicated that, with the increase of web horizontal reinforcement ratio, shear resistance of lightweight aggregate concrete shear wall increase. When the web horizontal reinforcement ratio is smaller than the web vertical reinforcement ratio, shear resistance increases distinctly. When

the web horizontal reinforcement ratio is larger than the web vertical reinforcement ratio (0.392%), the increase proportion of shear resistance reduced. After the web horizontal reinforcement ratio is larger than 2%, the shear resistance of wall increases no more. It is because that the failure of wall in this status is exceed reinforcement failure, which behaves that most of the steels are not yielding until the wall failure.
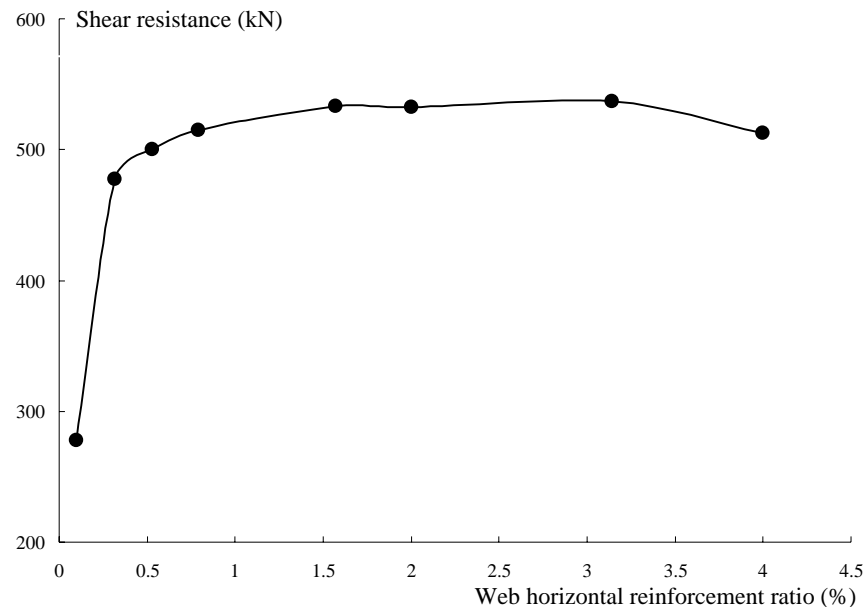
Fig.7-17 Influence curve of web horizontal reinforcement ratio on shear resistance

7.3.3 Web vertical reinforcement ratio

Fig.7-18 (a) shows the calculated results of shear resistance of six lightweight aggregate concrete walls. The only difference between these walls and specimen LW-1 is the web vertical reinforcement ratio, which changed from 0.1% to 3.14%. Because the shear span ratios of these walls are 1.43, which means that either the flexure or the shear failure will occur in them, so that the influence of web vertical reinforcement ratio on the shear resistance of wall is not obviously.

Fig.7-18 (b) shows the calculated results of shear resistance of another seven lightweight aggregate concrete walls. One difference between these walls and specimen LW-1 is the web vertical reinforcement ratio, which changed from 0.1% to 6%. The other difference is the shear span ratio, which are 2.5 for all the seven walls. It can be seen that, for shear wall with shear span ratio of 2.5, their shear resistance increase obviously with the increase of web vertical reinforcement ratio. This phenomenon also proves that, for the shear wall with larger shear span ratio, in which flexure failure will occur, web vertical reinforcements have definitive effect on the shear resistance.

Shear resistance (kN)
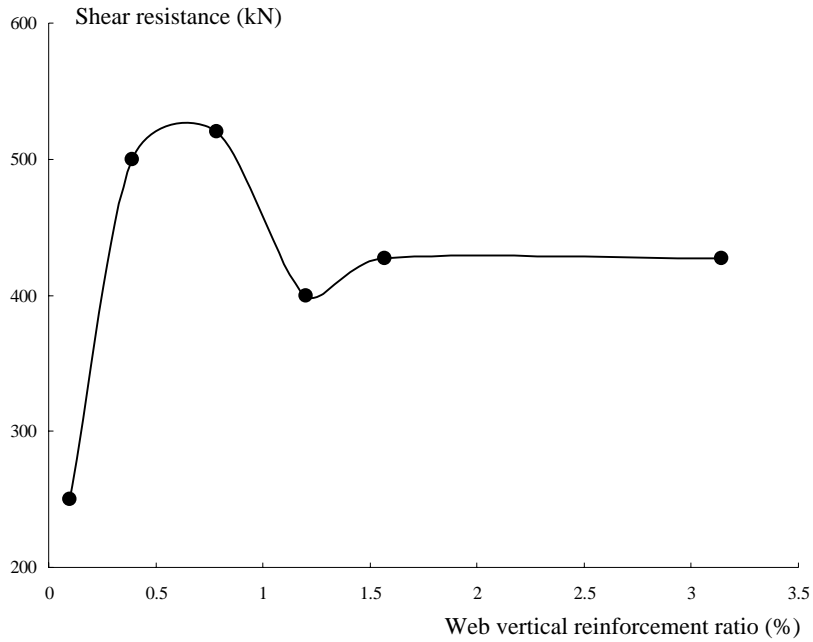
(a) Walls with shear span ratio of 1.43

Shear resistance (kN)
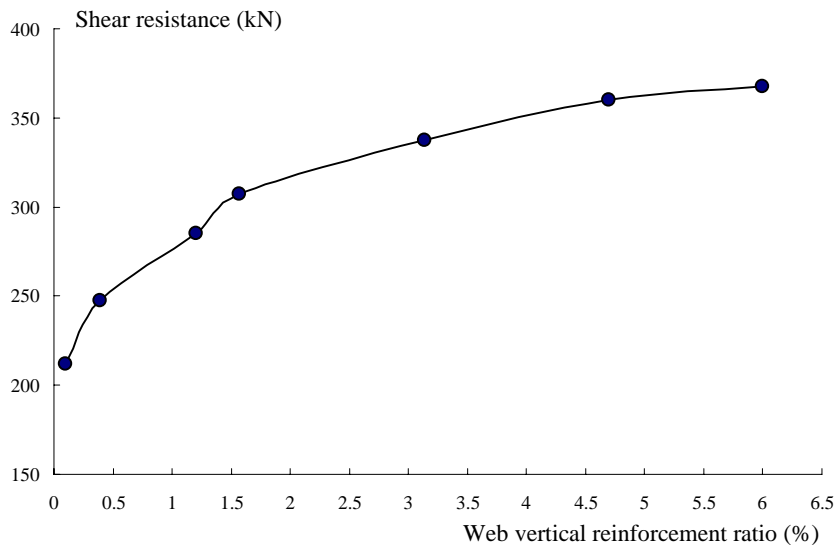
(b) Walls with shear span ratio of 2.5

Fig.7-18 Influence curve of web vertical reinforcement ratio on shear resistance

7.3.4 Column width

Taking the column width to web depth ratio (h_c / h) as X-axis and shear resistance as Y-axis, Fig.7-19 is the influence curve of column width on the shear resistance of shear walls. The only parameter changed here is width dimension in cross section of column, which let the ratio h_c / h vary from 1.0 to 4.0. It indicates that, shear resistance of lightweight aggregate concrete wall can be increased by widening the column width. Before the column width to

web depth ratio is less than 2.5, the increase is linear. After the column width to web depth ratio is larger than 2.5, its increase has light influence on the shear resistance. The reason is that, if the dimension of column is too small, shear wall will be quickly destroyed due to the low shear strength of column. After the column width is relatively large, failure of shear wall will occur in the web. So there is little use to increase the dimension of column.
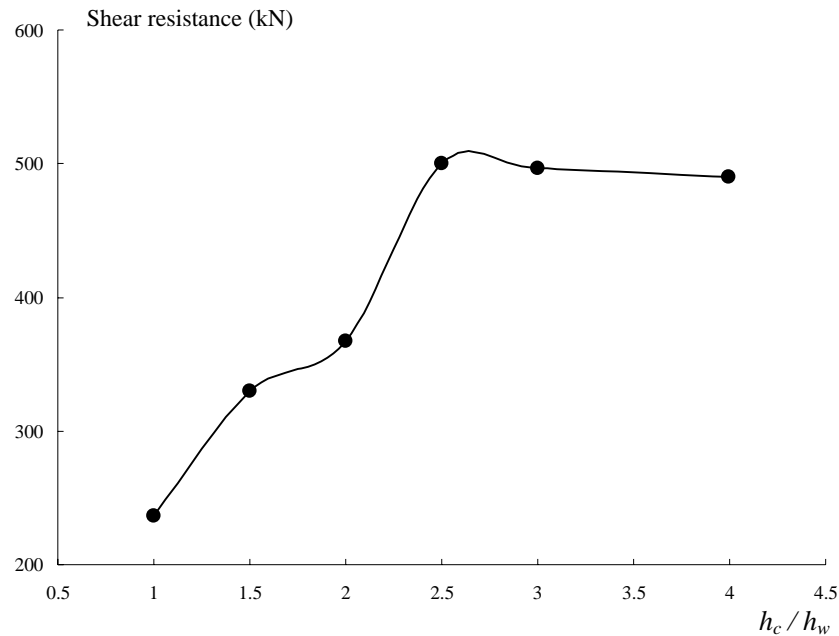
Fig.7-19 Influence curve of column width on shear resistance

7.3.5 Column longitudinal steel ratio
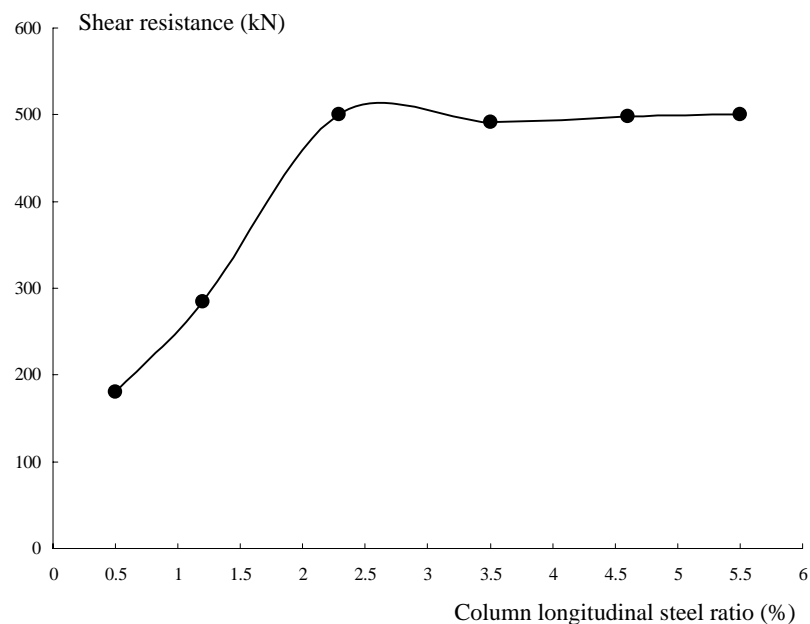
Fig.7-20 Influence curve of column longitudinal steel ratio on shear resistance

Six lightweight aggregate concrete shear walls with different longitudinal steel ratio in columns, 0.5% to 5.5%, are calculated in this study. The other parameters of them are the same as those of specimen LW-1. From Fig.7-20 it can be seen that, increasing the longitudinal steel in column can improve the shear resistance of shear wall. Before the column longitudinal steel ratio is less than 2.5%, the increase is almost linear. After the column longitudinal steel ratio is larger than 2.5%, its increase has light influence on the shear resistance. The reason is that, if the column longitudinal steel ratio is too small, shear wall will be quickly destroyed due to the low bending strength of column. After the column longitudinal steel ratio is relatively large, failure of shear wall will occur in the web. So there is little effect to increase the longitudinal steel in column.

7.3.6 Concrete compressive strength

Fig.7-21 provides the calculated results of shear resistance for five lightweight aggregate concrete shear walls. The only different of these walls to specimen LW-1 is the concrete compressive strength, which vary from 20 MPa to 45 MPa. It indicates that concrete compressive strength has obvious effect on the shear resistance of shear wall. With the increase of concrete compressive strength, shear resistance of walls increase distinctly. The reason of it is that, after diagonal cracks appear in the web, part of shear resistance of wall is provided by the concrete compressive diagonal struts and moreover, web failure will not occur until concrete is crushed when the strain in concrete at shear compressive zone reaches to ultimate value.
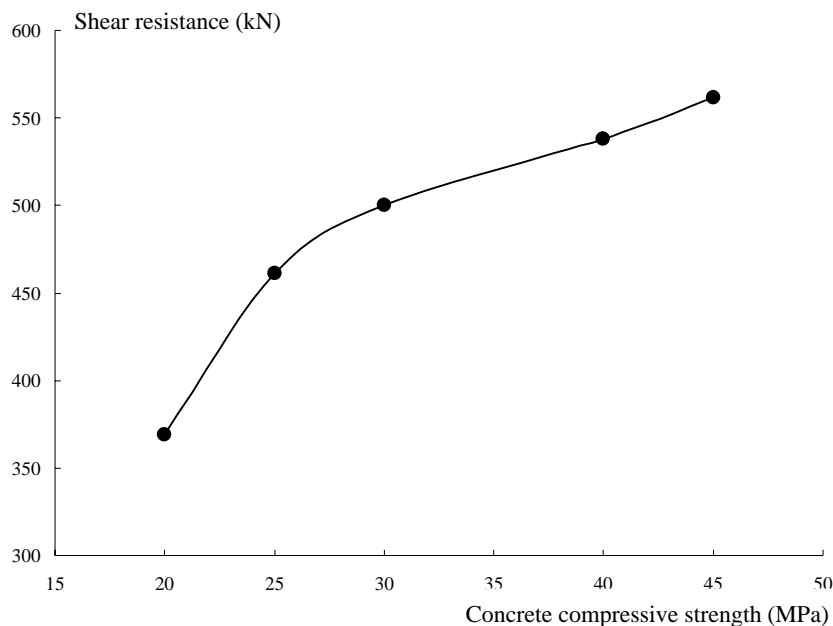
Fig.7-21 Influence curve of concrete compressive strength on shear resistance

Chapter 8

Conclusions and Recommendations for Further Research

The major objective of this study was to conduct experimental and theoretical studies on the seismic behaviour of lightweight aggregate concrete shear wall with different modes of reinforcement. Four shear walls were tested under cyclic loading up to failure to study the shear strength, flexural strength, deformation capacity and seismic behaviour of lightweight aggregate concrete shear wall. Reinforcement details were representative to construction practice in regions of low to moderate seismic risk. Based on the analysis of the experimental results, the influence of lightweight aggregate and diagonal reinforcement on the shear capacity, the deformation, the hysteretic behaviour and the ductility of shear walls were discussed in detail. The finite element method was used to model the behaviours of lightweight aggregate concrete shear wall with conventional and diagonal web reinforcements. With the proper elements and the proper material models for concrete and steel bar, non-linear finite element analyses of four specimens were preformed by the software ANSYS 8.0. The results were compared with the experimental results. The stress redistribution in shear walls and the strain developments in steels and concrete are also discussed in detail based on the analytical and tested results. Furthermore, some numerical experiments which focus on the influence factors of shear resistance of lightweight reinforced concrete shear wall were processed. The former chapters have provided all the research work in detail. Some valuable conclusions and some recommendations for further research work are summarized as follows.

8.1 Conclusions from experimental study

- Walls with lightweight concrete exhibited high shear capacity and large ductility, and they all showed a satisfactory energy dissipation mechanism. With appropriate confinement of the boundary elements, brittle modes of failure were avoided. All specimens tested here failed in a predominantly flexural shear mode, characterized by concrete crushing and reinforcement buckling at the confined edges. The test data discussed herein appeared that

lightweight reinforced concrete shear wall can be used as structural walls in seismic zones. Because of the lighter weight, the better thermal insulation and the greater fire resistance properties of lightweight concrete, lightweight reinforced concrete shear wall provides a new way for wall system structures in seismic zones.

- Pinching of the hysteretic loops caused by horizontal sliding, bonding-slip of vertical bars and shear crack opening were significant in the conventionally reinforced specimen, and considerably less in the specimens with web diagonal reinforcement. It was found that, walls with diagonal web reinforcement displayed the ability to dissipate more energy at a given level of lateral deformation than walls with conventional web reinforcement. Increasing the amount of diagonal web reinforcement increased the energy dissipation capacity of the walls.

- Walls with diagonal web reinforcement experienced less shear distortion in the lower portion than walls with conventional web reinforcement. Shear distortion did increase, however, after the diagonal web reinforcement yielded. Web crushing was not observed in walls with diagonal web reinforcement. Diagonal web reinforcement also helped to prevented deterioration of the concrete strength in the compressive struts. The decrease in force in the concrete struts and the decrease in inelastic shear distortion improved the shear transfer capacity of concrete in the web and prevented web crushing.

- Diagonal web reinforcement is one approach to control structural damage reliably during earthquakes. For loading cycle to a specified lateral displacement, walls with diagonal web reinforcement exhibited smaller crack widths and dissipated more energy than conventionally reinforced walls.

- Walls with conventional reinforcement and additional bidiagonal bars experienced satisfactory energy dissipation capacity and relatively slow rigidity attenuation. Compared with specimen LW-3, in which all the web reinforcements were diagonal steels, specimen LW-4 which reinforced with four intersect inclined bars behaved similar seismic properties. So that, due to the economic reason and the difficulties associated with placement of diagonal bars during construction, the placement of fewer inclined bars together with conventional reinforcements like specimen LW-4 provided an attractive alternative for the web reinforcement in walls.

8.2 Conclusions from theoretical study

- For shear design of reinforced concrete walls, ACI 318-05 and EC 8 present some notable differences. The design according to EC 8 leads to a less economic design than in case of a design according to ACI Code. The EC 8 design is conservative, as compared to the ACI Code design.

- Although the proposed material models in this investigation were not capable of reproducing all observed aspects in lightweight reinforced concrete shear walls, the finite element analysis could still provide a wide-range of information that were useful for the study of the behavior of lightweight reinforced concrete shear walls. The calculated and tested results of horizontal load versus top displacement curves of four specimens showed a good agreement. Moreover, the load–strain responses in steel for four walls were

captured well by the numerical simulation. The finite element models of four lightweight aggregate concrete shear walls, constructed in ANSYS 8.0 using elements SOLID 65 and LINK 8 in this study, could capture the non-linear response of these systems under earthquake load conditions.

- The dedicated element employed a smeared crack model to allow for concrete cracking with the option of modeling the reinforcement in a distributed or discrete manner. For a known compressive strength of concrete, which can be measures from concrete cubes, existing rules for the elastic modulus and concrete tensile strength were adequate for inclusion in the numerical models. It was found that for the optimum modeling strategy, controlling mesh density, defining appropriate material properties and accurately locating the internal reinforcement were very important.

- The load–stress development curves of concrete and steel rebar for four specimens with different reinforcement based on the finite element model results were compared in detail. It indicated that, diagonal web reinforcement was effective in transferring shear force to the foundation and the shear forces carried by the compressive struts were evidently reduced due to the existing of diagonal web reinforcement.

- Due to the practicability of finite element model developed for four specimens, it is possible to continue to do some numerical experiments by this way. The influence on the shear resistance of lightweight aggregate concrete shear walls of some factors, such as strength of concrete, shear span ratio, web reinforcement, column dimension and column reinforcement, were studied by this finite element method.

8.3 Recommendations for further work

Several other subjects related to this research have been identified that it needs further investigation. Experimental and analytical research works needed later are summarized below.

- More experimental study are still needed which focus attentions on the lightweight concrete shear walls with different shear aspect ratio, different web reinforcement ratio, and different concrete strength or with vertical load applied on the top of the walls.

- Although the current ACI design equation provides a conservative estimate of the shear strength of walls with diagonal web reinforcement, further study is needed to develop a proper design expression for shear walls with diagonal web reinforcement.

- Comparison of experimental results for conventional reinforced concrete shear walls with that for lightweight reinforced concrete shear walls is needed for validating if lightweight reinforced concrete shear wall is a good alternative to conventional reinforced concrete shear wall used in seismic regions.

- More research works should be done to find a better way to simulate the behavior of lightweight reinforced concrete shear walls under cyclic loads. So that the ductility, the crack development, the failure region, etc. of this system can be studied in detail.

Bibliography :

[ACI99]   ACI Committee 318. "Building Code Requirements for Structural Concrete (318-99) and Commentary (318R-99)", *American Concrete Institute*, Farmington Hills, Mich. 1999, pp.391.

[ACIL99] ACI Committee 213, Guide for Structural Lightweight Aggregate Concrete (*ACI 213R-87 Reapproved 1999*), 1999.

[ACI05] ACI 318 – 05, "Building Code Requirements for Structural Concrete with Design Applications ", *2005 Portland Cement Association*, Ninth edition, First printing, 2005.

[Agr76] Agrawal, A.B., L.G. Jaeger, and A.A. Mufti, "Crack Propagation and Plasticity of Reinforced Concrete Shear-Wall under Monotonic and Cyclic Loading", *Conference on Finite Element Methods in Engineering*, Adelaide, Australia, December 1976.

[Akt80] Aktan, H.M. and R.D. Hanson, "Nonlinear Cyclic Analysis of Reinforced Concrete Plane Stress Members", *Special Publication SP63-6*, American Concrete Institute, 1980, pp.135-152.

[Alm95] Almusallam T.H. and Alsayed H, "Stress-strain Relationship of Normal, High-Strength and Lightweight Concrete", *Magazine of Concrete Research*, 1995, 47, No. 169, pp. 39-44.

[ANS05] ANSYS, *ANSYS User' Manual Revision 10.0*, ANSYS, Inc., Cannonsburg, Pennsylvania, 2005

[Arn86] Arnould M., Virlogeux M., "Granulats et bétons légers", *Paris: Presses ponts et chaussées*, 1986 (in French).

[Bar93] Bardhan-Roy BK et al., "Structural Lightweight Aggregate Concrete", *J. L. Clarke, Blackie Academic & Professional,* 1993.

[Bat79] Bathe, K.J. and S. Ramaswamy, "On Three-Dimensional Nonlinear Analysis of Reinforced Concrete Structures", *Nuclear Engineering and Design*, Vol.52, 1979, pp. 385-409.

[Baz79]   Bazant, Z.P. and L. Cedolin, "Blunt Crack Band Propagation in Finite Element Analysis", *Journal of the Engineering Mechanics Division*, ASCE, Vol. 105, No. EM2, April 1979, pp. 397-315.

[Bel94]   Belarbi, A. and Hsu, T.T.C., "Constitutive Laws of Concrete in Tension and Reinforcing Bars Stiffened by Concrete", *ACI   Structural Journal*, Vol.91, 1994, pp. 465-474.

[Ber79]   Bergan, N.B. and I. Holand, "Nonlinear Finite Element Analysis of Concrete Structures", *Computer Methods in Applied Mechanics and Engineering*, Vol. 17, No. 18, 1979, pp.443-467.

[Bol89]   Bolander, J.E. and J.K. Wight, "Towards Realistic FE Models for Reinforced Concrete Shear Wall Dominant Buildings subjected to Lateral Loadings", *Report No. UMCE89-2*, Department of Civil Engineering, The University of Michigan, Ann Arbor, Michigan, January 1989, pp. 192.

[Bol91]   Bolander, J.E. and J.K. Wight, "Finite Element Modeling of Shear-Wall-Dominant Buiding", *Journal of Structural Engineering*, ASCE, Vol.117, No.6, June 1991, pp. 1719-1739.

[Cav03]   Cavaleri, L., Miraglia, N. and M. Papia, "Pumice Concrete for Structural Wall Panels", *Engineering Structures*, Vol.25, 2003, pp. 115-125.

[CEB96]   CEB.,"RC Elements under Cyclic Loading: State of the Art Report", *London: Thomas Telford Services Ltd.*, 1996.

[CEB96a]   CEB., "RC Frames under Earthquake Loading: State of the Art Report", *London: Thomas Telford Services Ltd.*, 1996a.

[Cer80]   Cervenka, V. and K.H. Gerstle, "Inelastic Analysis of Reinforced Concrete Panel : Theory", *Publication of International Association for Bridge and Structural Engineering*, Vol. 31-II, 1971, pp.31-45.

[Cer80]   Cervenka, V., "Inelasitc Finite Element Analysis of Reinforced Concrete Panels under Inplane Loads", *Ph.D. Dissertation*, Department of Civil Engineering, The University of Colorado, Boulder, Colorado, 1980, pp. 239.

[Cha01]   Chadchart Sittipunt et al. "Cyclic behavior of reinforced concrete structural walls with diagonal web reinforcement", *ACI Structural Journal*, V.98, N0. 4, July-August 2001, pp. 554-562.

[Che05]   Chee-Kiong Soh, Susanto Teng, Yu Liu, "Computational Experiment of Reinforced Concrete Structural Elements Using Damage Mechanics", *Structural Concrete Research Group*, School of Civil and Environmental Engineering, Nanyang Technological University.

[Dan04]   Daniel, P., and Frank J.V., "Compression Field Modeling of Reinforced Concrete Subjected to Reversed Loading: Verification", *ACI   Structural Journal*, V.101, No.2, March-April 2004, pp. 155-164.

[Dar76]   Darwin, D. and D.A.W. Pecknold, "Analysis of RC Shear Panels under Cyclic Loading", *Journal of the Structural Division*, ASCE, Vol.107, No. ST2, February 1976, pp. 355-369.

[Der79]   Derecho, A. T.; Ghosh, S. K.; Iqbal, M.; and Fintel, M., "Strength, Stiffness, and Ductility Required in Reinforced Concrete Structural Walls for Earthquake Resistance", *ACI Journal*, *Proceedings* V.76, No.8, Aug. 1979, pp. 875-895.

[Ebe95]   Eberhard, M. O., and Meigs, B. E., "Earthquake-Resisting System Selection Statistics for Reinforced Concrete Buildings", *Earthquake Spectra*, Earthquake Engineering Research Institute, V.11, No.1, Feb. 1995, pp. 19-36,

[Eur00]   European Committee for standardization, 2000, Draft No.1, *Eurocode-8*, Design Structures for Earthquake resistance, Brussels.

[Eur05]   Designers' Guide to EN1992-1-1 and EN1992-1-2, *Eurocode2*: Design of Concrete Structures, General Rules and Rules for Buildings and Structural Fire Design, 2005.

[Fil83]   Filippou, F.C., Popov, E.P. and Bertero, V.V., "Effects of Bond Deterioration on Hysteretic Behavior of Reinforced Concrete Joints", *Berkeley: Earthquake Engineering Research Center*, Univ. of California, EERC 83-19.

[Fin74]   Fintel, M., "Ductile Shear Walls in Earthquake Resistant Multistory Buildings", *ACI Journal*, *Proceedings* V.71, No.6, June 1974, pp. 296-365.

[Ino85]   Inoue, N., N. Koshika, and N. Suzuki, "Analysis of Shear Wall Based on Collins Panel Test", *Finite Element of Reinforced Concrete Structures*, ASCE, May 1985, pp. 288-299.

[Izu89]   Izumo, J., H. Shin, K. Maekawa, and J. Okamura, "Analytical Model for RC Panels under Cyclic Load", *Structural Design, Analysis, and Testing*, Proceedings of the sessions related to design, analysis and testing at Structures Congress´89, ASCE, May 1989, pp.39-48.

[Jam92]   James G.MacGregor, "Reinforced Concrete Mechanics&Design", *Prentice-Hall*, 2nd ed., 1992, 848 pp.

[Jof71]   Jofriet, J.C. and G.M. McNeice, "Finite Element Analysis of Reinforced Concrete Slab", *Journal of the Structural Division*, ASCE, Vol.97, No. ST3, March 1971, pp.785-806.

[Joh02]   Johnn P. Judd and Fernando S. Fonseca, "Nonlinear Wood Diaphragm and Shear Wall Analysis", *Proceedings, 2nd International Conference on Engineering Materials*, August 16-19, San Jose, California, Canadian Society for Civil Engineering and Japan Society of Civil Engineers, Montreal, Quebec, Vol. 1, pp. 391-401.

[Kap91]   Kappos, A.J., "Analytical prediction of the Collapse Earthquake for R/C Buildings: Suggested Methodology", *Earthquake Engineering and Structural Dynamics*, Vol.20, 1991, pp.167-176.

[Kar69]   Karsan, I.D. and Jirsa, J.O., "Behavior of Concrete under Compressive Loading", *Journal of the Structural Division*, ASCE, Vol.95, 1969, pp. 2543-2563.

[Kaw01]   Kwak, H.G. and D.Y. Kim, "Nonlinear analysis of RC shear walls considering tension-stiffening effect", *Computers and Structures*, Vol.79, 2001, pp.499-517.

[Kaw02]   Kwak, H.G. and Song, J.Y. , "Cracking Analysis of RC Members UYsing Polynomial Strain Distribution Function", *Engineering of Structural*, Vol.24, 2002, pp. 455-468.

[Kaw04]   Kwak, H.G. and D.Y. Kim, "Cracking Behavior of RC Shear Walls Subject to Cyclic Loadings", *Computers and Concrete*, Vol.1, No.1 (2004) 77-98.

[Kup73]   Kupfer, H.B. and Gerstle, K.H., "Behavior of Concrete under Biaxial Stresses", *Journal of Engineering Mechanic Division*, ASCE, Vol.99, 1973, pp.852-866.

[Lin75]   Lin, C.S. and A.C. Scordelis, "Nonlinear Analysis of RC shell of General Forms", *Journal of the Structural Division*, ASCE, Vol.101, No.ST3, March 1975, pp. 523-538.

[Lux03]   Lu xinzheng and Jiang jianjing, "Analysis for Concrete Structure under Complex Stress Condition with Solid 65 FEA Element of Ansys", *Building structure*, 33(6), 2003, pp.22-24.

[Man01]   Mansour, M., Lee, J.Y. and Hsu, T.T.C., "Cyclic Stress-strain Curves of Concrete and Steel Bars in Membrane Element", *Journal of the Structural Division*, ASCE, Vol.127, 2001, pp. 1402-1411.

[Mas90]   Massicotte, B., J.G. MacGregor, and A.E. Elwi, "Behavior of Concrete Panels Subjected to Axial and Lateral Loads", *Finite Element of Reinforced Concrete Structures*, ASCE, May 1985, pp. 11-30.

[Mey82]   Meyer, C. and K.J. Bathe, "Nonlinear Analysis of R/C Structures in Practice", *Journal of the Structural Division*, ACSE, Vol. 108, No. ST7, July 1982, pp. 1605-1622.

[Men73]   Menegotto, M. and Pinto, P.E., "Method of Analysis for Cyclically Loaded Reinforced Concrete Plane Frames including Changes in Geometry and Nonelastic Behavior of Element under Combined Normal Force and Bending", *In: IABSE, Proceedings of IABSE Symposium on Resestance and Ultimate Deformability of Structures Acted on by Well Defined Repeated Loads*, Lisbon, Spain

[Mik89]   Mikame, A., H. Yoshikawa, I. Shiraishi, Y. Kamiyama, S. Iizuka, K. Sato, K. Kawasaki, and H. Noguchi, "Parametric Analyses of RC Shear Walls by FEM", *Structural Design, Analysis, and Testing*, Proceedings of the sessions related to design, analysis and testing at Structures Congress´89, ASCE, May 1989, pp. 301-310.

[Min04]   Ming li Cao and Li-jiu Wang, "Research on MgO-$MgCl_2$-H_2O System Ceramsite Exempted from Sintering", *Proceeding of the International Workshop on Sustainable Development and Concrete Technology Center for Transportation Research and Education Iowa State University Ames Iowa USA*, Beijing China, May 20-21, 2004:141-158.

[Moh02]   Mohammad N. Shirali, "Seismic Resistance of a Hybrid Shearwall System", *Dissertation*, Fachbereich 13-Bauingenieurwesen der Technischen Universität Darmstadt, 2002.

[Mon02]   Monique C. Hite and Harry W. Shenton III, "Modeling the Nonlinear Behavior of Wood Frame Shear Walls", *15th ASCE Engineering Mechanics Conference*, June 2-5, 2002, Columbia University, New York, NY.

[Nue81]   Nuelle, L. M., and Sumner, S. S., "A Preliminary Evaluation of Shale-oil Resources in Missouri", *Missouri Department of Natural Resources*, Division of Geology and Land Survey, Information Circular 27, 31 p, 1981.

[Oes76]   Oesterle, R. G.; Fiorato, A. E.; Johal, L. S.; Carpenter, J. E.; Russell, H. G.; and Corley, W. G., "Earthquake Resistant Structural Walls – Tests of Isolated Walls", *Report to National Science Foundation, Construction Technology Laboratories, Portland Cement Association*, Skokie, I11., Oct. 1976, 315 pp.

[Oes79]   Oesterle, R. G.; Aristizabal-Ochoa, J.D.; Fiorato, A. E.; Russell, H. G.; and Corley, W. G., "Earthquake Resistant Structural Walls – Tests of Isolated Walls, Phase II", *Report to National Science Foundation, Construction Technology Laboratories, Portland Cement Association*, Skokie, I11., Oct. 1979, 325 pp.

[Oes84]   Oesterle, R. G.; Aristizabal-Ochoa, J.D.; Shiu, K. N.; and Corley, W. G., "Web Crushing of Reinforced Concrete Structural Walls", *ACI Journal*, *Proceedings* V.81, No.3, May-June 1984, pp.231-241.

[Oes86]   Oesterle, R. G. "Inelastic Analysis for In-Plane Strength of Reinforced Concrete Shearwalls", *PhD dissertation,* Department of Civil Engineering, Northwestern University, Evanston, I11., June 1986, 332 pp.

[Ozc89]   Ozcebe, G. and M. Saatcioglu, "Hysteretic Shear Model for Reinforced Concrete Members", *Journal of Structural Engineering*, ASCE, Vol. 115, No. 1, January 1989, pp. 132-148.

[Pau77]   Paulay, T., "Ductility of Reinforced Concrete Shearwalls for Seismic Areas", *Reinforced Concrete Structures in Seismic Zones,* SP-53, N. M. Hawkins, ed., American Concrete Institute, Farmington Hills, Mich., 1977, pp. 127-147.

[Pen97]   Penelis, G. G., and Kappos, A.J., "Earthquake-resistant concrete structures", *E & FN Spon*, London, UK, 1997

[Qin99]   Qin Weizu., "Some Aspects of the Utilization of Fly Ash to Develop High Performance Concrete", *Journal of Building Materials*, 1999(2): 153-158(in Chinese).

[Ric04]   Ricard W. Furlong, Cheng-Tzu Thomas Hsu, and Ali S., "Mirza Analysis and Design of Concrete Columns for Biaxial Bending ", *ACI Structural Journal*, Vol. 101 No.3, May-June 2004, pp. 413-423.

[Rou87]   Roufaiel, M.S.L. and Meyer, C., "Analytical Modelling of Hysteretic Behavior of R/C Frames", *Journal of Structural Engineering*, ASCE, Vol.113, 1987, pp. 429-444.

[Roy60]   Roy E. Gorton, "The Effects of Preheating Shale for Bloated Lightweight Aggregate", *A Thesis Submitted to State University of New York College of Ceramics at Alfred University*, Alfred, New York, 5 May 1960.

[Ste87]   Stevens, N.J., S.M. Uzumeri, and M.P. Collins, "Analysis Modelling of Reinforced Concrete Subjected to Monotonic and Reverses Loading", *Publication No. 87-1*, Department of Civil Engineering, University of Toronto, Toronto, Canada, January 1987.

[Sto84]   Stone, C. G., and Bush, W. V., "General Geology and Mineral Resources of the Caddo River watershed", *Arkansas Geological Commission Information Circular 29*, 32 p, 1984.

[Sit93]   Sittipunt, C., and Wood, S. L., "Finite Element Analysis of Reinforced Concrete Shear Walls", *A Report to the National Science Foundation*, Research Grant BCS 89-12992, Department of Civil Engineering, University of Illinois at Urbana-Champaign Urbana, Illinois, December 1993.

[Sitp93]   Sittipunt, C., and Wood, S. L., "Finite Element Analysis of Reinforced Concrete Shearwalls", *Civil Engineering Studies : Structural Research Series*, No. 584, University of Illinois, Urbana, Ill., Dec. 1993, 384 pp.

[Sit95]   Sittipunt, C., and Wood, S. L., "Influence of Web Reinforcement on the Cyclic Response of Structural walls", *ACI Structural Journal*, V.92, No.6, Nov-Dec. 1995, pp. 745-756.

[Sot85]   Sotomura, K. And Y. Murazumi, "Nonlinear Analysis of Shear Walls with Numerous Small Openings", *Finite Element of Reinforced Concrete Structures*, ASCE, May 1985, pp. 300-307.

[Ste87]   Stevens, N.J., S.M. Uzumeri, and M.P. Collins, "Analytical Modelling of Reinforced concrete Subjected to Monotonic and Reversed Loadings", *Publication No.87-1*, Department of Civil Engineering, University of Toronto, Toroto, Canada, January 1987.

[Ste91]   Stevens, N.J., Uzumeri, S.M., Collins, M.P. and Will, G.T., "Reinforced Concrete Subjected to Reversed Cyclic Shear Experiments and Constitutive Model", *ACI Structural Journal*, V.88, 1991, pp. 135-146.

[Sui73]   Suidan, M. and W.C. Schnobrich, "Finite Element Analysis of Reinforced Concrete", *Journal of the Structural Division*, ASCE, Vol.99, No. ST10, October 1973, pp. 2109-2122.

[Tao94]   Tao Hejin;Yu Qingrong and Shi Xinya, " Experimental Study on Behaviors of Reinforced Ash Ceramsite Concrete Shear Walls", *Journal of Building Structure*, V. 15, No. 4, Aug. 1994, pp. 20-30.

[Tas82]   Task Committee on Finite Element Analysis of Reinforced Concrete Structures, *State-of-the-Art Report on Finite Element Analysis of Reinforced Concrete*, American Society of Civil Engineers, New York, N.Y., 1982, 545 pp.

[Tom05]   Tom Kuennen, "Exploring the Synthetic Aggregates Alternative", *The Magazine For Aggregates Professionals*, October 2005.

[Ued85]   Ueda, M. and T. Kawai, "Discrete Limit Analysis of R/C Shear Walls", *Finite Element of Reinforced Concrete Structures*, ASCE, May 1985, pp. 277-287.

[Val72]   Valliappan, S. and T.F. Doolan," Non-linear Stress Analysis of Reinforced Concrete", *Journal of the Structural Division*, ASCE, Vol. 90, No. ST4, April 1972, pp. 885-898.

[Vec82]   Vecchio, F.J. and M.P. Collins, "The Response of Reinforced Concrete to In-plane Shear and Normal Stresses", *Publication No. 82-03*, Department of Civil Engineering, University of Toronto, March 1982.

[Vec89]   Vecchio, F.J., "Nonlinear Finite Element Analysis of Reinforced Concrete Membranes", *ACI Structural Journal*, Vol.86, No.1, January-February 1989, pp. 26-35.

[Vec93]   Vecchio, F.J. and Collins, M.P., "Compression Response of Cracked Reinforced Concrete", *Journal of the Structural Engineering*, ASCE, Vol.119, 1993, pp.3590-3610.

[Vec99]   Vecchio, F.J., "Towards cyclic load modelling of reinforced concrete", *ACI Structural Journal*, V.96, pp.193-202.

[Wan78]   Wang P.T., Shah S.P. and Naaman A.E., "Stress-strain Curve for Normal and Lightweight Concrete in Compression", *American Concrete Institute Journal Proceedings*, 1978, 75, No. 11, pp. 603-611.

[Will75]   Willam, K. J., and Warnke, E. D., "Constitutive Model for the Triaxial Behavior of Concrete", *Proceedings, International Association for Bridge and Structural Engineering*, Vol. 19, ISMES, Bergamo, Italy, p. 174 (1975).

[Will82]   Willam, K. J., University of Colorado, Boulder, (*Private Communication*) (1982).

[Woo91]   Wood, S. L., "Observed Behavior of Slender RC Walls Subjected to Cyclic Loadings", *Inelastic Response and Design of Earthquake-Resistant Concrete Structures*, SP-127, S. K. Ghosh, ed., American Concrete Institute, 1991, Farmington Hills, Mich., pp. 334-344.

[Xu91]   Xu, C. "Analytical Model for Reinforced Concrete under Cyclic Loading*", Ph.D. Dissertation*, Department of Civil Engineering, University of Illinois at Urbana-Champaign, Urbana, Illinois, 1997.

[Yam89]   Yamaguchi, H. And S. Nomura, "Analysis of RC Walls by Plastic-Fracturing Theory", *Structural Design, Analysis and Testing, Proceedings of the sessions related to design, analysis and testing at Structures Congress'89*, ASCE, May 1989, pp. 204-213.

[Y.H.05]   Y.H. Chai and John D. Anderson, "Seismic Response of Perforated Lightweight Aggregate Concrete Wall Panels for Low-rise Modular Classrooms", *Engineering Structures*, V. 27, 2005, pp.593-604.

[Yuz72]   Yuzugullu, D., "Finite Element Approach for the Prediction of Inelastic Behavior of Shear Wall-Frame System", *Ph.D. Dissertation*, Department of Civil Engineering, University of Illinois at Urbana-Champaign, Urbana, Illinois, 1972.

[Zha90]   Zhang M.H., O.E. Gjorv., "Microstructure of the Interfacial Zone between Lightweight Aggregate and Cement paste", *Cement Concrete Research. 20(4)*, 1990: 610-618

[Zha02]   Zhang Yong, Ding Qingjun, etc. "The Study on the Transition Zone of Lightweight Aggregate Concrete", *Concrete*.2002 (10): 29-31 (in Chinese).

[Zhe06]   Zheng Xiuhua, Zhang Baosheng, Yuan jie, Kong lijuan, Xu chi, Guo yongzhi, "Microstructure and Mechanical Properties of Shale Ceramsite Concrete", *School of Material Science and Engineering*, Harbin Institute of Technology, Harbin 150001, China.

[Zhu00]   Zhuang Yizhou, "Mechanical Properties of Self-combusted Gangue Reinforced Concrete Shear Walls under Low-cyclic Load", *Journal of Zhejiang University*, Engineering Science, V.34, No. 3, may 2000, pp. 325-330.

Lebenslauf

Persönliche Daten:	Werasak Raongjant
	Schulenburger LandStr.50
	30165, Hannover, Deutschland
	6 M. 1 Klongmadur, Kratumbann,
	Samutsakorn, 74110, Thailand
	Geb. Am 19. Oktober 1974 in Thailand
	Verheiratet

Hochschulausbildung:

Juni 1992-März 1995
Studium der Bauingenieurwesen an der Technische Universität Rajamangala, Uthenthawai kampus in Thailand
Abschluss: Dip.Con

Juni 1995-April 1998
Studium der Bauingenieurwesen an der Technische Universität King Mongkut Thonburi in Thailand
Abschluss: B.Eng

Juni 1998-October 2000
Studium der Bauingenieurwesen an der Technische Universität King Mongkut Thonburi in Thailand
Abschluss: M.Eng

Berufstätigkeit:

Seit Oktober 2000
Mitarbeiter an der Technische Universität Rajamangala in Thailand